# The Ubiquitin Proteasome System as a Regulator of Neuronal Function

Thesis submitted for the degree of
Doctor of Philosophy
at the University of Leicester
by

**Katie Puddefoot**
BSc Honours (The University of Bath)

Department of Neuroscience, Psychology and Behaviour
University of Leicester
December 2022

# Covid Impact Statement

This thesis was completed between the summer of 2019 to December 2022. During this time, the University of Leicester closed all laboratories from March 2020 to September 2020 due to the Covid-19 pandemic. During these six months, no data collection could occur. I received a three month funded extension to compensate for time lost. As such, some planned experiments had to be dropped or modified in order for this thesis to be submitted in time.

On return to the laboratory, access was restricted to reduce staff numbers. As such, much of this PhD was undertaken with very little technical support, including reduced access to fish breeding. On a personal note, during this PhD I became the primary carer for my husband throughout the Covid-19 pandemic, which again further limited my time in the laboratory. In addition to this, departmental restructuring occurred during this period, causing further disruption.

# Abstract


## The Ubiquitin Proteasome System as a Regulator of Neuronal Function

*Katie Puddefoot*

Homeostatic balance between protein synthesis, turn over and degradation is vital for the stability and viability of all living cells. The primary function of the Ubiquitin Proteasome System is to degrade intracellular proteins, however perturbation of this system has been associated with the pathogenesis of neurodegenerative diseases. There is also mounting evidence for the role of the proteasome in the healthy functioning of neurons, however an investigation into the effect of proteasomal inhibition on the physiology, morphology and behaviour within a vertebrate species has yet to be carried out.

In Chapters 3 and 4, whole-cell patch clamp technique has been used to determine how pharmacological inhibition of the proteasome influences the synaptic and intrinsic properties of motoneurons within the spinal cord of larval zebrafish. Proteasomal inhibition increased the frequency of glycinergic miniature inhibitory post-synaptic currents during chronic and short-term incubations. However, proteasome inhibition did not affect glutamatergic miniature excitatory post-synaptic currents or firing properties of motoneurons.

In Chapter 5, changes in the synaptic properties of the neuromuscular junction and the morphology primary motoneurons following pharmacological proteasomal inhibition were investigated. Proteasomal inhibition increased the frequency of miniature endplate potentials, suggesting that inhibition of the proteasome selectively affects neurotransmitter release at specific synapses. Thereafter, using immunohistochemistry, the effect of proteasomal inhibition on the morphology of primary motoneurons was assessed. Inhibition of the proteasome does not affect the outgrowth of primary motoneurons or the formation of neuromuscular junctions.

Finally, in Chapter 6, the effect of proteasomal inhibition on the free-swimming behaviour of larval zebrafish was assessed. Inhibition of the proteasome does not affect overall swimming distance or time spent swimming. However, proteasomal inhibition increased velocity of swimming, suggesting that changes in synaptic transmission due to inhibited proteasomes affects the locomotive behaviour of larval zebrafish.

# Acknowledgements

I would first and foremost like to thank my supervisor, Joe McDearmid, for all his wisdom, guidance and support during my PhD. Joe has been an excellent supervisor and there is no doubt that I would not have been able to complete this thesis without him. I am sincerely grateful to him for giving me this opportunity and offering up his time so willingly.

I would like to thank the Midlands Integrative Bioscience Doctoral Training Partnership for providing me with the funding for this PhD and for delivering such excellent training opportunities to help develop my research skills.

I want to thank McDearmid lab members past and present for all their help during my PhD. I would also like to thank all the technical staff at the University of Leicester who have helped to make my time in the lab easier with their support. A special mention for Neal Rimmer, who even post-PhD has been a much needed technical and emotional support. A big thank you to all my PhD friends, especially Josh Whittingham, Jordan Cassidy and Zoe Baily who have all helped to make my time at Leicester a little bit easier.

I would also like to thank my wonderful husband Ben Symonds for all his support and for never seeming to get annoyed at my constant complaining. His encouragement has kept me motivated and his incredible work ethic has been a source of inspiration throughout.

Finally, I would like to thank my family, especially my Mum and Dad. They raised me to pursue my dream and keep going even when the task felt beyond impossible. Thank you for being an emotional (and financial!) support over the years so that I have been able to complete this chapter.

# Contents

# Table of Figures

# List of Tables

## Abbreviations

| | |
|---|---|
| **α**-bgt | alpha-bungarotoxin-ATTO-633 |
| ACh | Acetylcholine |
| AChR | Acetylcholine Receptor |
| ACTN1 | Actinin Alpha 1 |
| ALS | Amyotrophic Lateral Sclerosis |
| AMPA | **α**-amino-3-hydroxy-5-methyl-4-isoxazolepropionic acid |
| AO | Acridine Orange |
| APC | Anaphase Promoting Complex |
| APC/C | Anaphase Promoting Complex/Cyclosome |
| aS | Alpha Synuclein |
| ASK1 | Apoptosis-signalling-kinase 1 |
| ATP | Adenosine triphosphate |
| BAK | Bcl-2 antagonist killer |
| BAX | Bcl-2 associated x protein |
| BB | Bridge Balance |
| Bcl2 | B cell lymphoma-2 |
| BFA | Brefeldin a |
| BID | BH3-interacting domain |
| CaP | Caudal Primary |
| Cdh1 | Cadherin 1 |
| CFTR | cystic fibrosis transmembrane conductance regulator |
| CiD | Circumferential Descending Neurons |
| CMA | Chaperone Mediated Autophagy |
| CoLo | Commissural Local |
| Comm | Commissureless |
| CoPA | Commissural Primary Ascending |
| CoSA | Secondary Ascending Commissural Interneuron |
| CSF-cNs | Cerebrospinal fluid-contacting neurons |
| DIAP1 | *Drosophila* inhibitor of apoptosis |
| dlc | dorsolateral commissural |
| DLK-1 | Delta Like Non-Canonical Notch Ligand 1 |
| DMSO | Dimethyl Sulfoxide |
| DNA | Deoxyribonucleic Acid |
| dpf | Days Post Fertilisation |
| DRG | Dorsal Root Ganglion |
| Dronc | Death regulator Nedd2-like caspase |
| DUBs | Deubiquitinating Enzymes |
| EJC | Excitatory Junction Current |
| ENaC | Epithelial Sodium Channel |
| ER | Endoplasmic Reticulum |
| ERAD | ER-Associated Degradation |
| ERM | Embryonic Red Muscle |

| | |
|---|---|
| EW | Embryonic White Muscle |
| *faf* | fat facets |
| FSN-1 | F-box/SPRY domain-containing protein 1 |
| Fzr | Fizzy-related protein |
| GABA | Gamma Aminobutyric Acid |
| GLR-1 | Glutamate Receptor 1 |
| GTP | Guanosine-5'-triphosphate |
| HECT | Homologous to the E6-AP Carboxyl Terminus |
| *hiw* | highwire |
| hpf | hours post fertilisation |
| IEGs | Immediate Early Genes |
| IN | Interneuron |
| IRE1**α**1 | Inositol Requiring Enzyme 1 |
| iS | Intermyotomal Secondary |
| JAABA | Janelia Automatic Animal Behaviour Annotator |
| JNK | c-Jun N-terminal Protein Kinase |
| KD | Knock-Down |
| KO | Knock-Out |
| KYN | Kynurenic Acid |
| L-LTP | Late Long Term Potentiation |
| LAMP2 | Lysosomal Associated Membrane Protein 2 |
| LB | Luria Broth |
| LTD | Long-Term Depression |
| LTF | Long-Term Fascilitation |
| LTP | Long-Term Potentiation |
| M-Cell | Mauthner neuron |
| mEPC | miniature endplate current |
| mEPSC | mini Excitatory Postsynaptic Current |
| MiP | Middle Primary |
| mIPSC | mini Inhibitory Postsynaptic Current |
| MNs | Motoneurons |
| mRNA | Messenger Ribonucleic Acid |
| MS | mass spectrometry |
| $Na_v$ | Voltage Gated Sodium Channels |
| Nedd4 | neuronal precursor cell expressed developmentally downregulated-4 |
| Nedd4-2 | neuronal precursor cell expressed developmentally downregulated-4 type 2 |
| NMDA | N-methyl-D-aspartic acid |
| NMJ | Neuromuscular Junction |
| nMLF | nucleus of the medial longitudinal fasciculus |
| NMP | Neuronal Membrane Proteasomes |
| PERK | Protein Kinase RNA-like ER Kinase |
| PEST | protein sequence linked to degradation |
| PFA | Paraformaldehyde |

| | |
|---|---|
| PLM | Posterior Lateral Microtubule |
| PMN | Primary Motor Neuron |
| PSD | Post-synaptic Density |
| PSD-95 | post-synaptic density protein 95 |
| PTX | Picrotoxin |
| Ra | Access Resistance |
| Rap | Receptor-associated protein |
| RB | Rohon Beard |
| RGC | Retinal ganglion cells |
| RIDD | IRE1-dependent decay |
| RING | Really Interesting New Gene |
| Rm | Membrane Resistance |
| RNA | Ribonucleic Acid |
| Robo | Roundabout |
| ROI | Region of Interest |
| RoP | Rostral Primary |
| RPM-1 | Regulator Presynatpic Morphology 1 |
| RT | Room Temperature |
| SCF | Skip1, Cullin, F-box |
| SILAC | stable isotope labelling with amino acids in cell culture |
| SMN | Secondary Motor Neuron |
| SNA | Spontaneous Neuronal Activity |
| SNT | Simple Neurite Tracer |
| SOD1 | Superoxide Dismutase 1 |
| STF | Short-Term Fascilitation |
| STY | Strychnine |
| SV | Synapric Vesicles |
| SV2 | Synaptic Vesicle Protein 2 |
| TRN | Touch Receptor Neurons |
| TRAF2 | (TNFR)-Associated Factor 2 |
| tRNA | Transfer Ribonucleic Acid |
| TTX | Tetrodotoxin citrate |
| Ub | Ubiquitin |
| *ubcD1* | E2 ubiquitin-conjugating enzyme D1 |
| unc-11 | Un-coordinated 11 |
| UPR | Unfolded Protein Response |
| UPS | Ubiquitin Proteasome System |
| USP14 | Ubiquitin Specfic Peptidase 14 |
| VeLD | Ventral Longitudinal Descending Neurons |
| Vm | Membrane Voltage |
| WGD | Whole-Genome Duplication |
| WT | Wild Type |
| XBP1 | X Box Binding Protein 1 |

| | |
|---|---|
| ZNP-1 | Zebrafish Neuropilin Protein |

# Chapter 1 General Introduction

Protein synthesis, folding, processing and turnover are central to the control of protein homeostasis (proteostasis) in eukaryotic cells. Dysfunction of any of these processes can lead to cellular stress and apoptosis (Hipp et al., 2019). Protein turnover, the process in which proteins are synthesised and then degraded, is an energy dependent process. As such, it must be tightly regulated to ensure that it is as efficient as possible. Furthermore, loss of proteostasis is a hallmark of aging, and dysfunctional proteostasis has been implicated in many neurodegenerative diseases (Basisty et al., 2018). Here, I will discuss the role of intracellular protein synthesis and degradation pathways, as well as giving an insight into the fail safes that are put in place if these systems go wrong.

## 1.1 Degradation pathways

There are two main intracellular degradation pathways: the ubiquitin proteasome pathway and the lysosomal-autophagic pathway (Cuervo and Dice, 1998). The system by which proteins undergo proteasomal degradation is referred to as the Ubiquitin Proteasome System (UPS). The UPS is exclusively intracellular and is primarily used for the degradation of transient or misfolded proteins. Alternatively, the lysosomal pathway, which degrades both intracellular and extracellular components, is primarily used to breakdown large protein complexes and whole organelles (Dunn, 1994, Yu et al., 2018, Yang and Wang, 2021).

As the name suggests, the principal degradation machinery of the lysosomal pathway are 'lysosomes'; organelles which contain hydrolytic enzymes that can degrade proteins, nucleic acids and lipids (Dell'Angelica et al., 2000, Yang and Wang, 2021). Lysosomes contain proton-pumps which pump in $H^+$ to create an acidic environment (pH 4.8). The acidic interior environment of the lysosome is important for the action of acidic hydrolases, which function inside lysosomes to degrade target substrates (Yang and Wang, 2021). These organelles are formed via a pinching off from a section of the late Golgi apparatus (Bonam et al., 2019).

Extracellular and plasma membrane proteins can be degraded via lysosomal fusion with vesicular endosomes. Secretory proteins can be degraded in a similar fashion, by a process called crinophagy, whereby proteins in secretory vesicles fuse with the lysosome (Cuervo and Dice, 1998). Intracellularly, proteins are trafficked to the lysosome by three processes: macroautophagy, microautophagy and chaperone-mediated direct transport through the

membrane of the lysosome (Cuervo and Dice, 1998). Macroautophagy is the most common method of degradation in the cytosol and involves the formation of a double membrane bound vesicle termed an autophagophore. The autophagophore can then fuse with the lysosome which can degrade sequestered components into macromolecules to then be recycled within the cell. Macroautophagy is frequently used to breakdown organelles, cytosolic proteins and microbes. As the breakdown of components via the lysosome is a catabolic process, macroautophagy can be used in situations of cellular stress to generate energy that is lost during protein synthesis (Cuervo and Dice, 1998, Bernales et al., 2006, Feng et al., 2014). Macroautophagy is a constant process within cells, however it can be increased in times of cellular stress, including being induced through the process of the Unfolded Protein Response (UPR; (Parzych and Klionsky, 2014). During microautophagy, the lysosomal membrane takes up cytoplasmic elements for degradation via a process of membrane invagination. Whilst microautophagy was initially thought to be used for small regions of the cytosol, further research has revealed it can also be used to degrade peroxisomes, mitochondria, parts of the nucleus and the endoplasmic reticulum as well as cytosolic proteins and enzymes. Microautophagy, is therefore, an umbrella term used for non-specific degradation directly via the lysosome as the process by which these different structures and components are degraded varies depending on the target of degradation. (Cuervo and Dice, 1998, Li et al., 2012, Schuck, 2020).

Finally, chaperone-mediated autophagy (CMA) is the process via which proteins are unfolded through the action of molecular chaperones and then translocated across the lysosomal membrane for degradation (Dice, 2007). This form of autophagy is triggered by prolonged cellular stress, often due to starvation. Protein substrates bound to molecular chaperones are trafficked to the lysosomal membrane upon-which, they bind to the receptor lysosomal-associated membrane protein 2 A (LAMP2A). Proteins are then translocated into the lysosomal lumen, whereby they are degraded hydrolytically (Dice, 2007, Parzych and Klionsky, 2014). Whilst previously CMA had only been described in mammalian cells, it has recently been described in medaka fish (Lescat et al., 2020).

## 1.2 Proteasome structure and function

The UPS is the process by which misfolded proteins are degraded within cells, preventing their accumulation into proteinaceous aggregates and allowing for the recycling of essential amino acids (Adams, 2003). The proteasome is a large protein complex, the function of which is to degrade proteins within the cell through proteolysis. The system is closely linked to ubiquitin (Ub), which is used to tag proteins for trafficking and subsequent degradation by the proteasome (Tanaka, 2009).

### 1.2.1 The ubiquitinating enzymes

Until the 1980s, it was thought that most cellular proteins were highly stable with slow turnover rates. However, work by Hershko *et al,* revealed that turnover is rapid and mediated by ubiquitination via three main ubiquitinating enzymes E1, E2 and E3 (Wilkinson et al., 1980, Ciechanover et al., 1982, Hershko et al., 1984). The three enzymes have been found to tag specific proteins with ubiquitin in an ATP dependent manner, which acts as a signal for degradation by the 26S proteasome. The synchronised interaction of the three ubiquitin enzymes is depicted in Figure 1 and discussed in the following sections.

The first enzyme in this cascade is the E1- activating enzyme. This is the most conserved of the three enzymes, with only eight human isoforms of E1 identified (Groettrup et al., 2008, Barghout and Schimmer, 2021). E1 is the activating enzyme, which binds to ubiquitin to form an activated E1-ubiquitin complex that can then be recognised by the E2-conjugating enzyme. E1 binds initially to both ubiquitin and MgATP, catalysing a C-terminal ubiquitin acyl-adenylation reaction. From here, the catalytic cysteine of the E1 attacks the ubiquitin adenylate, resulting in a E1-S-ubiquitin complex containing a thioester bond between the E1 and the ubiquitin moiety (Schulman and Harper, 2009). The E1 enzyme, then transfers the ubiquitin protein to the surface of the E2-conjugating enzyme via a transthiolation reaction (Stewart et al., 2016, Olsen and Lima, 2013).

Finally, the E3-ligases complete the process of ubiquitinating target proteins. There are two main subfamilies of E3-ligases- RING (Really Interesting New Gene) and HECT (Homologous to the E6-AP Carboxyl Terminus) domain families, that act via two different mechanisms of action. Of these, the subfamilies can be categorised further to include single catalytic domains or multi-subunit enzymes (Fulga and Van Vactor, 2008, Deshaies and

Joazeiro, 2009, Weber et al., 2019). The functional diversity of E3 ligases allow them to interact with specific protein targets, making E3 enzymes the most targeted step in the UPS enzyme cascade (Morreale and Walden, 2016). The action of E3 ligases also control the speed of protein turnover, as different E3 ligases can carry out ubiquitination at different rates. There are some E3 ligases which can slowly produce polyubiquitin chains, even in the absence of a protein target, so that when they encounter a substrate, ubiquitination is fast (Ronchi and Haas, 2012).

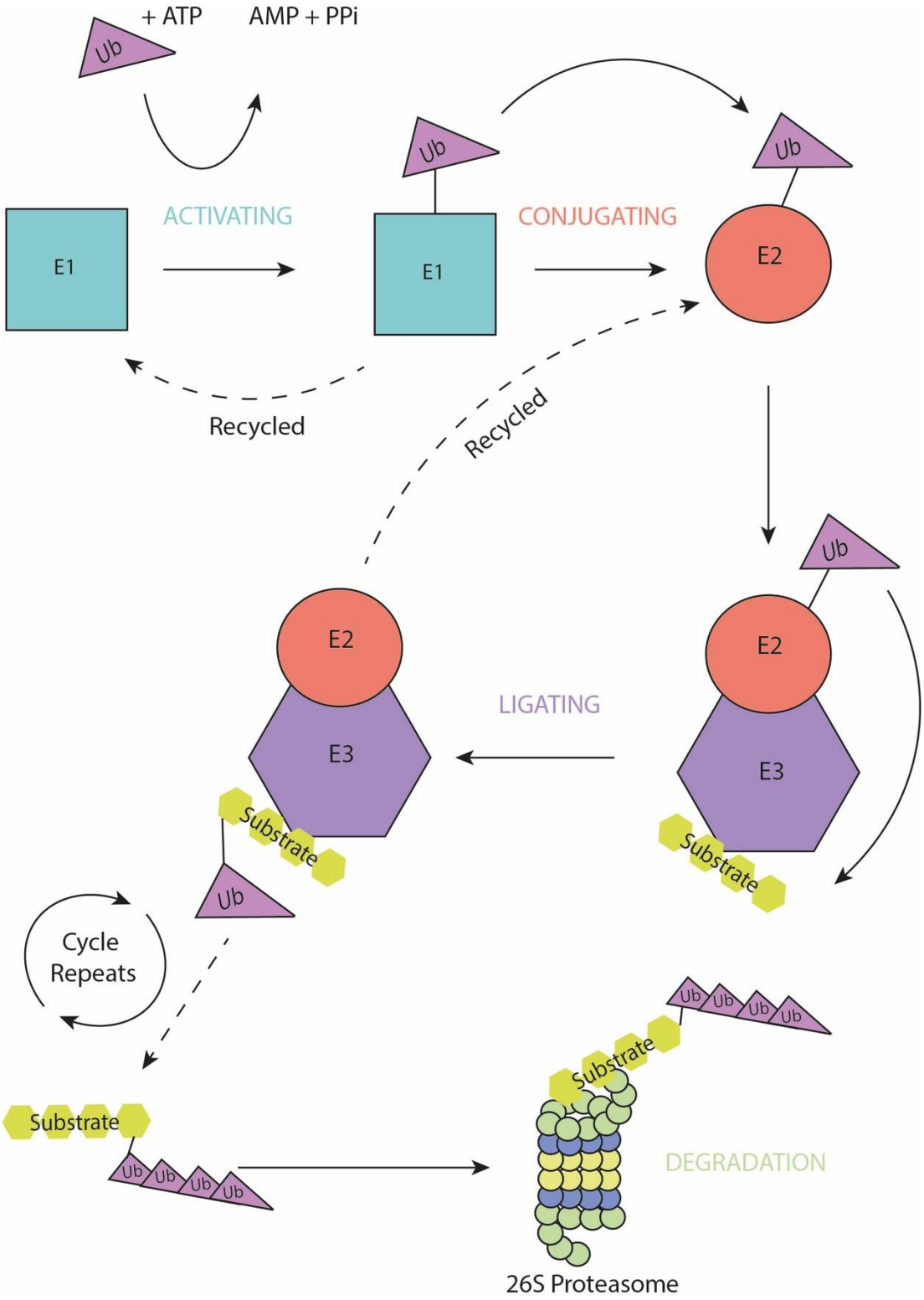


*Figure 1. A schematic of the ubiquitin enzyme cascade*

*Figure 1 displays the action of the E1, E2 and E3 enzymes that are required for correct tagging of a substrate protein with a poly-ubiquitin chain. First the E1 activating enzyme attaches a ubiquitin moiety to its surface in an energy dependent process. ATP is hydrolysed to AMP and inorganic pyrophosphate (PPi), producing the energy required for ubiquitin to attach to the E1 enzyme via a thioester bond. Next, the ubiquitin molecule is transferred from the E1 Activating enzyme to a cysteine residue on the E2 Conjugating enzyme. Finally, the ubiquitin is transferred to the substrate via the action of the E3 Ligating enzyme. This can occur via two main transfer system - a scaffold transfer or with E3 acting as intermediary complex. This process is repeated in order for a poly-ubiquitin chain to be transferred to the substrate. Four ubiquitin molecules attached to a substrate is the standard signal for degradation via the 26S proteasome.*

#### *1.2.1.1 Ring E3-ligases*

RING finger domains and RING finger-like ubiquitin ligases function as a scaffold to transfer the ubiquitin molecule from the E2-conjugating enzyme onto the substrate protein (Metzger et al., 2014a). This means that there is a direct transfer of the ubiquitin from the E2 straight onto the target protein. RING finger domains carry two catalytic zinc residues, which form a structure that acts as a platform in conjugation with a central alpha helix for E2 binding. U-box domains (Deshaies and Joazeiro, 2009, Metzger et al., 2014b). RING finger domain E3s can act as singular subunits or together in multicomplex enzyme structures. SCF complexes (Skp1, Cullin, F-Box) are an example of a multicomplex RING finger domain E3. SCF complexes usually consist of a Skp1 linker protein, followed by a scaffold protein such as Cul1 and finally a RING finger domain. This complex is highly diverse, with many different combinations of the subunits resulting in a high level of substrate recognition specificity (Willems et al., 2004).

#### *1.2.1.2 HECT E3-ligases*

The mechanism of action of HECT E3-ligases works to use the E3 as an intermediary complex, which accepts the ubiquitin from the E2-conjugating enzyme before transferring it onto the final target substrate. Therefore, the catalytic action of a HECT E3 is a two-step process. Firstly, a second transthiolation reaction transfers the ubiquitin from the E2 enzyme onto a catalytic cysteine of the E3, followed by a second step, whereby the ubiquitin is transferred from the E3 onto a lysine residue of the substrate protein. The N terminus of the HECT domain contains the E2 docking site, whereas the C terminus contains the catalytic cysteine. A flexible hinge region between the two termini allows for the HECT domain to easily transition the ubiquitin from the E2 to the E3 enzyme (Weber et al., 2019).

Whilst there are only eight different types of E1-activating enzyme and tens of different types of E2-conjugating enzymes, there are over 600 different variants of E3-ligases that have been identified in humans (Weber et al., 2019). Thus, E3-ligases allow for the huge diversity displayed by the UPS, as in addition to there being such heterogeneity in the E3 families, there is added complexity as different combinations of E2 and E3 enzymes working together can result in the same target substrate being tagged for different eventual fates (Hegde, 2010).

### 1.2.2 The structure of the proteasome

The 20S proteasome is a barrel like structure consisting of four heptameric ring complexes. Each 20S complex comprises two identical β rings which are stacked together, sandwiched between two α rings. The internal β rings each contain three catalytic subunits, which degrade proteins into shorter polypeptide chains. The two flanking α units act as a pore gate, narrowing the opening of the proteasome to 13 Å to ensure tight control over exit and entry (Lecker et al., 2006, Schrader et al., 2009). The structure of the 26S proteasome is shown in Figure 2.

Specialised β-subunits have also been identified, including β1i, β5i and β5t. These are associated with the immunoproteasome (i) and thymoproteasome (t). These specialised subunits can be inserted into the proteasome to produce more complex, specialised structures as well as altering the catalytic activity of the proteasomes with which they are associated (Dahlmann, 2016, Livneh et al., 2016).

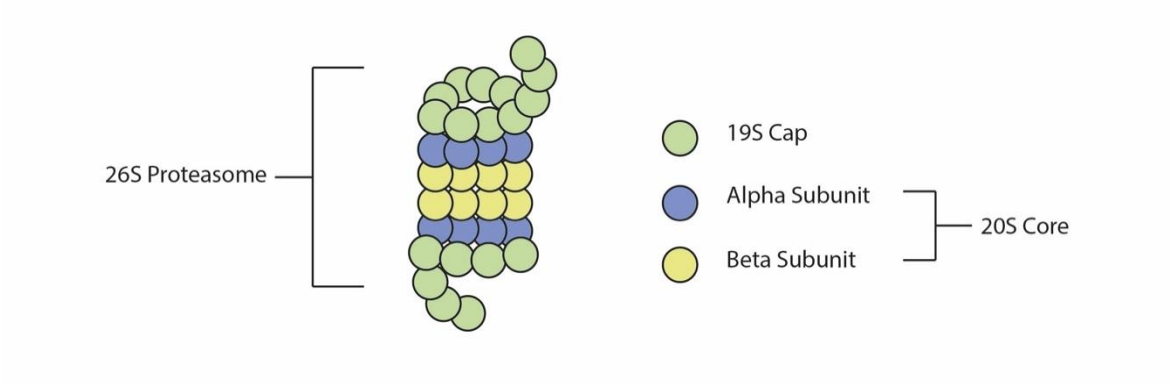


*Figure 2. The 26S Proteasome.*

*The 26S Proteasome Structure. A schematic of the 26S proteasome. The 26S proteasome is constituted 20S core subunits capped at either end by two 19S subunits. The 20S core subunit comprises eight alpha subunits and eight beta subunits, stacked in concentric rings. The beta subunits contain the proteolytic activity required for the breakdown of protein substrates, whilst the alpha subunits act as a substrate binding recognition as well as helping to mechanically unfold proteins.*

The 26S proteasome is a complex comprised of two subcomplexes; the 20S catalytic core and the 19S regulatory particle. The 20S core is a hollow cylindrical structure, which is capped at either end by a 19S subcomplex. The 19S subcomplex contains 18 different subunits that give it both its structure and function (Lecker et al., 2006). Within this structure are two key recognition sites for Ub-tagged proteins. These domains are the S5a (psmd4a and psmd4b in zebrafish) and Adrm1 (adrm1a and adrm1b in zebrafish). Once

bound to a substrate, the 19S proteasome helps to unfold and deubiquitylate proteins before the target passes into the 20S proteasome to be broken down into shorter lengths of polypeptide (Liu and Jacobson, 2013).

The 20S proteasome also requires additional assembly. The 20S core exists as two complexes containing $\alpha 7\beta 7$ subunits and assembled into two rings stacked together, which then dimerise to produce the final 20S core particle containing the four heptameric rings. The incorporation of the PSMD4 ($\beta 7$) subunit into each 'half proteasome' allows for the subsequent assembly of the complete 20S core particle (Ramos et al., 2004).

#### *1.2.2.1 Proteasome heterogeneity*

Whilst the structure of the proteasome is highly conserved across species, studies have shown that the 26S proteasome can be display subunit heterogeneity and differential subcellular distribution cell types to produce heterogeneity in the population of proteasomes present. The first studies to find this heterogeneity were carried out in developing *Drosophila melanogaster* and found that subunits could change throughout development in a cell-type-specific manner, expressing different isoforms of alpha and beta subunits (Haass and Kloetzel, 1989, Yuan et al., 1996, Dahlmann et al., 2000, Klare et al., 2007). Differential expression of proteasome alpha subunits have been shown to be important during neural crest development in the chick embryo (Hutson et al., 1997) and studies in *Drosophila* have shown specific changes in proteasome subunit expression throughout development (Haass and Kloetzel, 1989). Further to this, studies have shown that even within the same cell, depending on subcellular localisation the proteasome can be modified to have different activity rates (Palmer et al., 1996). In particular, post-translational modifications have been shown to be important for regulating enzymatic activity of the proteasome (Mason et al., 1996, Upadhya et al., 2006, Tsimokha et al., 2020).

Heterogeneity of the proteasome has also been shown in tissue-specific expression of subunit isoforms. Studies carried out looking at differences in proteasome populations within heart and liver tissue of mice showed that differing patterns in post-translational modifications resulted in molecular differences in the proteasomes isolated from the different organs. These molecular differences showed corresponding changes in the resulting catalytic activity of the proteasomes present in the different tissue types.

Moreover, these molecular differences resulted in differing responses to the proteasome inhibitors epoxomicin and Z-Pro-Nle-Asp-H (Drews et al., 2007, Gomes et al., 2009).

The discovery of immunoproteasome and thymospecific proteasome subunits (βi and ti) also gave further evidence to the heterogeneity of the 20S proteasome. The 20S core is made up of six concentric rings of β1, β2 and β5 subunits, each containing protease activity. As there are duplicated rings within this structure, this gave rise to the idea that immunoproteasome units could be inserted in place of one of the canonical rings in order to alter the specific function of certain proteasomes. Evidence for this was found in cultured murine pancreatic-β-cells which showed expression of proteasomes containing a mixture of both β and βi subunits following cytokine stimulation (Freudenburg et al., 2013). More recently, studies have revealed the existence of a 20S proteasome complex that specifically binds to neuronal plasma membranes in both mammalian neurons (Ramachandran and Margolis, 2017) and *Xenopus laevis* tadpoles (He et al., 2022). Hence, despite eukaryotic proteasomal complexes being highly conserved throughout evolution, modifications to the structure of the complex results in differing roles for the proteasome within cells (Livneh et al., 2016).

### 1.2.3 The function of the proteasome

The proteasome first recognises ubiquitin tagged substrates through substrate recognition sites on the 19S regulatory particle. The S5a and Adrm1 domains are vital for this recognition process. Whilst the N-terminus of S5a interacts with the 20S catalytic core, the C-terminus contains two Ub interacting motifs (UIM), which bind to Ub-tagged proteins. Adrm1 functions in much the same way; however, it contains only one UIM. The recognition domains bind to Ub-tagged proteins; however, target proteins have two sites of recognition required for proteasomal degradation (Young et al., 1998).

Eukaryotic proteins contain large unstructured stretches of amino acids that act as initiation sites for degradation by the proteasome. Studies have found that whilst the Ub-tag binds to regions of the 19S proteasome, the unstructured regions bind to the 20S proteasome, acting as the initiation site for protein unfolding. As proteasome mediated degradation is ATP dependent, it is thought that the translocation of the protein to the 20S proteasome and the subsequent unfolding happen concurrently (Lee et al., 2001, Prakash et

al., 2004). The current view is that disordered regions of the target polypeptide chain initiate degradation through endopeptidase activity instead of the previously held view that proteins degrade from a free amino or carboxyl terminus through sequential hydrolysis (Liu et al., 2003).

Once substrates have been recognised by the 19S cap, the protein must next be unfolded in order for degradation to occur. The $\alpha$ subunits of the 20S proteasome act as a pore, creating an aperture into the proteasome of 13 Å. This means that proteins are mechanically forced through this pore, thus aiding the unfolding of the protein so that it sequentially enters the main barrel containing the proteolytic $\beta$ subunits. Of the 7 subunits that make up the $\beta$ rings, 6 have proteolytic properties which break down substrate proteins into short polypeptides (Kumar Deshmukh et al., 2019). Polypeptides are then allowed to leave the proteasome via a second RP, often another 19S proteasome complex, and can then be further degraded in the cytosol.

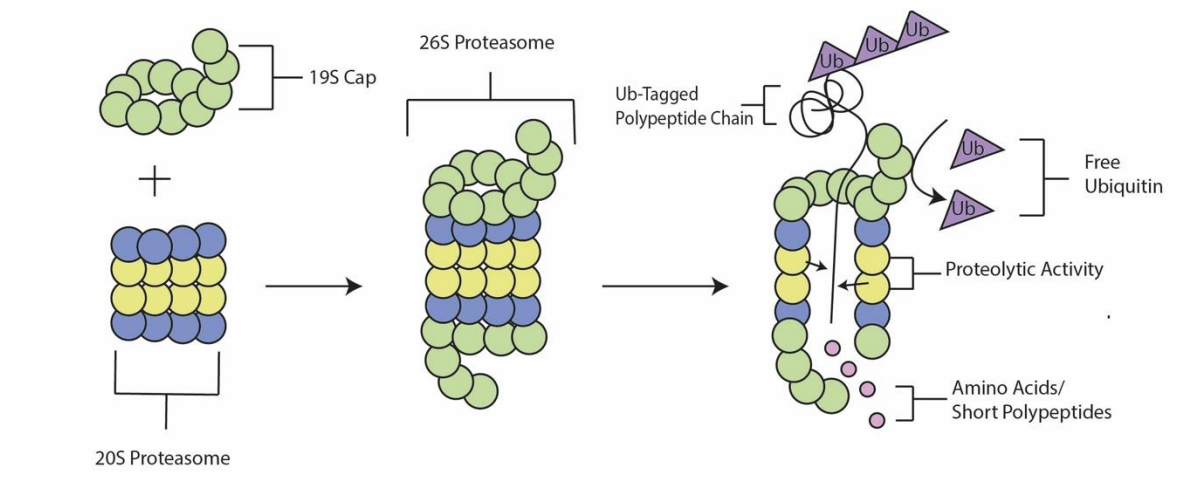


*Figure 3. The Functioning Proteasome*

*The 26S proteasome is combined of the 20S core particle and two 19S cap units that stack on either end of the 20S core. The 19S particle contains substrate recognition and binding regions. Upon binding to a substrate, DUBs contained within the 19S cap remove the ubiquitin chain so that the free ubiquitin can then be recycled. The substrate is sequentially translocated into the 20S core. The alpha subunits create a small opening, so that the protein becomes mechanically unfolded as it moves through the core of the proteasome. Proteolytic activity of the beta subunits breaks down the substrate protein into smaller polypeptides that can then be recycled.*

### 1.2.4 Deubiquitinating enzymes

An additional layer of control is added to the UPS via the action of deubiquitinating enzymes (DUBS, Figure 4). These enzymes function to remove ubiquitin tags from substrate proteins before they can be degraded by the UPS, or in conjunction with the 19S subcomplex (Chen et al., 2017b) so that ubiquitin can be reused in the cell. This is

important, as it adds an element of local control, allowing the cell to change its response rapidly and prevent the unnecessary degradation of cell signalling proteins (Kowalski and Juo, 2012b). These enzymes also allow the cell to reuse existing ubiquitin moieties, which can then re-enter the pool of free ubiquitin within cells. This recycling of ubiquitin ensures that this process is energetically efficient, especially as this is such a common post-translational modification that is not only involved in degradation, but also transport of proteins within the cell (He et al., 2016, Kim and Goldberg, 2017).

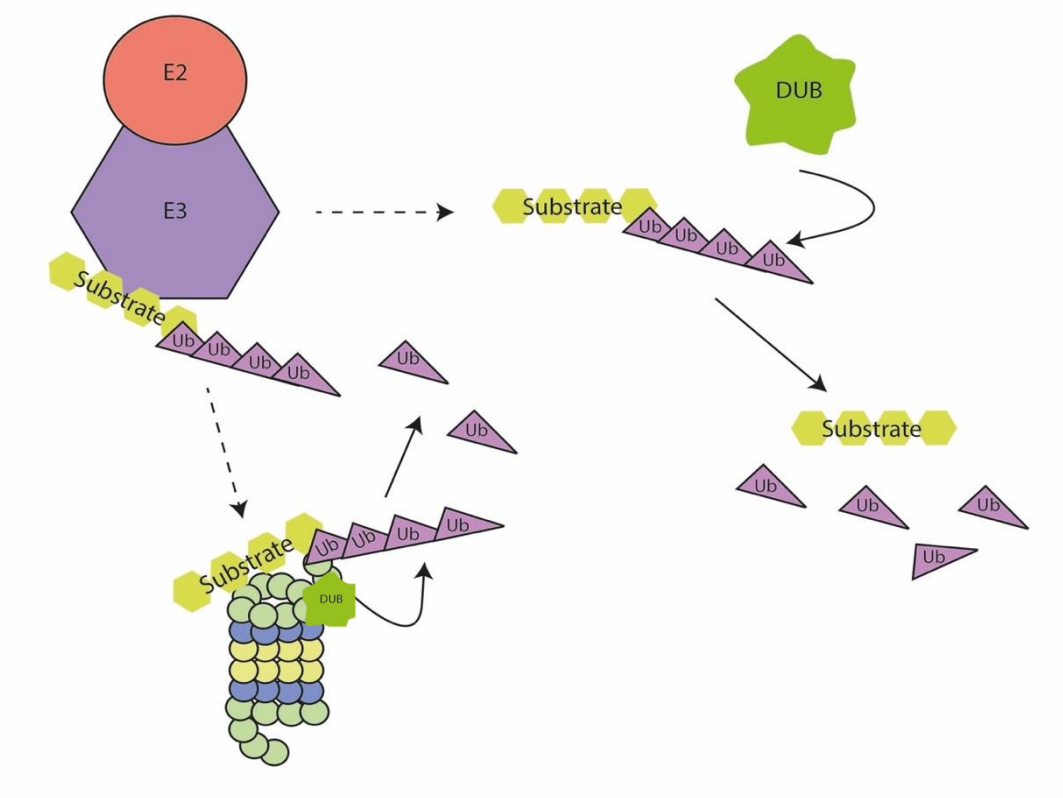


*Figure 4. A schematic showing the role of DUBs in the UPS*

*DUBs function to remove ubiquitin from tagged proteins. DUBs can work alone, but key subunits of the 19S cap also contain deubiquitinating action, allowing Ub to be removed from substrates so that free Ub can be recycled instead of degraded by the core particle. Alternatively, DUBs are also present in the cytosol and are available for dynamic removal of ubiquitin from substrates tagged for degradation if the cellular situation has changed and that protein is still required. DUBs allow for an extra layer of local control over protein degradation.*

Whilst the proteasome functions as the end-point for misfolded proteins, other processes are in place to prevent the accumulation of misfolded proteins within cells. The endoplasmic reticulum (ER) is the major cellular organelle involved in the correct folding of proteins synthesised by ribosomes, as well as aiding the assembly of multi-protein complexes. Proteins undergo post-translational modification and subsequent folding whilst

within the ER, but if proteins cannot appropriately fold, the Unfolded Protein Response (UPR) can be triggered. Activation of the UPR results in a cellular cascade that can either mitigate the accumulation of misfolded proteins or, in the case of terminal UPR, trigger cellular apoptosis to prevent further damage to the cell. Activation is a two-stage process involving the activation of ER stress sensors, which in turn cause activation of specific UPR responsive genes. There are three main signalling pathways involved in the manifestation of the UPR, which are each linked to an individual stress sensor. These sensors are IRE1, ATF6 and PERK (Nogalska et al., 2015). Downstream signalling of the UPR often involves the upregulation of transcription factors involved in mitigating protein misfolding or which are pro-apoptotic (Hetz and Saxena, 2017b).

Following the activation of the UPR, misfolded proteins are removed via retrograde trafficking to the cytosol and then degraded by the 26S proteasome. This system of protein removal and degradation is referred to as ER-associated degradation (ERAD) (Hetz and Papa, 2018). The ER, and its associated processes, is highly vulnerable to stress, as small changes in the environment can cause perturbations to the varied pathways and processes involved. Therefore, it is unsurprising that both the UPR and ERAD have been implicated in the pathogenesis of neurodegenerative diseases (Hetz and Saxena, 2017b).

ER stress can occur for a variety of reasons. As the ER works close to its maximum capacity for protein post-modifications and subsequent folding, small changes in the cellular environment can cause the build-up of misfolded proteins. Common stressors of the ER include perturbation of calcium homeostasis and direct interaction with aggregated proteins associated with neurodegeneration including alpha synuclein (aS) and tau (Hetz and Saxena, 2017a).

### 1.2.6 Pharmacological inhibitors of the proteasome

In this thesis, inhibition of the proteasome was achieved using three pharmacological inhibitors of the proteasome. An introduction to these inhibitors and their mechanisms of action are outlined below. Proteasome inhibitors were first synthesised as tools to better understand the function of the proteasome within cells. Peptide aldehyde inhibitors, such as MG115 (a precursor to MG132) were synthesised first and showed that the proteasome is important for the degradation of both long and short-lived proteins within cells (Rock et al.,

1994). From there, interest in proteasome inhibitors as pharmaceuticals for the treatment of human diseases, especially cancers associated with liquid tumours, increased and licensed drugs such as bortezomib (Velcade), carfilzomib (Kyoprolis) and ixazomib (Ninlaro) were produced (Kisselev, 2021).

#### *1.2.6.1 MG132*

MG132 (carbobenzyl-Leu-Leu-Leu-aldehyde) is a synthetic proteasome inhibitor that is soluble in organic solvents. It is a potent, cell permeable, pan-inhibitor of the proteasome, capable of interacting with all of the catalytic subunits of the 20S proteasome (β1, β5, β7). MG132 is a tripeptide aldehyde inhibitor that shows the strongest inhibition of chymotryptic-like activity of the proteasome (β5) subunits (Crawford et al., 2006). The structure of MG132 is based on pre-existing serine and cysteine proteases (Thibaudeau and Smith, 2019). The peptide aldehyde group of MG132 is the active site of the drug, forming a tetrahedral adduct with the threonine active site within β subunits (Kisselev and Goldberg, 2001) However, this group is also capable of binding to and inhibiting cathepsins and calpains (Goldberg, 1998, Thibaudeau and Smith, 2019, Myung et al., 2001). MG132 is widely used in a research environment, however due to its off-target effects, a more specific inhibitor was synthesised (bortezomib, boronated MG132) as a licensed therapy instead of MG132 (Lee et al., 2010, Adams, 2003).

#### *1.2.6.2 Lactacystin*

Lactacystin is a natural peptide that is a potent, irreversible inhibitor of the proteasome. It shows higher specificity compared to MG132 but also has also been shown to have off-target effects by inhibiting cathepsin A (Kozlowski et al., 2001). Lactacystin is not an active inhibitor of the proteasome but at physiological temperature and pH, it undergoes spontaneous conversion into *clasto*-lactacystin β-lactone (β-lactone), which is a potent inhibitor of the β5 subunits of the 20S core (Ōmura and Crump, 2019). β-lactone is cell permeable, however once it enters cells it can react with glutathione (a substance produced by the amino acids glycine, cysteine and glutamic acid involved in cellular redox reactions (Sies, 1999)) producing lactathione which does not react with the proteasome. Lactathione

is a stable product, which can readily be converted back to β-lactone and as such acts as a stable reservoir for the prolonged release of active proteasome inhibitor (Dick et al., 1997). However, due to these kinetics this makes lactacystin the least stable of the proteasome inhibitors, with a half-life of about 20-hours (Kisselev and Goldberg, 2001). Lactacystin is an expensive proteasome inhibitor, hence it is not used as widely in research as MG132 (Thibaudeau and Smith, 2019).

#### *1.2.6.3 Bortezomib*

Bortezomib (Velcade) is a potent, synthetic inhibitor of the proteasome which is a licenced therapy for the treatment of multiple myeloma and mantle-cell lymphoma (Raedler, 2015). Bortezomib is a peptide boronate inhibitor of the proteasome that is synthesised from the lead compound MG132. Peptide boronates are more potent proteasome inhibitors then peptide aldehydes, but have a similar mechanism of action, forming tetrahedral adducts with the active threonine of β subunits. Peptide boronates are incapable of interacting with other cysteine proteases, due to the size of the boronate active group. As such, they show increased specificity compared to peptide aldehydes. They are also more metabolically stable, less readily oxidised than MG132 or degraded as easily by cytochrome p450 enzymes (Kisselev and Goldberg, 2001, Lee et al., 2010, Thibaudeau and Smith, 2019).

## 1.3 The role of the UPS in synaptic plasticity and neuronal development

The role of the UPS in synaptic plasticity has been widely researched for many years. It has been shown to have effects both on pre-synaptic and post-synaptic neurons, receptor trafficking and long-term potentiation (LTP; Figure 5). Here, the various roles for the UPS in synaptic plasticity are discussed.

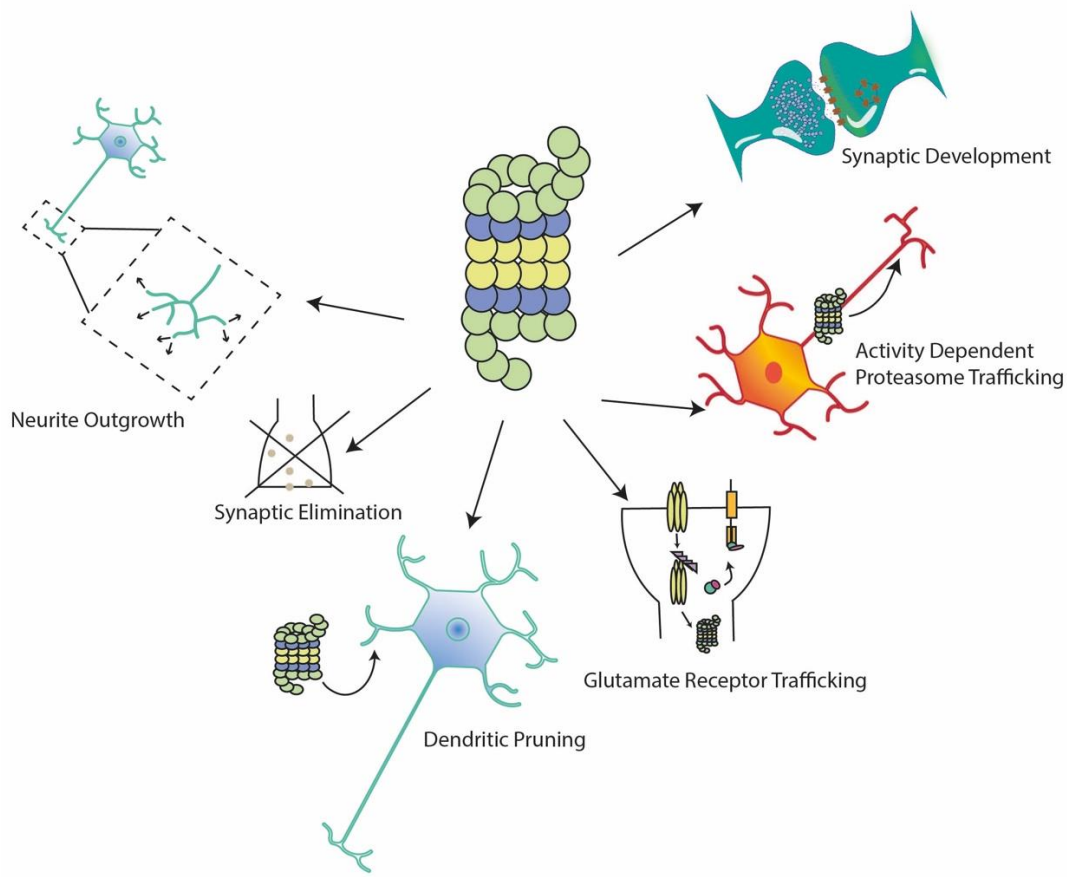


*Figure 5 The Role of the UPS in Synaptic Plasticity.*
*The Ubiquitin Proteasome System (UPS) has been implicated in synaptic plasticity. This includes in the developing system, where synaptic elimination and dendritic pruning are important for the maturation of neuronal networks from a larval to an adult phase. The UPS is also important for neurite outgrowth and synaptic development. However, the proteasome is also required for maintaining the plasticity of neurons in the adult brain. This has been shown via the proteasome's role in receptor trafficking and in activity dependent shuttling of the proteasome to the post-synapse.*

### 1.3.1 Neurite growth and synaptic development

Early experiments into the role of the UPS in synaptic plasticity came from work in *Drosophila*. A balancing act between fat facets (*faf*) and Highwire (*hiw*), first showed that synaptic growth and function is regulated by ubiquitin-dependent degradation mechanisms at the *Drosophila* neuromuscular junction (NMJ). *Faf* encodes for a deubiquitinating enzyme, which when overexpressed, causes an increase in the number of synaptic boutons, a change in the arborisation pattern of neurites and disruption of synaptic function. *Hiw* is an E3-ubiquitin-ligase which contains a RING-H2 domain and has been found to negatively regulate the MAP3K Wallenda (*Drosophila* homolog of DLK-1 , regulates the JNK pathway) thus controlling synaptic growth and neurotransmission (Collins et al., 2006). Loss-of- *hiw* function phenocopies *faf* overexpression, suggesting that increasing deubiquitination or decreasing

ubiquitination, both give rise to similar phenotype of neurite overgrowth and NMJ disorganisation (Wan et al., 2000a, DiAntonio et al., 2001b).

Experiments carried out in *Caenorhabditis elegans* highlighted the role of RPM-1, a guanine nucleotide exchanger with a RING-H2 finger domain, in the organisation of pre-synaptic structures, by acting in a similar fashion to *hiw*. Loss-of-function mutations in RPM-1 lead to a disorganised structure of neurons in the NMJ of the *C.elegans,* with extended axonal growth in mechanosensory neurons and MN (motoneuron) overgrowth of both axons and dendritic branching (Schaefer et al., 2000). RPM-1 is homologous to the *hiw* gene in *Drosophila* and was also found to be localised to the presynaptic terminal, where it functions during synaptogenesis, preventing the over production of presynaptic structures (Schaefer et al., 2000, Zhen et al., 2000a). RPM-1 loss-of-function was further found to prevent the termination of axon outgrowth, leading to an overextension of axon growth in PLM (posterior touch receptor neurons) axons (Li et al., 2008). RPM-1 was thought to act as an E3-ubiquitin ligase due to the presence of the RING-H2 domain, however an interaction between RPM-1, FSN-1 (a novel F-box protein) and a *C.elegans* homologue of SKP1, Cullin, forms an SCF complex at presynaptic periactive zones, that has a role in protein degradation (Liao et al., 2004). RPM-1 regulates a p38 MAP kinase pathway at presynaptic terminals, specifically targeting DLK-1, a MAPKKK, by ubiquitination, marking DLK-1 for degradation (Nakata et al., 2005). The two studies in combination showed that RPM-1 acts as an E3-ubiquitin-ligase forming a complex with other proteins that regulates synaptic structure and morphology through negatively regulating the p38 MAP kinase pathway (Nakata et al., 2005).

The discovery of a post-mitotic role for anaphase promoting complex/cyclosome (APC/C), revealed new functions for E3-ubiquitin-ligases in synapse development. APC is an E3-ubiquitin-ligase, which usually carries out a role in mediating the cell-cycle in mitotic cells. At *Drosopholia* NMJs, a diverse role for APC in both muscular and neuronal cells was found. In neurons, APC was found to regulate synaptic growth and development, acting as a by downregulating Liprin-$\alpha$ (a synaptic scaffold protein) and decreasing synaptic bouton number. Inhibition of Cdh1, a regulatory protein that associates with APC/C, was found to enhance axonal growth in rat neurons (Konishi et al., 2004). In *Drosophila*, the Cdh1 homologue, Rap/Fzr loss-of-function mutations led to reductions in synaptic bouton size and shape, as well as an increase in spontaneous neurotransmitter release and an overall change in *Drosophila* locomotion (Wise et al., 2013a).

### 1.3.2 Synaptic pruning and development

In addition to synaptic growth and morphology, a role for the UPS in synaptic elimination has also been elucidated. A gene in *Drosophila*, *ubcD1*, encodes for an E2-ubiquitin-conjugating enzyme that has been implicated in development (Treier et al., 1992a). Metamorphosis in *Drosophila* leads to synaptic pruning of class IV dendritic aborization (C4da) sensory neurons, mediated by the UPS. Synaptic pruning of these cells involves the larval dendrites breaking away from the soma and being fully degraded, allowing them to mature into adult neurons (Kuo et al., 2005). UbcD1 aids the degradation of C4da dendrites, by regulating local caspase action. First, ubcD1 degrades DIAP1, an E3-ubiquitin-ligase needed to degrade the caspase Dronc. Upon ubcD1-dependent degradation of DIAP1, Dronc can then be activated, giving rise to the elimination of specific dendrites (Kuo et al., 2006a). This level of local and temporal specificity of the UPS is an example of how the system is essential for neuronal development.

### 1.3.3 Glutamate receptor trafficking

Postsynaptic strength can be determined by a number of features including receptor number on the postsynaptic membrane. The discovery that GLR-1 (a class of glutamate receptor) in *C.elegans* are ubiquitinated, first gave rise to the idea synaptic strength may be regulated by the UPS through control of AMPA receptor turnover. Overexpression of ubiquitin decreases the density of GLR-1 receptors at synapses. However, this phenotype could be rescued by mutations in *unc-11*, a gene encoding AP180. AP180 is a clathrin adapter protein which is involved in the endocytosis of post-synaptic elements following ubiquitination. As such, these experience revealed that AP180 is responsible GLR-1 abundance at synapses and that this process is regulated by the UPS (Burbea et al., 2002a). In the mammalian system, glutamatergic receptor trafficking has been shown to be mediated via clathrin-associated endocytosis (Carroll et al., 1999).

Further evidence for UPS-mediated regulation of GLR-1 receptor abundance was derived from studies of LIN-23, a substrate for an SCF (Skp1, Cullin, F-box) complex found in *C.elegans*. Loss-of-function mutations in LIN-23 caused an increase in GLR-1 receptor density.

This would suggest that the UPS is important for the regulation of GLR-1 abundance at the synapse (Dreier et al., 2005).

APC (anaphase promoting complex) in both *C.elegans* and *Drosophila* has been shown to be essential for glutamate receptor trafficking. APC is an E3 ubiquitin ligase complex associated with protein degradation (Peters, 2006). In *C.elegans*, temperature-sensitive mutations in APC led to a rise in the number of GLR-1 subunits expressed in the ventral nerves. Specifically APC was found to have a role in GLR-1 recycling, as mutations in clathrin-dependent endocytosis, prevented the increased abundance of GLR-1 as a result of APC mutations (Juo and Kaplan, 2004). Similarly, in *Drosophila* muscle cells, APC/C (anaphase promoting complex/cyclosome) was found to have similar effects to that in *C.elegans*, regulating neurotransmitter release through controlling GluR-IIa. Mutations in APC led to an increase in GluR-IIa, thus controlling synaptic transmission via the regulation of glutamate receptor subunits (van Roessel et al., 2004).

## 1.4 The UPS and neurodegeneration

The UPS has been well characterised for its role in neurodegeneration and neuronal aging (Figure 6). A shared hallmark of neurodegenerative diseases is the presence of proteinaceous plaques within neurons. Whilst these differ in specific composition and morphology, components such as the presence of ubiquitin and heat shock proteins are found consistently in many types of neurodegenerative plaques (Dale et al., 1991, Spillantini et al., 1997, Armstrong et al., 2008a). The presence of ubiquitin within these inclusions, shows evidence of potential disruption to the UPS during neurodegeneration.

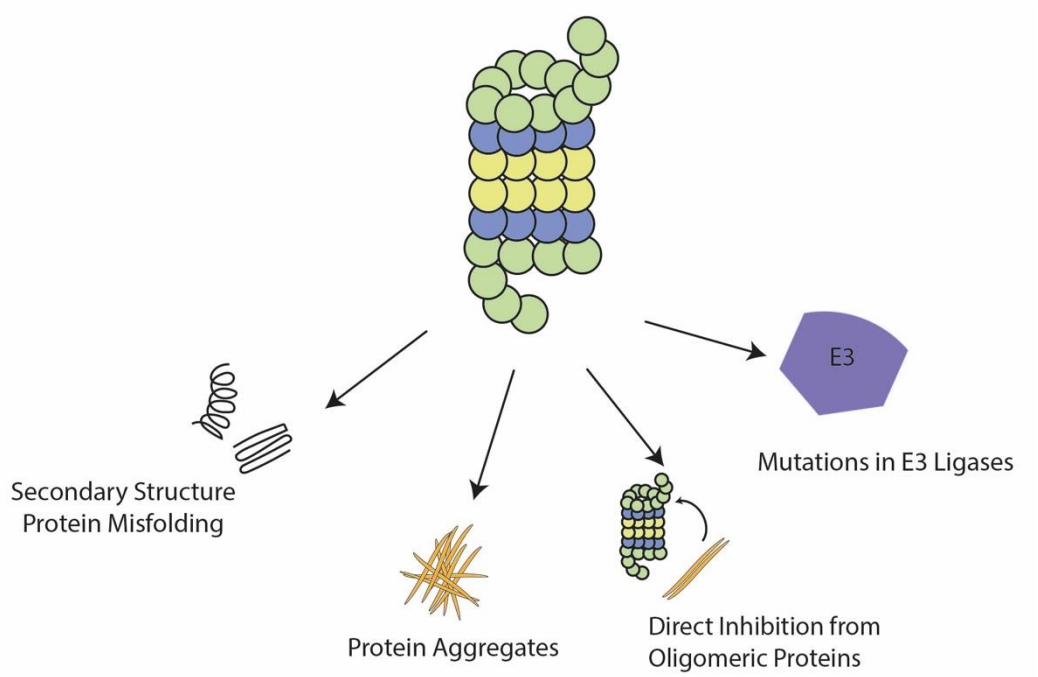


*Figure 6. The UPS and Neurodegeneration.*

*The UPS has been implicated in pathogenesis of neurodegenerative diseases including Parkinson's and Alzheimer's disease. Misfolding of the secondary structure of proteins can lead to a conversion of alpha-helix to beta-sheet formation, increasing the likelihood of proteins aggregating due to the exposure of inappropriate amino acids on the surface of the protein. This can lead to an increase in protein aggregation, a major hallmark of neurodegenerative diseases. There is evidence for the role of certain oligomeric proteins directly inhibiting the proteasome, primarily certain dipeptides produced in C9orf72 ALS patients. Finally, mutations in E3 ligases have been associated with genetic forms of neurodegenerative diseases. An example of this would be Parkin, an E3 ligase which has mutations associated with familial Parkinson's disease.*

### 1.4.1 Abnormal protein structure in neurodegeneration

Abnormal protein structure is often seen as the initial point in the cascade towards protein aggregation. Changes to post-translational modifications can cause inappropriate labelling of proteins, protein misfolding or proteins being trafficked to the incorrect locations within the cell (Stefani, 2008, Del Monte and Agnetti, 2014). Changes to the cellular environment including macromolecular concentration changes or changes to pH can also lead to aberrant protein folding (Stefani, 2008, Shamsi et al., 2017b). As well as these extrinsic factors, mutations in the DNA sequence encoding proteins can lead to direct changes in their folding behaviour. There is mounting evidence that protein conformation changes from alpha-helix structure to beta-sheet formations are highly prevalent in aggregated proteins (Ding et al., 2003). Whilst these changes could be adopted due to changes in the cellular environment, mutations in the DNA sequence can also lead to this beta-sheet formation (Ding et al., 2005, Shivu et al., 2013, Valastyan and Lindquist, 2014). This phenomenon has been

seen in aS (alpha synuclein), a protein implicated in plaques associated with the pathogenesis of Parkinson's disease (PD). The aS protein normally adopts a structure of four coiled-coil alpha helices. However, when it adopts a fibril formation, the alpha helices reassemble into beta-sheets (Davidson et al., 1998, Tuttle et al., 2016)

A hallmark of AD is the presence of amyloid beta (Aβ) plaques. The perturbation of the amyloid cascade, which produces Aβ proteins, leading to an increase in the production of the toxic oligomer $A\beta_{42}$, is referred to as the Amyloid Cascade Hypothesis (Glenner and Wong, 1984, Hardy and Higgins, 1992). In AD, $A\beta_{42}$ has been found to be misfolded, leading to the inappropriate production of dimers or multimers of the peptide, in addition to toxic fibrils (Lee and Ham, 2011). As with aS, amyloid beta has also been found to undergo alpha-helix to beta-sheet transition under certain conditions (Chen et al., 2017a).

The UPS does not have a direct role in the mechanisms of protein misfolding. However, the UPS should efficiently remove misfolded proteins from the cellular environment before they can aggregate. Hence, the presence of protein aggregates could suggest that the proteasome is dysfunctional or impaired.

### 1.4.2 Protein aggregation

Accumulations of misfolded proteins are referred to as protein aggregates. These are a hallmark of many neurodegenerative diseases including Lewy Bodies in PD and dementia, amyloid plaques in AD and Huntingtin (Htt) lesions in Huntington's disease (HD) (Armstrong et al., 2008b, Shamsi et al., 2017a). Both misfolded proteins and protein aggregates have been shown to have a direct inhibitory effect on the 26S proteasome.

αS has been found to inhibit the 26S proteasome in an aggregated state when in the presence of βS (beta-synuclein), but not in its monomeric state. *In vitro*, aggregated αS was found to inhibit the action of 20S proteasomes, with enhanced degradation in the presence of βS (Snyder et al., 2005). Similarly, misfolded and aggregated PrP, a protein associated with Prion disease, can block the opening of the 20S core of the proteasome *in vitro* using purified human. 20S proteasomes and aggregated PrP from mice (Andre and Tabrizi, 2012, Deriziotis et al., 2011). In both cases, there is reduced proteolytic activity from the proteasome. Impairment of the proteasome can also occur through hyper-phosphorylated tau aggregates binding to the recognition site of the 19S core of the proteasome and hence reducing protein degradation and causing a back-up of ubiquitinated proteins (Ren et al., 2007). Mutations in

c9orf72 are the most common cause of ALS and frontotemporal dementia (FTD). This mutant contains a hexanucleotide repeat expansion, which can produce toxic dipeptides of various lengths and amino acid composition. In HEK293T cells, expressing human β4 proteasome subunits, the proline/arginine dipeptide were HA (human influenza hemagglutinin) tagged and incubated with the cells. Using streptavidin beads pulled down proteasome-dipeptide complexes, showing direct binding of dipeptides with the proteasome. Further experiments using polyubiquitinated proteins incubated with human proteasomes and dipeptides, showed the degradation of ubiquitinated substrates was impaired (Gupta et al., 2017).

### 1.4.3 Mutations in E3 Ligases

Whilst most neurodegenerative diseases are sporadic in nature, a small subset can be caused by genetic components. With particular relevance to this thesis, E3 ligase mutations have been associated with both neurodevelopmental disorders and neurodegeneration, indicating that perturbations in the ubiquitination enzymes can cause neurological effects (George et al., 2018).

The best characterised of the neurodegenerative gene mutants is *Parkin* (PARK2), a RING-between-Ring family E3 ligase (Riley et al., 2013). Whilst loss of function of Parkin is most strongly associated with a juvenile recessive form of Parkinsonsim, it has also been implicated in more common sporadic cases of PD as well as AD, ALS and Huntington's disease (HD) (Zhang et al., 2016). Multiple Parkin mutations have been found in PD patients, spanning from single base pair indels to the deletion of large numbers of nucleotides. However, despite the variation in mutations in Parkin, the mechanism of PD molecular pathology remains the same; through the loss-of-function of Parkin (Dawson and Dawson, 2010). This results in decreased catalytic activity leading to aberrant ubiquitination of target proteins and preventing the efficient degradation of substrate proteins.

Parkin is also implicated in sporadic cases of PD, where no genetic causes have been identified. The most likely causes of loss-of-function of *Parkin* in these cases is through oxidative and dopaminergic stress causing DNA damage (Dawson and Dawson, 2014). The substrates of Parkin have yet to be fully elucidated. However, some Parkin substrates that have been identified have links to protein trafficking (Syx5, Vps4) (Martinez et al., 2017) and outer membrane mitochondrial proteins present on depolarised mitochondria (MFN/miro)

(Koyano et al., 2019), implicating the loss-of-function of Parkin with many other cellular processes that are also associated with Parkinsonism pathology.

The role of the UPS in neurodegeneration shows how vulnerable neurons are to perturbations in protein metabolism.

## 1.5 Zebrafish as a model organism

The embryonic zebrafish offers a unique opportunity to pair physiology, imaging and behaviour together within an intact spinal network, making them a suitable model for studying vertebrate nervous systems. The zebrafish genome has been fully sequenced showing many genetic similarities to humans; 71.4% of human genes have zebrafish orthologue (Howe et al., 2013). Zebrafish embryos develop externally and are completely transparent, making them an excellent tool for electrophysiology and *in vivo* imaging experiments. By 4-dpf, larval zebrafish are capable of displaying a variety of locomotive behaviours, making them suitable for behavioural experiments. Larval zebrafish are a good model for pharmacology studies, as they can be bathed in solutions containing drugs and can absorb them through the skin.

The focus of this thesis was motoneurons (MNs) of the larval zebrafish spinal cord. These are a useful vertebrate model cell as they are easily accessible for electrophysiological recordings and have been well characterised previously. Their connections to the musculature offer the ability to link the physiology of the neurons to changes in the growth of neural processes and changes at the neuromuscular junction (NMJ). This can then be further linked to the locomotive behaviour of the zebrafish, as any physiological or morphological changes in the MNs should show a direct change in behaviour.

## 1.6 Zebrafish Development

The different stages of embryonic development have been well characterised in the zebrafish (Kimmel et al., 1995). Embryogenesis happens over defined periods, starting with the zygote period from 0 - ¾ hour post fertilisation (hpf). Development then cycles through the blastula period (2 ¼ - 5 ¼ hpf), gastrula period (5 ¼ - 10 hpf), segmentation period (10 – 24 hpf), pharyngula period (24 – 48 hpf), the hatching period (48 – 72 hpf) before finally entering the early larval period (≤48 hpf). During the larval period (48 – 120 hpf), the larva

develops an inflated swim bladder and there is further anterio-dorsal protrusion of the mouth (Kimmel et al., 1995).

### 1.6.1 The Neuronal Circuitry for Locomotion

In all vertebrates, locomotor movements are generated through orchestrated communication between networks of spinal neurons, brain and brainstem neurons and sensory feedback systems (Arber, 2012). Within the spinal cord, spinal circuits are comprised of primary motoneurons (PMNs), secondary motoneurons (SMNs) and spinal interneurons (INs) which work in conjunction to produce basic locomotive movement. This ability for motor activity outside of sensory input has given rise to the concept of the central pattern generator (CPG) in all vertebrate species (Wilson and Wyman, 1965, Goulding, 2009).

CPGs are found throughout the nervous system of vertebrates and are important neural circuits that control rhythmic behaviours including locomotion and feeding (Katz, 2016). CPGs in the spinal cord can produce basic motor outputs without the need for sensory inputs, although sensory feedback is required for more complex behaviour to meet the needs of the animal (Stein, 2014). In the larval zebrafish, spinal CPGs produce swimming behaviours without the need for supraspinal inputs (Downes and Granato, 2006). Spinal cord CPGs function through a balance of both inhibitory (glycinergic) and excitatory (glutamatergic) synapses, allowing for the regulation of both reflexive and rhythmic behaviours including swimming (Schmid et al., 1991, Schmid et al., 1996, Callister and Graham, 2010). Here, I will discuss the different cell types involved in larval zebrafish locomotion.

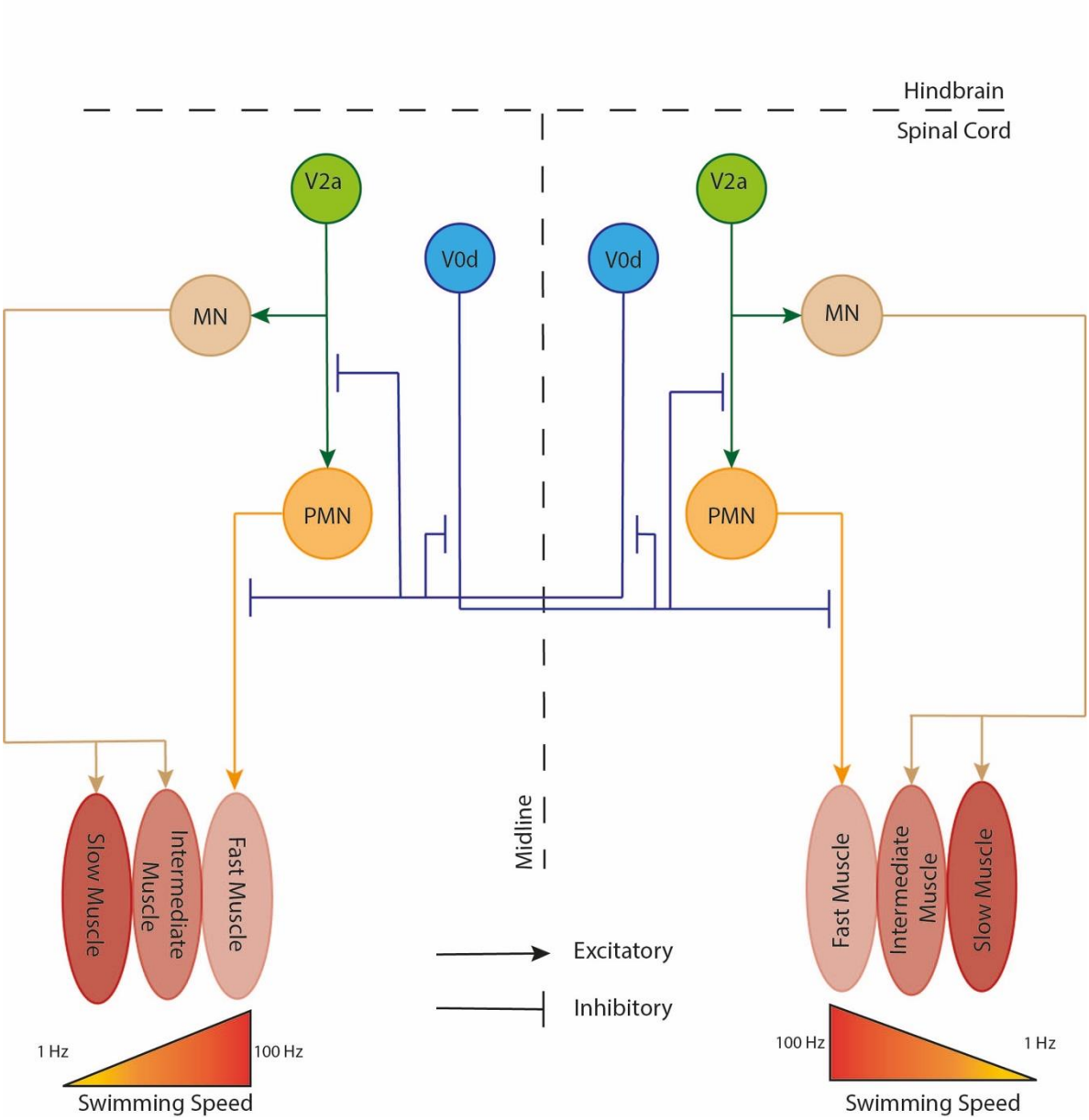


*Figure 7.A schematic of the zebrafish spinal cord CPG.*
*The CPG in zebrafish consists of a network of spinal neurons consisting of MNs, excitatorty V2a INs and inhibitory commissural INs which work in conjunction to produce basic locomotor movement without the need for sensory input. V2a excitatory INs provide the synaptic drive to MNs, sufficient for them to elicit action potentials, which in turn cause muscle contractions. V0d INs provide inhibition to the contralateral or ipsilateral side of the zebrafish trunk to prevent activation of both sets of MNs at the same time, allowing for the undulating body movement which characterises zebrafish swimming. A gradient of muscular fibres from red, intermediate and white allows for control of swimming speed with red muscle fibres activated during slow swimming and white muscle fibres activated during fast swimming.*

### *1.6.1.1 Supraspinal connections and their role in swimming*

Supraspinal input from neurons in the mid and hindbrain are required to provide synaptic drive to the spinal neurons (Kimmel et al., 1982). Reticulospinal neurons located in both the mid and the hindbrain are required for swimming behaviours including prey-capture, and to process sensory input from auditory and visual stimuli (Berg et al., 2018b).

Neurons in the nucleus of the medial longitudinal fasciculus (nMLF) located in the midbrain control swimming speed and steering in larval zebrafish. nMLF neurons project to the MNs (Wang and McLean, 2014) and control the duration of tail movements (Severi et al., 2014) as well as postural control needed for steering during swimming (Thiele et al., 2014). These neurons have also been linked to prey-capture behaviour in larvae aged 7-dpf (Gahtan et al., 2005).

Within the hindbrain, are a set of reticulospinal neurons involved in locomotion which provide direct inputs to the MNs, arranged into seven clusters, organising the neurons into segmental homologues (Metcalfe et al., 1986). Within the hindbrain are included two Mauthner neurons (M-Cell), large crescent shaped cells found bilaterally within the hindbrain with axonal projections down the contralateral side to the soma, making direct contact with spinal neurons along the full length of the spinal cord (Fetcho and Faber, 1988). Whilst M-Cells provide direct contact with the MNs, they also provide inputs to INs within the spinal cord to enhance fast swimming responses as required. The M-cells receive direct sensory input in the form of auditory stimuli from the VIIth cranial nerve, visual stimuli from the optic tectum and stimuli from the lateral line. The M-Cells are responsible for the initiation of C-bend escape responses as a result of external stimuli (Eaton and Hackett, 1984, Eaton et al., 1977). Ablation of the M-Cell, and two of its homologues MiD2cl and MiD3cm, results in no escape responses being elicited (Liu and Fetcho, 1999). Hence, hindbrain reticulospinal neurons are important within the motor network for ensuring that sensory information in form of auditory and visual stimuli, result in an escape response away from the direction of the stimuli (Korn and Faber, 2005).

#### *1.6.1.2 Motoneurons*

The MNs of the spinal cord represent the executive neurons of locomotion, they produce the final output to the musculature that results in the rhythmic body patterning required for swimming (Grillner and El Manira, 2020, Arber, 2012, Berg et al., 2018b). The PMNs facilitate the fastest swimming speed and they are the first to develop in the zebrafish larvae (Bernhardt et al., 1990, Myers et al., 1986b, Myers, 1985). PMNs are easily identified as they have the largest somata (11.3 +/- 1.4 µM in diameter) of the MNs and are positioned most dorsally located MNs in the spinal cord. Of the PMN class, there are three distinct types

of neuron: rostral primary (RoP), middle primary (MiP) and caudal primary (CaP) (Myers et al., 1986b). One of each type of these neurons is present within each hemisegment of the spinal cord, with the RoP in closest proximity to the rostral vertical myosepta and the CaP being closest to the caudal vertical myosepta (Sato-Maeda et al., 2008, Menelaou and McLean, 2012). Each PMN has one distinct axon, which leaves the somata and travels vertically whereupon it turns caudally and travels along the lateral edge of the spinal cord. The axons of all PMNs within the same hemisegment then exit the spinal cord at the same position. CaP axons are the first to exit the spinal cord, followed by the axons of RoPs and MiPs (Myers et al., 1986a).

Each type of PMN innervate muscles in a different pattern: CaPs innervate ventral musculature, whilst the MiPs innervate dorsal musculature. RoPs are the intermediate PMN that innervate the musculature between the CaPs and MiPs. There is some debate over the presence of a fourth primary motor neuron type, the Variable Primary (VaP), which innervates the space between the MiPs and RoPs. However, its role is argued as to whether it is a true distinct class of PMN or whether there are simply two different types of RoP- a ventral RoP (vRoP) and a dorsal RoP (dRoP) (Menelaou and McLean, 2012). Whilst the axons of PMNs are well established by 120-hpf, there is very little dendritic outgrowth into the musculature at this age. Dendritic growth continues throughout development (Bernhardt et al., 1990). PMNs can also be identified by their distinctive firing patterns. Using whole-cell current clamp recordings, PMNs which are stimulated to 2x rheobase (the minimum current required to elicit an action potential) fire tonically, displaying a pattern of continuous firing throughout the duration of the injected current step (Menelaou and McLean, 2012).

The innervation patterns of SMNs are not as clearly defined as those of the PMNs. SMNs are therefore characterised based on their dorsoventral innervation, as opposed to soma location within the spinal cord (Menelaou and McLean, 2012). Another distinguishing feature of SMNs is their branched nature in comparison to PMNs, where branching reaches far deeper muscles, indicating a preference for innervating slower muscle. There are two main groups of SMNs, the first of which encompasses the dorsoventrally projecting cells (dvS), the ventrally restricted cells (vS) and cells which are dorsally restricted (dS). This group of SMNs covers the full range of each muscle hemisegment (Menelaou and McLean, 2012).

The second class of SMNs is distinguished by a single axon which runs the length of the intermyotomal boundary. These SMNs follow a nomenclature based on this

intermyotomal boundary and are therefore called the intermyotomal secondaries (iS). There are two further subtypes of iS- those with collaterals (iS-c) i.e. branching from the main axon, and those without (iS-nc). As with other PMNs and the dorsoventral SMNs, the iS motor neurons cover the full range of musculature within each somite (Menelaou and McLean, 2012). MNs display different firing properties dependent on their dorsoventral location within the spinal cord. Whole-cell current clamp recordings revealed ventral most SMNs exhibit burst firing, whilst those located more dorsally generate a 'chattering' firing pattern. Tonic firing, displayed by PMNs, is defined as a train of action potentials with continuous firing during the depolarising step of the current clamp recording. Burst firing is defined as a single action potential or one short train of a couple of action potentials at the start of the depolarising step, followed by a period of no firing. 'Chattering' firing pattern involves short trains of action potentials followed by periods of inactivity. Multiple 'chattering' episodes can occur across the depolarising step, however unlike tonic firing, 'chattering' firing involves distinct periods of inactivity between action potential trains (Menelaou and McLean, 2012, Saint-Amant and Drapeau, 2000). Bursting cells receive the least amount of synaptic drive, with drive sequentially increasing as MNs display chattering and then tonic firing. This suggests that increases in swimming frequencies, correlate with increases in firing pattern (Menelaou and McLean, 2012).

The order of MN recruitment in larval zebrafish dictates swimming speed, smaller MNs drive slow swimming speeds, with larger MNs sequentially added to the recruited pool as swimming speed increases (McLean et al., 2007, Menelaou and McLean, 2012). Therefore, progressive recruitment of larger MNs results in faster swimming speeds. Whilst this recruitment order also represents the location of MNs within the spinal cord, the branching pattern of MNs also correlates to their order of recruitment. MNs located more dorsally in the spinal cord, and which are involved in slow to intermediate swimming speeds, have the ability to branch into neighbouring hemisegments, whilst larger lateral MNs are restricted to branching only within their own myotomal segment (Ampatzis et al., 2013). In the adult zebrafish, PMNs are almost exclusively recruited for escape responses and have little involvement in normal swimming patterns (Ampatzis et al., 2014).

#### *1.6.1.3 Interneurons*

In addition to PMNs and SMNs, there are also INs present in the spinal cord that assist with the smooth transition between swimming speeds during development and generate the rhythm for co-ordinated MN activation. Excitatory and inhibitory INs work in conjunction, providing inputs to MNs to control the output to the musculature that produces the resultant behaviour. The two main classes of INs in the spinal cord of larval zebrafish are the V2a excitatory INs and the V0 excitatory (V0v) and inhibitory (V0d) INs (Berg et al., 2018b). V2a INs provide the major excitatory drive to MNs to produce rhythmic swimming patterns.

V2a glutamatergic excitatory INs provide the main source of excitatory drive to descending MNs (Eklöf-Ljunggren et al., 2012, Ljunggren et al., 2014). Three V2a INs exist projecting to slow, intermediate and fast MNs in order to control swimming speeds. Slow V2a INs have the lowest threshold and maintain excitation throughout the CPG. As faster swimming speeds are required, excitatory drive is increased through the recruitment of subsequent V2a INs which provide excitatory drive to the appropriate MN. (Ampatzis et al., 2014, Ausborn et al., 2012, Song et al., 2018, Song et al., 2020). Optogenetic activation of V2a INs provides sufficient excitatory drive to elicit a behavioural output, whilst ablation of V2a INs results in abnormal locomotion (Eklöf-Ljunggren et al., 2012, Ljunggren et al., 2014). Studies have shown that MNs can also retrogradely control excitatory input from V2a INs through gap junction coupling in adult zebrafish (Song et al., 2016).

The order of recruitment of INs differs to MNs: as INs are not recruited based on their topographic recruitment pattern. As swimming speed increases, INs driving faster speeds are activated, whilst INs that drive slower speeds are silenced. As such, there is a shift in the pool of INs active at different swimming speeds, as opposed to MNs which are sequentially recruited as speed increases (Ausborn et al., 2012, McLean et al., 2007). Recent studies have shown that there are two distinct classes of V2a INs which separately control the timing and amplitude of locomotor behaviour. Separated through distinctive intrinsic properties, type I V2a INs display tonic firing. Type I V2a INs ensure that rhythmic synaptic drive is provided to MNs to elicit swimming behaviour, whilst type II V2as are associated with controlling the intensity and duration of motor bursts (Menelaou and McLean, 2019).

Inhibitory INs are also important for locomotion providing body patterning rhythmicity, allowing for the undulating movement of the trunk. Whilst the inhibitory commissural INs on the contralateral side are active, inhibition is provided to the MNs on the ipsilateral side (Grillner, 2003, Satou et al., 2020, Cohen and Harris-Warrick, 1984, Alford and Williams, 1989). One way to study excitatory and inhibitory drive to MNs is to use larvae which are bathed in tubocurarine, a acetylcholine receptor antagonist, to prevent muscle contractions allowing researchers to isolate neurons involved in 'fictive swimming' (Buss and Drapeau, 2001). Using this approach, researchers applied strychnine and found that the alternating pattern of burst firing associated with fictive swimming became synchronised. This suggests that it is glycinergic INs which are required for alternating body patterning (Cohen and Harris-Warrick, 1984, Buss and Drapeau, 2001). Inhibitory INs synapse with contralateral V2a INs, MNs and inhibitory INs in order to control alternating body movement (Cohen and Harris-Warrick, 1984, Nishino et al., 2010, Satou et al., 2020, Grillner and Kozlov, 2021). In embryonic and larval zebrafish, glycine is depolarising at resting potentials (Brustein and Drapeau, 2005). Studies suggest that the reversal potential for $Cl^-$ is close to action potential threshold (around -47 mV). As such, glycine appears to provide a source of depolarising drive to MNs whilst also preventing overexcitation by providing a source of membrane shunting when the cell is depolarised beyond threshold (Payne et al., 2003, Reynolds et al., 2008).

A specific inhibitory IN has also been linked exclusively to escape responses, with no input during normal swimming. Comissural Local (CoLo) inhibitory INs receive direct inputs from the M-Cell. Ablation of these neurons impairs C-bend auditory and visual startle responses (Satou et al., 2009).CoLos also ensure that if both M-Cells are stimulated simultaneously, that only the contralateral muscles on the side of the M-Cell that fired first contract and produce a resultant startle response (Satou et al., 2020).

#### *1.6.1.4 Musculature*

Two different types of muscle tissue are present within larval zebrafish, embryonic white (EW) and embryonic red (ER) muscle fibres. Adult zebrafish develop a third class of musculature, intermediate muscle fibres. ER fibres are aerobic whilst EW fibres are anaerobic, allowing for the different speeds and durations of movement elicited by the

recruitment of the different muscle fibres (van Raamsdonk et al., 1982, Buss and Drapeau, 2002).

The muscle fibres are utilised in different speeds of swimming, with EW muscle fibres involved in fast swimming responses and ER fibres involved in slower swimming speeds. Hence, in larval zebrafish up to 4-dpf, the muscle fibres presently mostly consist of layers of EW fibres with a superficial single layer of ER muscle (van Raamsdonk et al., 1982, Buss and Drapeau, 2000). ER and EW muscle fibres are active in fictive swimming episodes, but as swimming speed increases ER fibres are no longer activated, whilst EW muscle fibres remain active. This muscle recruitment strategy remains in place throughout development and into the adult zebrafish (Buss and Drapeau, 2000).

## 1.7 Zebrafish as a model for studying proteasomal regulation of neurons

In this thesis, I have used the larval zebrafish (up to 4-dpf) to study the effect of proteasomal inhibition on the synaptic and intrinsic properties of MNs. Larval zebrafish express 20S proteasomes and previous studies have shown that proteasome inhibitors are capable of inhibiting zebrafish proteasomes (Winder et al., 2011, Daroczi et al., 2009, Rosas et al., 2019, Khan et al., 2012). Spinal cord preparations were utilised in this study, as they offer the opportunity to study how the inhibition of the proteasome affects neurons involved in an intact neuronal network, allowing me to link together changes in physiology, morphology and behaviour.

## 1.8 Aims and objectives

The aim of this thesis was to identify the effects of proteasomal inhibition on neuronal function in larval zebrafish intact spinal preparations. Using this model, I aimed to study how proteasomal inhibition affects the synaptic and intrinsic properties of MNs following chronic (overnight; Chapter 4) and short (1-hour; Chapter 3) incubation with proteasome inhibitors. Thereafter, I aimed to investigate the effects of proteasomal inhibition on synaptic transmission at the NMJ, as well as effects on MN dendritic growth and branching and the formation of NMJs (Chapter 5). Finally, I investigated the effects of proteasomal inhibition on the locomotion of larval zebrafish, with a focus on free-swimming behaviour (Chapter 6).

# Chapter 2 Methods

### 2.1.1 Zebrafish Care

Adult AB Wild Type (WT) zebrafish (*Danio rerio*) were reared according to standard protocols in accordance with guidelines from the Animals and Scientific Procedures Act 1986. Embryos were maintained on a 14:10 light:dark cycle at 28.5 °C, in system water. Zebrafish embryos for this study were used at 4-days post fertilisation (dpf) and were staged according to Kimmel (Kimmel et al., 1995).

### 2.1.2 Pharmacological Agents

Pharmacological inhibitors of the proteasome were used in these studies. MG132 (Hellobio), a synthetic proteasome inhibitor was dissolved in DMSO to produce a 100 mM stock. Lactacystin (Hellobio), a natural proteasome inhibitor was dissolved in $dH_20$ to produce a 10 mM stock. Bortezomib (PS-341, Hello Bio), a synthetic proteasome inhibitor was dissolved in DMSO to produce a 100 mM stock solution. Control solutions contained the same concentration of DMSO as was present in the test condition.

### 2.1.3 Electrophysiological Reagents

At all times unless otherwise stated, zebrafish embryos were perfused using standard Evans solution. Unless otherwise stated, 10 µM d-tubocararine was added to the Evans solution to prevent muscle contractions of the zebrafish during recordings.

| **Reagent** | Concentration (mM) | Supplier |
|---|---|---|
| NaCl | 134 | Fisher Scientific |
| KCl | 2.9 | Fisher Scientific |
| $CaCl_2$ | 2.1 | Fisher Scientific |
| $MgCl_2$ | 1.2 | Fisher Scientific |
| HEPES | 10 | Melford |
| Glucose | 10 | Fisher Scientific |
| d-tubocurarine | 0.01 | Fisher Scientific |

*Table 1. Evans Solution.*

In order to elucidate glutamatergic miniature excitatory post-synaptic potentials (mEPSPs), $Mg^{2+}$ free Evans solution was used to remove the $Mg^{2+}$ block from N-methyl-D-aspartate receptors (NMDAR) and to prevent single channel events from being blocked. Three pharmacological ion channel inhibitors were used in addition to the $Mg^{2+}$ free Evans solution: 1 µM tetrodotoxin (TTX) was used to prevent activation of voltage gated $Na^+$

channels; 100 µM strychinine (STY) was used to inhibit glycine receptors and 50 µM picrotoxin (PTX) was used to inhibit GABA receptors. All three toxins were used simultaneously in order for mEPSCs to be elucidated.

For glycinergic miniature inhibitory post-synaptic potentials (mIPSPs) recordings, Evans solutions containing pharmacological inhibitors were also used. 1 µM TTX and 50 µM PTX were used with 50 µM kynurenic acid to prevent inhibit glutamatergic receptors α-amino-3-hydroxy-5-methyl-4-isoxazoleprpionic (AMPAR)/Kainate receptors and NMDAR.

Unless otherwise stated, a K-gluconate intracellular solution was used to backfill electrodes (Table 2). In the case of glycinergic mIPSP recordings, caesium chloride replaced the k-gluconate in the intracellular solution. Intracellular solutions were kept on ice throughout experiments.

| **Reagent** | **Concentration (mM)** | **Supplier** |
|---|---|---|
| K-Gluconate | 125 | Acros |
| $MgCl_2$ | 5 | Fisher Scientific |
| EGTA | 10 | Melford |
| HEPES | 10 | Melford |
| $Na_2ATP$ | 4 | Sigma |

*Table 2. K-Gluconate Intracellular Solution.*

### 2.1.4 Zebrafish Embryo Preparation

Zebrafish embryos were first anaesthetised in 0.02% tricaine and then spinalised, by removing the head with a sharp pair of forceps. Spinalised fish were then placed in Evans solution until they were needed for experiments. Prior to electrophysiological recordings, the spinalised fish were pinned to a Slygard 184 dish by placing tungsten wire pins through the notochord. The skin was then removed from the preparation using fine forceps, exposing the underlying musculature.

### 2.1.5 Application of Proteasome Inhibitors

Three different methods of application of proteasome inhibitors were used throughout these experiments. In bath application experiments, fish were prepared and cells were whole-cell patch clamped in Evans solution with appropriate toxins (TTX, STY, PTX or KYN). Electrophysiological recordings were then taken from motor neurons for 10 minutes as a control recording. After 10 minutes, Evans solution with appropriate toxin and proteasome inhibitor were then applied to the preparation via the perfusion system. The preparation was

allowed to incubate for 15 minutes, before a further 5 minute recording was taken in the presence of inhibitor.

A one-hour incubation period was also tested, where fish were spinalised and placed directly in Evans solution containing proteasome inhibitor. After the one-hour incubation, fish were prepared for electrophysiological recordings and motor neurons were whole-cell patch clamped. Throughout experiments, fish remained exposed to proteasome inhibitors for up to two hours. Appropriate controls were set up in a similar fashion.

In the third application method, proteasome inhibitors were applied to zebrafish embryos in an overnight incubation. 10 embryonic zebrafish were placed in 20 ml system water with proteasome inhibitor and left overnight in an incubator at 28.5 °C. Upon spinalising the following day, zebrafish spinalised preparations were placed in Evans solution with the appropriate proteasomal inhibitor. Control conditions contained the same concentration of DMSO as test conditions. Throughout experiments, all solutions perfused with the preparations contained proteasomal inhibitor or corresponding control solution.

### 2.1.6 Motor Neuron Electrophysiology Recordings

Zebrafish preparations were perfused with Evans solution containing TTX and other appropriate ion channel inhibitors. Borosilicate glass pipettes (Harvard Apparatus) were pulled using a SU-P97 pipette puller (Sutter) to produce tips with resistance 4 – 5 Ω for electrophysiological recordings. Wide-bore glass pipettes were also pulled using a SU-P97 pipette puller and used to remove the musculature from somites 6-9 of the spinalised zebrafish preparation to expose the underlying musculature. Pipettes used for electrophysiological solution were backfilled with intracellular solution containing sulforhodamine B dye (Sigma) and mounted to a pipette holder with a silver chloride electrode.

Whole-cell patch clamp recordings were taken from MNs within the spinal cord. Recroding pipettes were placed in a pipette holder and lowered into the bath solution using a micromanipulator (PatchStar; Scientifica). Voltage and current clamp recordings were acquired using a Multiclamp 700b amplifier (Molecular Devices), Digidata 1440A (Molecular Devices) and pClamp software (Molecular Devices). Standard corrections for pipette capacitance, fast and slow capacitance and bridge balance (for current clamp recordings) were used. Electrical signals were filtered at 10 kHz with a gain of 10 with a sampling rate of

10,000 Hz. Cells with an access resistance (Ra) above 20 MΩ were not used for recordings. Voltage clamp recordings were taken for 10 minutes. Increases of Ra post-recording above 20 MΩ were discarded from analysis. For current clamp recordings, the recordings were discarded if the Bridge Balance exceeded 20 MΩ.

Whole-cell voltage clamp recordings were taken in the presence of appropriate ion channel inhibitors and proteasome inhibitor or control conditions. Cells were held at -65 mV with Rs compensation set to 70% with a 2.42 kHz filter. A gap free protocol was used to monitor miniature post-syanptic currents. Whole-cell current clamp recordings taken to study firing properties of neurons were also taken. Current clamp protocols involved a 400ms 10 pA depolarising step protocol applied to cells until 2x Rheobase was reached.

For 1-hour and overnight application of proteasome inhibitors, recordings were taken from up to three individual cells per fish preparation. To ensure that cells were not patched multiple times, cells were filled with sulforhodamine B dye and were selected from different myotomal segments.

### 2.1.7 Embryonic White Muscle Cell Electrophysiological Recordings

Pinned zebrafish preparations were perfused with Evans solution containing TTX and the top layer of ER muscle fibres were removed using gentle suction with a wide-bore glass pipette. Borosilicate glass pipettes (Harvard Apparatus) were pulled using a SU-P97 pipette puller (Sutter Instruments) to produce a pipette resistance of 3 – 5 MΩ and backfilled with Cs-gluconate solution containing sulforhodamine B dye. EW muscle cells were whole-cell patch clamped and voltage clamp recordings were taken as outlined in the above method for MN recordings. Only one cell per fish was recorded for EW muscle cell recordings.

### 2.1.8 Statistical Analysis of Electrophysiological Recordings

Analysis of recordings was carried out using Clampfit (Molecular Devices). A power spectrum analysis was carried out on glutamatergic recordings using normal distribution to determine the extent of electrical noise. Recordings were filtered using a Low Pass Gaussian filter set to 1000 Hz and electrical noise filtering was carried out based on the power spectrum analysis. Power spectrum analysis identifies harmonics within the data set, in order to remove extraneous noise from recordings which occurs at 50 Hz (due to electrical noise). A template

search was then used on a 300 s section of the recording to identify mEPSPs and mIPSPs frequency. An average of these identified mEPSPs/mIPSPs was then used to determine the amplitude, half-width and rise time. For current clamp recordings, a threshold search was applied to determine the number of action potentials within the 400 ms step. Firing rate was calculated for cells at 2 x Rheobase.

In order to counter the effect of pseudoreplicates in the case of multiple cells being recorded from the same fish, a linear mixed effect model was used to statistically analyse data, taking fish number into consideration as a random factor. A normality test was first carried out to ensure data was normally distributed. A significance threshold of $p < 0.05$ was used for linear mixed effects model analysis.

Control and test recordings taken from the same cell within individual fish were analysed using a paired t-test ($p < 0.05$) to determine significance. A unpaired t-test ($p < 0.05$) was also used to analyse EW muscle recordings, as only one cell was recorded per fish.

### 2.1.9 Body Length Measurements

Zebrafish larvae were treated overnight with either 50 μM bortezomib, 10 μM MG132, 0.01% DMSO or 0.05% DMSO. The following day, larvae were anaesthetised in 0.02% tricaine and fixed in 4% PFA (paraformaldehyde) containing PBS (phosphate buffered saline) for 2 hours before being placed in a Sylgard dish. Larvae were aligned on their lateral side and tungsten wire pins were placed through the swim bladder and notochord. Larvae were visualised using x20 lens on Nikon SMZ800 (Nikon) dissection microscope. Images were taken using Moticam 1000 (Moticam) camera. Body length measurements were taken from the tip of snout to the tail along the body axis. Measurements were calculated using Fiji (Schindelin et al., 2012).

### 2.1.10 Ub-R- YFP Plasmid Injection

Ub-R-YFP was a gift from Nico Dantuma (Addgene plasmid # 11948 ; http://n2t.net/addgene:11948 ; RRID:Addgene_11948). The plasmid was provided in an agar stab of DH5alpha bacteria, which was streaked onto LB Agar plates containing 50 μg/ml kanamycin. Colonies were allowed to grow overnight at 37°C. One colony was then selected and added to 5ml LB Broth containing 50 μg/ml kanamycin and cultured overnight at 37°C in a shaking incubator at 100 rpm. Isolation of the plasmid DNA was carried out using GeneJet MiniPrep Plasmid DNA kit (ThermoFisher) using 5 ml of overnight culture. All centrifugation

purification steps were carried out at 12,000 rpm. The concentration of DNA was calculated to be 67.2 ng/μl using the Nanodrop (ThermoFisher). The isolated plasmid DNA was sent for sequencing at GATC Eurofins. Primers for the EGFP-N1 vector backbone were purchased from Millipore from sequences provided by Addgene: CGTCGCCGTCCAGCTCGACCAG. Sequence alignment was carried out using BLAST2 sequence alignment tool and verified reference sequences provided by Addgene. Sequence similarity was determined to be 100%.

The Ub-R-YFP plasmid was then cloned using GeneJet MidiPrep Plasmid DNA kit (ThermoFisher) to produce a larger quantity of DNA. LB Agar plates with 50 μg/ml kanamycin were streaked with a glycerol stock of Ub-R-YFP plasmid stored at -80 °C. The culture was left to grow overnight at 37 °C upon which one colony was picked and grown up in 5 ml LB broth inoculated with 50 μg/ml kanamycin at 37 °C in a shaking incubator at 250 rpm for 8 hours. The starter culture was then diluted to 1:10,000 in LB broth and incubated overnight at 37 °C at 250 rpm. The plasmid DNA was then isolated using the GeneJet MidiPrep Plasmid DNA kit (ThermoFisher). The final concentration of plasmid was 300.1 ng/μl measured using the Nanodrop (ThermoFisher). Aliquots of plasmid were frozen at – 20 °C until required.

AB WT zebrafish were set up for breeding with a divider to separate males and females. The divider was then removed in the morning to allow breeding to occur. Fertilised embryos were collected between the 1 to 4 cell stage (Kimmel et al., 1995) and placed in agar plates to be injected. The plasmid was diluted to 75 ng/μl and mixed with 0.2% fast green dye. Sharp electrodes were pulled using borosilicate filtered glass pipettes. Pipettes were filled with dye and plasmid, before being loaded onto a microinjector (μPump). Embryos were injected at the yolk-blastomere boundary, so that plasmid was injected directly into the cytoplasm of the embryos up until the 4-cell stage of development. Embryos were transferred to a petri dish containing system water and kept at 28.5 °C until 3-dpf. At 3-dpf microinjected fish were incubated with MG132, bortezomib or control conditions overnight, before being spinalised and imaged on the Olympus FV1000 Confocal microscope at x10 lens.

### 2.1.11 Immunohistochemistry

All antibody staining was carried out on fish at 4-dpf. All antibodies and concentrations are listed in Table 3. Fish were first fixed in 4% PFA for 2 hours at RT. A permeabilization step using ice cold acetone for 1 hour, followed by RT acetone for 0.5 hour was used for all whole-mount zebrafish spinal cord staining. Fish were then left in block solution (10% milk

powder/BSA, 1% DMSO, 0.1% Triton-X) for one hour and incubated overnight at RT with primary antibody. The following day, fish were incubated in block solution for 1 hour and then incubated overnight in secondary antibody. Fish were then cleared in 60% glycerol before being mounted on microscope slides with Anti-Fade Fluorescence Mounting Media (Abcam) and imaged. Images were taken on the Olympus FV1000 confocal scanning microscope at x40 lens.

To stain for NMJs, alpha-bungarotoxin-ATTO-633 ($\alpha$-bgt) (Alomone Labs) was used at 10 ng/ul and added for 0.5 hours before primary antibody incubation. In this protocol, no acetone permeabilization step was utilised.

| Antibody | Manufacturer | Concentration Used |
|---|---|---|
| **Primary** | | |
| SV2 Goat anti-mouse | Developmental Studies Hybridoma Bank | 1:100 |
| ZNP1 Goat anti-mouse | Developmental Studies Hybridoma Bank | 1:100 |
| **Secondary** | | |
| Alexa-488 conjugated anti-mouse | Invitrogen | 1:2000 |

*Table 3. Immunohistochemistry.*

### 2.1.12 Acridine Orange Staining

Larvae (3-dpf) were incubated overnight in either MG132, Bortezomib or control conditions and 10 ng/ml of acridine orange (AO) stain. The following morning, larvae were spinalised and mounted in Anti-Fade Fluorescence Mounting Media (Abcam) before being imaged at x10 lens on the Olympus FV1000 confocal microscope.

### 2.1.13 Image Aqcuisition

All images were acquired using the Olympus FV1000 laser scanning confocal microscope. Z-stack images were taken in 1 μM sections. High sensitivity detectors were used for all image acquisition. For acquisition of images from larvae stained with Alexa-488 conjugated antibodies, a laser at wavelength 488 nm was used. For larvae stained with YFP fluorescence, a 535 nm wavelength laser was used to acquire images. Images of larvae stained with AO were acquired using a 500 nm wavelength laser. For acquisition of images from larvae treated with α-bgt-ATTO-633, a 633 nm wavelength laser was used.

### 2.1.14 Image Analysis

All images obtained on the Olympus FV1000 confocal microscope were analysed using Fiji (2012). Images were first converted into 8-bit images in greyscale, in order for auto-thresholding to be carried out. A macro was used to subtract background and auto-threshold using the Li algorithm. The Li algorithm is a histogram based, auto-threshold option which binarises 8-bit greyscale images, allowing for the segmentation of background and 'object'

based on a greyscale algorithm threshold (Li and Lee, 1993). The 'Analyze Particles' plug-in was then used for total staining analysis, as this compares the percentage of background to 'object' for binarized images. For whole mount immunohistochemistry staining, regions of interest (ROI) were selected using the polygon tool to exclude myotomal boundary staining from total staining analysis. ROI were drawn around the lateral and ventral myotomal segment from somites 6 and 7 of the larvae in order to exclude the myotomal boundary. This was carried out as the myotomal boundaries exhibit autofluorescence and should be excluded from analysis. Auto-threshold using the Li algorithm as described above was then used to analyse total percentage stain using Fiji. An unpaired t-test was used ($p < 0.05$) to determine significance in total percentage stain.

Further analysis was carried out on ZNP-1 antibody stained larvae using Simple Neurite Tracer (SNT) a plugin designed for use in Fiji (Longair et al., 2011). Images were processed into a Z-stack and SNT was used to trace all present neurites in one myotomal segment from the dorsal side of the zebrafish larvae. SNT statistics for total cable length traced and number of branches were extracted.

For SV2 and $\alpha$-bgt co-staining analysis, Pearson's Correlation Coefficient was calculated using CoLoc2, a plugin through Fiji to determine the degree of colocalization between pre- (SV2) and post- ($\alpha$-bgt) synapses of the NMJ (Bolte and Cordelières, 2006). An unpaired t-test ($p > 0.05$) was then used to determine significance in the degree of co-localisation in larvae treated with proteasome inhibitors compared to control treated larvae.

For images from larvae microinjected with the UB-R-YFP plasmid and for larvae treated with AO, a Fiji macro was used to subtract background and set the image threshold as described above for ZNP1 staining. Total percentage stain for the whole image was then compared between drug and control conditions. An unpaired t-test ($p > 0.05$) was used to determine significance.

### 2.1.15 Free-Swimming Behaviour Analysis

Larval zebrafish 3-dpf were first incubated overnight with either MG132, Bortezomib or control conditions. Free swimming behavioural experiments were carried out in a room heated to 28 °C. Recordings were taken with fish aged 4-dpf staged according to Kimmel *et al* (Kimmel et al., 1995). A single larvae was placed in a 55 mm diameter petri dish with 2 ml system water containing appropriate proteasome inhibitor or control condition and allowed

to acclimatise for 10 minutes. Videos were captured using a DragonFly2 DR2-HIBW camera for 5 minutes using FlyTrap2 software with a frame rate of 15 frames/s.

Videos were converted for analysis using any2ufmf software (Branson et al., 2009) and then fish were tracked using Ctrax software (Branson et al., 2009). Tracking errors were corrected in MatLab (2022) and distance and velocity data extracted from these files. R was used to analyse the output from the CTrax tracking data to calculate the total distance covered (R Development Core Team, 2022). Janelia Automatic Animal Behaviour Annotator (JAABA) was used as a machine learning tool to automatically analyse specific behaviours, including beat-glide-swimming (Kabra et al., 2013). Beat-and-glide swimming periods were identified based on velocity parameters. Thigmotaxis, or 'wall-hugging' behaviour was defined as the time spent within a 5 mm distance of the arena edge.

# Chapter 3 Investigating the effect of overnight incubation with proteasome inhibitors on the synaptic and intrinsic properties of motoneurons

## 3.1 Introduction

The focus of this chapter is on the role of the proteasome on the intrinsic and synaptic properties of neurons. As has been described in Chapter 1, the UPS has been implicated in a variety of processes, including in nervous system development and degeneration. Whilst previous studies have examined the role of the proteasome in neurotransmission, these have been limited in their scope (Rinetti and Schweizer, 2010, Speese et al., 2003). Previous experiments have utilised either invertebrate models or mammalian cell-culture, and hence an understanding of the proteasome in the context of intact neural networks remains lacking. Therefore, in this chapter I aimed to investigate how inhibition of the proteasome affects the spontaneous release of neurotransmitter within spinal neurons of larval zebrafish, as spontaneous events give an indication of the functional state of synaptic connections. I also aimed to assess the effect of pharmacological proteasome inhibition on the intrinsic properties of MNs by investigating the firing properties of these neurons.

Here, I aim to identify previously reported experiments looking into the role of the UPS and its implications for vertebrate neuronal network function. I will start by discussing how neurons within the spinal cord are organised within spinal networks in order to allow locomotive behaviours to occur.

### 3.1.1 Central Pattern Generators and the importance of inhibitory and excitatory synapses

CPGs are present in the spinal cord of all vertebrates and are responsible for the production of rhythmic movements such as locomotion, swimming, feeding and breathing. In the larval zebrafish, CPGs within the spinal cord consist of MNs, inhibitory and excitatory INs and muscle fibres (see Chapter 1). MNs receive inhibitory and excitatory synaptic inputs from INs within the spinal cord and projections from the mid and hindbrain regions. At larval stages, the major neurotransmitter systems involved in locomotion are glycine and glutamate within the spinal cord and acetylcholine (Ach) at the level of the muscle. These synaptic inputs are important for producing the co-ordinated movement required for undulating body movements which characterise swimming behaviour.

### 3.1.2 Spontaneous and Evoked Neurotransmitter Release

There are three main modes in which synapses can release vesicles of neurotransmitter: via activity-induced release either synchronously (happening within milliseconds of an action potential) or asynchronously (happening within tens of milliseconds or seconds after an action potential) or through spontaneous activity-independent release (Fon and Edwards, 2001, Ramirez and Kavalali, 2011, Kaeser and Regehr, 2014). Synaptic veiscles can be segregated into three main pools; the readily releasable pool (RRP), the recycling pool and the reserve pool (Rizzoli and Betz, 2005). The RRP vesicles are ready to be immediately released upon neuronal stimulation, whilst the recycling pool requires moderate stimulation to be released and is constantly replenished with new vesicles. Finally, the reserve pool of vesicles are only released upon intense neuronal stimulation and constitute the largest of the three vesicle pools (Rizzoli and Betz, 2005).

Activity-induced release of neurotransmitter requires an action potential, whereby an electrical signal is propagated down the axon of the pre-synaptic cell. Upon depolarisation of the pre-synapse, $Ca^{2+}$ ion channels are opened, resulting in an influx of calcium into the synapse. This in turn triggers the pool of readily releasable vesicles to dock to the pre-synaptic membrane active zone, resulting in the subsequent release of neurotransmitter from the fused vesicle into the synaptic cleft (Leenders et al., 1999, Katz, 1969, Katz and Miledi, 1967). During spontaneous release, action-potential independent mechanisms result in a single quanta of neurotransmitter being released into the synaptic cleft (Katz and Miledi, 1963, Kavalali et al., 2011, Heuser et al., 1979, Fatt and Katz, 1950, Fatt and Katz, 1952). Here, I will discuss the current views surrounding spontaneous neurotransmitter release and how it differs from evoked transmission.

The classical hypothesis of spontaneous neurotransmitter release holds that it is the product of an imperfect system of vesicle fusion following the propagation of an action potential, hence vesicular release occurs randomly from the same pool of vesicles, docking at the same active zone as vesicles involved in activity-dependent release (Van der Kloot et al., 2000, Diamond and Jahr, 1995, Isaacson and Walmsley, 1995). More recent studies show the importance of $Ca^{2+}$ signalling in spontaneous release, revealing that release is not a

random event, but is correlated with the influx of $Ca^{2+}$ (Williams and Smith, 2018, Williams et al., 2012).

Moreover, in addition to a set mode of release, spontaneous transmission has a distinct role in the function of healthy neurons (Kaeser and Regehr, 2014). There is evidence that spontaneous release is required for maintenance of synaptic homeostasis, including the regulation of dendritic spine growth and synaptic plasticity (McKinney et al., 1999, Tyler and Pozzo-Miller, 2003, Crawford et al., 2017, Ramirez and Kavalali, 2011, Ramirez et al., 2017, Reese and Kavalali, 2015). In CA1 pyramidal cells, spontaneous glutamate release is sufficient to maintain dendritic spines following deafferentation and allows for spinogenesis even in the presence of TTX and inhibitors of protein synthesis (McKinney et al., 1999, Tyler and Pozzo-Miller, 2003).

In rat hippocampal cultures, spontaneous neurotransmission appears to occur from a distinct pool of releasable vesicles segregated from vesicles associated with evoked release (Fredj and Burrone, 2009). Differences in the recycling pool of spontaneous and evoked release have also been suggested in hippocampal cultures using styryl-dyes (Sara et al., 2005), although there is still some disagreement about this as other studies have shown no difference in recycling pools (Groemer and Klingauf, 2007). Using hippocampal cultures taken from mice deficient in the SNARE protein synaptobrevin showed that in these neurons, no segregation of evoked and spontaneous release pools could occur (Sara et al., 2005). This suggests that SNARE proteins are important in the molecular machinery distinguishing evoked and spontaneous release events. Hence, despite some disagreement, more recent evidence suggests that there are differences within vesicle pools contributing to different types of vesicular release.

Spontaneous neurotransmission has also been implicated in synaptic homeostasis and post-synaptic efficacy. Inhibition of postsynaptic glutamate receptors in *Drosophila* resulted in an increase in spontaneous neurotransmitter release at the NMJ. Spontaneous release events induce homeostatic synaptic scaling in the absence of both neuronal activity and protein synthesis, suggesting that spontaneous neurotransmission has an important role in synaptic homeostasis (Frank et al., 2006). Synaptic scaling of AMPA receptors and pre-synaptic glutamate release is also impaired as a result of genetic knock-down of SNARE proteins involved in spontaneous, but not evoked, release events in mouse hippocampal neurons (Crawford et al., 2017).

Spontaneous release events have been associated with synaptic plasticity and mechanisms associated with learning and memory formation, including synaptic potentiation. Synaptic potentiation and facilitation are important processes required for synaptic strengthening and synaptic depression respectively. LTP is the process by which synapses are strengthened and synaptic transmission increased as a result of brief, tetanic high-stimulation activity (Bliss and Lømo, 1973, Malenka et al., 1999). Conversely, LTD occurs with low-frequency stimulation for long periods of time (10-15 minutes) resulting in the depression of neurotransmission for several hours at specific synapses (Ito and Kano, 1982). Both LTP and LTD are dependent on the activation of NMDA receptors, with the main determinant between potentiation and depression being the volume of $Ca^{2+}$ influx following NMDA activation. A large influx in $Ca^{2+}$ results in LTP, whereas a small influx results in LTD (Collingridge et al., 2010). LTP and LTD have been associated as the mechanisms behind learning and memory formation. LTP and LTD can be broken down into different phases, beginning with the induction of LTP/LTD leading to early-LTP/LTD (E-LTP/LTD), followed by a maintenance phase which eventually results in late-LTP/LTD (L-LTP/LTD). Initiation occurs through stimulation of NMDA receptors and subsequent downstream signalling resulting in L-LTP/LTD involving gene transcription and protein synthesis (Huang, 1998). Short-term potentiation and facilitation can also occur, resulting in a transient increase or decrease in neurotransmitter release.

In *Aplysia,* during short-term facilitation (STF), spontaneous neurotransmission acts to increase membrane insertion of AMPA-like receptors, hence triggering the post-synaptic mechanisms involved in LTF (Jin et al., 2012a, Jin et al., 2012b). Furthermore, depleting the vesicles from within the recycling pool of spontaneous neurotransmitter release triggers synaptic potentiation via an increase in AMPA receptors in rat and mouse CA1 hippocampal neurons (Nosyreva et al., 2013).

In sum, spontaneous neurotransmission has been shown to be important for the growth of dendritic spines, synaptic efficacy and homeostasis and the induction and maintenance of synaptic plasticity in both vertebrate and invertebrate model systems. In addition to there being a distinct functional role for spontaneous neurotransmission in neurons, evidence suggests that the mechanisms of release also vary between evoked and spontaneous neurotransmission.

Key proteins involved in the molecular machinery of release events have been proposed as being differentially involved in spontaneous and evoked neurotransmission (Kavalali, 2015). There are differences in the SNARE proteins that are involved in segregating vesicle pools and allowing fusion of vesicles to the active zone. Synaptobrevin has been shown to be important for the segregation of recycling pools of vesicles (Sara et al., 2005). Furthermore, abrogation of all synaptobrevin proteins blocked evoked neurotransmitter release, but not spontaneous release at the NMJ in a murine knock-out model, suggesting that spontaneous release mechanisms occur independently of synaptobrevin (Liu et al., 2019). In *Drosophila,* synaptotagmin mutants altered the rate of spontaneous neurotransmission (Littleton et al., 1994). In murine cortical neurons, $Ca^{2+}$ binding to synaptotagmin-1 was sufficient to induce spontaneous neurotransmitter release, suggesting that synaptotagmin-1 acts as a calcium sensor modulating spontaneous release. As with the study in *Drosophila*, point-mutations in murine synaptotagmin-1 altered the affinity for $Ca^{2+}$ binding and as such, led to defects in spontaneous neurotransmitter release (Xu et al., 2009). Synaptotagmin-12, a $Ca^{2+}$ independent isoform of synaptotagmin, has also been identified as a selective modulator of spontaneous release events (Maximov et al., 2007). Therefore, whilst there is some disagreement about the existence of segregated pools of vesicles between spontaneous and evoked release, the molecular machinery behind these release events appears to be distinct.

### 3.1.3 The Proteasome and Neurotransmission

The proteasome has been implicated in the regulation of both the pre- and the post-synaptic domains in developing and mature neurons. Here, I will discuss the literature evidencing the role of the proteasome in the function of pre and postsynaptic domains.

#### *3.1.3.1 The Proteasome and the Pre-Synapse*

Synaptic proteins are continuously turned over in a matter of hours to days, allowing for the constant rebuilding of synaptic machinery involved in neuronal signalling (Cohen et al., 2013, Price et al., 2010, Speese et al., 2003). In both mammalian post-natal development (Kano and Watanabe, 2019, Faust et al., 2021) and during larval to adult development in invertebrate species (Fulga and Van Vactor, 2008, Kuo et al., 2005), synaptic remodelling has been shown to be highly important for the healthy functioning of neurons.

Previous experiments have implicated the UPS in the healthy functioning of pre-synaptic neurotransmission (Rinetti and Schweizer, 2010, Yao et al., 2007, Speese et al., 2003, Kalla et al., 2006, Willeumier et al., 2006). The dynamic ubiquitination and subsequent degradation of proteins involved in the formation of cytomatrix scaffolding proteins have been implicated in the release of SVs from the pre-synaptic cleft during neurotransmission (Speese et al., 2003, Ivanova et al., 2016, Kalla et al., 2006, Zhao et al., 2003).

Experiments carried out at the *Drosophila* NMJ first identified an increase in neurotransmission following both pharmacological and genetic perturbation of the proteasome . Researchers observed an increase in evoked EPC amplitude, indicating an increase in neurotransmission in both *Drosophila* treated with MG132 and *Drosophila* dominant temperature-sensitive mutants which disrupted the β6 proteasome subunit at varying temperatures. In these genetic and pharmacological models of proteasome inhibition, researchers identified specific increases in DUNC-13, a protein involved in the regulation of synaptic vesicle priming. Previous work had identified Munc-13 (the mammalian homolog of DUNC-13) as a key pre-synaptic protein involved in the regulation of neurotransmitter release (Betz et al., 1998) and had shown that DUNC-13 is a substrate for the UPS (Aravamudan and Broadie, 2003). Hence, the authors concluded that the accumulation in DUNC-13 following perturbation of the proteasome in *Drosophila* strengthened synaptic neurotransmission.

Consequently, more studies were published focusing on the proteasome and its role in the degradation of pre-synaptic proteins. Further pre-synaptic substrates of the proteasome were identified, including Rab3-interacting molecule-1 (RIM1). RIM proteins are found within the active zone of synapses and act as scaffolding molecules important for mediating vesicle priming and release (Wang et al., 1997). Previous work has shown that the $Zn^{2+}$ finger binding domain of RIMs can bind with Munc-13, activating the protein and resulting in regulation of pre-synaptic vesicle release (Deng et al., 2011). RIM1 is a substrate for SCRAPPER, an E3 ligase, and hence levels of RIM1 are regulated by proteasomal degradation (Yao et al., 2007). In *scrapper*-knockout mice, RIM1 displayed an increased half-life and showed increased frequency of glutamatergic mEPSCs. This study concluded that RIM1 is important for neurotransmitter release and that it is regulated by the UPS (Yao et al., 2007). These studies on DUNC-13 and RIM1 gave rise to the hypothesis that

ubiquitination of certain proteins within the pre-synaptic SV release machinery allowed for the regulation of synaptic transmission.

By contrast, later experiments carried out in cultured hippocampal neurons also detected an increase in neurotransmission following pharmacological inhibition of the proteasome, without detecting an increase in Munc13, or RIM1. Increases in both spontaneous and evoked release of excitatory and inhibitory neurotransmitter was detected within 10 minutes of perfusion of cells with proteasome inhibitors MG132 and lactacystin (Rinetti and Schweizer, 2010). Equally, an increase in spontaneous neurotransmission was detected when E3 ligases Fbx20/SCRAPPER were depleted in hippocampal neurons (Yao et al., 2007, Tada et al., 2010), suggesting that the observed increase is specifically due to changes in protein ubiquitination rather than degradation.

Vesicle pools have also been shown to be regulated by the proteasome. Using FM-Dye staining, a styryl-dye which binds to vesicular membranes, researchers visualised changes to vesicle numbers within the recycling pool of cultured hippocampal synapses in response to proteasome inhibition. Prolonged exposure to proteasome inhibitors of over an hour, showed that the recycling pools of SVs increased in size following proteasomal inhibition with β-lactone (the active form of lactacystin, see introduction; (Willeumier et al., 2006). At the *Drosophila* NMJ, perturbation of the proteasome resulted in increased RRP size and increased pre-synaptic $Ca^{2+}$, adding weight to a role for the proteasome in the regulation of vesicular pools. Proteasomal inhibition also abolished homeostatic plasticity. The *Drosophila* NMJ displays pre-synaptic homeostatic plasticity through perturbation of glutamate receptors, leading to an increase in pre-synaptic vesicle release (Petersen et al., 1997, Frank et al., 2006). Proteasomal inhibition using lactacystin abolished the induction of homeostatic plasticity at the NMJ following application of glutamate receptor antagonist, philanthotoxin-433 (PhTX), at the *Drosophila* NMJ (Wentzel et al., 2018). Taken together, these studies show that the proteasome is involved in the regulation of vesicle pools and has a role in modulating homeostatic plasticity.

#### *3.1.3.2 The Proteasome and the Post-Synapse*

Evidence also suggests UPS involvement in post-synaptic neurons and in the induction and maintenance of LTD (Burbea et al., 2002b, Zhao et al., 2003, Limanaqi et al.,

2019, Ehlers, 2003, Dong et al., 2014). This post-synaptic role for the UPS has implications for memory formation (Hegde, 2017), psychiatric disorders such as schizophrenia (Rubio et al., 2013) and methamphetamine addiction (Limanaqi et al., 2019).

Early studies showed that proteins found in the post-synaptic density (PSD) of mammalian neurons had multiple ubiquitinated proteins present, although specific protein targets had not yet been identified (Chapman et al., 1994). Further to this, neuronal activity regulates PSD proteins, and this regulation has been shown to be dependent on proteasome mediated degradation (Ehlers, 2003). One such specific PSD protein complex found to be regulated by the UPS in *C.elegans* studies was the GlR-1 receptor. The GlR1 receptor is a non-NMDA glutamate receptor homolog found in *C.elegans* and is important for long-term memory formation (Rose et al., 2003). Glr1 receptors were shown to be ubiquitinated, with Ub attachments occurring at site lysine sites within the sequence. Mutations at all 4 lysine residues (GlR1-4KR), prevented the formation of Ub-GlR1 conjugates. The mutation resulted in increased *GlR1*-4KR positive puncta, suggesting that the inability to degrade these receptors results in their increased expression at post-synaptic sites. Behavioural studies carried out in the *GLR1*-4KR mutants displayed behavioural defects (an decrease in forward motion) similar to model in which a consitutively activated GlR1 receptor was expressed, hence displaying increased synaptic strength. As such, although the researchers did not measure synaptic strength directly, they inferred that the changes in behaviour were due to synaptic strengthening as a result of increased GlR1 expression (Burbea et al., 2002b). This study suggests that the proteasome is involved in post-synaptic regulation, as the UPS modulates post-synaptic receptors and hence can alter synaptic response to neurotransmission.

In cultured hippocampal neurons, the proteasome has also been shown to regulate glutamate receptors. Application of AMPA (glutamate receptor agonist) induces endocytosis of the AMPA-like receptors GluR1 and GluR2. Pre-treatment for 20 minutes with proteasome inhibitors MG132, lactacystin or $ZL_3VS$ prevented the AMPA induced internalisation of GluR1 and GluR2 (Patrick et al., 2003). Further work has shown that PSD-95, a scaffolding protein shown to bind to AMPA receptors, is a target for proteasomal degradation and could underlie the mechanism of proteasomal regulation of AMPA trafficking (Colledge et al., 2003). When NMDA receptors are activated, PSD-95 is ubiquitinated by the E3 ligase, Mdm2, and the number of AMPA receptors on the post-

synaptic membrane decreases. 1-hour pre-incubation with proteasome inhibitors MG132 and lactacystin followed by application of NMDA prevented the loss of PSD95 and the decrease in AMPA expression (Colledge et al., 2003). The results of these studies suggest that the proteasome is required for trafficking of glutamate receptors and suggests that the proteasome has a conserved role in regulating post-synaptic density across species.

Other receptors have since also been found to be regulated by the proteasome, including G-protein coupled receptors (Alonso and Friedman, 2013) and dopamine receptors (Limanaqi et al., 2019). Taken together, these studies show an important role for the proteasome in the regulation of post-synaptic proteins, in particular glutamate receptors which are required for the induction and maintenance of synaptic plasticity.

Proteasome inhibition has been shown to affect synaptic plasticity in studies both looking at long-term potentiation (LTP) and long-term depression (LTD) (Dong et al., 2014, Schwarz et al., 2010). Murine hippocampal slice pre-incubated for 30-minutes with proteasome inhibitor β-lactone enhanced the induction of L-LTP, but inhibited the maintenance of L-LTP. Proteasome inhibition stabilised protein synthesis within dendrites, hence enhancing the induction of LTP (Dong et al., 2008). As with LTP, E-LTD is also enhanced upon 30-minute pre-incubation with MG132 and lactacystin followed by low-frequency tetanic stimulation for 155 minutes due to similar mechanisms to E-LTP (Li et al., 2015). However, proteasome inhibition prevented the transcription of key proteins involved in the maintenance phase of LTP, including brain derived neurotrophic factor (BDNF). BDNF is a CREB-inducible gene and transcription of BDNF is required for L-LTP to occur (Lu et al., 2008). Inhibition of the proteasome prevents the degradation of ATF4, a protein which represses CREB transcription. Hence the proteasome regulates LTP through the degradation of key proteins throughout the initiation and maintenance phase which allow for subsequent gene transcription to occur in L-LTP (Dong et al., 2008, Dong et al., 2014).

Aside from the Rinetti and Schweizer study, there is a paucity of research into how inhibition of the proteasome affects the physiological properties of neurons. Whilst the Rinetti paper confirmed previous studies showing an increase in neurotransmission as a result of proteasome inhibition (Speese et al., 2003, Zhao et al., 2003), no studies have been performed investigating the role of proteasome inhibition in intact vertebrate neural networks. Hence, more research is needed to determine the effects on the intrinsic and

extrinsic properties of neurons that have been exposed for longer time points to proteasome inhibitors.

### 3.1.4 Regulation of Action Potentials and Firing by the UPS

#### *3.1.4.1 The UPS and Ion Channels*

It has been shown that ion channels can be regulated through ubiquitination, whereby E3 ligases interact with ion channels leading to their internalisation from the plasma membrane into the cytosol of neurons. Nedd4-2, is an E3-ligase containing a HECT binding domain that has been identified as a key regulator of ion channels. Identified substrates of Nedd4-2 include membrane bound proteins, whereby upon ubiquitination they can be internalised and turned-over (Goel et al., 2015). A number of ion channels have been identified as substrates for Nedd4-2, including sodium channels (Rougier et al., 2005, Fotia et al., 2004). In HEK-293 cells, expression of $Na_v1.1$, 1.3 and 1.5 became downregulated by Nedd4-2 (Rougier et al., 2005). A pull-down assay showed that murine neuronal Nedd4-2 binds to $Na_v$ channels via their PY motif whilst Far-Western analysis carried out in *Xenopus* oocytes confirmed that Nedd4-2 interacts with all six $Na_v$ channels via the PY motif (Fotia et al., 2004). Brefeldin a was used to determine if Nedd4-2 accelerated the rate of internalisation of $Na_v$ channels. Brefeldin a (BFA) is a lactone which inhibits protein transport from the ER to the Golgi apparatus and therefore prevents newly synthesised channels from being trafficked to the membrane. In cells transfected with Nedd4-2 and incubated with BFA, the half-life of $Na_v1.5$ decreased, suggesting that Nedd4-2 increased the internalisation of $Na_v1.5$ whilst BFA prevented the trafficking of new channels to the membrane (Rougier et al., 2005).

The aforementioned post-translational regulation has also been shown to control neuronal excitation, as downregulation of Nedd4-2 leads to hyperexcitability in DRG neurons, which has been linked to neuropathic pain disorders (Laedermann et al., 2013). Using the spared nerve injury model of neuropathic pain in mice, it was shown by pull-down assay that Nedd4-2 had decreased expression in DRG neurons, but $Na_v1.7$ and 1.8 showed an increase in density. KO of Nedd4-2 also resulted in an increase in $Na_v1.7$ and 1.8 channels. These results show that *in vivo* ubiquitination of $Na_v$ channels alters neuronal excitability and channel density (Laedermann et al., 2013).

Whilst ubiquitination of $Na_v$ channels can result in their degradation via the proteasome or the lysosome, it can also lead to the recycling of these channels depending on the type of ubiquitination that occurs (Bongiorno et al., 2011). More recent studies have shown that Nedd4 family ligases tend to carry out K63 ubiquitination, which is more often associated with proteasome independent events such as autophagy (Maspero et al., 2013, Kristariyanto et al., 2015). Hence, it could be that whilst sodium channels are ubiquitinated by E3 ligases, they are not subsequently degraded via the 26S proteasome.

Other channels involved in mediating neuronal excitability have also been identified as substrates for the UPS and more specifically, have been shown to be targeted for degradation via the proteasome. The $KCa_2$ family of ion channels are responsible for producing after hyperpolarising potentials (AHP) which regulates neuronal excitability following a train of action potentials (Lin et al., 2008). A study focusing on $KCa_{2.2}$, small-conductance calcium channel, which mediates the AHP following an action potential and therefore, restrict the frequency of firing, observed that $KCa_{2.2}$ is regulated by the proteasome. In rat brain slices treated with gabazine (a GABA antagonist, reduces GABA-mediated inhibition and results in hyperpolarisation of neurons), $KCa_{2.2}$ is downregulated via interaction with an unidentified E3 ligase.. The co-application of proteasome inhibitor MG132 and gabazine for 60-minutes reduces the downregulation of $KCa_{2.2}$ and reduced the gabazine induced epileptiform activity in treated brain slices. This suggests that $KCa_{2.2}$ channels are regulated specifically by the proteasome (Müller et al., 2018). This is noteworthy as previous studies have suggested that ion channels are primarily degraded via the lysosome (Bongiorno et al., 2011).

In addition to the above, potassium channels (Kv) involved in the repolarisation of the membrane following an action potential (Hille, 1992), have also been shown to be regulated via the proteasome. $Kv_{7.2}$ channel subunits, which are associated with the inhibition of burst and repetitive firing of action potentials and are required for the maintenance of the resting membrane potential (Brown and Passmore, 2009, Chow and Leung, 2020), accumulate in the presence of proteasome inhibitor MG132 (Kim et al., 2018). Moreover, perturbation of proteasome degradation of $Kv_{7.2}$ subunits may be relevant to disease as point mutations in $Kv_{7.2}$ (M518V) in patients diagnosed with early onset epileptic encephalopathy, exhibit enhanced degradation of this channel (Devaux et al., 2016).

Whilst evidence suggests that ion channels are regulated by the UPS, as yet no study has been completed looking into the effect of proteasome inhibitors on the firing properties of neurons. Hence, in this chapter I plan to address this gap in the literature.

## 3.2 Aims and Objectives

The aims of this chapter were to observe the effects of chronic proteasomal inhibition on spontaneous neurotransmission using MNs of the developing zebrafish spinal cord. Whilst similar experiments to this have been previously carried out (Rinetti and Schweizer, 2010) in cultured mammalian cells, my aim was to better understand the effect of proteasome inhibition in the context of intact neural network function. As such, by examining synaptic effects of proteasome inhibition, as well as the intrinsic firing properties of MNs in the intact zebrafish spinal cord at 4-dpf, a better understanding of the physiological role of the UPS will be obtained. Intrinsic properties were studied in terms of neuronal excitability, by assessing the effect of proteasome inhibition on firing properties of MNs. Moreover, the effects of proteasome inhibition on synaptic properties were assessed through changes to spontaneous neurotransmitter release.

First, I used the Ub-R-YFP plasmid to test that the proteasome inhibitors MG132 and bortezomib can penetrate the larval zebrafish spinal cord and disrupt 26S proteasome function. I hypothesised that chronic pharmacological inhibition of the proteasome will result in an increase in the frequency of mIPSCs and mEPSCs in these cells, as seen in previous studies using mammalian neurons (Rinetti and Schweizer, 2010, Xie et al., 2017). Therefore, I performed electrophysiological experiments on MNs that have been incubated overnight in proteasome inhibitors, MG132, bortezomib and lactacystin, to assess for changes in spontaneous synaptic transmission and intrinsic firing properties of these cells.

## 3.3 Results

### 3.3.1 Use of UB-R-YFP Plasmid to determine effectiveness of pharmacological proteasome inhibitors

I first used the UB-R-YFP plasmid to determine that proteasome inhibitors were inhibiting the zebrafish proteasome in-situ. The UB-R-YFP plasmid is translated into a fluorescent protein with an N-end rule degradation signal, which is tagged for degradation via the UPS. Inhibition of the proteasome results in the accumulation of fluorescent protein in the larvae (Imamura et al., 2012). Larvae were microinjected with plasmid at the 1-cell stage, before being incubated overnight in either 10 µM MG132, 50 µM bortezomib or appropriate controls and imaged at 4-dpf. Representative images are shown in Figure 8.

YFP fluorescence was only detected in larvae treated with MG132 (n = 4, Figure 8 D-F) or bortezomib (n = 4, Figure 8 J-L). No YFP fluorescence was detected in larvae treated with 0.01% DMSO control (n = 4, Figure 8 A-B) or 0.05% DMSO control (n = 4, Figure 8 G-I). These results indicate that the proteasome inhibitors MG132 and bortezomib are sufficient to inhibit the zebrafish proteasome.

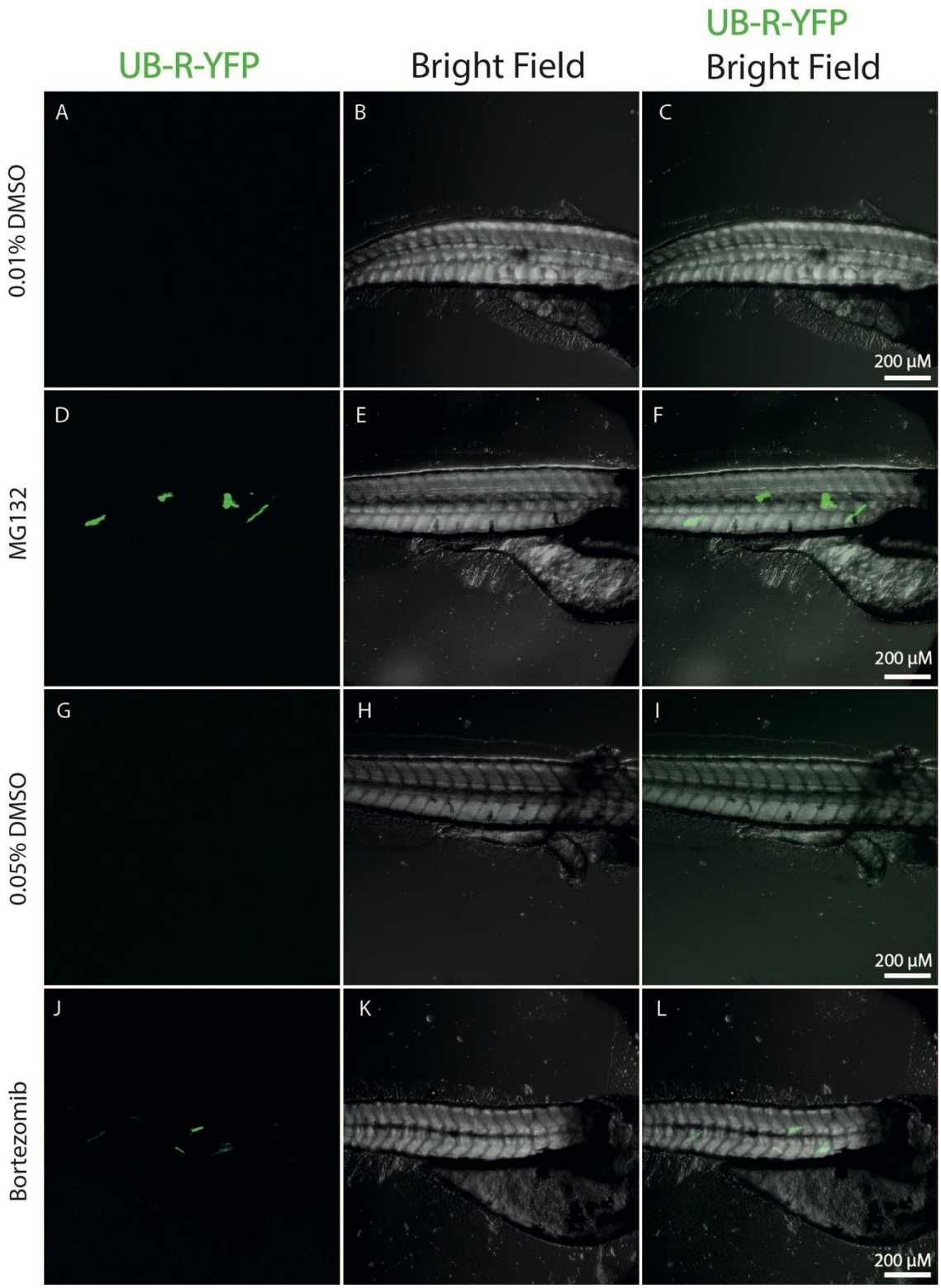


*Figure 8. UB-R-YFP Microinjected Embryos Treated with Proteasome Inhibitors.*

*1-cell stage embryos were microinjected with 75 ng/µl of UB-R-YFP plasmid. Embryos were left for 3 nights and then treated with either control DMSO, 10 µM MG132 or 50 µM bortezomib. Larvae were then spinalised and mounted for imaging on Olympus FV1000 confocal microscope.Larvae were orientated with posterior (left) to anterior (right). A-L) Confocal images of zebrafish larvae injected with UB-R-YFP plasmid and treated with (A-C) 0.01% DMSO, (D-F) 10 µM MG132, (G-I) 0.05% DMSO, (J-L) 50 µM bortezomib. Left panel shows UB-R-YFP fluorescence, middle panel shows a bright field image of the larvae and the right panel shows bright field image overlayed with UB-R-YFP fluorescence. UB-R-YFP fluorescence was only visible in larvae treated with proteasome inhibitors MG132 (n = 4) or bortezomib (n = 4) and no fluorescence was detected in 0.01% DMSO (n = 4) treated larvae or 0.05% DMSO treated larvae (n = 4).*

### 3.3.2 The effects of chronic proteasome inhibition on larval zebrafish development

During experiments, it was noted that larval zebrafish treated overnight with 50 µM bortezomib did not appear to have inflated swim bladders in comparison to age matched DMSO control larvae. To better understand if proteasome inhibitors were having general effects on larval development, I compared the standard length of zebrafish treated with bortezomib (50 µM) and MG132 (10 µM) compared to control larvae. As individual larvae can develop at different rates, measuring development in terms of dpf is not a good indication of developmental age. Standard length is instead often used, as it gives a better indication of developmental progress (Parichy et al., 2009). This image is displayed in Figure 9.

The total body length of the larvae was determined for each treatment condition. In line with previously published work (Kimmel et al., 1995), each fish measured 3.7 mm. Examination of larvae treated with MG132 or bortezomib revealed no statistical difference in length compared to control. Therefore, no differences in total body length are displayed between larval zebrafish treated overnight with proteasome inhibitors compared to control conditions.

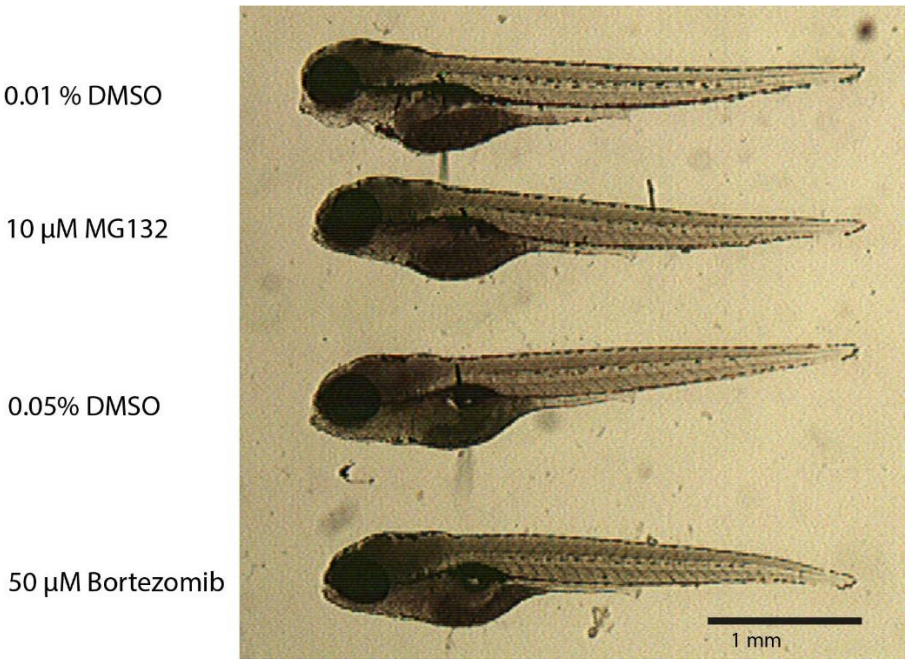


*Figure 9. Larval Zebrafish (4-dpf) treated with proteasome inhibitors show no difference in overall length*

*Larval zebrafish were treated overnight with either 10 µM MG132, 50 µM Bortezomib, 0.01% DMSO or 0.05% DMSO. Larvae were pinned and measurements taken. Overall length of larvae was determined to be 3.7 mm in each condition. No difference in overall length was determined for proteasome treated fish compared to control treated fish.*

### 3.3.3 Effect of chronic proteasome inhibition on parameters of Glycinergic mIPSCs

In order to study changes how the proteasome regulates the intrinsic properties of MNs in larval zebrafish, I first asked how chronic proteasome inhibition influenced synaptic properties by examining mPSCs in zebrafish MNs. I started with determining the effects of proteasomal inhibition on glycinergic mIPSCs.

Fish were first incubated overnight in MG132 dissolved in system water containing 0.01% DMSO (10 µM, N = 24, n = 15) or system water containing 0.01% DMSO control (N = 23, n = 13). Following incubation with MG132, the frequency of glycinergic mIPSCs increased significantly ($p = 0.000526$, MG132: $3.90 \pm 1.64$ Hz, control: $1.93 \pm 1.10$ Hz; Figure 10 A, C and E). However, the amplitude ($p = 0.988$, MG132: $-43.05 \pm 15.09$ pA, controls: $-45.34 \pm 19.19$ pA; Figure 10 A, C and F)., half-width ($p = 0.581$, MG132: $3.34 \pm 1.19$ ms, controls: $2.805 \pm 1.21$ ms; Figure 10 A, C, G) and rise time $p = 0.353$, MG132: $0.56 \pm 0.13$ ms, controls: $0.53 \pm 0.10$ ms; Figure 10 A, C, H) of glycinergic mIPSCs was not significantly different between MNs of control and drug treated fish. These results suggest that chronic (overnight) incubation with the proteasome inhibitor MG132 specifically increases the frequency of glycinergic mIPSCs.

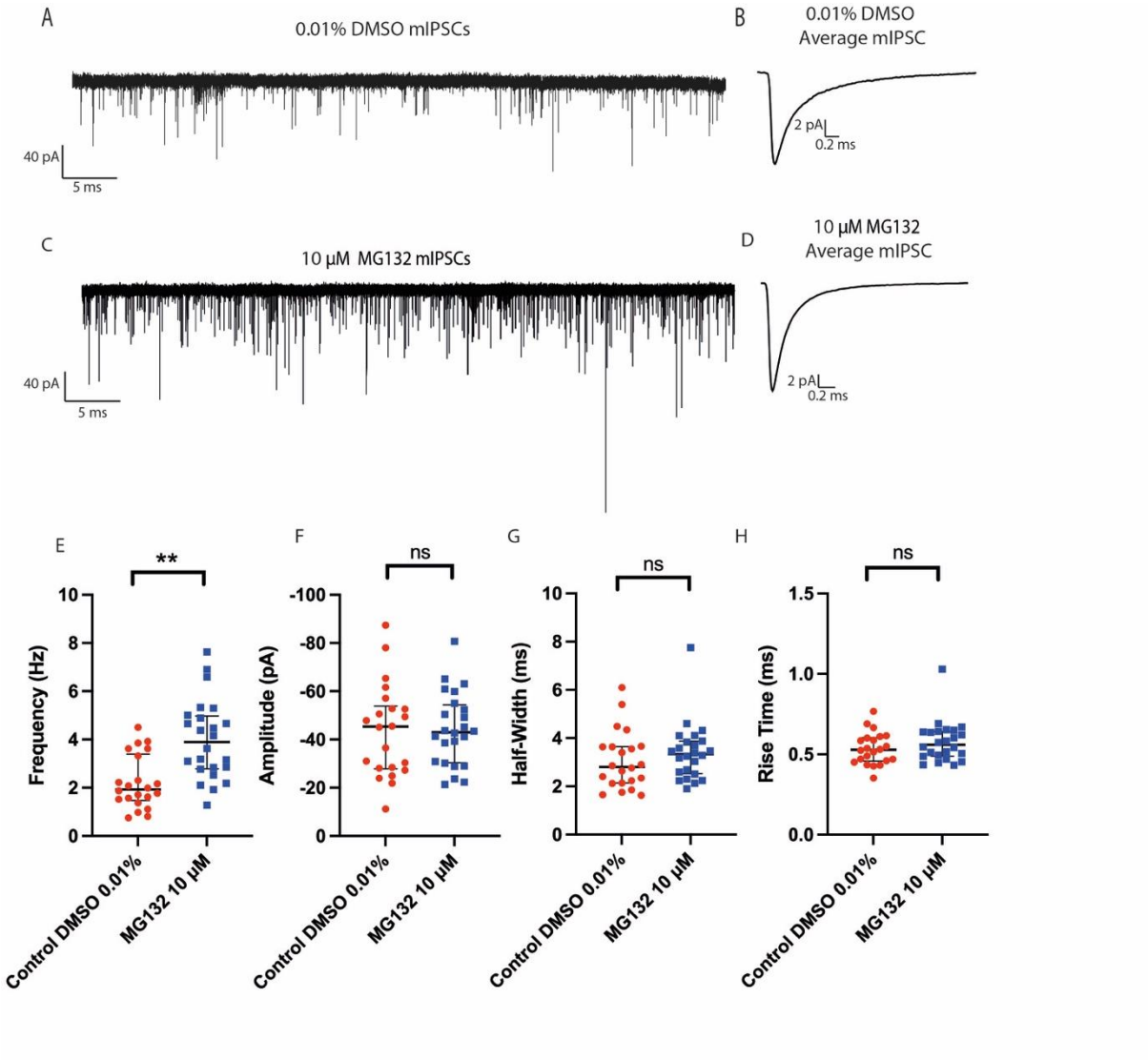


*Figure 10. Chronic incubation with proteasome inhibitor MG132 increased the frequency of glycinergic mIPSCs in larval zebrafish MNs.*

*Glycinergic mIPSCs following overnight incubation with 10 µM MG132 or control 0.01% DMSO. A-B) An example 60 s trace of a MN voltage clamp recording of glycinergic mIPSCs following control treatment and an average mIPSC trace. C-D) Example 60 s trace of MN glycinergic mIPSCs following 10 µM MG132 incubation and an average mIPSC trace. E-H) Median with interquartile range plots for glycinergic mIPSC frequency, amplitude, half-width and rise time for both fish treated in control conditions and with MG132. Treatment with MG132 caused a significant increase in the frequency of mIPSCS, but no change in the amplitude, half-width or rise time of glycinergic mIPSCs.*

To determine whether the observed effects of MG132 were due to specific inhibition of the proteasome, MNs were exposed to lactacystin. Following overnight incubation with lactacystin (10 µM, N = 15, n = 8), there was a significant increase in the frequency ($p = 0.003$, lactacystin: $1.60 \pm 0.66$ Hz, control: $0.90 \pm 0.25$ Hz; Figure 11A, C, E)and half-width ($p = 0.004$, lactacystin: $3.30 \pm 0.90$ ms, control: $2.37 \pm 0.37$ ms; Figure 11A, C, G) of glycinergic mIPSCs compared to control (N = 12, n = 7). However, there was no change in the amplitude ($p = 0.689$, lactacystin: $-20.13 \pm 9.88$ pA, controls: $-19.24 \pm 7.82$ pA; Figure 11A, C, F) or the rise time (0.084, lactacystin: $0.50 \pm 0.12$ ms, controls: $0.33 \pm 0.07$ ms); Figure 11A, C, H) of glycinergic mIPSCs. These data suggest that chronic (overnight) exposure to lactacystin induced an increase in glycinergic mIPSCs consistent with results obtained for MG132 chronic incubation. However, in addition, lactacystin increased the half-width of mIPSC.s.

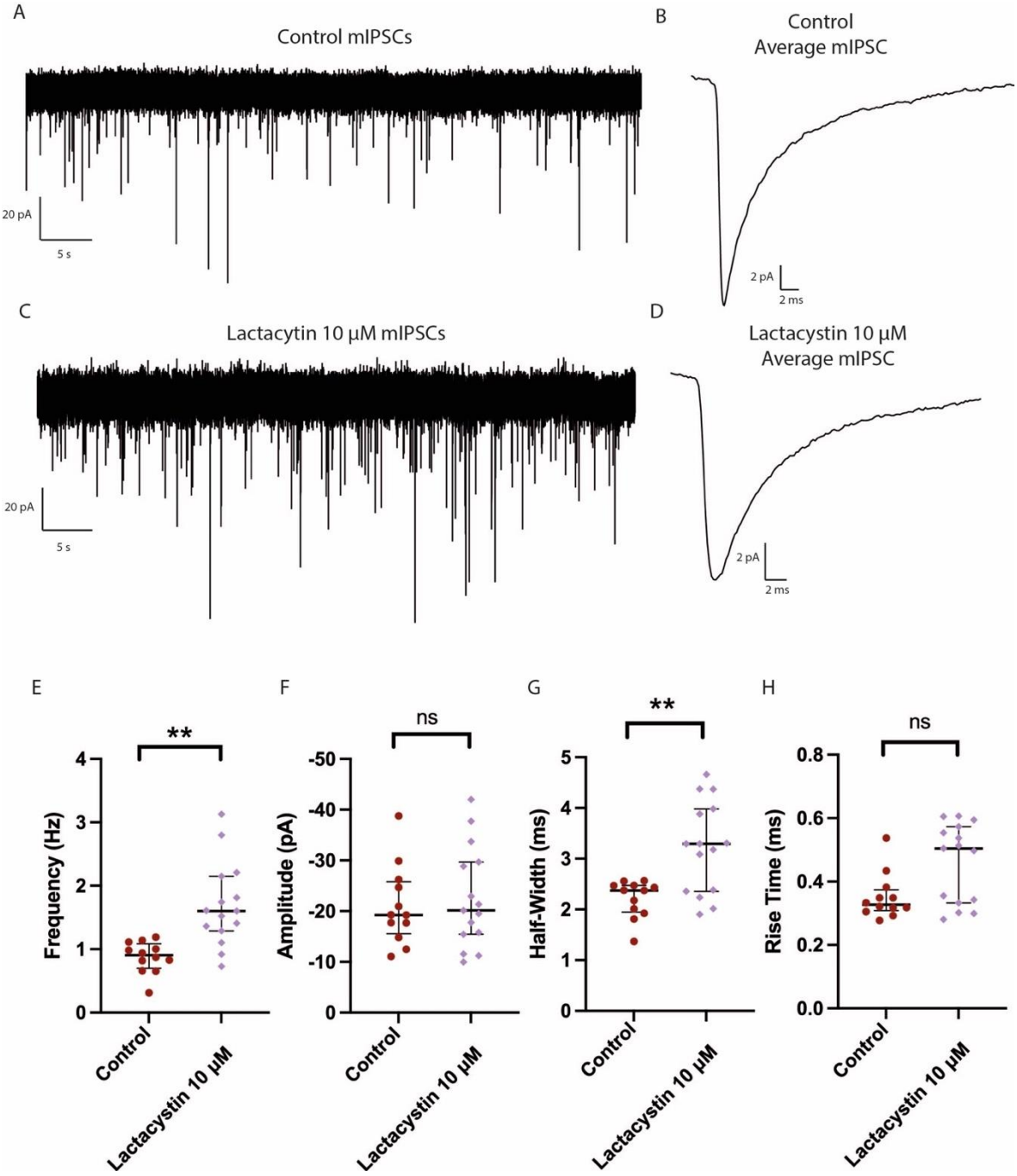


*Figure 11. Chronic incubation with proteasome inhibitor lactacystin increased the frequency and half-width of glycinergic mIPSCs in larval zebrafish MNs*

*A-B) Example 60 s mIPSC trace following overnight control treatment and an average mIPSC. C-D) Example 60 s trace of mIPSCs following overnight treatment with lactacystin and an average mIPSC trace. E-H)Median with interquartile range plots showing mIPSC frequency, amplitude, half-width and rise time for individual MNs treated in control conditions or lactacystin. Lactacystin incubation produced an increase in both the frequency and half-width of glycinergic mIPSCs, but did not change the amplitude or the rise time of mIPSCs.*

As chronic (overnight) lactacystin incubation induced additional changes in half-width of glycinergic mIPSCs compared to MG132 treatment, I next tested the effects of a third proteasome inhibitor: bortezomib. Overnight exposure with 25µM bortezomib resulted in no significant change in the frequency ($p = 0.165$, bortezomib: $1.53 \pm 0.64$ Hz, controls: $1.70 \pm 0.78$ Hz; Figure 12 A, C, E), amplitude ($p = 0.582$, bortezomib: $-20.83 \pm 6.97$ pA, controls: $-24.01 \pm 9.64$ pA; Figure 12A, C, F), half-width ($p = 0.745$, bortezomib: $0.76 \pm 0.31$ ms, controls: $0.86 \pm 0.32$ ms; Figure 12 A, C, G) or rise time ($p = 0.897$, bortezomib: $0.29 \pm 0.06$ ms, controls: $0.31 \pm 0.06$ ms; Figure 12 A, C, H) of glycinergic mIPSCs treated bortezomib (25 µM, N = 8, n = 10) or control (N = 7, n =10) as shown in Figure 12.

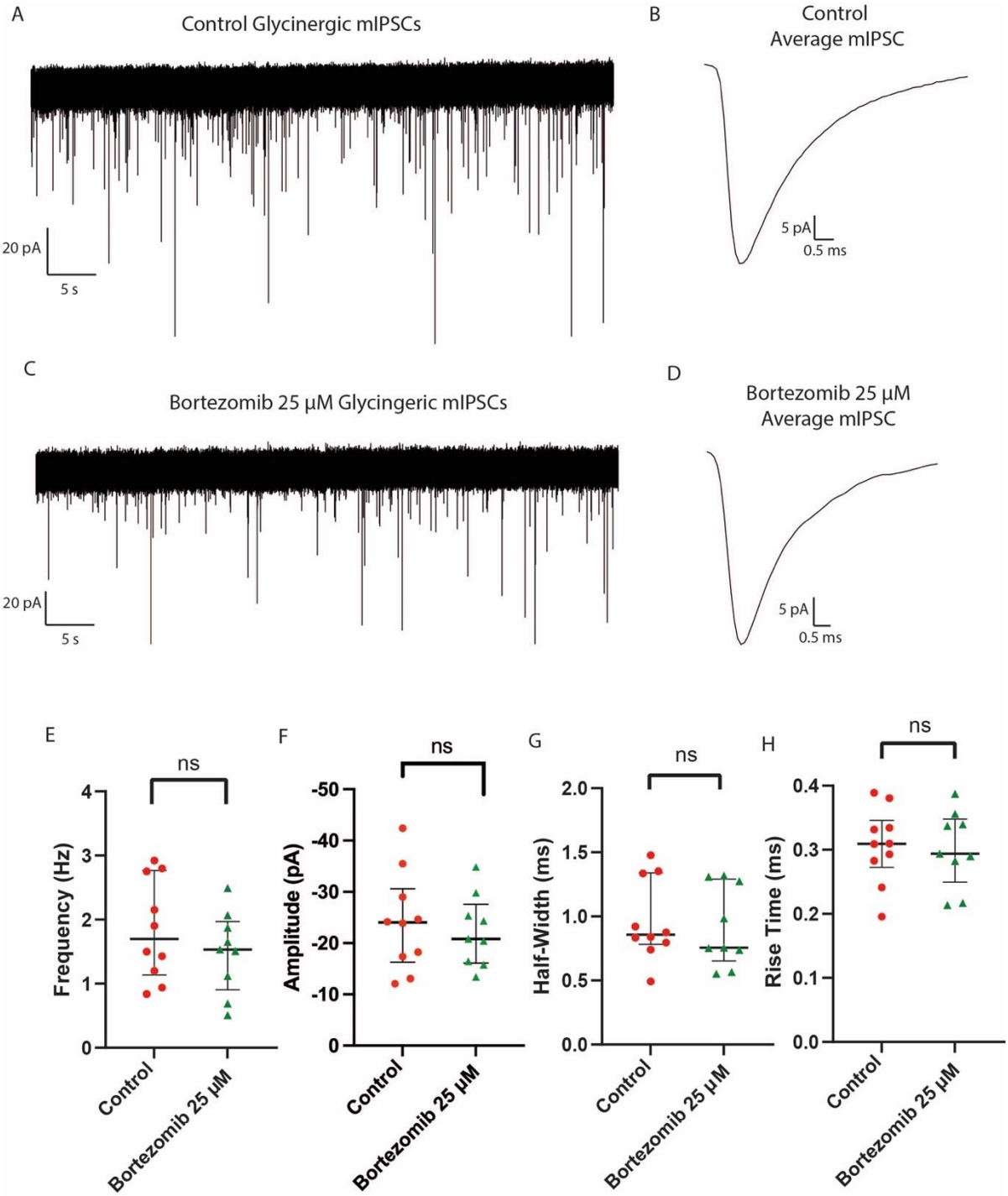


*Figure 12. Chronic incubation with proteasome inhibitor bortezomib (25 µM) did not significantly affect glycinergic mIPSCs in larval zebrafish MNs.*

*Glycinergic mIPSC voltage clamp recordings following overnight treatment with 25 µM bortezomib or 0.025% DMSO control. A-B) An example 60 s control recording taken from a larval zebrafish MN following overnight treatment with 0.025% DMSO control and an average mIPSC from the trace presented in A. C-D) Example 60 s recording of glycinergic mIPSCs from a zebrafish MN treated overnight with 25 µM bortezomib and an average mIPSC from the trace displayed in C. E-H) Median with interquartile range plots showing frequency, amplitude, half-width and rise time of mIPSCs treated in control or bortezomib 25 µM overnight. There was no change in frequency (p = 0.165), amplitude (p = 0.677), half-width (p = 0.745) or rise time (p = 0.897) detected between control and drug treated fish*

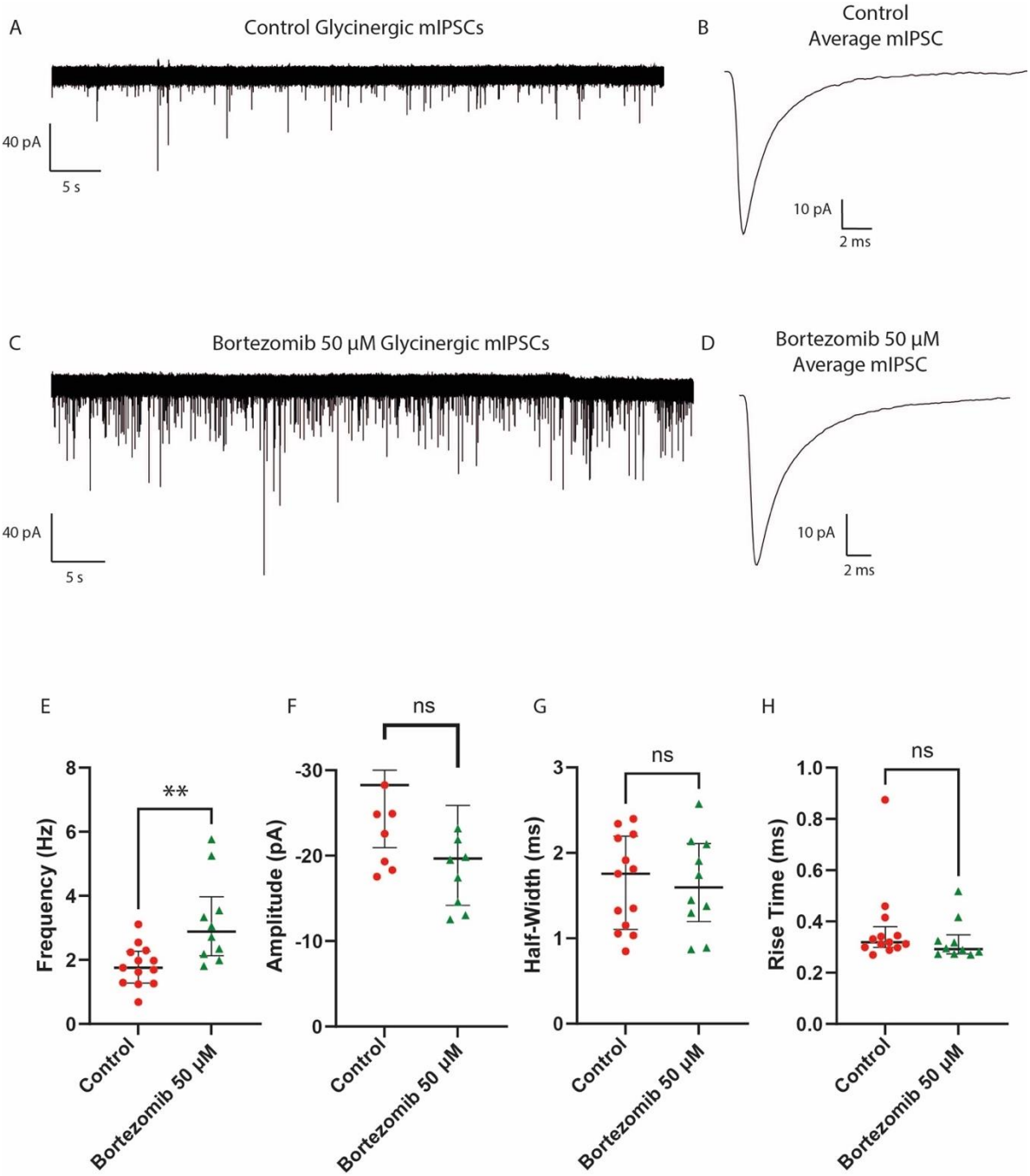


*Figure 13. Chronic incubation with proteasome inhibitor bortezomib (50 µM) significantly increased the frequency of glycinergic mIPSCs from larval zebrafish MNs.*

*Glycinergic mIPSCs voltage clamp recordings from larval zebrafish MNs following overnight treatment with 50 µM bortezomib or control. A-B) An example 60 s glycinergic mIPSC recording taken following overnight control conditions and an average mIPSC taken from recording shown in A. C-D) Example 60 s glycinergic mIPSC recording taken following overnight treatment with 50 µM bortezomib and an average mIPSC taken from the recording in C. E-H) Median with interquartile range plots showing the frequency, amplitude, half-width and rise time of glycinergic mIPSCs following overnight treatment in either 50 µM bortezomib or 0.05% DMSO control. A significant increase in the frequency ($p = 0.00499$) was detected following 50 µM bortezomib treatment, however no change in the amplitude ($p = 0.0862$), half-width ($p = 0.952$) or rise time ($p = 0.259$) was determined.*

By contrast, treatment with 50 µM bortezomib (N = 9, n = 5) had marked effects on mIPSC frequency when compared to control (N = 12, n = 8). Here, glycinergic mIPSCs showed a significant increase in frequency (p = 0.005, bortezomib: 2.88 ± 1.35 Hz, controls: 1.76 ± 0.64 Hz) Figure 13A, C, E) consistent with results obtained for MG132 and lactacystin chronic treatment. No statistical difference was observed in the amplitude (p = 0.0862, bortezomib: -19.67 ± 9.24 pA, controls: -28.25 ± 10.23 pA; Figure 13A, C, F), half-width (p = 0.952, bortezomib: 1.60 ± 0.56 ms, controls: 1.76 ± 0.54 ms; Figure 13A, C, G) and rise time (p = 0.259, bortezomib: 0.29 ± 0.08 ms, controls: 0.319 ± 0.16 ms; Figure 13A, C, H) of glycinergic mIPSCs in fish treated with 50 µM bortezomib compared to controls.

The data displayed here shows a consistent increase in the frequency of glycinergic mIPSCs across all 3 pharmacological inhibitors of the proteasome used. However, lactacystin treatment showed a significant increase in half-width compared to larvae treated in control solution, an effect that was not seen with either MG132 or bortizomib.

### 3.3.4 Effect of chronic proteasome inhibition on parameters of Glutamatergic mEPSCs

In order to determine the effects of chronic proteasomal inhibition on the spontaneous release of glutamate, larval zebrafish (3-dpf) were incubated overnight in three different pharmacological inhibitors of the proteasome; MG132, lactacystin and bortezomib. Whole-cell voltage clamp recordings were taken from primary motoneurons of larval zebrafish (4-dpf) to identify glutamatergic mEPSCs. Proteasome inhibitors were dissolved in the recording solution throughout experiments.

Larvae were first incubated overnight in MG132 dissolved in DMSO (10 µM, N = 7, n = 15) or system water containing 0.01% DMSO as a control (N = 11, n = 15). Recordings taken from MNs from fish treated with MG132 showed no significant difference in average frequency p = 0.13, MG132: 3.80 ± 1.84 Hz, controls: 3.62 ± 1.14 Hz; Figure 14A, C, E), amplitude (p = 0.121, MG132: -13.17 ± 3.20 pA, controls: -15.83 ± 3.92 pA; Figure 14A, C, F), half-width (p = 0.89, MG132: 0.73 ± 0.14 ms, controls: 0.74 ± 0.15 ms; Figure 14A, C, G) or rise time (p = 0.914, MG132: 0.35 ± 0.03 ms, controls: 0.35 ± 0.03 ms; Figure 14A, C, H) of glutamatergic mEPSCs compared to control MNs. In conclusion, chronic (overnight) MG132 treatment did not significantly change the frequency or other parameters of glutamatergic mEPSCs.

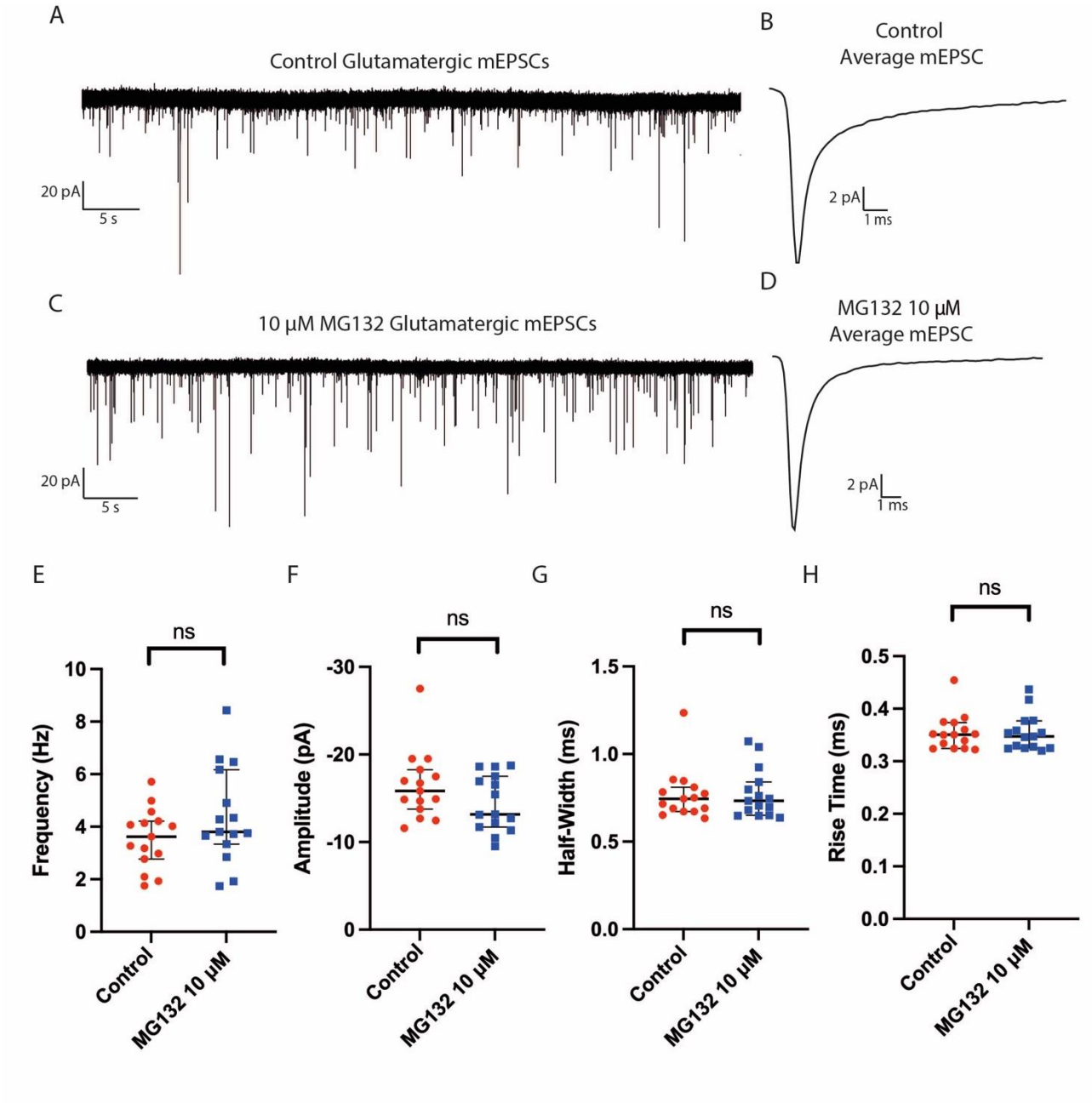


*Figure 14. Chronic incubation with proteasome inhibitor MG132 did not affect glutamatergic mEPSCs from larval zebrafish MNs.*

*The effect of 10 µM MG132 overnight incubation on glutamatergic mEPSCs . A-H. Whole-cell voltage clamp recordings of glutamatergic mEPSCs taken from MNs of zebrafish (4 dpf) spinal cord. A) Representative trace showing one minute voltage clamp recording of mEPSCs following overnight treatment with DMSO. B) An average glutamatergic mEPSC following DMSO treatment. C) Representative trace showing one minute voltage clamp recording of glutamatergic mEPSCs following overnight treatment with 10 µM MG132. D) An average glutamatergic mEPSC following 10 µM MG132. E-H) Median and interquartile range plots showing the frequency (E), amplitude (F), half-width (G) and rise time (H) of glutamatergic mEPSCs between MNs treated with 10 µM MG132 (N = 7, n = 15) and 0.01% DMSO control (N = 11, n = 15). No significant difference was found following overnight treatment with MG132 10 µM in frequency, amplitude, half-width or rise time of mEPSCs.*

Zebrafish larvae were next incubated overnight with 10 μM lactacystin (Figure 15) to determine if similar results could be obtained as were seen with MG132 (Figure 14). No significant change was observed in the frequency ($p = 0.456$, lactacystin: $2.56 \pm 1.49$ Hz, controls: $2.30 \pm 0.98$ Hz; Figure 15A, C, E), half-width ($p = 0.879$, lactacystin: $0.63 \pm 0.14$ ms, controls: $0.68 \pm 0.17$ ms; Figure 15A, C, G)or rise time ($p = 0.763$, lactacystin: $0.23 \pm 0.07$ ms, controls: $0.24 \pm 0.06$ ms; Figure 15A, C, H) of glutamatergic mEPSCs occuring in MNs of larvae treated with lactacystin (10 μM, N = 5, n = 11) or in control (N = 6, n = 12). However, there was a significant decrease in the amplitude of average mEPSCs ($p = 0.015$, lactacystin: $-16.21 \pm 4.78$ pA, controls: $-24.32 \pm 8.54$ pA; Figure 15A, C, F).

As with the data collected for glycinergic mIPSCs, differing results with MG132 and lactacystin were obtained for glutamatergic mEPSCs. MNs treated with lactacystin showed decreased glutamatergic mEPSCs amplitude compared to control treated MNs, whereas MG132 treated MNs showed no statistical difference in glutamatergic mEPSCs.

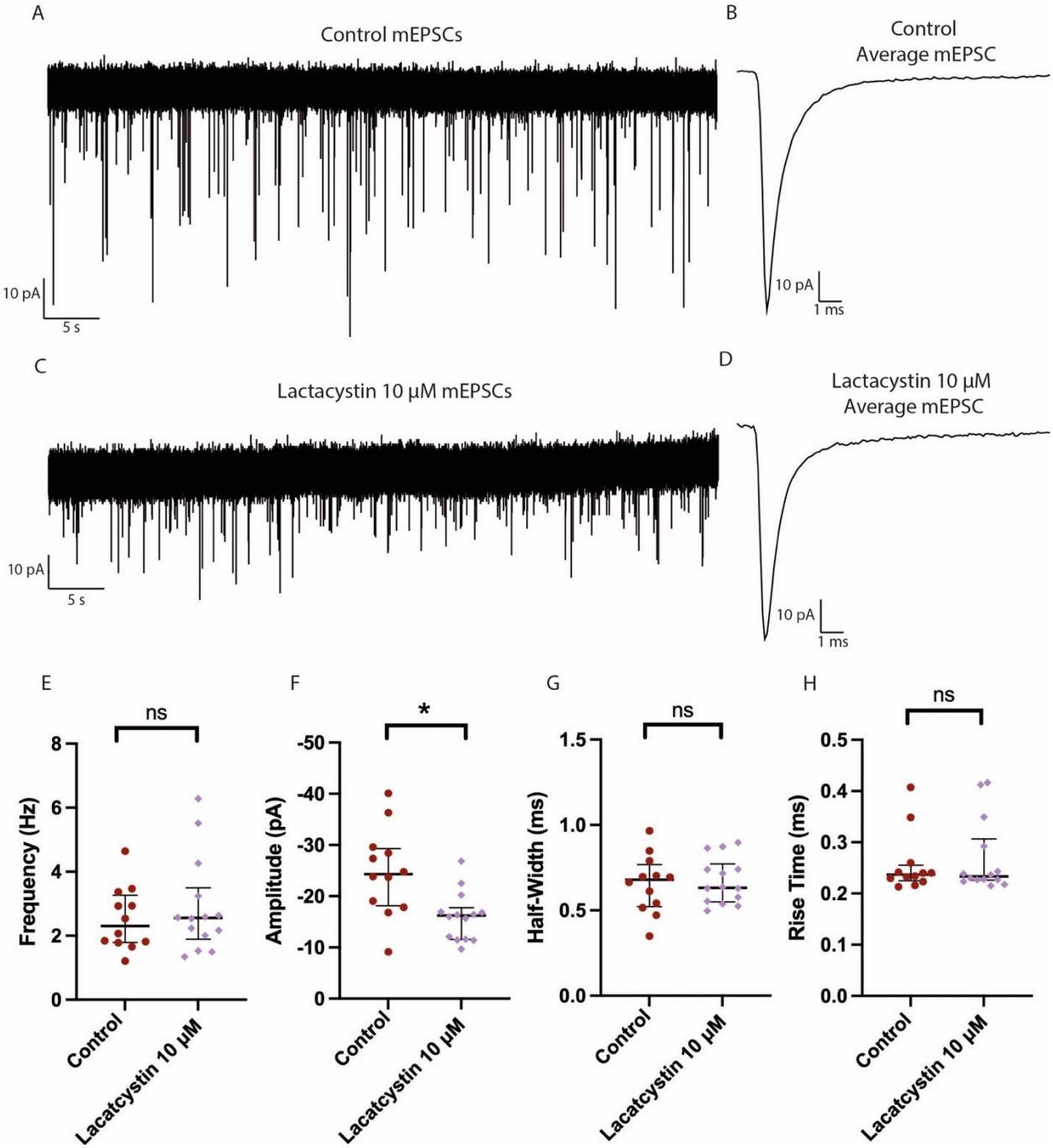


*Figure 15. Chronic incubation of proteasome inhibitor lactacystin decreased amplitude of glutamatergic mEPSCs from larval zebrafish MNs.*

*The effect of 10 µM lactacystin overnight incubation on glutamatergic mEPSCs. A-H. Whole-cell voltage clamp recordings of glutamatergic mEPSCs taken from MNs of zebrafish (4 dpf) following either overnight treatment with 10 µM lactacystin or control condition. A-B) Representative trace of mEPSCs following treatment with $dH_2O$ control and an average mEPSC taken from this representative trace. C-D) Representative minute trace of mEPSCs following treatment with 10 µM lactacystin and an average mEPSC taken from this trace. E-H) Median and interquartile range plots showing mEPSC frequency, amplitude, half-width and rise time after control and lactacystin incubation.. There was a significant decrease (p = 0.0151) in mEPSC amplitude with lactacystin treatment.*

Overnight treatment with 25µM bortezomib (N = 8, n = 11) resulted in no significant change in the frequency (p = 0.246, bortezomib: 1.16 ± 0.53 Hz, control: 1.49 ± 0.81 Hz; Figure 16A, C, E), amplitude (p = 0.582, bortezomib: -22.29 ± 6.07 pA, control: -21.18 ± 5.58 pA; Figure 16A, C, F) or rise time (p = 0.285, bortezomib: 0.23 ± 0.008 ms, control: 0.26 ± 0.03 ms; Figure 16A, C, H) was determined compared to control conditions (N = 7, n = 11). However, a significant decrease in the half-width (p = 0.0167, bortezomib: 0.52 ± 0.03 ms, control: 0.61 ± 0.16 ms; Figure 16A, C, G) was observed between fish treated with bortezomib (25 µM) compared to fish treated in control conditions.

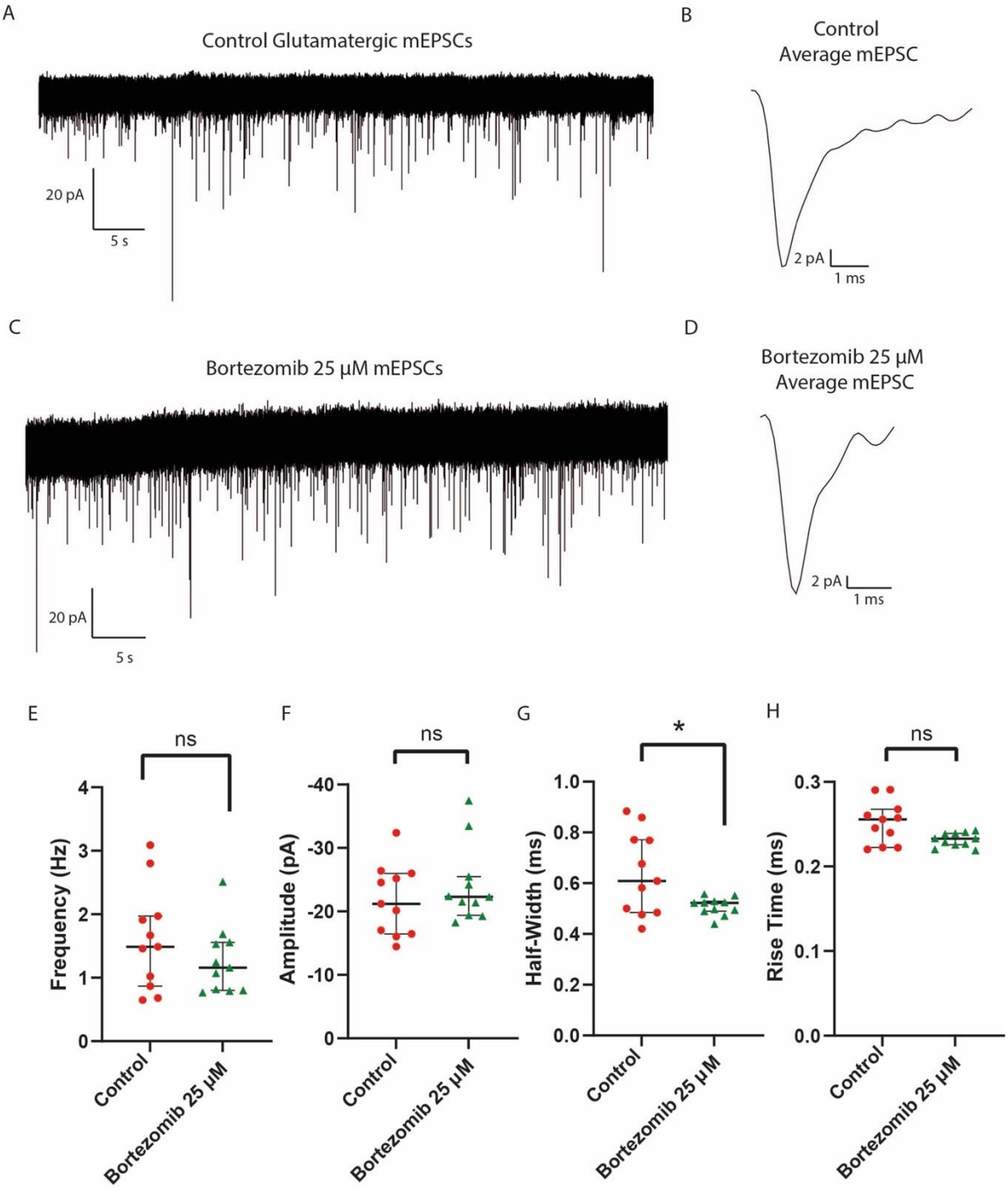


*Figure 16. Chronic incubation with proteasome inhibitor bortezomib (25 µM) decreased glutamatergic mEPSC half-width of larval zebrafish MNs.*

*The effect of 25 µM bortezomib overnight incubation on glutamatergic mEPSCs .A-H. Whole-cell voltage clamp recordings of glutamatergic mEPSCs from MNs of zebrafish (4 dpf). A-B) Representative voltage clamp traces of mEPSCs treated overnight with control 0.025% DMSO saline and an average mEPSC taken from this trace. C-D) Representative voltage clamp traces of mEPSCs from MNs treated overnight with 25 µM bortezomib and an average mEPSC taken from this trace. E-H) Median with interquartile range plots of mEPSC frequency, amplitude, half-width and rise time. A significant decrease (p = 0.0167) in mEPSC half-width was determined for mEPSCs following bortezomib treatment compared to control conditions.*

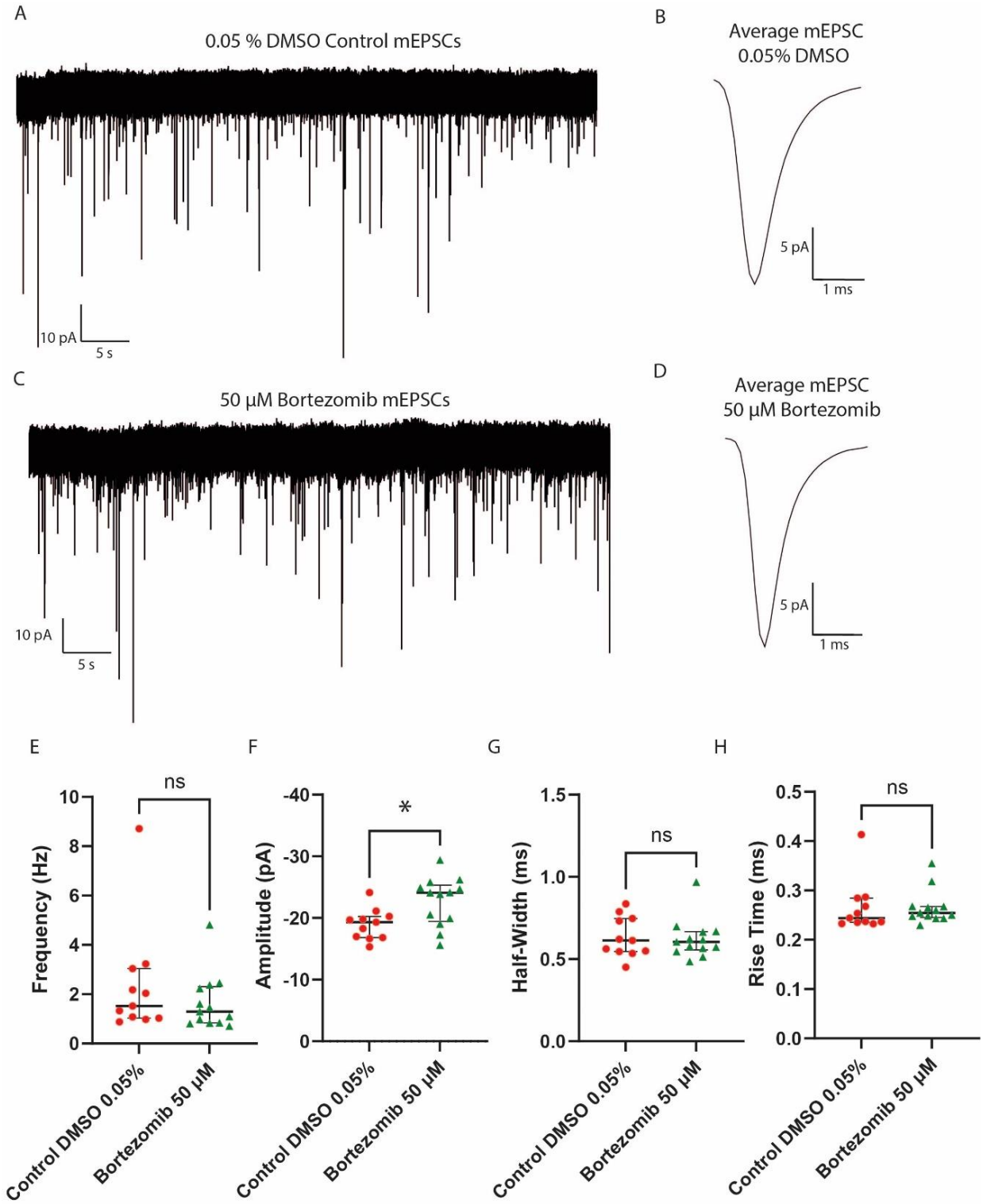


*Figure 17. Chronic incubation of MNs with proteasome inhibitor bortezomib (50 µM) increased amplitude of glutamatergic mEPSCs from larval zebrafish MNs.*

The effect of 50 µM bortezomib overnight incubation on glutamatergic mEPSCs. A-H. Glutamatergic mEPSC whole-cell voltage clamp recordings from MNs of zebrafish (4 dpf) treated overnight with either control 0.25% DMSO or 50 µM bortezomib. A-B) Representative trace of mEPSCs from MNs treated in control conditions and an average mEPSC from this trace. C-D) Representative trace of mEPSCs from MNs treated with 50 µM bortezomib and an average mEPSC from this trace. E-H) Median with interquartile range plots showing mEPSC parameters frequency, amplitude, half-width and rise time for cells treated with control conditions or 50 µM bortezomib. A significant increase in the amplitude ($p = 0.0183$) of mEPSC treated with 50 µM bortezomib compared to control conditions was determined

Zebrafish larvae treated overnight with 50µM bortezomib (N = 7, n = 12) compared to control 0.05% DMSO (N = 5, n = 10) showed no significant difference in frequency (p = 0.274, bortezomib: 1.30 ± 1.13, controls: 1.52 ± 2.26; Figure 17A, C, E), half-width (p = 0.993, bortezomib: 0.60 ± 0.12, controls: 0.61 ± 0.12; Figure 17A, C, G) or rise time (p = 0.443, bortezomib: 0.25± 0.03, controls: 0.24± 0.05; Figure 17A, C, H) of glutamatergic mEPSCs. However, a significant increase in the amplitude (p = 0.0183, bortezomib: -24.08 ± 3.94, controls: -19.32 ± 2.48; Figure 17A, C, F) mEPSCs was observed. The significant increase in glutamatergic mEPSC amplitude following bortezomib (50 µM) treatment was not observed with bortezomib (25 µM) treatment or MG132 treatment. However, consistent with MG132 and lactacystin treatment, no significant change in glutamatergic mEPSC frequency, half-width or rise time was observed following bortezomib (50 µM) incubation.

No consistent change in glutamatergic mEPSC parameters were observed across all MG132, lactacystin or bortezomib incubations. This contrasted with data collected for glycinergic mIPSCs, which showed a significant increase in mIPSC frequency following overnight treatment with all 3 proteasome inhibitors tested here. These data suggest that in the intact zebrafish spinal cord, chronic block of the proteasome primarily affects the properties of glycinergic synapses.

### 3.3.5 Effect of chronic proteasome inhibition on the firing properties of larval MNs

As I had seen changes in the synaptic properties of MNs following proteasomal inhibition, I next investigated the effect of chronic proteasome inhibition on intrinsic MN firing properties. To this end, 3-dpf zebrafish larvae were incubated in MG132 (10 µM), lactacystin (10 µM) and bortezomib (25 µM, 50 µM). Subsequently, recordings were taken from MNs at 4-dpf. For each condition, action potential firing, amplitude, half-width, rise time, threshold voltage and rheobase were analysed.

Fish incubated overnight in system water containing MG132 dissolved in DMSO (10 µM, N = 13, n =8) or system water containing 0.01% DMSO as the control (N = 11, n = 7) showed no significant difference in median MN firing frequency (p = 0.0655, MG132: 167.5 ± 32.14 Hz, controls: 122.5 ± 37.58 Hz; Figure 18 A, C, F), amplitude (p = 0.451, MG132: 16.68 ± 2.17 mV, controls: 17.31 ± 3.70 mV; Figure 18 A, C, E), half-width (p = 0.902,

MG132: 0.2611 ± 0.028 ms, controls: 0.2580 ± 0.007 ms; Figure 18A, C, G), rise-time (p = 0.234, MG132: 0.1152 ± 0.016 ms, controls: 0.1101 ± 0.009 ms; *18* Figure 18 A, C, H) or rheobase (p = 0.452, MG132: 120.0 ± 23.97 pA, controls: 100.0 ± 28.73 pA; Figure 18 A, C, I). However, there was a significant decrease in voltage threshold (p = 0.0101, MG132: -47.20 ± 4.22 mV controls: -44.20 ± 3.63 mV; Figure 18 A, C, I) for MNs treated with MG132 (10 μM) compared to control.

These data suggest that incubation with MG132 increases the voltage threshold of MNs without affecting firing frequency, rheobase and action potential waveform (amplitude, half-width and rise time).

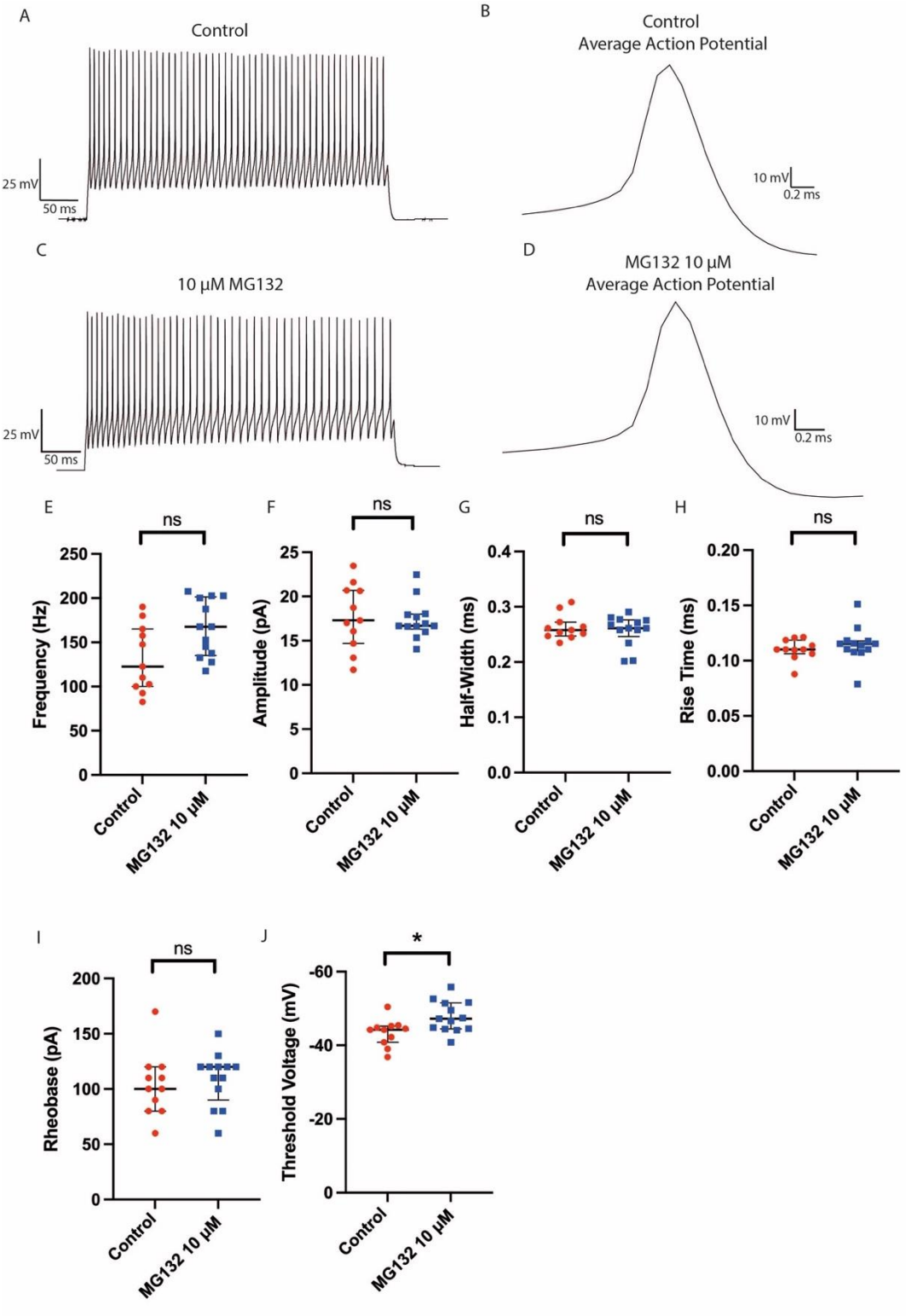


*Figure 18. Chronic incubation of proteasome inhibitor MG132 increased the threshold voltage of action potential generation of MNs from larval zebrafish.*
*Firing Properties of MNs treated overnight with MG132 (10 µM) or in control 0.01% DMSO. A current clamp step protocol was used with a 400ms 10 pA step pulse to analyse firing properties. Firing properties were analysed at 2 x Rheobase. A-B) An example recording of MNs treated in control DMSO and an average action potential taken from the firing train shown in A. C-D) An example recording of an MN treated in control and an average action potential taken from the firing train shown in C. E-J) Median with interquartile range plots displaying the firing frequency, amplitude, half-width, rise time, rheobase and threshold voltage for MNs treated with control or MG132 (10 µM). A significant increase in the threshold voltage was determined in MNs treated with MG132 (10 µM) compared to control. Asterix determine significance (* = p > 0.05).*

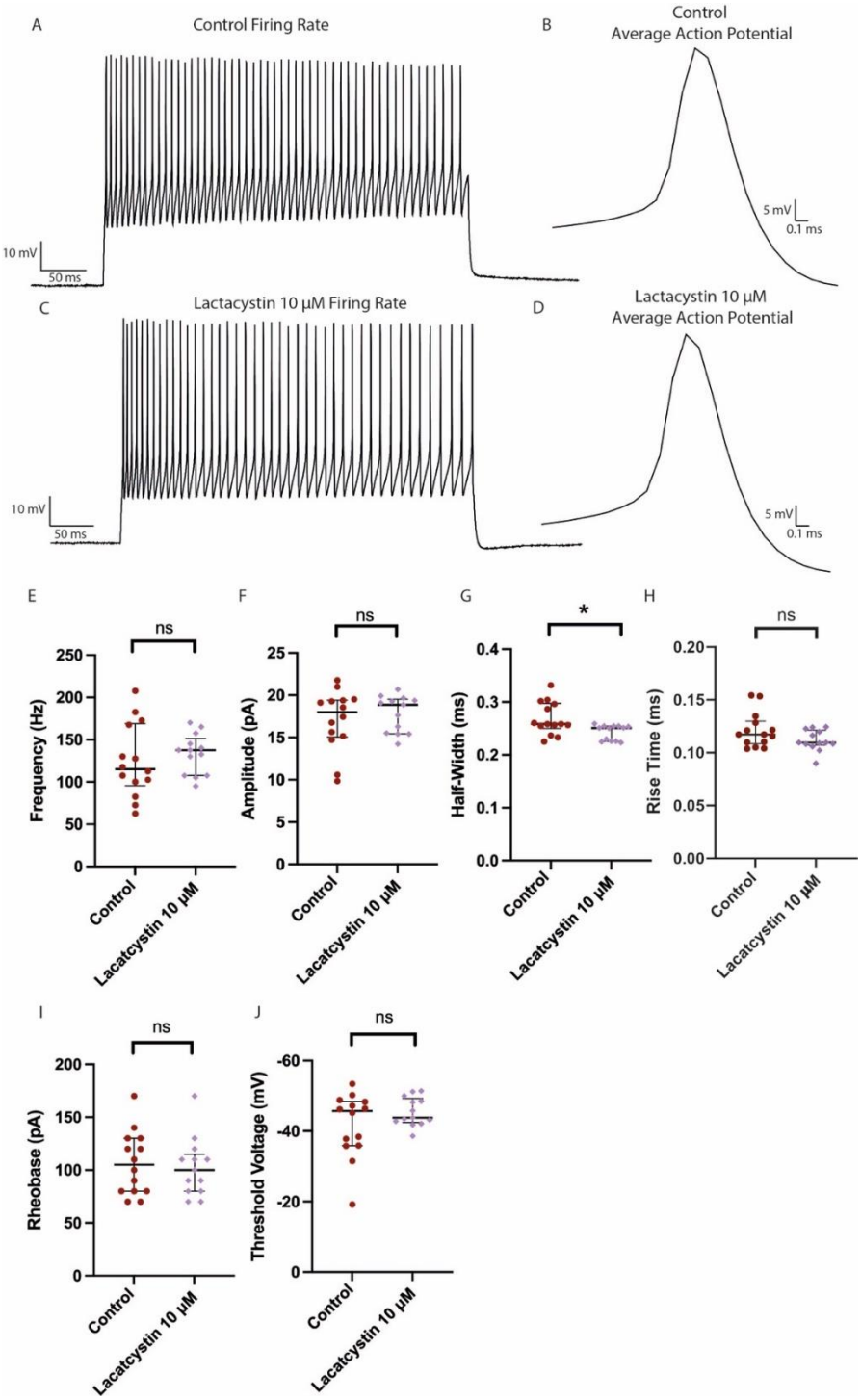


*Figure 19 Chronic incubation with proteasome inhibitor lactacystin decreased half-width of action potentials from larval zebrafish MNs.*

*Firing properties of MNs from 4 dpf larval zebrafish treated overnight with lactacystin (10 µM) or control conditions. Current clamp recordings with a 400 ms 10 pA pulse step were analyed at 2 x Rheobase. A-B) An example control recording and an average action potential taken from the train displayed in A in control conditions. C-D) An example recording of a 400 ms firing train taken at 2 x rheobase and an average action potential taken from the train displayed in C for MN treated with lactacystin (10 µM). E-J) Median with interquartile range plots showing firing frequency, amplitiude, half-width, rise time, rheobase and threshold voltage for MNs treated in either lactacystin (10 µM) or control conditions. A significant decrease in the half-width was found between the lactacystin (10 µM) and conrol treated MNs*

Fish were next incubated in lactacystin (10 μM; N = 13, n = 6) overnight or in control conditions (N = 14, n = 8) and the results are displayed in. Following drug treatment, there was no significant difference determined between the median frequency ($p = 0.486$, lactacystin: 137.5 ± 23.74 Hz, controls: 115.0 ± 43.26 Hz; Figure 19 A, C, E), amplitude ($p = 0.51$, lactacystin: 18.87 ± 2.15 mV, controls: 18.0 ± 3.57 mV; Figure 19 A, C, F), rise time ($p = 0.0839$, lactacystin: 0.1095 ± 0.01 ms, Control: 0/1172 ± 0.02 ms; Figure 19A, C, H), threshold voltage ($p = 0.222$, lactacystin: -43.80 ± 4.04 mV, controls: -45.70 ± 9.17 mV; Figure 19A, C, I) and rheobase ($p = 0.704$, lactacystin: 100.0 ± 27.74 pA, controls: 105.0 ± 30.03 pA; Figure 19A, C, J) of MN firing properties compared to control conditions. However, there was a significant decrease in the half-width of action potentials recorded from MNs treated with lactacystin (10 μM) compared to controls ($p = 0.00824$, lactacystin: 0.2508 ± 0.014 ms, controls: 0.2584 ± 0.031 ms; Figure 19A, C, G). This suggests that chronic (overnight) incubation with proteasome inhibitor lactacystin resulted in a significant decrease in the half-width of action potentials recorded from MNs.

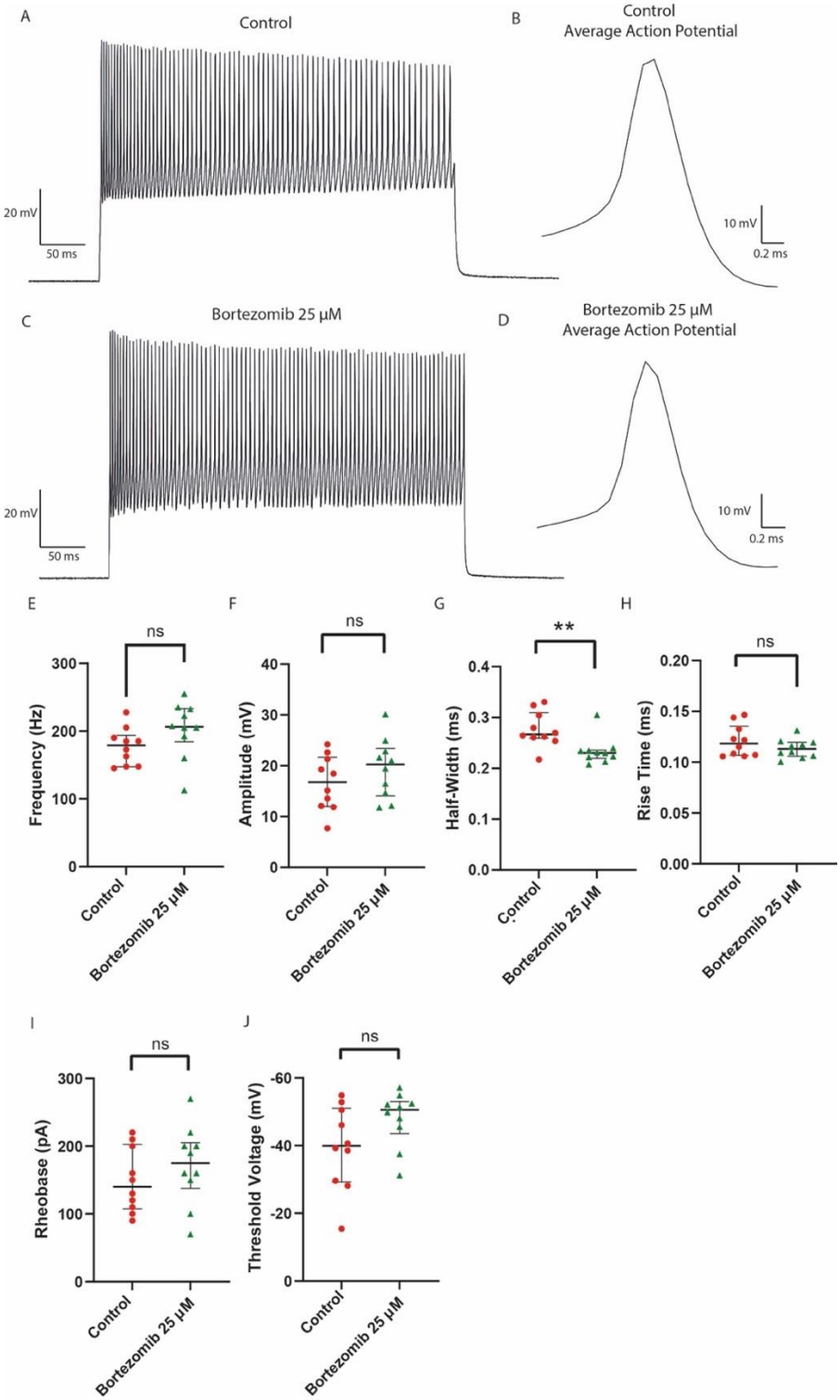


*Figure 20. Chronic proteasome inhibition with bortezomib (25 µM) decreased half-width of action potentials from larval zebrafish MNs.*

*Firing properties for MNs from 4 dpf zebrafish treated overnight with either bortezomib (25 µM) or 0.025% DMSO control. Current clamp protocol using a 400 ms 10 pA step was analysed at 2 x Rheobase for all neurons. A-B) An example 400 ms firing train taken from a current step at 2 x rheobase for a MN treated with control DMSO and an average action potential taken from A. C-D) An example 400 ms firing train taken from a current step at 2 x rheobase for a MN treated with bortezomib (25 µM) and an average action potential taken from C. E-J) Median with interquartile range plots showing firing frequency, amplitude, half-width, rise time, rheobase and threshold voltage for fish treated overnight with either bortezomib (25 µM) or 0.025% control DMSO. A significant decrease in action potential half-width (p = 0.00391) was determined between drug treated and control MNs.*

Finally, fish were incubated in either (25 μM, N = 10, n = 5) or (50 μM, N = 12, n = 5) bortezomib or control containing 0.025% DMSO (N = 10, n = 4) or 0.05% DMSO. (N = 10, n = 4). For MNs treated with 25 μM bortezomib, there was no significant change in the firing frequency (p = 0.1120, bortezomib: 206.3 ± 41.04 Hz, control: 178.8 ± 27.13 Hz; Figure 20 A, C, F), action potential peak amplitude (p = 0.237, bortezomib: 20.24 ± 5.85 mV, control: 16.79 ± 5.39 mV; Figure 20 A, C, E), rise time (p = 0.216, bortezomib: 0.1131 ± 0.009 ms, control: 0.1184 ± 0.015 ms; Figure 20 A, C, H), rheobase (p = 0.317, bortezomib: 175.0 ± 57.89, control: 140.0 ± 47.25 pA; Figure 20 A, C, I) or threshold voltage (p = 0.0713, bortezomib: -50.60 ± 8.019 mV, control: -39.90 ± 12.41 mV; Figure 20 A, C, J) compared to MNs treated with control conditions. However, there was a significant decrease in the half-width (p = 0.00391, bortezomib: 0.2302 ± 0.09757 ms, control: 0.2669 ± 0.1133 ms; Figure 20 A, C, G) of action potentials from bortezomib (25 μM) treated MNs compared to control cells.

Results obtained for MNs treated with bortezomib (25μM) action potential firing frequency, amplitude, rise time and rheobase were consistent for results obtained following MG132 (10 μM) and lactacystin (10 μM) incubation. The significant decrease in half-width obtained following 25 μM bortezomib incubation was not observed with MG132 treatment, however this was observed following lactacystin treatment (Figure 19).

Fish were incubated overnight with bortezomib (50 µM, N = 6, n = 10) or control saline containing 0.05% DMSO (N = 9, n = 12) to determine which concentration should be used for further experiments in this thesis. No significant difference was detected for frequency (p = 0.9180, bortezomib: 201.3 ± _41.55 Hz, controls: 175.0 ± _19.65 Hz; Figure 21A, C, E), amplitude (p = 0.303, bortezomib: 17.36 ± _4.81 mV, controls: 22.11 ± _3.89 mV; Figure 21A, C, F), half-width (p = 0.229, bortezomib: 0.2171 ± _0.018 ms, controls: 0.2190 ± _0.015 ms; Figure 21A, C, G), rise time (p = 0.0829, bortezomib: 0.1048 ± _0.017 ms, controls: 0.1099 ± _0.011 ms; Figure 21A, C, H), rheobase (p = 0.648, bortezomib: 150.0 ± _27.46 pA, controls: 135.0 ± _55.79; Figure 21A, C, I) or threshold voltage (p = 0.164, bortezomib: -48.30 ± _6.89, controls: -46.85 ± _4.99; Figure 21A, C, J) for MNs treated with bortezomib (50 µM) compared to control. These data indicate that chronic (overnight) incubation with bortezomib (50 µM) did not have a significant effect on the firing properties of MNs. Overall, chronic (overnight) incubation of larvae with MG132, lactacystin and bortezomib show no consistent changes in frequency, amplitude, half-width, rise time, rheobase or threshold voltage of firing properties.

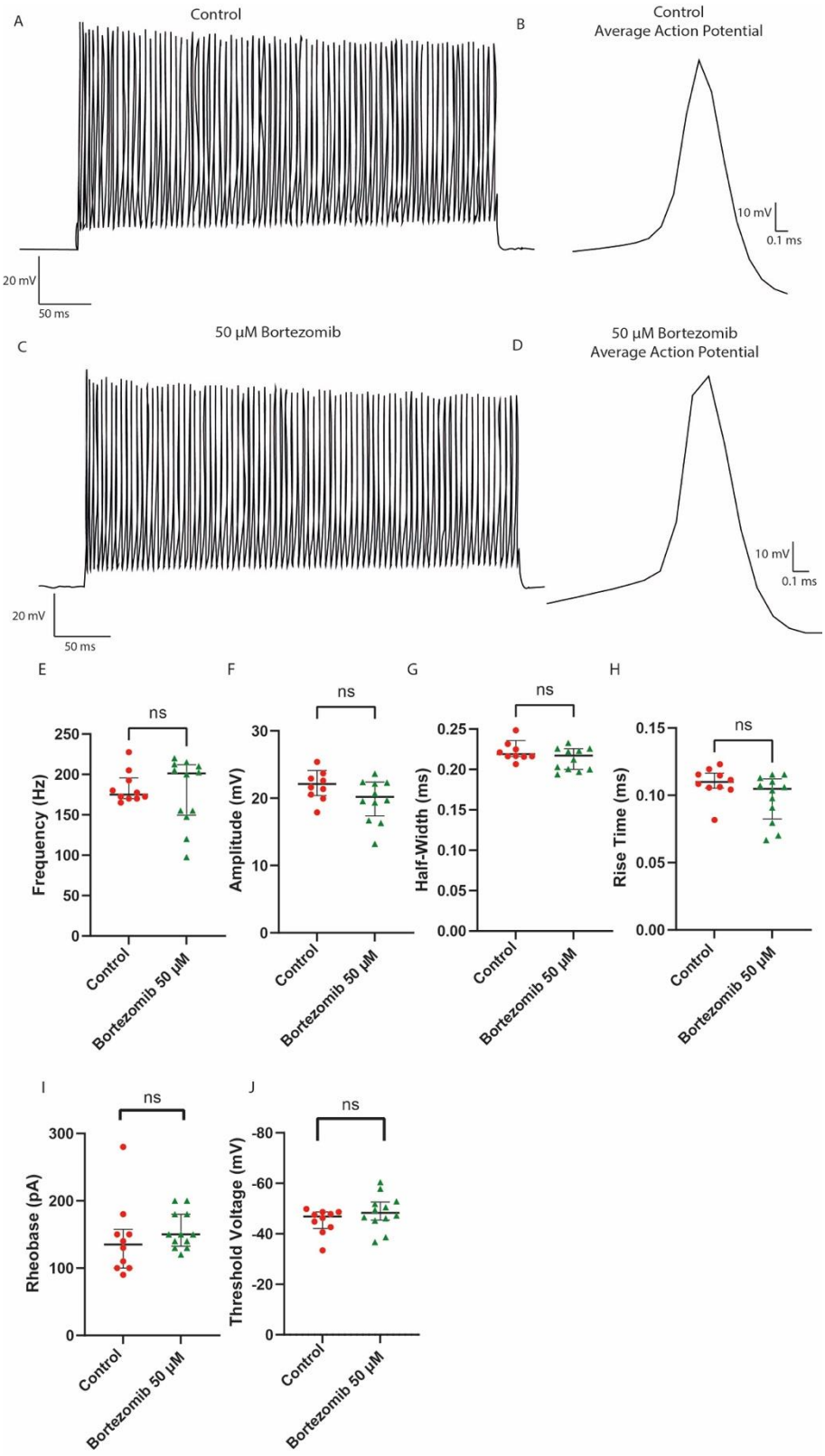


*Figure 21. Chronic incubation of proteasome inhibitor bortezomib (50 µM) did not affect firing properties of larval zebrafish MNs*

*Firing properties for MNs from 4 dpf zebrafish treated overnight with either bortezomib (50 µM) or 0.05% control DMSO. A-B) An example firing train from a 400 ms current step at 2 x rheobase of a MN treated with control DMSO and an average action potential from the firing train shown in A. C-D) An example firing train from a 400 ms current step at 2 x rheobase of a MN treated with bortezomib (50 µM and an average action potential from the firing train shown in C. E-J) Median with interquartile range plots showing firing frequency, amplitude, half-width, rise time, rheobase and threshold voltage for fish treated overnight with bortezomib (50 µM) or DMSO control. No significant difference was detected between parameters of firing properties between drug and control treated fish.*

## 3.1 Discussion

In this chapter, I have shown using the UB-R-YFP plasmid that proteasome inhibitors MG132 and bortezomib are sufficient to inhibit the larval zebrafish proteasome. No difference in overall body length was determined between larval zebrafish treated with proteasome inhibitors compared to control treated larvae. Finally, I have shown that chronic incubation with proteasome inhibitors results in an increase in the frequency of glycinergic mIPSCs. No significant increase in the frequency of mEPSCs or firing frequency was observed across all 3 drugs used here.

### 3.3.6 Using UB-R-YFP to Determine Proteasome Inhibition

Previous studies in zebrafish have used both MG132 and bortezomib as pharmacological inhibitors of the proteasome (Winder et al., 2011, Khan et al., 2012, Daroczi et al., 2009). However, for this thesis I wanted to test that MG132 and bortezomib were sufficient to inhibit the zebrafish 26S proteasome. The UB-R-YFP plasmid acts as a YFP-based substrate in the zebrafish, giving a visual fluorescent read out of proteasomal inhibition (Menéndez-Benito et al., 2005, Imamura et al., 2012).

Using the UB-R-YFP in larval zebrafish in this thesis, I only observed YFP fluorescence in microinjected larvae that had been incubated overnight with MG132 or bortezomib. None of the microinjected DMSO control fish showed YFP fluorescence at 4-dpf. Therefore, I have shown that the zebrafish 26S proteasome is inhibited using MG132 and bortezomib. I used MG132 and bortezomib during these experiments, but not lactacystin. This was due to costs and time constraints.

### 3.3.7 Total Body Length Measurements

Zebrafish larvae were treated overnight in either MG132, bortezomib or DMSO controls. Total body length measurement were taken to determine if proteasome inhibition resulted in difference in the overall length of the larvae. No difference in total body length was determined for proteasome inhibitor treated fish compared to control.

During experiments, it was noted that 50 µM bortezomib treated fish displayed a visible lack of swim bladder. Total body length measurements indicate that there is no difference in the length of bortezomib treated larvae compared to controls and no other

morphological differences were observed in drug treated larvae compared to controls. It was also noted during these experiments that bortezomib treated fish displayed different swimming patterns compared to control larvae. Therefore, it could be that the lack of swim bladder is due to an inability of the larvae to swim to the surface to fill their swim bladder. The swim bladder is a gas-filled sac which is essential for buoyancy and maintaining swimming position within the water column (Pandelides et al., 2021). It has previously been shown that there is a crucial window during larval development in which the swim bladder inflates in order to allow for the progression of swimming behaviour. In this period, larvae require access to the air-water boundary, so that they can swim to the surface and gulp air to inflate the swim bladder (Chapman et al., 1988, Goolish and Okutake, 1999). Further examination of swimming behaviour will therefore be completed in Chapter 6 of this thesis, to analyse differences in locomotion between proteasome inhibitor treated larval zebrafish and control larvae.

### 3.3.8 Effects of Overnight Proteasome Inhibition on Glycinergic mIPSCs

In order to examine the effects of overnight incubation with proteasomal inhibitors on MN glycinergic mIPSCs, I used whole-cell patch clamp technique in voltage clamp configuration. These experiments showed that in the presence of proteasome inhibitors (MG132, lactacystin and bortezomib), the frequency of glycinergic mIPSCs increased indicating a presynaptic effect, most likely caused by an increase in the number of glycinergic vesicles being released or an increase in the number of synapses connecting with the MNs. Whilst 25 µM bortezomib was not sufficient to induce this increase in glycinergic mIPSC frequency, increasing the concentration to 50 µM was sufficient to observe an increase. This was an expected result, as previous work by Rinetti & Schweizer had shown an increase in spontaneous inhibitory neurotransmitter in cultured rat hippocampal cells in the presence of both MG132 and lactacystin (Rinetti and Schweizer, 2010) and studies carried out in *Drosophila* had shown that inhibition of the proteasome increased pre-synaptic neurotransmission through synaptic strengthening (Speese et al., 2003).

These results could be due to the increase in pre-synaptic proteins available for neurotransmission release, particularly Munc13 and RIM1, which accumulated at the *Drosophila* NMJ following proteasomal inhibition in previous studies (Speese et al., 2003). However, these proteins were not found to be accumulated in mammalian hippocampal

neurons used by Rinetti and Schweizer, indicating potential species differences (Rinetti and Schweizer, 2010).

Recent findings, however, now dispute that changes in synaptic transmission following proteasome inhibition are due to changes in specific proteins involved in vesicle release accumulating as they cannot be degraded by the UPS. In 2017, a neuronal plasma membrane 20S proteasome complex (NMP) was discovered to be involved in the degradation of intracellular, unstructured proteins, resulting in the excretion of extracellular peptides which upon release, induced activity-dependent increases in calcium signalling (Ramachandran and Margolis, 2017). NMPs were found to only consist of 20S proteasomes missing their 19S cap, indicating that they are only capable of degrading unstructured proteins. The authors also showed that NMPs were not present immediately in neuronal cell culture, but around by DIV8. Further work revealed that nascent polypeptides, which are newly synthesised and hence not structured, are the main target of NMP degradation (Ramachandran et al., 2018). These findings were carried out in brain slices or cultured cortical neurons, however a 2022 study investigating the role of NMPs in *Xenopus* tadpole optic tectum was published, showing that NMPs are present in other vertebrate species. In this study, the authors found that acute inhibition of NMPs for up to 6 hours, was capable of increasing spontaneous neuronal activity and that NMP inhibition resulted in defects in the learning behaviour of the visuomotor system (He et al., 2022).

Whilst there is currently no evidence that these complexes exist in zebrafish, the existence of NMPs in *Xenopus* tadpoles in addition to in mammalian neurons adds weight that these are likely to be conserved structures across vertebrate species (He et al., 2022). In the context of the results obtained in this chapter, the discovery of NMPs raises interesting questions. If inhibition of NMPs is sufficient to spontaneously increase neuronal activity, this could be the mechanism by which synaptic transmission increases due to proteasomal inhibition. Further work would be required to establish if these complexes are the cause of the increase in mIPSCs observed in this chapter.

Increases in glycinergic mIPSC frequency displayed here could also indicate morphological changes to the neurons as a result of proteasome inhibition. Previous studies in developing systems have shown that proteasomal inhibition can affect neurite outgrowth, as well as synaptic strengthening and synaptic pruning (Speese et al., 2003, DiAntonio et al., 2001a, Collins et al., 2006). Hence, these results could indicate that there

are more glycinergic synapses being formed onto MNs as a result of proteasomal inhibition. As the larval zebrafish spinal cord continues to rapidly grow and mature between 3-dpf and 4-dpf, I aim to investigate the effects of overnight inhibition on the morphology of spinal neurons in Chapter 5 of this thesis.

I observed no difference in the amplitude, half-width or rise time of glycinergic mIPSCs treated with MG132 or bortezomib compared to control conditions. Lactacystin treatment did result in an increase in the half-width of mIPSCs, however as this was not seen with either MG132 or bortezomib treatment this was likely due to an off-target effect of lactacystin rather than a direct result of proteasome inhibition. Lactacystin has been shown to inhibit cathepsin A, a lysosomal enzyme (Ostrowska et al., 1997, Kozlowski et al., 2001). Hence, additional changes to mIPSC kinetics seen with lactacystin, but not with MG132 or bortezomib, could indicate that these changes are due to off-target inhibition of an enzyme involved in the lysosomal pathway of protein degradation rather than specific inhibition of the proteasome alone.

### 3.3.9 Effects of Overnight Proteasome Inhibition on Glutamatergic mEPSCs

As with glycinergic mIPSCs, the effect of overnight incubation of proteasome inhibitors on motoneuron glutamatergic mEPSCs was determined using whole-cell patch clamp technique in voltage clamp configuration. These experiments showed that there was no change in mEPSC frequency in MNs treated with proteasome inhibitors compared to controls. This was an unexpected result, as work carried out by Rinetti and Schweizer (2010) had shown that proteasomal inhibition resulted in an increase in the frequency of spontaneous excitatory neurotransmitter release (Rinetti and Schweizer, 2010).

These differences with previously published results could be due to the time scale of proteasomal inhibitor application. Rinetti and Schweizer (2010) used a cell culture model of rat hippocampal neurons and incubated these neurons over a time scale of minutes to 4-hours. Hence there are both species and cell type differences, on top of differences in incubation period length between these two studies which could account for the differences in neurotransmitter release that have been observed (Rinetti and Schweizer, 2010). Studies carried out in *Drosophila* showed that evoked EJC amplitude increased following 1-hour of proteasome inhibition suggesting an increase in pre-synaptic efficacy (Speese et al., 2003). Whilst these previous studies both showed similar findings, work carried out in *Drosophila*

attributed the effect to an increase in DUNC18 (*Drosophila* protein homologous to Munc13) which is involved in synaptic vesicle release, whilst no change in the levels of Munc13 or RIM1 proteins were observed following proteasome inhibition in hippocampal cultures. Hence, it was unclear whether the mechanism of increased neurotransmitter release was due to changes in synaptic vesicle release machinery, or if this was a species difference between mice and *Drosophila*.

However, new research has established the existence of NMPs in neuronal tissue from mice and *Xenopus* tadpoles (Ramachandran and Margolis, 2017, Ramachandran et al., 2018, He et al., 2022). As mentioned above, the existence of NMPs could go some way towards explaining the increase in glycinergic mIPSCs observed following the inhibition of the proteasome in this chapter. Inhibition of NMPs has been shown to increase spontaneous neuronal activity, however the cell types tested in this research have been limited in their scope. The authors have argued that this increase in spontaneous activity is due to accumulation of proteins from the nascent proteome. Emerging evidence suggests that alterations to the proteome following neuronal activity can vary depending on the activity pattern of neurons tested, hence this could suggest cell-type-specific differences in the mechanism of NMP proteome regulation (Schanzenbächer et al., 2016, Hartman et al., 2006, Bowling et al., 2016).

Do proteomic changes within individual cell types due to NMP inhibition vary as a result of homeostatic scaling of nascent proteins? This could go some way towards explaining the differences in glycinergic and glutamatergic synaptic transmission that I have seen in this chapter as a result of proteasome inhibition. Further work would, therefore, be needed to determine if NMPs are present in zebrafish and if they account for the differences in pre-synaptic transmission I have shown here.

Research on the NMP is new and therefore, limited in its scope of cell types and model systems tested. Hence, the results I have seen here could be due to other mechanisms. Heterogeneity of proteasome complexes is important for modulating the activity of proteasomes present in a cell-type-specific manner (Gomes et al., 2009). During development proteasomes are modified to become more complex structures in line with the developing organism (Haass and Kloetzel, 1989, Yuan et al., 1996, Hutson et al., 1997). Hence, I could be seeing cell-type-specific differences here due to differences in proteasome composition present within the different interneurons. Glutamatergic signalling to PMNs

comes predominantly for V2a interneurons whereas glycinergic inputs come predominantly from V0d interneurons (See Introduction). Further work could therefore be carried out to identify if there are molecular differences in the structure of proteasomes present resulting in these differing responses in mIPSC or mEPSC tansmission.

Further to this, these results could also indicate a difference in proteasome regulation of pre-synaptic release machinery involved in excitatory and inhibitory synapses. Previous studies of proteasome regulation of synaptic transmission has focused on the idea that the proteasome regulates key proteins involved in synaptic vesicle release, including Munc13 and RIM1 and did not discriminate between inhibitory and excitatory synapses (Rinetti and Schweizer, 2010). The currently held view is that vesicle release machinery does not differ between inhibitory or excitatory synapses. However, a rise in improved technology in recent years have started to show distinct differences in the architecture and dynamics of inhibitory synapses compared to excitatory synapses (High et al., 2015, Tao et al., 2018, Park et al., 2020). Hence, researchers are starting to question whether vesicle release machinery is the same between different neurotransmitters. The increase in the frequency of spontaneous mIPSCs, but not mEPSCs seen in these results could therefore be due to differences in synaptic neurotransmitter release mechanisms between inhibitory and excitatory synapses in the zebrafish being differentially affected by proteasome inhibition.

No significant difference in the rise time of mEPSCs was detected for treatment with MG132, lactacystin or bortezomib. However, changes in amplitude were determined for chronic treatment with lactacystin and bortezomib. Lactacystin caused a significant decrease in the amplitude of mEPSCs, whilst bortezomib induced a significant increase in the amplitude of mEPSCs. As no change in amplitude was observed following MG132 treatment or bortezomib (25 µM) treatment, these differences in amplitude with lactacystin and bortezomib are likely due to differences in the pharmacology of the two inhibitors.

Increases in mEPSC amplitude following chronic exposure to proteasome inhibitors have been previously reported in cultured hippocampal neurons (Jakawich et al., 2010, Srinivasan et al., 2021). Chronic exposure over a period of 12-24 hours slowly increases mEPSC amplitude over exposure time to proteasome inhibitor lactacystin and MG132 in hippocampal cultured neurons. These studies concluded that the slow increase in mEPSC amplitude was due to changes in neuronal activity and post-synaptic receptor density following inhibition of protein degradation (Jakawich et al., 2010). Hence, the increase in

mEPSC amplitude I observed here following 50 µM bortezomib incubation could be a true effect of chronic proteasomal inhibition.

The aforementioned studies also showed that the increase in mEPSC amplitude occurred slowly over the period of 12-24 hours (Jakawich et al., 2010). As such, the disparity in results between what I have observed in this thesis compared to previously published data could be due to differences in model used and time-period of incubation. A monolayer cell culture model does not present the same access issues as an *in vivo* larval zebrafish. As the increase in mEPSC amplitude occurred slowly, the exposure time could be different for the MNs I have used in this study as permeabilisation of the drug through the skin and tissues of the larvae to reach the MNs is likely to be slower than in cell-culture. Hence, I may not be seeing the same effect, as the chronic exposure time to MG132 may not have been sufficient to see increases in mEPSC amplitude. Whilst incubation time was the same with 50 µM bortezomib, the higher concentration of this drug may account for the differences seen.

The decrease in mEPSC amplitude I have shown following chronic incubation with lactacystin is not consistent with previously published results. This could be due to differences in the model systems used. Whilst exposure time would be different between a cell-culture model compared to a larvae, cell-type differences could also exist between mammalian hippocampal neurons and zebrafish MNs. In the hippocampal cell culture neurons, authors concluded that the slow increase in mEPSC amplitude was as a result of post-synaptic receptor remodelling, with particular emphasis on increased AMPA receptor expression. Further work would be needed to determine if this decrease in mEPSC amplitude following chronic exposure to lactacystin had an effect on post-synaptic AMPA receptor density. This work is beyond the scope of this thesis.

### 3.3.10 Effects of Overnight Proteasome Inhibition on Firing Properties

To examine the effects of overnight proteasomal inhibition on the firing properties of MNs, whole-cell patch clamp technique in the current clamp configuration was used. Depolarising current clamp steps were applied to MNs until step size had reached 2 x rheobase to observe repetitive spiking responses. These experiments showed that overnight incubation with all three proteasomal inhibitors did not affect the amplitude or rise time of

action potential firing compared to control cells. There was also no significant difference found in the rheobase of cells treated with proteasome inhibitors compared to control.

Action potentials are formed due to the orchestrated opening and closing of $Na^+$ and $K^+$ voltage-gated ion channels. Hence, using current clamp to inject depolarising currents onto MNs causes the opening of $Na^{2+}$ channels and elicits action potentials once rheobase has been reached. The repolarisation of the membrane is dependent on potassium ions. Results obtained here showed no changes in spiking frequency with either for MG132, lactacystin or bortezomib treatment, indicating there was no difference in the number of action potentials generated. No changes were observed in amplitude or rise time of the action potentials following proteasome inhibition. This suggests that the proteasome does not have an observable effect on sodium channel kinetics. Rheobase was also not affected by proteasome inhibition. This suggests that chronic inhibition of the proteasome is most likely not associated with changes in action potential threshold (Luque et al., 2017).

A significant decrease in the half-width was observed between cells treated with 25 µM bortezomib or lactacystin compared to control conditions. The half-width (or spike width) gives an idea of the speed of the action potential and is measured as the width of the spike at half the maximum peak. Hence, a decrease in half-width denotes a faster action potential. As a significant decrease in the rise time of action potentials was observed following lactacystin or bortezomib (25 µM) treatment, these results suggest that lactacystin and bortezomib are capable of modulating potassium channels to speed up the repolarisation of the membrane following an action potential. There is a lack of evidence in the literature studying the effects of proteasomal inhibition on action potential properties. These effects were not seen with MG132 or 50 µM bortezomib treatment, although 50 µM bortezomib showed a trend towards a decrease in half-width. These differences could be due to a true effect of proteasome inhibition and differences in the pharmacology of the proteasome inhibitors could account for the disparity in results seen here. Further work would be needed to determine if this were the case, however this was beyond the scope of this thesis.

Whilst there have been many studies implicating the proteasome in pre-synaptic vesicle release (Rinetti and Schweizer, 2010, Speese et al., 2003, Bingol and Schuman, 2006, Yao et al., 2007) and post-synaptic changes in receptors (Jakawich et al., 2010, Srinivasan et al., 2021), the effects of proteasome inhibition on ion channels controlling membrane

potential have been less well studied. Previous studies have shown that the UPS regulates specific ion channels, including $Kv_7$ channels and certain $Na^+$ channels (Fotia et al., 2004, Rougier et al., 2005, Kim et al., 2018). However, as yet no studies have conclusively linked proteasomal inhibition to changes in the firing properties of neurons. I have shown here that no changes to firing frequency, amplitude, rise time or rheobase occur as a result of proteasomal inhibition with the three different inhibitors tested here.

### 3.3.11 Conclusions

Overall, results obtained in Chapter 3 of this thesis have shown that the larval zebrafish proteasome is inhibited by the three drugs used in the following experiments (Figure 8). During whole-cell patch clamp recordings, evidence suggests that overnight inhibition of the proteasome with three different proteasome inhibitors causes a specific increase in glycinergic mIPSC frequency, without consistently affecting mIPSC amplitude, half-width or rise time. Glutamatergic mEPSCs and firing properties of MNs are not affected by proteasomal inhibition. Whilst certain drug conditions did produce changes in amplitude, half-width and rise time, these were not repeatable across all three drugs tested.

MNs in spinalised fish receive synaptic inputs from both glutamatergic excitatory INs and glycinergic inhibitiory INs (Berg et al., 2018b). These results suggest that there could be cell type specific differences in pre-synaptic release machinery, which is regulated differently by the proteasome. However, these results could also be due to differences in the time scale of proteasome inhibition. Previously reported experiments have carried out acute application of proteasome inhibitors for 10-mins (Rinetti and Schweizer, 2010), hence the differing results seen here could be due to longer term proteasome inhibition.

Therefore, in Chapter 4 of this thesis, I will investigate if the effect of increased mIPSC frequency is observed over shorter incubation periods with proteasome inhibitors. Due to the cost involved in using lactacystin and the inconsistent results obtained when measuring glycinergic mIPSCs, in the preceding chapters I will use 10 µM MG132 and 50 µM bortezomib. For Chapter 4, I will incubate spinalised larval zebrafish (4-dpf) with 10 µM MG132 and 50 µM bortezomib for 1-hour to assess the effects of shorter incubation periods on proteasomal regulation of MN extrinsic and intrinsic properties.

# Chapter 4 The Effect of Short-Term Proteasome Inhibition on the Synaptic and Intrinsic Properties of Motoneurons

## 4.1 Introduction

### 4.1.1 Acute Proteasomal Inhibition

Studies have shown that the proteasome is involved in regulating synaptic transmission. In Chapter 3 of this thesis, I showed that chronic (overnight) incubation with proteasome inhibitors was sufficient to produce an increase in glycinergic mIPSCs using three different proteasome inhibitors. However, previous studies have shown that the UPS is capable of modulating synapses within shorter time periods. Here, I will outline the previous studies carried out looking at acute proteasomal inhibition and its effects on neurons.

#### *4.1.1.1 Acute Proteasomal Inhibition and Synaptic Transmission*

Key protein targets of the UPS were first identified in *Drosophila*, including DUNC-13, a vesiclular release machinery protein. Short (< 1 hour) incubation periods with lactacystin and epoxomicin (proteasome inhibitors) resulted in accumulation of DUNC-13 at the *Drosophila* NMJ. Moreover, sharp electrode recordings provided evidence of increased synaptic strengthening due to an increase in mEJC amplitude within tens of minutes (Speese et al., 2003). Building from this, work in rat hippocampal cell culture showed that following 10-minute bath application of proteasome inhibitors (MG132 and lactacystin), there was an increase in glycinergic and glutamatergic miniature and evoked synaptic currents. By contrast, proteasome inhibition did not affect presynaptic protein targets Munc-13 (murine homolog of DUNC-13) and RIM1, as had previously been shown in *Drosophila* (Speese et al., 2003). Further investigation revealed that application of E1-ubiquitinating enzyme inhibitors mirrored the effect of proteasome inhibition on spontaneous and evoked synaptic transmission, with no accumulation of RIM1 and Munc-13. Munc-13 and RIM1 are both pre-synaptic protein targets of the proteasome, that associate together and enhance docking and release of pre-synaptic vesicles. Hence, if increases in vesicle release were due to the proteasome being unable to degrade these pre-synaptic proteins, accumulation of RIM1 and Munc-13 would be observed. However, authors so no such increase in RIM1 or Munc-13 protein following inhibition of the proteasome or the E1-ubiquitinating enzymes.

These results indicated that instead of accumulation of synaptic proteins, the UPS regulates synapses through ubiquitination and subsequent proteasomal degradation of specific target proteins involved in vesicular release. (Rinetti and Schweizer, 2010).

In the aforementioned studies, changes in pre-synaptic vesicle release were observed within a short time frame (tens of minutes), indicating that the proteasome exerts rapid and dynamic effects on the abundance presynaptic proteins. However, subsequent studies of cultured hippocampal neurons from mice revealed no effect of proteasome inhibition on accumulation of Munc-13. Using a Munc-13-EYFP line, a stable mouse strain which expresses fluorescent functional Munc-13 protein ubiquitously throughout neurons, time lapse microscopy of cultured neurons treated with MG132 showed no increase in Munc-13 fluorescence (Kalla et al., 2006). These contrasting observations could arise from species-specific, age-dependent differences or differences between neuron subtypes (Rinetti and Schweizer, 2010, Speese et al., 2003).

A proteomic study showed that inhibition of the UPS for 4-hours with lactacystin did not significantly increase the degradation of most synaptic proteins. SILAC (stable isotope labelling with amino acids in cell culture) and Mass Spectrometry (MS) is a technique which can be used to measure how application of pharmacological agents can affect the degradation of thousands of protein targets. Using primary cultures from rat hippocampal neurons in combination with lactacystin treatment, researchers identified only a small subset of proteins where the half-life was significantly reduced with the application of proteasome inhibitors. Key targets included AMPA-type glutamate receptor subunit GluA2, Nedd4 (an E3 ligase), Norbin (a protein involved in metabotropic glutamate receptor trafficking) and SNAP-$\alpha$ (a protein involved in trafficking between the ER and the Golgi apparatus). Conversely, proteasomal inhibition resulted in the suppression of synaptic protein synthesis, with over 1400 proteins being differentially synthesised following application of lactacystin. The proteomic profile was indicative of the unfolded protein response, with increased expression of proteins involved in the ER stress response. Hence, researchers concluded that the main effects of proteasomal inhibition on the proteomic profile of the cell were linked to changes in protein expression as opposed to increased protein degradation. Moreover, no differences in spontaneous network activity of cortical neurons following lactacystin application for 10-20 hours were observed , indicating that

synaptic transmission was not impaired as a result of proteasome inhibition (Hakim et al., 2016).

#### *4.1.1.2 Role of the UPS During Synaptic Activity*

The possible role of the UPS in short-term regulation of synapse efficacy has also been studied using time-lapse imaging of vesicle dynamics. FM-dyes have been used to characterise vesicle pools following proteasomal inhibition. FM-dyes are lipophilic dyes which bind to the outer plasma membrane and emit fluorescence within the hydrophobic space. Tissue preparations are bathed in saline containing the dye and then stimulated, evoking vesicle release into the extracellular space. These vesicles then absorb the dye, before they are endocytosed back into the tissue and can then be imaged (Jelínková et al., 2019, Gaffield and Betz, 2006). These dyes were used to label recycling vesicles in cultured rat hippocampal neurons and showed that a-15-minute exposure to proteasome inhibitors was sufficient to increase the size of the recycling pool. A 76% increase in the vesicular recycling pool was observed within a 2-hour period of block. This increase was not observed when network activity was inhibited with the sodium channel blocker TTX, indicating that evoked synaptic release is required for this effect (Willeumier et al., 2006).

There is growing evidence that localisation of the proteasome is dynamically regulated by neuronal activity. Neuronal activity was induced in rat hippocampal neurons using KCl solution to depolarise neurons. The 19S subunit Rpt1 was fused to GFP and expressed in hippocampal cell culture, allowing for the rapid identification of 26S proteasomes *in situ*. Within tens of minutes of KCl application, rapid translocation of the proteasome from dendritic spines to pre-synaptic terminal occurred (Bingol and Schuman, 2006).

Subsequent work revealed that proteasome translocation was dependent on autophosphorylated CaMKII, which acted as a scaffold protein for proteasomes to bind to within dendritic spines in hippocampal cell culture (Bingol et al., 2010). Taken together, these studies indicate that neuronal activity stimulates an orchestrated process of proteasome trafficking to the synapse, providing support for the idea that proteasomes are important for synaptic function.

Fast ubiquitination of PSD-95 has been observed following neuronal activity. PSD-95 is a scaffolding protein associated with the post-synaptic density of excitatory synapses and interacts directly with the cytoplasmic tails of AMPA receptors to anchor them to they

synapse (Sheng, 2001). In cultured hippocampal neurons, stimulation of NMDA-type glutamate receptors with the agonist NMDA caused rapid ubiquitination of PSD-95 within 10 minutes of NMDA application (Colledge et al., 2003). These results suggest that the proteasome can act rapidly within cells in response to neuronal activity to regulate AMPA receptor number at the post-synaptic membrane during synaptic plasticity.

Recent research has revealed the existence of neuronal-specific 20S membrane proteasome complexes (NMPs) in both cultured mammalian brain tissue and *Xenopus* tadpoles (Ramachandran and Margolis, 2017, He et al., 2022). NMPs have been shown to regulate neuronal network activity through their ability to degrade intracellular proteins and remove peptides into the extracellular space which can be used as signalling molecules. These signalling peptides have yet to be identified, but evidence shows that the intracellular protein targets of NMPs are nascent proteins. Nascent proteins are those which are still bound to the ribosomes and, therefore, are not fully formed or folded into their final confirmation. Hence, they are candidates for 20S proteasome degradation, as they do not need to be ubiquitinated or have a 19S cap to unravel their native folding. Using mass-spectrometry, it was shown that KCl-induced depolarisation of mouse cortical cultures increased nascent peptide production when in cultures treated with the NMP specific proteasome inhibitor, bio-epoxomicin, compared to control. These changes can be observed between 1-2 hours following neuronal stimulation (Ramachandran et al., 2018). This suggests that NMPs may play a role in the regulation of activity-dependent changes in neuronal function, through their ability to affect the nascent proteome of neurons.

## 4.2 Aims and Objectives

In Chapter 3, I investigated the effect of chronic (overnight) incubation with proteasome inhibitors and observed an increase in the frequency of glycinergic mIPSC occuring on MNs of larval zebrafish. In this chapter, I investigate the effects of short-term (10-60 min) exposure to proteasome inhibitors on synaptic input to MNs of the larval zebrafish spinal cord. Subsequently I examine the effects of short-term exposure to proteasome inhibitors on the intrinsic firing properties of MNs.

## 4.3 Results

### 4.3.1 The effect of short-term proteasome inhibition on glycinergic mIPSCs parameters

To investigate the effects of short-term proteasome inhibition on glycinergic synapses, larvae were first incubated for 1-hour in 10 µM MG132 before performing whole cell voltage clamp recordings of MNs exposed to the sodium channel blocker TTX (1 µM), the pan-specific glutamate receptor antagonist kynurenic acid (10 mM) and the GABA inhibitor picrotoxin (100 µM). Under these conditions, glycinergic mIPSCs were isolated for study.

A significant increase in the frequency of glycinergic mIPSCs MNs of MG132 preparations than those observed in controls ($p = 0.0128$, MG132: $3.28 \pm 1.56$ Hz, control: $1.78 \pm 1.05$ Hz; Figure 22A, C, E). By contrast, mean amplitude ($p = 0.191$, MG132: $-19.39 \pm 5.77$ pA, control: $-19.45 \pm 10.25$ pA; Figure 22A, C, F), half-width ($p = 0.507$, MG132: $2.06 \pm 0.42$ ms, control: $1.85 \pm 0.44$ ms; Figure 22A, C, G) and rise time ($p = 0.272$, MG132: $0.50 \pm 0.041$ ms, control: $0.47 \pm 0.054$ ms; Figure 22A, C, H) of mIPSCs recorded from MNs pre-treated with 10 µM MG132 ($N = 8$, $n = 12$) were not significantly different from those occurring in control cells ($N = 13$, $n = 9$). These results were consistent with previously reported results in Chapter 3 following chronic incubation with MG132. Short (1-hour) incubation with MG132 results increased glycinergic mIPSCs, with no change to other parameters.

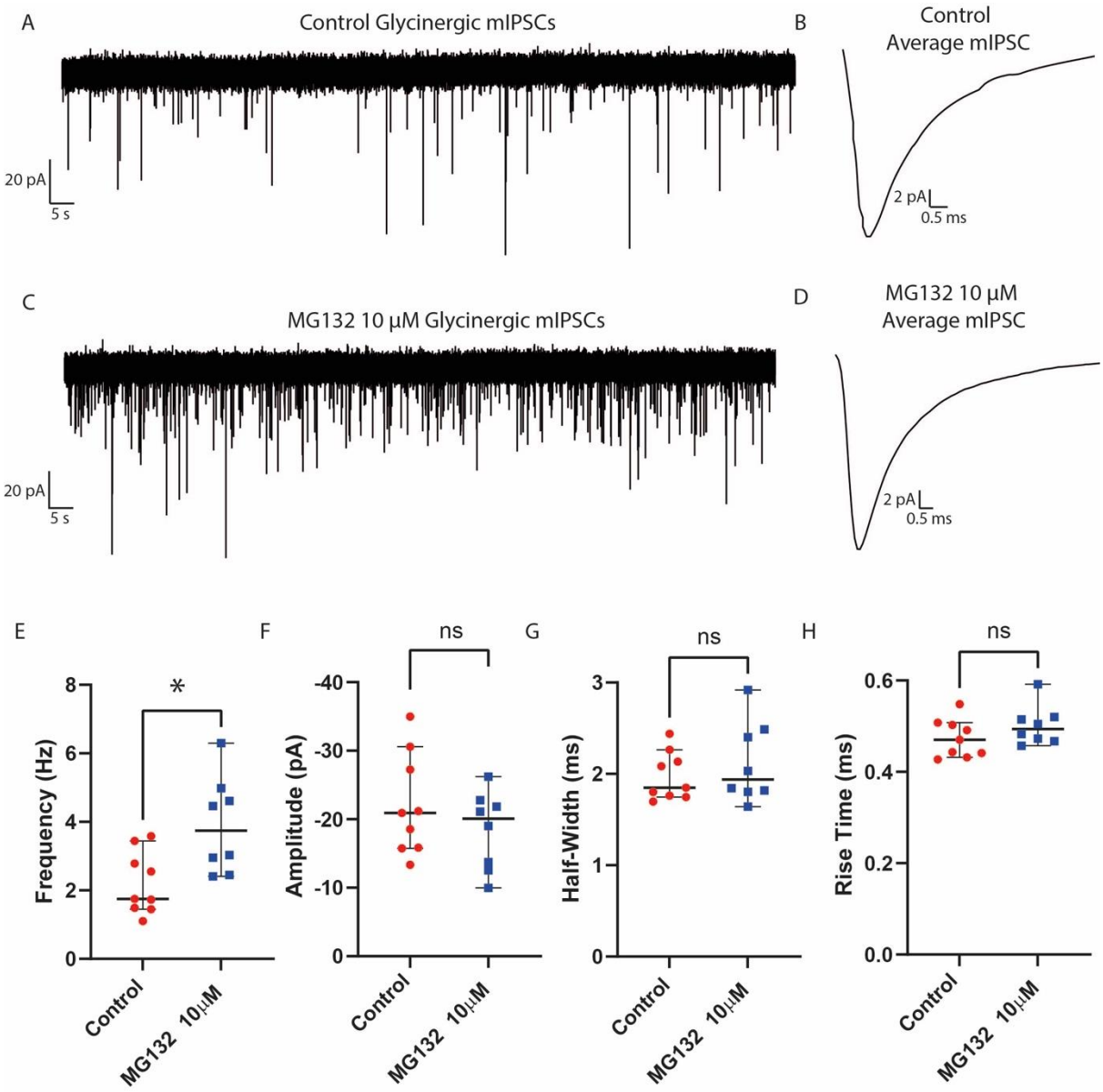


*Figure 22. Short incubation with proteasome inhibitor MG132 increases the frequency of glycinergic mIPSCs isolated from MNs in spinal cord of zebrafish larvae.*

*A-B) An exemplar voltage clamp trace of glycinergic mIPSCs taken from a MN treated for 1-hour with 0.01% DMSO control saline and an average mIPSC (B) taken from the trace displayed in A. C-D) An exemplar voltage clamp trace of glycinergic mIPSCs take from a MN treated for 1-hour with 10 µM MG132 and an average mIPSC (D) taken from the trace displayed in C. E-H) Median with interquartile range plots displaying mIPSC paramaters frequency, amplitude, half-width and rise time for MNs treated with 10 µM MG132 compared to DMSO control.. No significant difference was determined for mIPSC amplitude, half-width or rise time for MNs treated in either MG132 or control. A significant increase ($p = 0.0128$) in mIPSC frequency was detected between cells treated for 1-hour in 10 µM MG132 and control DMSO. * = $p < 0.05$.*

To determine whether the observed effects on mIPSC frequency were due to selective blockade of the proteasome, the effects of a 1-hour pre-treatment with bortezomib (50µM, N = 7, n = 10) were examined in comparison to control (N = 7, n = 10). A significant increase in the frequency ($p = 0.0049$, bortezomib: 1.66 ± 0.65 Hz, control: 1.08 ± 0.36 Hz; Figure 23A, C, E) of glycinergic mIPSCs was observed following short (1-hour) incubation with bortezomib. No significant difference in amplitude ($p = 0.0761$, bortezomib: -29.51 ± 10.88 pA, control: -36.72 ± 8.40 pA; Figure 23A, C, F) was observed. However, there was a significant decrease in the half-width ($p = 0.0374$, bortezomib: 1.11 ± 0.38 ms, control: 1.38 ± 0.12 ms; Figure 23A, C, G) and the rise time ($p = 0.0169$, bortezomib: 0.28 ± 0.04 ms, control: 0.33 ± 0.056 ms; Figure 23A, C, H) of mIPSCs following treatment with bortezomib. Thus, short (1-hour) incubation with bortezomib increased glycinergic mIPSC frequency as observed following short (1-hour) MG132 application or chronic (overnight) application of bortezomib. Additionally, short (1-hour) incubation with bortezomib decreased half-width and rise time of glycinergic mIPSCs.

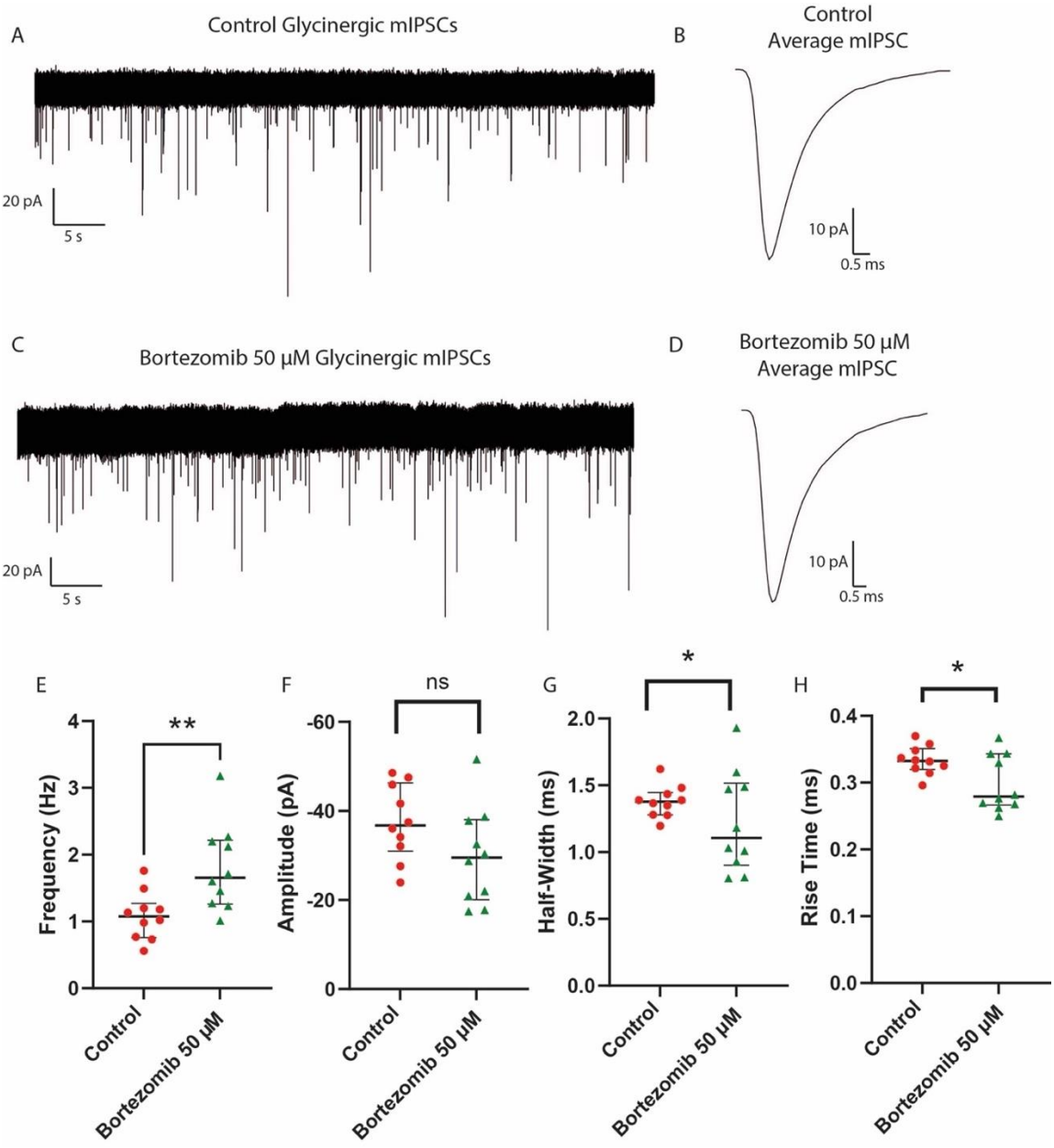


*Figure 23. Short incubation with proteasome inhibitor bortezomib increases the frequency of glycinergic mIPSCs isolated from MNs in spinal cord of zebrafish larvae.*

*Larvae (4-dpf) were spinalised incubated for 1-hour in 50 µM bortezomib. Whole-cell voltage clamp recordings were taken from MNs of the zebrafish spinal cord. A-B) A-B) An exemplar voltage clamp trace of glycinergic mIPSCs taken from a MN treated for 1-hour with 0.05% DMSO control saline and an average mIPSC (B) taken from the trace displayed in A. C-D) An exemplar voltage clamp trace of glycinergic mIPSCs take from a MN treated for 1-hour with 50 µM Bortezomib and an average mIPSC (D) taken from the trace displayed in C. E-H) Median with interquartile range plots displaying mIPSC paramaters frequency, amplitude, half-width and rise time for MNs treated with 50 µM Bortezomib compared to DMSO control. No significant difference was determined for mIPSC amplitude for MNs treated in either Bortezomib or control. A significant increase in glycinergic mIPSC frequency was determined*

### 4.3.2 The effect of short proteasome inhibition on glutamatergic mEPSCs parameters

Next, the effects of short-term proteasome inhibition on glutamatergic synapses was investigated. Here, larvae were first incubated for 1-hour in MG132 (10 µM, N = 10, n =7) or saline containing 0.05% DMSO (N = 10, n = 9) before performing whole cell voltage clamp recordings of MNs exposed to the sodium channel blocker TTX (1 µM), the glycine receptor antagonist strychnine (100 µM) and the GABA receptor antagonist picrotoxin (100 µM). In keeping with chronic incubation experiments (See Chapter 3), a one hour pre-treatment with MG132 yielded no significant difference in glutamatergic mEPSC frequency ($p = 0.0679$, MG132: $3.03 \pm 1.58$ Hz, control: $2.60 \pm 0.47$ Hz; Figure 24A, C, E ), amplitude ($p = 0.612$, MG132: $-16.46 \pm 4.01$ pA, control: $-14.89 \pm 5.58$ pA; Figure 24A, C, F) , half-width ($p = 0.585$, MG132: $0.77 \pm 0.39$ ms, control: $0.83 \pm 0.17$ ms; Figure 24A, C, H) or rise time ($p = 0.567$, MG132: $0.34 \pm 0.06$ ms, control: $0.35 \pm 0.06$ ms; Figure 24A, C, G) in control and MG132 treated fish.

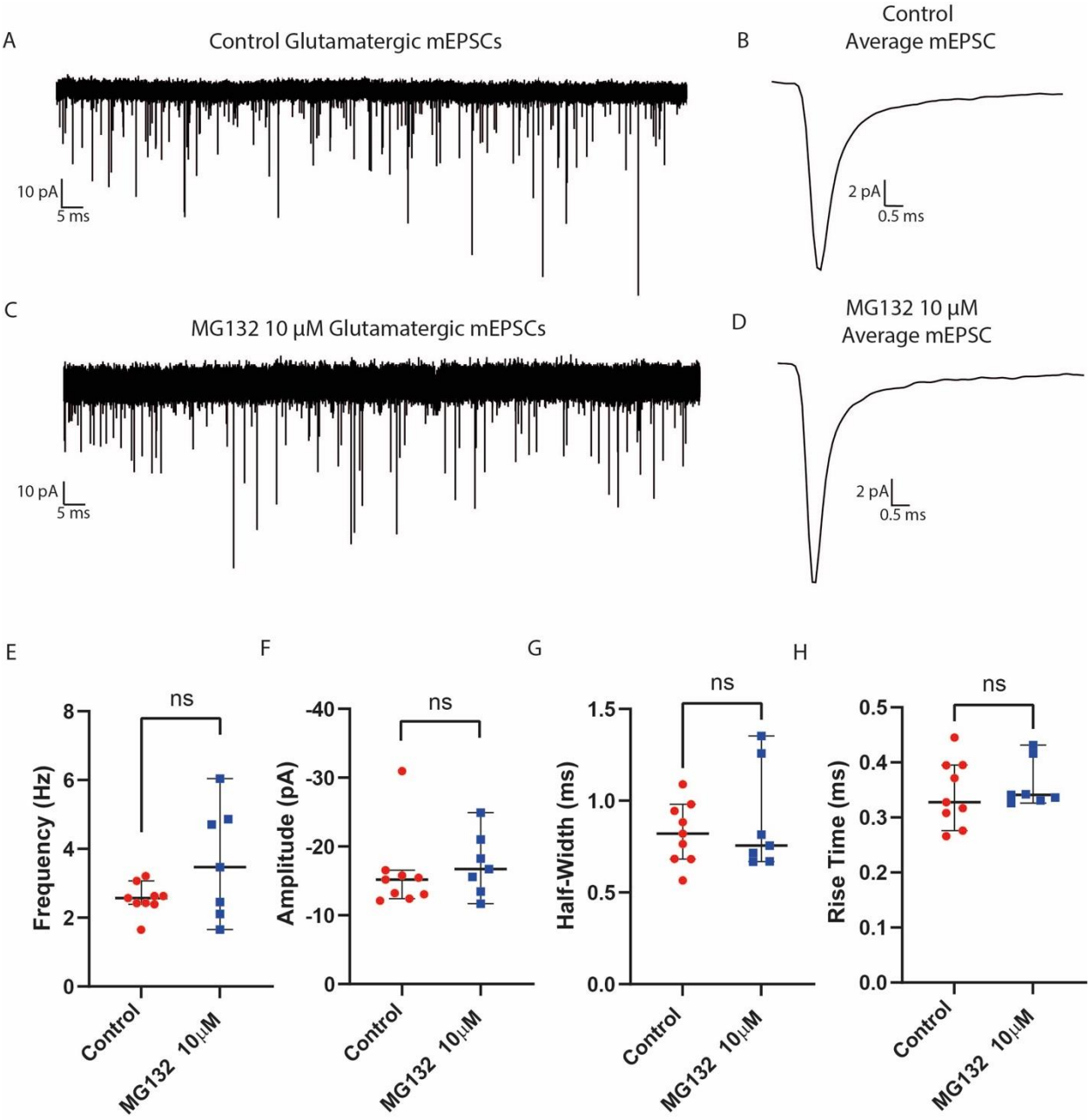


*Figure 24. Short incubation with proteasome inhibitor MG132 does not effect glutamatergic mEPSCs isolated from MNs in spinal cord of zebrafish larvae.*

*A-B) Example 60 s voltage clamp trace showing mEPSCs from a MN in the presence of 0.01% control DMSO saline and an average mEPSC (B) taken from the trace shown in A. C-D) Example 60 s voltage clamp trace showing mEPSCs from a MN in the presence of 10 µM MG132 in saline and an average mEPSC (D) taken from the trace displayed in C. E-H) Median with interquartile range plots displaying frequency, amplitude, half-width and rise time of mEPSCs from 1-hour incubation with either 10 µM MG132 or control DMSO saline. No significant difference was detected between mEPSC parameters between control and MG132 treated cells.*

Next the effects of a 1-hour pre-incubation with bortezomib (50µM) or control saline containing 0.05% DMSO on glutamatergic mEPSCs was examined. Pre-exposure to bortizomib (50 µM, N = 7, n = 10)) had no significant effect on the frequency (p = 0.016, bortezomib: 0.84 $\pm$ 0.74 Hz, control: 1.52 $\pm$ 1.20 Hz, Figure 25A, C, E), amplitude (p = 0.333, bortezomib: -26.36 $\pm$ 14.29 pA, control: -22.55 $\pm$ 7.15 pA, Figure 25A, C, F), half-width (p = 0.603, bortezomib: 0.70 $\pm$ 0.18 ms, control: 0.53 $\pm$ 0.16 ms; Figure 25A, C, H) or rise time (p = 0.412, bortezomib: 0.28 $\pm$ 0.04 ms, control: 0.24 $\pm$ 0.03 ms; Figure 25A, C, G) of mEPSCs when compared to cells bathed in control saline (N = 7, n = 10). In sum, these data suggest that the effects of short (one hour) proteasome inhibition has effects that parallel those observed with chronic (overnight) treatment, with no significant effect on glutamatergic mEPSC parameters.

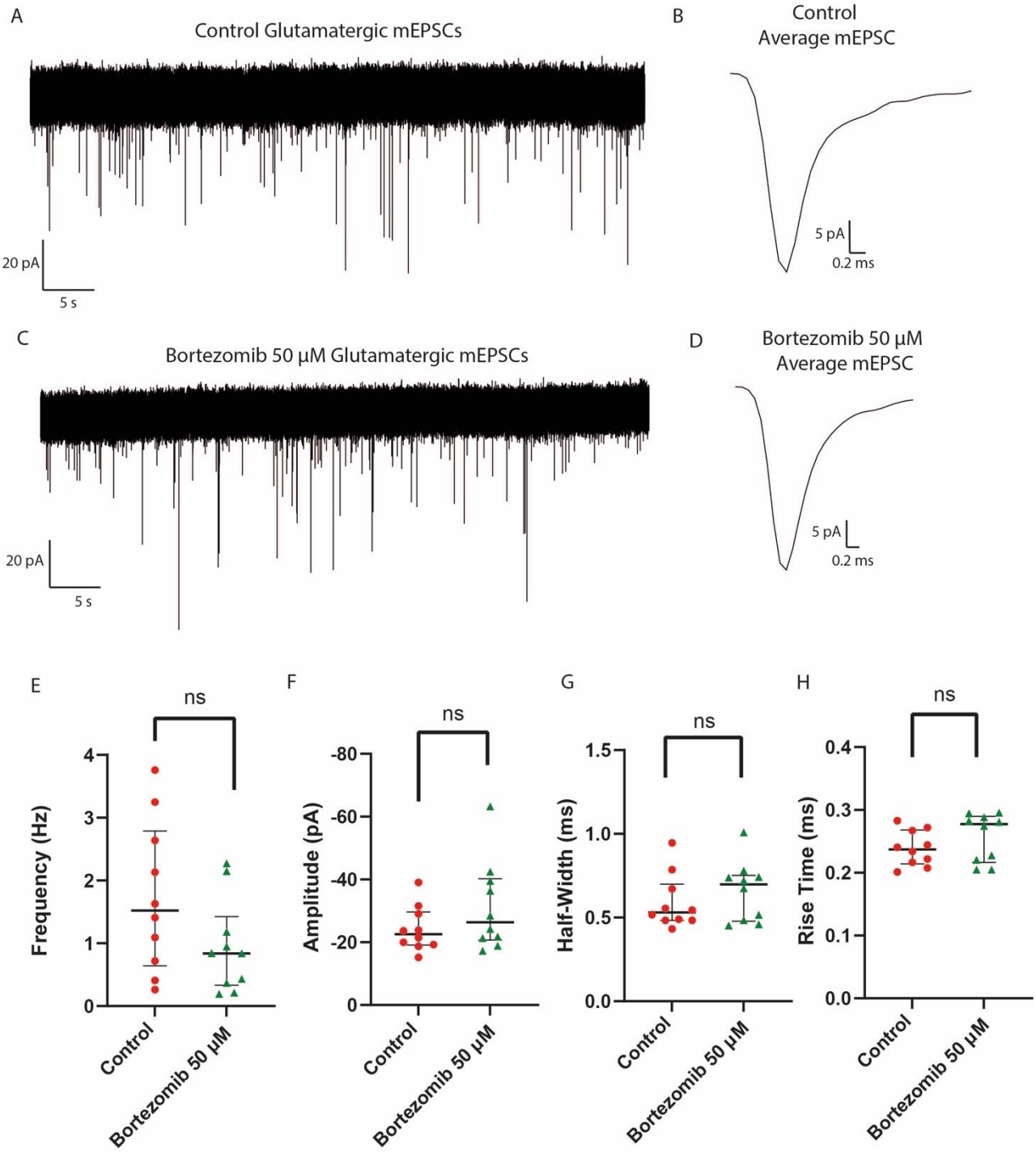


*Figure 25. Short incubation with proteasome inhibitor bortezomib does not effect glutamatergic mEPSCs isolated from MNs in spinal cord of zebrafish larvae.*

*A-B) Example 60 s voltage clamp trace of glutamatergic mEPSCs from MNs treated with 0.05% DMSO control saline and an average mEPSC (B) taken from the trace displayed in A. C-D) Example 60 s voltage clamp trace of glutamatergic mEPSCs from MNs treated with 50 µM Bortezomib and an average mEPSC (B) taken from the trace displayed in A. E-H) Median with interquartile range plots showing mEPSC paramters for cells treated with 50 µM Bortezomib compared 0.05% DMSO control saline. No significant difference was detected between mEPSC frequency, amplitude, half-width or rise time for cells treated with bortezomib compared to control.*

### 4.3.3 The effect of short proteasome inhibition on the firing properties of larval MNs

Next, I sought to determine whether brief 1-hour inhibition of the proteasome influenced intrinsic firing properties of MNs in the larval zebrafish spinal cord at 4-dpf, larvae were pre-incubated for 1-hour in MG132 (10 µM, N = 7, n = 12) or control saline containing 0.01% DMSO (N = 6, n = 11). Whole-cell current clamp protocols of 400 ms with 10 pA steps were used to determine firing properties.

No significant difference was observed between the frequency ($p = 0.864$, MG132: 152.50 ± 26.30 Hz, control: 152.5 ± 29.23 Hz; Figure 26A, C, E), amplitude ($p = 0.176$, MG132: 16.21 ± 3.89 mV, control: 18.76 ± 2.27 mV; Figure 26A, C, F), half-width ($p = 0.614$, MG132: 0.26 ± 0.017 ms, control: 0.26 ± 0.020 ms; Figure 26A, C, G), rise time ($p = 0.285$, MG132 0.11 ± 0.008 ms, control: 0.11 ± 0.014 ms; Figure 26A, C, H) or rheobase ($p = 0.139$, MG132: 95.00 ± 18.99 pA, control: 100.00 ± 24.94 pA; Figure 26A, C, I) for MNs treated with MG132 compared to control. However, there was a significant decrease in the threshold voltage of MNs treated with MG132 compared to controls ($p < 0.0001$, MG132: -62.25 ± 3.60 mV, control: -46.40 ± 10.10 mV; Figure 26 A, C, J).

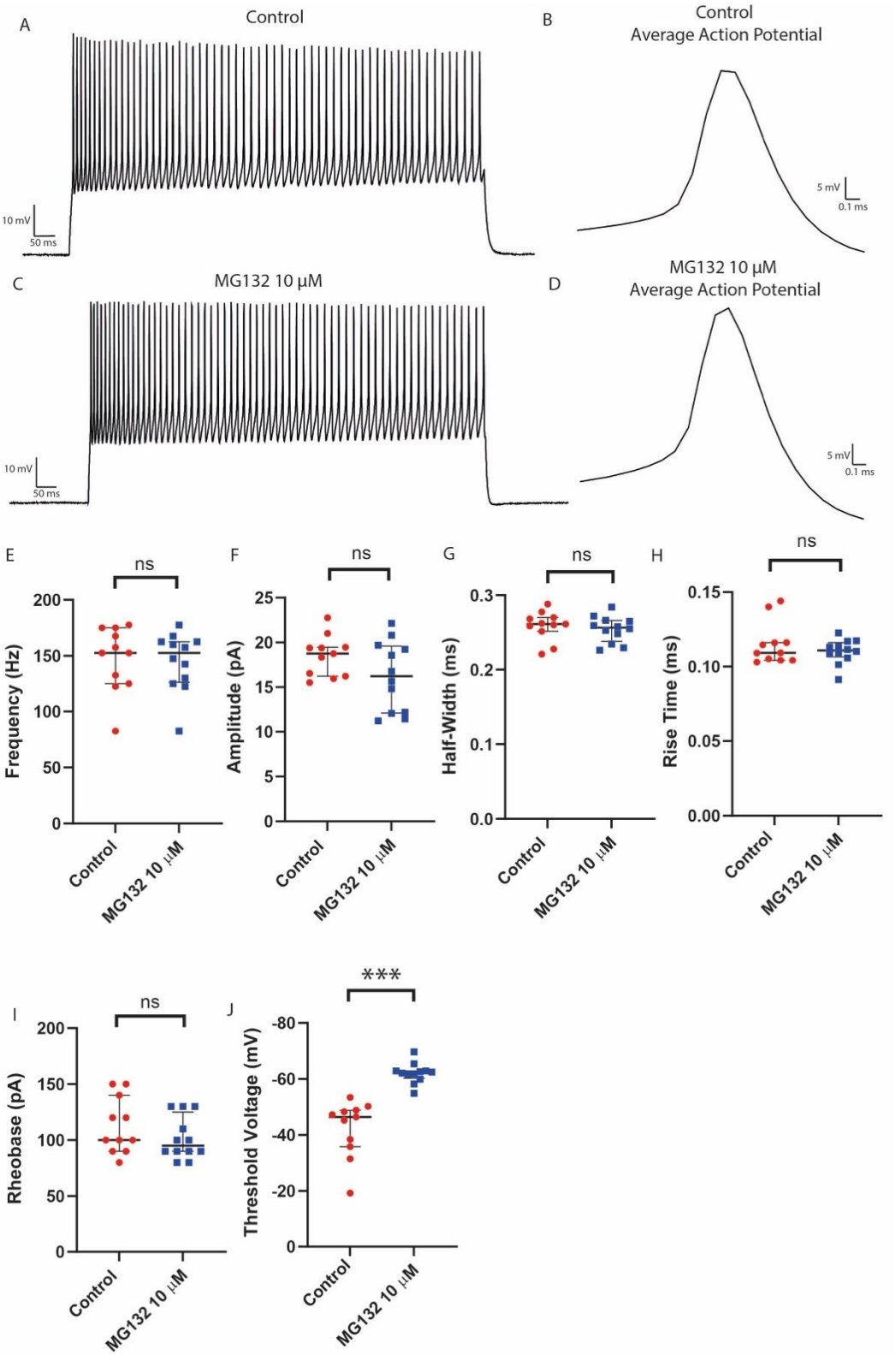


*Figure 26. Short incubation with proteasome inhibitor MG132 decreases threshold voltage for generating action potentials isolated from MNs in spinal cord of zebrafish larvae.*

*Current clamp protocols with 400 ms 10 pA steps were used and firing properties analysed at 2 x Rheobase. A-B) An exemplar 60 s current clamp trace from a MN treated with 0.01% DMSO control saline and an average action potential (B) taken from the trace shown in A. C-D) An exemplar 60 s current clamp trace from a MN treated with 10 µM MG132 and an average action potential (D) taken from the trace shown in C. E-J) Median with interquartile range plots showing action potential parameters. No significant difference was determined between the frequency, amplitude, half-width, rise time or rheobase for MNs treated with either 10 µM MG132 or 0.01% DMSO control. A significant decrease in threshold voltage of cells treated with MG132 compared to controls was observed. *** = $p < 0.0005$*

Firing properties were examined in MNs that had been pre-incubated in bortezomib (50 µM, N = 4, n = 10) and compared to larvae bathed in control saline containing 0.05% DMSO control (N = 5, n = 10). No significant difference in the frequency (p = 0.816, bortezomib: 165.0 ± 30.91 Hz, control: 181.3 ± 34.03 Hz,Figure 27 A, C, E), amplitude (p = 0.942, bortezomib: 19.92 ± 2.71 mV, control: 20.22 ± 4.88 mV; A, C, F), half-width (p = 0.0537, bortezomib: 0.22 ± 0.018 ms, control: 0.20 ± 0.021 ms;Figure 27 A, C, G), rheobase (p = 0.541, bortezomib: 115.0 ± 30.55 pA, control: 115.0 ± 37.25 pA; Figure 27A, C, I) threshold voltage (p = 0.28, bortezomib: -42.75 ± 3.01 mV, control: 46.85 ± 4.99 mV,Figure 27 A, C, J) were determined for cells treated with bortezomib compared to control. However, a significant increase was observed in action potential rise time (p = 0.00312, bortezomib 0.12 ± 0.12 ms, control: 0.10 ± 0.016 ms; Figure 27A, C, H).

To conclude, MG132 treatment resulted in an increased threshold voltage for action potential generation following short (1-hour) and chronic (overnight, Chapter 3) incubation. By contrast, bortezomib produced a selective increase in the action potential rise time following short (1-hour) pre-incubation.

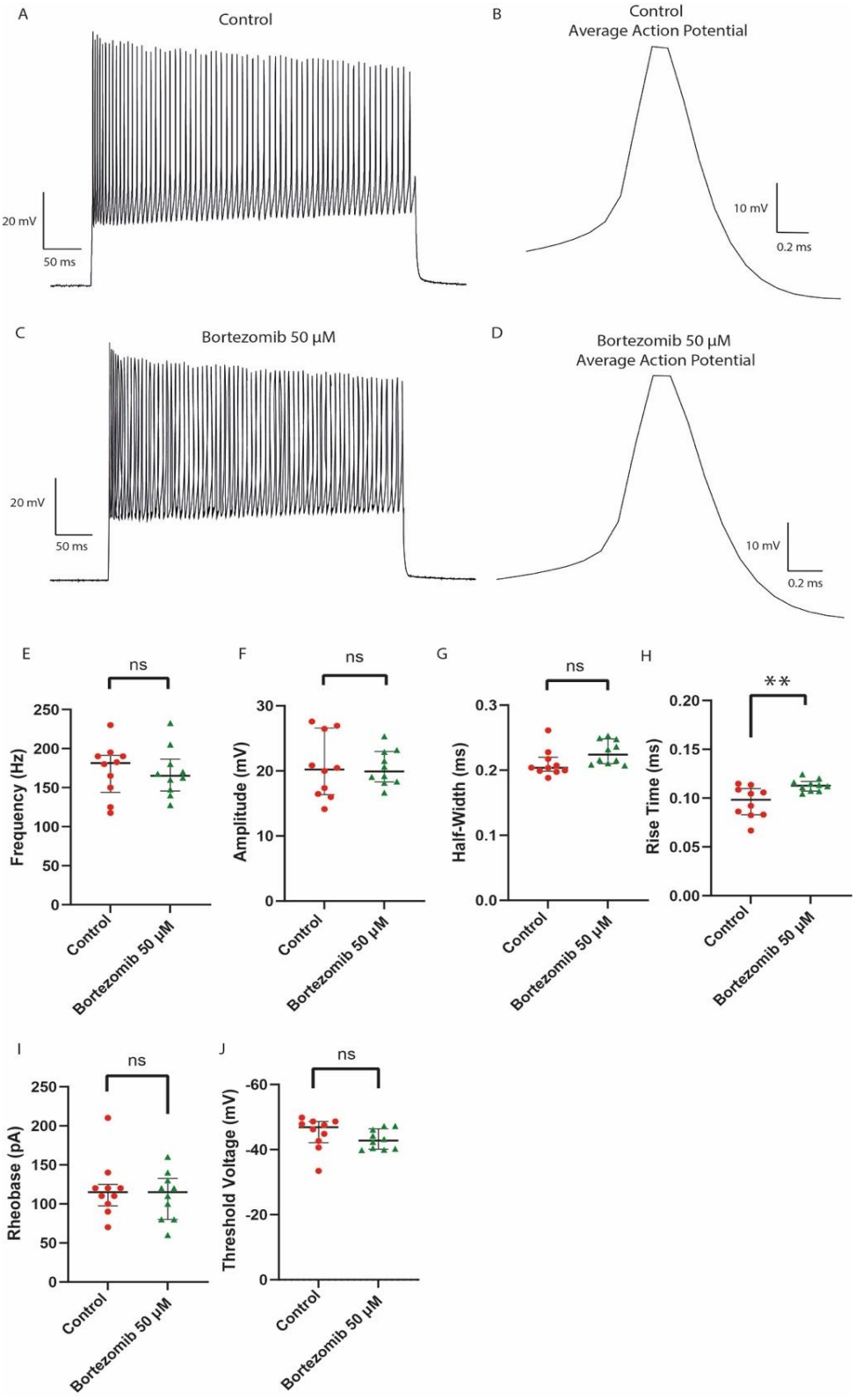


*Figure 27. Short incubation with proteasome inhibitor MG132 increases rise time of action potentials isolated from MNs in spinal cord of zebrafish larvae.*

*Current clamp protocols with 400 ms 10 pA steps were used and firing properties analysed at 2 x Rheobase A-B) An exemplar 60 s current clamp trace from a MN treated with 0.05% DMSO control saline and an average action potential (B) taken from the trace shown in A. C-D) An exemplar 60 s current clamp trace from a MN treated with 50 µM Bortezomib and an average action potential (D) taken from the trace shown in C. E-J) Median with interquartile range plots showing action potential parameters. No significant difference was determined between the frequency, amplitude, half-width, threshold voltage or rheobase for MNs treated with either 50 µM Bortezomib or 0.01% DMSO control. A significant increase in the rise time ($p = 0.00312$) of action potentials was determined for MNs treated with 50 µM Bortezomib compared to DMSO control. ** = $p < 0.005$.*

### 4.3.4 Control recordings to determine stability of glycinergic mIPSCs and glutamatergic mEPSCs over a 30-minute period

The stability of whole-cell patch clamp recordings can degrade over time due rundown arising from dialysis of the intracellular environment. In order to investigate the effects of shorter incubation periods (minutes rather than hours), I first carried out control experiments to determine the stability of 30-minute recordings from MNs.

First I isolated glycinergic mIPSCs using Evans physiological saline containing sodium channel blocker TTX (1 µM), pan-glutamate receptor antagonist kynurenic acid (10 mM) and pan-GABA receptor antagonist picrotoxin (100 µM). MNs (N = 5) were recorded for 10-minutes in control saline containing 0.01% DMSO, before bath perfusion with additional control saline for 10-minutes to mimic addition of proteasomal inhibitors. The recording was continued for a further 5-minutes for analysis.

No significant difference was detected in glycinergic mIPSC frequency ($p = 0.4486$, MG132: 4.45 ± 1.41 Hz, control: 3.96 ± 1.33 Hz; Figure 28 A, C, E, I), amplitude ($p = 0.6816$, MG132: -57.95 ± 24.74 pA, control: -43.92 ± 14.75 pA; Figure 28 A, C, F, J) or rise time ($p = 0.4167$, MG132: 0.51 ± 0.072 ms, control: 0.48 ± 0.067 ms; Figure 28 A, C, H, L) of mIPSCs during 30-minutes of recording in control saline. However, a significant increase in the half-width ($p = 0.0029$, MG132: 3.50 ± 0.99 ms, controls: 2.10 ± 0.61 ms; Figure 28 A, C, G, K) of glycinergic mIPSCs during 30-minute control recordings was observed. In summary, 30-minute control recordings of isolated mIPSCs showed significant increases in half-width, indicative of cellular rundown. However, they did not show significant increases in glycinergic mIPSC frequency.

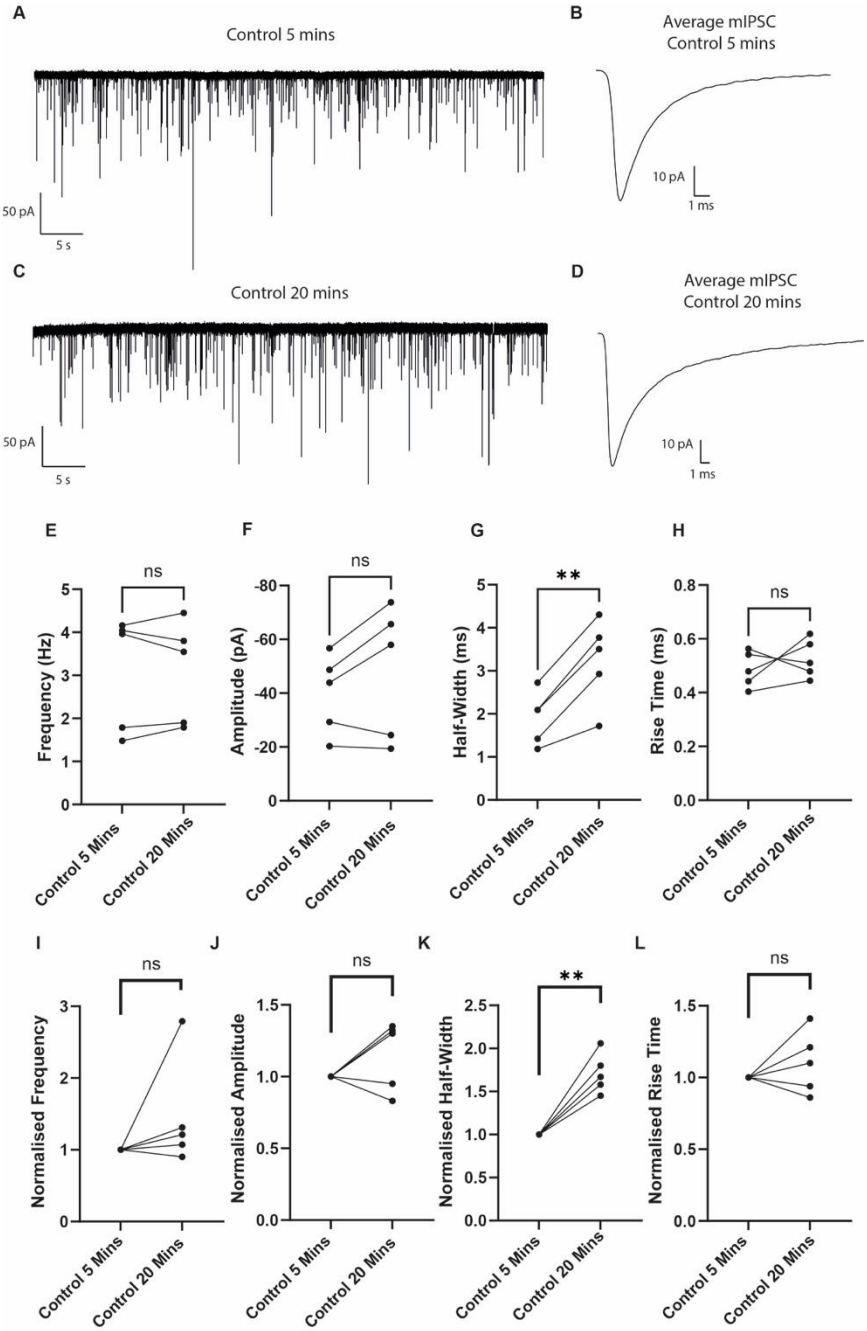


*Figure 28. Control recordings of glycinergic mIPSCs from MNs recorded for 25 minutes in control saline showed an increase in mIPSC half-width*

*A-D) Representative glycinergic mIPSC recordings from a MN treated for 25 minutes with control DMSO saline. A-B) An example 60 s trace of glycinergic mIPSCs from a MN treated with control saline for 7 minutes and an average mIPSC (B) from this trace. C-D) An example 60 s trace after 20 minutes of recording glycinergic mIPSCs in DMSO control saline. Further saline was introduced to the preparation after 7 minutes to simulate the application of MG132 saline in experiments displayed in Figure 31. E-H) Plots showing recordings for glycinergic mIPSC parameters in the first 5 minutes of recording and then after 20 minutes of recording in control DMSO saline. A significant decrease in the amplitude ($p = 0.0463$) of mIPSCs was detected after 20 minutes of recording. I-L) Plots showing normalised data for glycinergic mIPSC frequency, amplitude, half-width and rise time. A significant decrease in amplitude ($p = 0.0463$) of mIPSCs was determined after 20-minutes of recording. Significance values: $p < 0.005$ = **.*

A series of 30-minute control recordings were also obtained isolating glutamatergic mEPSCs. Experimental design remained the same as control recordings isolating glycinergic mIPSCs, however control saline in glutamatergic mEPSC recordings contained sodium channel blocker TTX, glycine receptor antagonist strychnine and GABA antagonist picrotoxin. Following 30-minute control recordings isolating glutamatergic mEPSC (N = 5), no significant difference was detected in the frequency ($p = 0.1788$, MG132: 2.16 ± 3.96 Hz, control: 4.68 ± 2.60 Hz; Figure 29 A, C, E, I), half-width ($p = 0.0532$, MG132: 0.66 ± 0.18, control: 0.77 ± 0.11 ms; Figure 29 A, C, G, K) or rise time ($p = 0.1332$, MG132: 0.38 ± 0.38 ms, control: 0.39 ± 0.044 ms; Figure 29 A, C, H, L) after 20-minutes of recording. A significant decrease in the amplitude ($p = 0.0463$, MG132: -13.85 ± 21.22 pA, controls: -24.88 ± 15.82 pA; Figure 29A, C, E, J) of mEPSCs was detected after 20-minutes of recording. The significant changes in amplitude and half-width for mEPSCs indicates that prolonged dialysis of MNs is occurring.

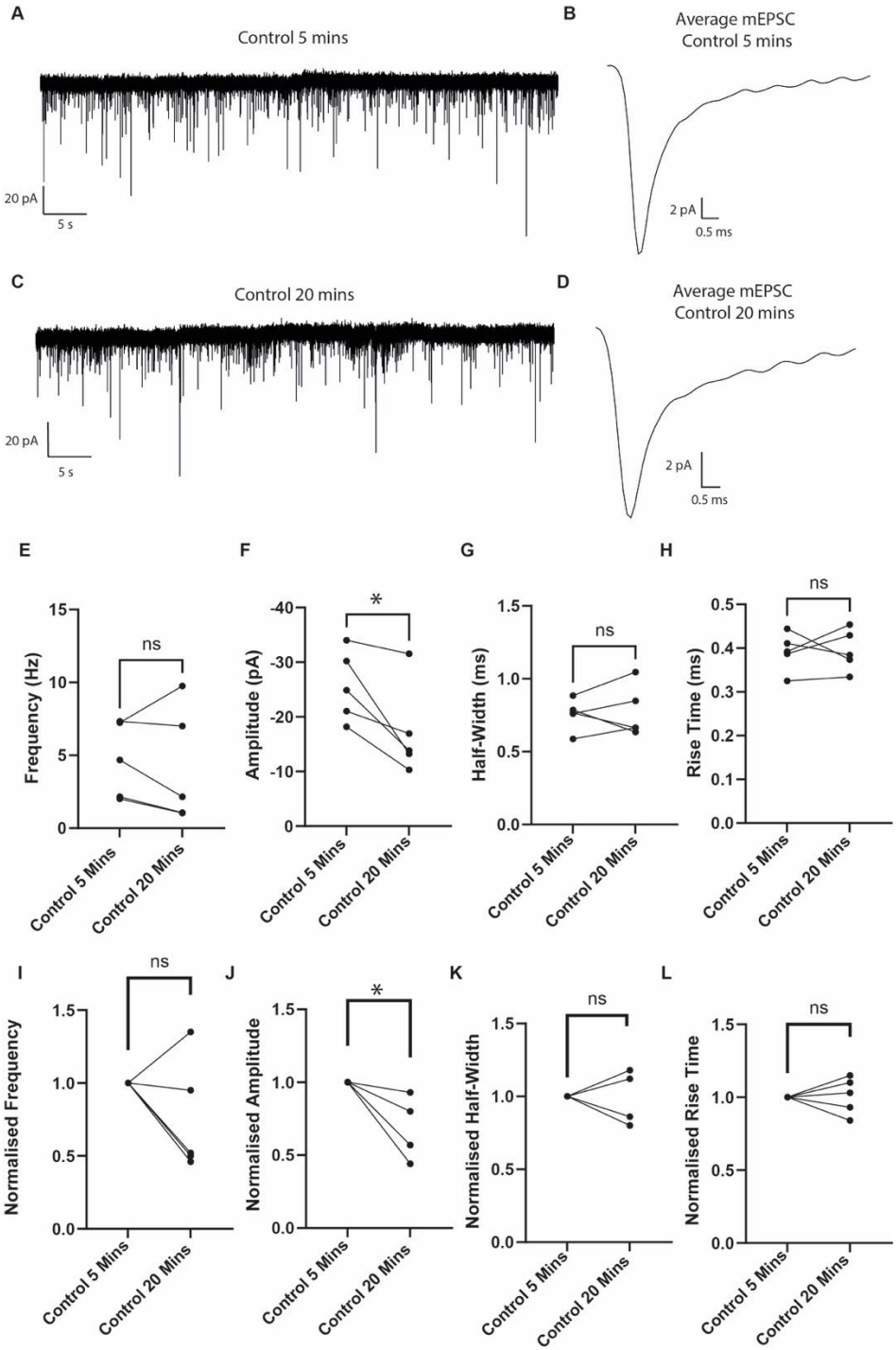


*Figure 29. Control recordings of glutamatergic mEPSCs from MNs recorded for 25 minutes in control saline showed a decrease in mEPSC amplitude.*

*A-D) Representative recordings from a MN treated for 25 minutes with control DMSO saline. A-B) An example 60 s trace of glutamatergic mEPSCs from a MN treated with control saline for 7 minutes and an average mEPSC (B) from this trace. C-D) An example 60 s trace after 20 minutes of recording mEPSCs in DMSO control saline. Further saline was introduced to the preparation after 7 minutes to simulate the application of MG132 saline in experiments displayed in Figure 31. E-H) Plots showing paired recordings for mEPSC parameters in the first 5 minutes of recording and then after 20 minutes of recording in control DMSO saline. A significant decrease in the amplitude ($p = 0.0463$) of mEPSCs was detected after 20 minutes of recording*

### 4.3.5 The effect of 15-minute application of proteasome inhibitor MG132 on glycinergic mIPSC parameters

As glycinergic mIPSCs frequency is not affected by dialysis of MNs during control recordings, I was able to investigate the effects of brief proteasome inhibition of synaptic release. The effect on mIPSCs was examined with whole-cell voltage clamp recordings of MNs in zebrafish larvae (4-dpf). Preparations were perfused with control Evans electrophysiology saline containing sodium channel blocker TTX, pan-glutamate receptor antagonist kynurenic acid and GABA receptor antagonist pictrotoxin. Control saline contained 0.01% DMSO. Recordings of mIPSCs were obtained from MNs bathed in control saline for 10 minutes before perfusion with MG132 (10 µM) for 15 minutes. Changes in mIPSC properties were monitored for a following 5 minutes, resulting in a 30 minute recording. A significant increase was detected for both mIPSC frequency ($p = 0.0061$, MG132: 2.38 ± 0.69 Hz, control: 1.47 ± 0.71 Hz; Figure 30 A, C, E, I) and half-width ($p = > 0.0001$, MG132: 2.93 ± 0.64 ms, control: 1.68 ± 0.62 ms; Figure 30 A, C, H, K). No significant difference between control and MG132 mIPSCs were detected for average mIPSC amplitude ($p = 0.09576$, MG132: -29.67 ± 15.50 pA, control: -32.06 ± 15.50 pA; Figure 30 A, C, F, J) or average rise time ($p = 0.0802$, MG132: 0.53 ± 0.64 ms, control: 0.48 ± 0.62 ms;,Figure 30 C, G, L).

In summary, bath application for 15-minutes with MG132 was sufficient to increase frequency of glycinergic mIPSCs, consistent with results obtained following short (1-hour, Chapter 4) and chronic (overnight, Chapter 3) MG132 treatment. Additionally, following 15-minute bath application of MG132 the half-width of glycinergic mIPSCs increased, consistent with 30-minute control recordings and likely due to the effects of dialysis during whole cell recording.

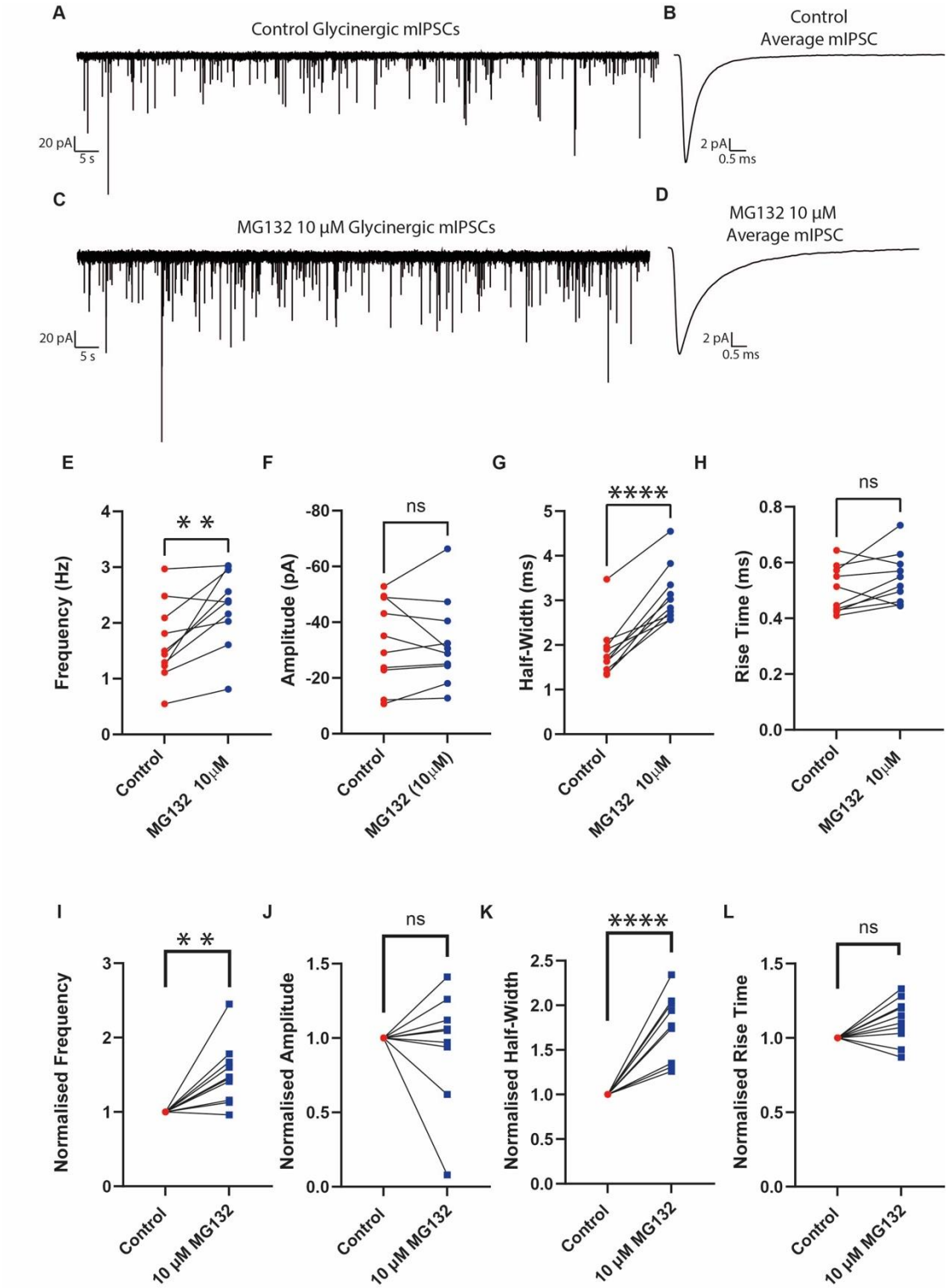


*Figure 30. 15 minute bath application of proteasome inhibitor MG132 increased frequency and half-width of glycinergic mIPSCs recorded from MNs of larval zebrafish.*

*A-D) Recordings of a representative MN treated with control saline for 10 minutes (A-B) followed by application of MG132 (10 µM) for 15 minutes (C-D). A-B) A representative 60 s trace of glycinergic mIPSCs from a MN treated with 0.01% DMSO and an average mIPSC taken from this trace (B). C-D) A representative 60 s trace of glycinergic mIPSCs after 15-minute application of MG132 and an average mIPSC taken from this trace (B). E-H) Plots displaying paired recordings of MNs treated for 10 minutes with control followed by a 15-minute application of 10 µM MG132 showing mIPSC parameters. A significant increase in both the frequency (p = 0.0061) and half-width (p => 0.0001) were detected following application of MG132.*

### 4.3.6 The effect of 15-minute application of proteasome inhibitor MG132 on glutamatergic mEPSC parameters

I next carried out whole-cell voltage clamp recordings isolating glutamatergic mEPSCs. As with recordings of glycinergic mIPSC larvae were first perfused for 10-minutes in control solution and then 15-minutes in MG132 (10 µM, N =10). After 15-minutes of drug application, the MN was recorded for a further 5-minutes and this was analysed in comparison to control. Addition of MG132 resulted in no significant change in glutamatergic mEPSC frequency ($p = 0.174$, MG132: 2.8 ± 0.66 Hz, control: 3.46 ± 1.08 Hz; Figure 31A, C, E, I) or, amplitude ($p = 0.3535$, MG132: -15.04 ± 4.04 pA, control: -15.00 ± 3.78 pA; Figure 31A, C, F, J). However, a significant increase in mEPSC half-width ($p = 0.015$, MG132: 0.85 ± 0.23 ms, control: 0.72 ± 0.13 ms; Figure 31A, C, G, K) and rise time ($p = 0.01$, MG132: 0.36 ± 0.037 ms, control: 0.34 ± 0.037 ms; Figure 31A, C, H, L) was observed. These results suggest that 10-minute bath application of MG132, no significant increase in frequency of events was observed. The observed increase in half-width and rise time is likely due to the dialysis of MNs during whole cell recordings.

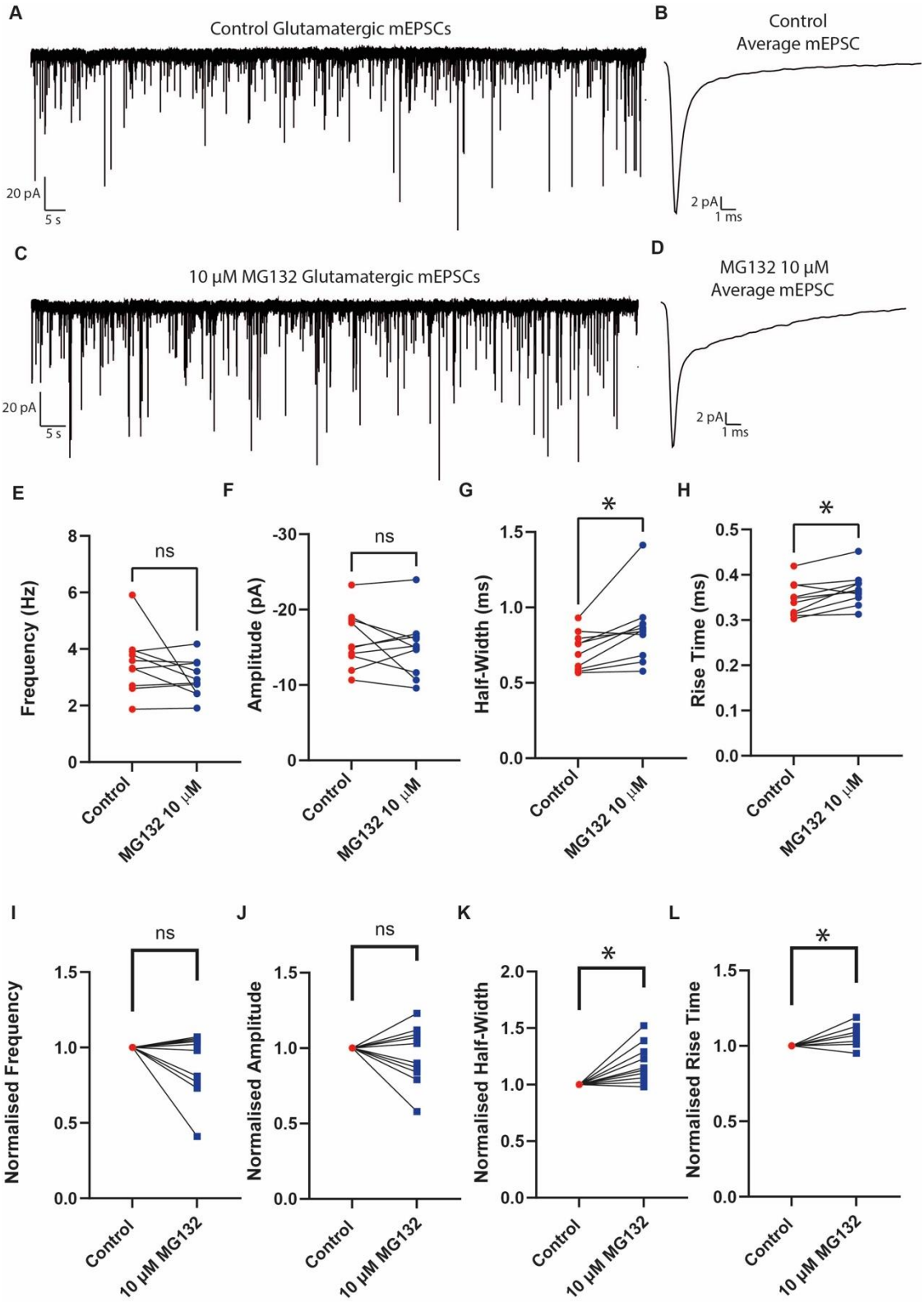


*Figure 31. 15-minute bath application of MG132 increased half-width of glutamatergic mEPSCs recorded from MNs of larval zebrafish.*

*A-D) Recordings of a representative MN treated with control saline for 7-minutes (A-B) followed by application of MG132 (10 µM) for 15-minutes (C-D). A-B) A representative 60 s trace of glutamatergic mEPSCs from a MN treated with control and an average mEPSC taken from this trace (B). C-D) A representative 60 s trace of glutamatergic mEPSCs after 15-minute application of 10 µM MG132 and an average mEPSC taken from this trace (B). E-H) Plots displaying paired recordings of MNs treated for 10 minutes with control followed by a 15-minute application of 10 µM MG132 showing mEPSC parameters. A significant increase in both the half-width (p = 0.015) and rise time (p = 0.01) were detected following application of MG132.*

## 4.4 Discussion

The aim of this chapter was to determine the timescale through which proteasome inhibition exerts its effects on the firing and synaptic properties of MNs. The data presented in this chapter shows that short (1-hour) incubation with both MG132 and bortezomib is sufficient to induce a selective increase in the frequency of glycinergic mIPSCs without affecting other mIPSC parameters. By contrast, 1-hour exposure to proteasome inhibitors had no effect on the frequency or kinetics of glutamatergic mEPSC. Further to this, 15-minute application of proteasome inhibitor MG132 was also sufficient to induce increases in glycinergic mIPSCs. The results observed with a 1-hour incubation of proteasome inhibitors mirror those observed with a longer, overnight incubation (see Chapter 3). This suggests that proteasome inhibition causes a rapid and specific increase in transmitter release at glycinergic synapses.

### 4.4.1 Effect of 1-hour Proteasome Inhibition on Glycinergic mIPSCs of MNs

In order to build on previous experiments carried out in Chapter 3, I investigated the use of a shorter (1-hour) incubation period with proteasome inhibitors to observe if the specific increases in glycinergic mIPSCs occur. As with Chapter 3, I chose to use proteasome inhibitors MG132 and bortezomib to test the effects of short (1-hour) incubation on glycinergic mIPSCs from MNs. Consistent with pervious results, I observed a specific increase in glycinergic mIPSCs following short (1-hour) incubation period with both MG132 and bortezomib. The increase in mIPSC frequency observed here is consistent with previously published work (Rinetti and Schweizer, 2010) showing that evoked and spontaneous release increase following application of MG132 and lactacystin.

The observed decrease in mIPSC half-width and rise time was also observed with short (1-hour) incubation with bortezomib, however this was not an effect observed with short (1-hour) MG132 exposure. The half-width and rise time of glycinergic mIPSC from bortezomib treated larvae also had a larger range compared to control treated MNs. As previous studies have reported the mean turn over time of zebrafish MNs GlyRs was 11.8 hours (Chow et al., 2017). As GlyR density would contribute to the amplitude, half-width or rise time of glycinergic mIPSCs, it is perhaps not surprising that their parameters were not affected by a 1-hour period of proteasome inhibition. Therefore, the observed decreases in

half-with and rise time of mIPSCs isolated from MNs treated with bortezomib are likely due to other post-synaptic changes.

Whilst receptors themselves may not have been internalised or turned over within this time frame, changes in mPSC kinetics are often associated with changes to the gating properties of receptors. Gating properties can be altered by subunit confirmations present within the receptor. Pre-synaptic neurotransmitter release has also been shown to induce post-translational modifications to receptors on the post-synaptic membrane, including phosphorylation which can alter receptor kinetics.

Post-translational modifications stimulated by pre-synaptic neurotransmitter release, including phosphorylation can alter subunit assembly, desensitisation and clustering of receptors. Changes in the gating properties of the receptors would account for changes in kinetics. Different subunit confirmations directly influence gating properties of ligand-gated receptors, including glycine receptors (Twyman and Macdonald, 1991, Barberis et al., 2011). Pre-synaptic neurotransmitter release can also influence post-translational modifications to receptors on the post-synaptic membrane. These modifications include phosphorylation, which can affect subunit conformation and clustering of receptors. (Swope et al., 1992, Han et al., 2013). Phosphorylation of the $\alpha$2 glycine subunit induces a conformational change in the ligand binding site, resulting in decreased mIPSC kinetics (Islam et al., 2018). Glycine receptors are regulated through ubiquitination and degradation by the proteasome, hence inhibition of the proteasome could be contributing to changes in receptor conformation (Lin and Man, 2013).

Clustering of receptors has also been shown to alter PSC kinetics, with receptor cluster sizing resulting in large variation in mIPSCs amplitude and kinetics (Lim et al., 1999, Oleskevich et al., 1999). Variations in receptor clustering can suggest differences in synaptic scaffolding proteins present. Gephyrin in particular has been associated with the clustering of inhibitory receptors GABA and glycine (Feng et al., 1998, Cabot et al., 1995). Whilst there is a lack of evidence that gephyrin is degraded by the proteasome, gephyrin does contain two PEST (a peptide sequence linked to protein degradation) sequences (Meyer et al., 2011, Tyagarajan et al., 2011, Prior et al., 1992). PEST sequences are motifs found within protein structures that are rich in proline, glutamic acid, serine and threonine which acts as a signal for rapid proteolysis within cells (Rechsteiner, 1990). PSD-95 (a scaffolding protein associated with excitatory synapses) contains PEST sequences and has been shown to be

ubiquitinated for subsequent proteasomal degradation (Colledge et al., 2003). As such, the existence of ubiquitination sites within the protein structure indicate that regulation by the proteasome could be possible. Hence, mIPSC kinetic changes displayed here could be due to increased gephyrin available to modulate receptor clustering. Further work would be needed to determine if these changes in mIPSC half-width and rise time were due to changes in receptor conformation. However, as the main focus of this chapter was on the increases to glycinergic mIPSC frequency, this further work was beyond the scope of this thesis.

The selective increase in glycinergic mIPSCs as a result of short (1-hour) incubation periods indicate that more quanta of glycine are being released into the synaptic cleft, resulting in an increase in mIPSCs. In these spinalised preparations, hindbrain connections are severed from the spinal cord, hence pre-synaptic connections would primarily come from interneurons that make up the CPG of the zebrafish spinal cord (Grillner, 2003).In the zebrafish spinal cord, MNs are innervated by INs from within the spinal cord (Berg et al., 2018a). These results indicate that there is an increase in input from the inhibitory INs innervating the MNs. This increase in synaptic input could be due to changes within the synapse resulting in increased release of vesicles due to changes in synaptic machinery or could be due to changes in the number of synapses innervating the MNs.

### 4.4.2 Effect of 1-hour incubation on glutamatergic mEPSCs of MNs

To investigate the effect of proteasome inhibition on MN glutamatergic mEPSCS, spinalised larvae were incubated for 1-hour with either MG132, bortezomib or control DMSO. As with glycinergic mIPSCs, whole-cell voltage clamp recordings of MNs were taken isolating glutamatergic mEPSCs. 1-hour incubation with proteasome inhibitors did not increase the frequency of glutamatergic mEPSCs. This was consistent with results obtained for Chapter 3, where overnight incubation with MG132, lactacystin and bortezomib did not cause changes to mEPSC frequency. As with results obtained for chapter 1, this contrasts with previously reported results (Rinetti and Schweizer, 2010, Xie et al., 2017). No effect on glutamatergic mEPSC amplitude, half-width or rise time was determined for 1-hour incubation with proteasome inhibitors. This was expected, as no change in glutamatergic

mEPSC frequency, rise time or half-width were determined using MG132 and bortezomib (50 µM) in Chapter 3.

Previously reported results looking at the effect of the proteasome on neurotransmitter release has focused on predominantly on rodent models including the use of a rodent hippocampal cell culture model to determine changes in both evoked and spontaneous neurotransmission (Rinetti and Schweizer, 2010). Species or cell type differences could, therefore, play a role in the different results observed here. New research implicates a role for NMPs in regulating neuronal activity through the degradation of the nascent proteome. Following inhibition of NMPs, nascent polypeptides accumulate in cells, inducing a spontaneous increase in neuronal activity (Ramachandran and Margolis, 2017, Ramachandran et al., 2018, He et al., 2022). The nascent proteome can vary in different cell types, hence inhibition of NMPs in certain cell-types could result in the accumulation of different nascent polypeptides (Wilson and Nairn, 2018, Alvarez-Castelao et al., 2017, Schanzenbächer et al., 2016). Hence, if NMPs are the cause of increased synaptic transmission following proteasome inhibition, this could explain the differential effects seen here with glutamatergic mEPSC and glycinergic mIPSC frequency as different nascent proteomes could be present in excitatory and inhibitory synapses.

### 4.4.3 Effect of 1-hour incubation on firing properties of MNs

No effect on firing frequency, amplitude, half-with or rheobase was determined for MNs treated for 1-hour with MG132 or bortezomib compared to MNs treated with control. This was expected, as no effect in these parameters was observed with overnight incubation.

However, a significant increase in the rise time of action potentials was observed for larvae incubated for 1-hour in 50 µM bortezomib compared to control. This difference in rise time was not observed during overnight incubation with 50 µM bortezomib. This increase in rise time could suggest a change in sodium channels present, as a faster rise time would indicate more sodium channels opening and hence increasing the depolarisation of the membrane faster. Voltage-gated sodium channels ($Na_v$) form clusters on excitable cells and have been shown to be degraded by the UPS (Ogino et al., 2015). Therefore, this effect could be a true effect of proteasome inhibition, resulting in increased density of $Na_v$.

However, as this effect was observed only after 1-hour incubation and not after overnight incubation, it is unlikely that this is an effect of greater receptor clustering. As the same effect was not seen with MG132, it is also unlikely that this is due to the effect of directly inhibiting the proteasome. The increase in rise time could be due to an off-target effect of bortezomib or could be due to large biological variability in the control data.

A significant decrease in the threshold voltage was observed following 1-hour incubation with MG132 compared to control data. A decrease in threshold voltage was also observed following overnight incubation with MG132. Threshold voltage is dependent on sodium channels which are important for the controlling the depolarisation of the membrane. $Na_v$ channels have previously been shown to be internalised and degraded via ubiquitination and subsequent proteolysis via the proteasome (See Chapter 3 Introduction) (Rougier et al., 2005, Fotia et al., 2004). Hence, proteasomal inhibition could result in increase sodium ion channels present on the neuronal membrane, lowering the threshold voltage required to elicit an action potential. However, as this decrease was not observed following overnight or 1-hour incubation with bortezomib, it is unlikely that this significant decrease in threshold voltage is due to the effect of proteasome inhibition. MG132 is also a known to inhibit calpains (Tsubuki et al., 1996). Calpains are calcium activated proteases present ubiquitously within cells (Croall and Ersfeld, 2007, Wu and Lynch, 2006). Calpains regulate $Na_v$ channels, with activated calpains being associated with a decrease in $Na_v$ expression (Magby and Richardson, 2015). Calpains have also been shown to be required for the proteolysis of the $\alpha$-subunit of $Na_v$ channels, resulting in the breakdown of $Na_v$ channels and their removal from the membrane (von Reyn et al., 2009). Threshold voltage has been shown to be dependent on ion channel densities, most notably $Na_v$ channel membrane density (Platkiewicz and Brette, 2010). Therefore, this variation in threshold voltage observed with MG132 could be due to its role as a calpain inhibitor instead of due to proteasome inhibition. Further work would need to be done to determine if these changes are due to calpain inhibition, however this is beyond the scope of this thesis.

### 4.4.4 The Effect of 15-Minute Application of MG132 on Glycinergic mIPSCs

A previous study in rat hippocampal cell culture had shown increases in mIPSC and mEPSC frequency after only 10-minute application of proteasome inhibitors . Amplitude and

kinetics of mIPSCs and mEPSCs remained unaffected in these experiments (Rinetti and Schweizer, 2010). Here, a 15-minute bath perfusion with MG132 (10 µM) showed no significant difference in the amplitude or rise time of mIPSCs compared to control. However, there was a significant increase in the frequency and the half-width of glycinergic mIPSCs following MG132 application. The increase in frequency of mIPSCs was consistent with data collected for overnight and 1-hour incubation with MG132. This suggests that the observed effects on glycine transmission occur rapidly (within minutes) and are capable of affecting pre-synaptic quanta release within that time frame.

However, the significant increase in the half-width of mIPSCs following 15-minute MG132 perfusion was not consistent with previous results for overnight or 1-hour incubation. The recordings carried out for the 15-minute application of proteasome inhibitors require recording from the MNs for 30 minutes. As this is longer than the 10-minute recordings previously carried out, I hypothesised that this increase in half-width could be due to rundown of the neurons due to dialysis. During whole-cell patch clamp recordings, the patched neuron is filled with extracellular solution within the patch pipette, hence washout of essential signalling molecules which homeostatically regulate receptor properties can occur when cells are held for long periods (Belles et al., 1988).

To assess if this was the case, I carried out control recordings for 30-minutes, with further application of control Evans solution after 15-minutes to simulate the introduction of MG132 Evans during mIPSC recordings. No significant difference was observed in the frequency, amplitude or rise time of glycinergic mIPSCs during 30-minute control recordings, however a significant increase in the half-width was determined. This is likely due to the length of the recording. In addition to this, the relatively small size of zebrafish MNs compared to the size of the patch clamp pipette means that increase in the overall series resistance start to occur over longer recording periods. Changes in series resistance, particularly changes in access resistance, leads to changes in recorded currents. Hence, the significant change in shape over time is likely due to changes in the quality of the patch overtime.

A significant difference in the frequency of glycinergic mIPSCs was not observed during control recordings. This suggests that the increase in frequency of mIPSCs was due to proteasomal inhibition during 30-minute recordings with MG132. This result indicates that the effects of proteasomal inhibition on glycinergic transmission can occur within minutes.

### 4.4.5 The Effect of 15-minute MG132 Application on Glutamatergic mEPSCs

Recordings of glutamatergic mEPSCs with 10-minute control saline and 15-minute bath application of MG132 (10µM) were also obtained. As with overnight and 1-hour application of MG132, no significant difference was determined between control recordings and recordings following 15-minute MG132 application for glutamatergic mEPSCs. However, a significant increase in half-width and rise time was observed following 15-minute application of MG132.

As with glycinergic mIPSC recordings with 15-minute application of MG132, due to changes in the half-width and rise time of mEPSCs following MG132 perfusion, I carried out 30-minute control recordings using DMSO control Evans solution to imitate the addition of MG132 after the initial 10-minute control period. During the control recordings, no significant difference in frequency, half-width or rise time was observed, however a significant decrease in the amplitude was determined. This significant change in amplitude indicates a decrease in the quality of the whole-cell patch clamp configuration, as perfusion of the intracellular patch solution into the cytoplasm can result in changes to the amplitude of recorded currents (Belles et al., 1988).

As a result of the 30-minute control recordings for both glycinergic mIPSCs and glutamatergic mEPSCs coupled with time constraints to the project, I decided not to repeat these experiments using bortezomib as the recordings were not stable enough to provide reliable results.

### 4.4.6 Conclusions

The results presented here in Chapter 5 show that shorter period incubations of 1-hour with proteasome inhibitors bortezomib and MG132, and tens of minutes with inhibitor MG132, are sufficient to increase glycinergic mIPSC frequency. Using both proteasome inhibitors, no increase in amplitude, half-width or rise time was detected in glycinergic mIPSCs following a 1-hour incubation. 1-hour incubation with proteasome inhibitors did not significantly change the frequency, amplitude, half-width or rise time of glutamatergic mEPSCs, which was a finding consistent with overnight incubation with proteasome inhibitors. Firing frequency, amplitude, half-width and rheobase were not affected by 1-hour application of proteasome inhibitors. Whilst rise time was increased with bortezomib 1-hour incubation and threshold voltage was decreased following MG132 incubation, as

these results were not consistent across both proteasome inhibitors, this could still be due to proteasomal inhibition, but I cannot rule out off-target effects of these drugs.

Following 15-minute bath application of MG132, glycinergic mIPSC frequency did increase, whilst no increase in glutamatergic mEPSCs was observed. However due to the changes in amplitude and half-width of mIPSCs and mEPSCs obtained during 30-minute control recordings, I determined that these recordings were not stable enough to draw true conclusions about the effect of 15-minute bath application of proteasome inhibitors.

Following both overnight and 1-hour application of proteasome inhibitors an increase in glycinergic mIPSCs was observed. I hypothesise that this effect is due to a change in the number of glycinergic synapses as a result of aberrant growth of axons and dendrites of MNs. Therefore, in Chapter 5 of this thesis I will investigate the effect of proteasome inhibition on mEPCs from embryonic white muscle cells (EWM). I will then use immunohistochemistry staining to determine the effect of proteasome inhibition on the growth of axons and dendrites of MNs in larval zebrafish (4-dpf).

# Chapter 5 The Effect of Proteasomal Inhibition on Synaptic Release at the Neuromuscular Junction and Outgrowth of Motoneurons

## 5.1 Introduction

In Chapter 3 and Chapter 4 of this thesis, I have shown that pharmacological inhibition of the proteasome results in an increase in the frequency glycinergic mIPSCs occuring on MNs, but has no effect on the frequency of glutamatergic mEPSCs. This effect on mIPSCs appears to occur on a rapid timeframe (within 15 minutes of proteasome inhibition). In this Chapter, I have chosen to focus on the effects of chronic incubation of proteasome inhibitors on neurotransmission at the NMJ. Moreover, I examine the effects of proteasome block on innervation of MN branching and NMJ formation in larval zebrafish.

### 5.1.1 Zebrafish Muscle Development

The axial musculature of teleost fish drive undulating body movement during swimming which propel the fish through the water. They are primarily composed of: red, intermediate and white muscle fibres. In adult zebrafish, a further two minor groups of musculature develop from the red and white muscle fibres; red muscle rim and scattered intermediate fibres respectively. Hatched larvae contain only red and white muscle fibres, with differentiation of intermediate muscle and the minor subgroups red muscle rim and scattered intermediate fibres occurring in the subsequent four weeks of development (van Raamsdonk et al., 1978, van Raamsdonk et al., 1982).

In zebrafish, axial muscle development starts during primary myogenesis within the paraxial mesoderm. During this period, somite segmentation and morphogenetic changes occur concurrently to give rise to distinct cell populations including adaxial cells, which are the pre-cursor for both red and white muscle fibres (Hollway et al., 2007, Stellabotte et al., 2007, Stellabotte and Devoto, 2007, Stickney et al., 2000).

As with MNs in the spinal cord, the different groups of muscle fibres develop to allow for the transition from burst swimming to sustained swimming (McLean et al., 2007, Brill and Dizon, 1979). The slow twitch red muscle fibres utilise aerobic metabolism, working at slower contraction speeds and fatiguing slowly, whereas fast twitch white muscle fibres utilise anaerobic metabolism to generate rapid contractions but are readily fatigable. The

red muscle fibres are situated in the superficial myotome, whereas white muscle fibres are found in the deep myotome layer (van Raamsdonk et al., 1982, Devoto et al., 1996, Buss and Drapeau, 2000). Electrophysiological data shows that the inner white muscle fibres generate action potentials whilst the outer red fibres do not (Buckingham and Ali, 2004).

Muscle fibres are innervated by motoneurons. Each of the three PMNs (CaP, MiP, RoP) found within a myotomal segment innervate individual muscle fibres. CaP and RoP (dRoP and vRoP) MNs innervate muscle fibres on the lateral side of the zebrafish whilst MiP motoneurons exclusively innervate dorsal musculature. CaP MN arbors branch into the deep ventral muscle, whilst RoP arbors innervate the dorsal musculature closest to the spinal cord of the ventral hemisegment. PMNs innervate musculature solely within their own hemisegment of the spinal cord and do not show overlapping innervation patterns into adjacent hemisegments. In addition to innervation from PMNs, individual muscle fibres also receive additional input from up to three SMNs (Westerfield et al., 1986).

Groups of muscle fibres and the MNs that innervate them are collectively known as motor units (Heckman and Enoka, 2012, Bello-Rojas et al., 2019). These motor units are involved in regulating swimming behaviours and speeds. 'Fast' motor units, consisting of fast twitch fibres and larger MNs, and 'slow' motor units containing slow twitch muscle fibres and smaller MNs (Fetcho, 1992).

### 5.1.2 The UPS and the Neuromuscular Junction

The NMJ is a specialised synapse made up of presynaptic motoneuron nerve terminals converging onto a post-synaptic muscle fibre. Action potentials from the motor nerve terminal result in the release of acetylcholine into the synaptic cleft, which binds to nicotinic acetylcholine receptors (nAchR) situated on the muscle fibre. This causes end plate potentials, which result in muscle fibre contraction (Rodríguez Cruz et al., 2020).

The UPS has been implicated in regulating the development and function of the NMJ (Bachiller et al., 2020, Kowalski and Juo, 2012a). For example, several different E3-ubiquitin ligases have been identified as key modulators of NMJ function and development: loss of function of the APC/C E3-ligase leads to overgrowth of pre-synaptic boutons at the *Drosophila* NMJ (van Roessel et al., 2004). Transgenic mice overexpressing PDZRN3, an E3-ligase located within skeletal muscles, was shown to lead to reduced growth and maturation

of the NMJ (Lu et al., 2007). Defects in E3-ligases have also been associated with neuromuscular disorders. In the congenital neuromuscular disorder nemaline myopathy, thread-like protein aggregates composing of ACTN1 (Actinin alpha 1; referred to as nemaline bodies) are present in patients. The *KBTD13* mutation in E3-ligase Cullin-3 causes the accumulation of ACTN1 nemaline bodies in skeletal muscle. KO of skeletal muscle Cullin-3 in mice showed disorganisation in the AChR (Acetylcholine receptor) clustering at the NMJ of skeletal muscle. In summary, dysfunction in the UPS due to specific mutations or KO of Cullin-3, an E3 ligase, results in defective NMJ maturation and AChR clustering, implicating defects in the UPS in the pathogenesis of neuromuscular disorders (Blondelle et al., 2019).

USP14, a DUB associated with the removal of Ub from substrates once they are bound to the proteasome, has been implicated as being associated with ataxia in mice (Chen et al., 2009, Wilson et al., 2002, Bhattacharyya et al., 2012). *Usp14* undergoes alternative splicing, resulting in the formation of a full length Usp14 protein which can associate with the 26S proteasome to aid in the removal of ubiquitin from tagged proteins. The *Usp14-ax*$^{J}$ mutant does not produce full-length Usp14 proteins. This phenotype can be rescued by introduction of full length Usp14 protein to ataxia mice (Crimmins et al., 2006). Furthermore, *Usp14-ax*$^{J}$ mice had developmental defects at the NMJ during the first 2 weeks of postnatal development. Pre-synaptic bouton changes occurred including accumulation of neurofilaments within the axon terminal and nerve terminal swelling including sprouting of the nerve terminals and aberrant aborisation. The post-synapses of the NMJ were also noted to be immature, with defects in the expression pattern of AChRs not displaying the typical 'pretzel-like structures' associated with mature NMJ post-synapses (Sanes and Lichtman, 2001). Moreover, mEPPs (miniature endplate potentials) recorded from *ax*$^{J}$ mice showed a decrease in frequency and an increase in amplitude, indicative of defects at the pre- and post-synapses of the NMJ (Chen et al., 2009, Wilson et al., 2002). Further work in *ax*$^{J}$ showed that these mice display reduced paired pulse facilitation at the NMJ, suggesting that proteasome disruption induces defects in synaptic vesicle recycling (Bhattacharyya et al., 2012). Hence, the use of *Usp14-ax*$^{J}$ and Usp14 KO models has shown that the UPS is important for the development and maturation of both the pre- and post-synapse of the NMJ and that defects in the UPS can result in aberrant nerve terminals throughout skeletal muscle.

### 5.1.3 The UPS and axonal arborisation

In the past 20 years, there has been increasing evidence of the role of the UPS in neurite outgrowth during development. One of the first studies to link the UPS to axonal pathfinding showed that a balance between protein synthesis and degradation is required for axonal outgrowth in *Xenopus* retinal cultures. Netrin-1 is an axon guidance molecule required for neurite outgrowth in retinal growth cones. In the presence of a chemotactic gradient of Netrin-1, retinal cultures stimulate neurite outgrowth towards the Netrin-1 gradient, as Netrin-1 stimulates the phosphorylation of initiation factors involved in protein synthesis to aid in axonal outgrowth (Ming et al., 2002). Inhibiting the proteasome using lactacystin prevented axonal outgrowth in response to a netrin-1 chemotactic gradient, resulting in chemoattraction towards the Netrin-1 gradient (Ming et al., 2002). Furthermore, antibody staining of ubiquitin-conjugates showed an increase in immunofluorescence following netrin-1 application to retinal cultures, indicating that the UPS is required at growth cones and plays a role in axonal outgrowth (Campbell and Holt, 2001).

Further work in *Xenopus* retinal ganglion cells (RGCs) showed that depressing UPS activity through expression of a dominant negative form of Ub (Finley et al., 1994), decreased terminal axon branching in the tectum. Nedd4, an E3 ligase, is expressed in RGC growth cones and is an upstream regulator of PTEN, a protein important for the regulation of the PI3K signalling pathway. PI3K signalling is involved in the reorganisation of cytoskeletal elements and in protein synthesis, hence PI3K and PTEN are important for regulating the morphology of neurons including axonal elongation, guidance and branching. (Cosker and Eickholt, 2007). Branching defects displayed by the dominant negative Ub mutant could be rescued by decreasing levels of PTEN, showing that the UPS is a regulator of neurite outgrowth through regulating the abundance of proteins involved in the PI3K pathway (Drinjakovic et al., 2010).

The E3 ligase Nedd4 has also been identified as a regulator of axonal outgrowth in *Drosophila*. During development, a variety of commissural axons arising from different neuronal cell types cross the midline of the CNS, whereby they continue to grow away from the midline. Hence, certain guidance cues are required to initially attract the axon growth cone towards the midline before being removed to prevent aberrant recrossing. The UPS has been implicated in the regulation of this process. The Slit receptor Roundabout (Robo) is

found in low levels prior to midline axonal crossing, but expression of this receptor is increased following the crossing of the midline. A mutant screen carried out in *Drosophila* produced a number of mutants where axons continue to cross and recross the midline. Previous work had shown that Robo is regulated by a transmembrane protein, Commissureless (Comm). A mutant screen of *comm* mutants showed that axons grow towards the midline, but instead of crossing become repelled and curl away from the midline. Overexpression of Comm results in a phenotype similar to that seen in Robo mutants, showing that Comm is required to downregulate Robo (Kidd et al., 1998). Further work in *Drosophila* showed that comm is a substrate for DNedd4 (*Drosophila* Nedd4) and hence, proteasomal degradation. Furthermore, using a yeast two-hybrid screen showed that comm must be bound to DNedd4 in order for downregulation of Robo to occur (Myat et al., 2002). Hence, the UPS is important for the regulating axon guidance cues needed for appropriate midline crossing in *Drosophila*.

Studies in mice have also shown the importance of the UPS in neurite outgrowth. The E3 ligase F-box protein complex FBXO31-SCF (Skip1/Cullin/F-box, hereby referred to as FBXO31) has been shown to regulate dendritic growth in the cultured mouse cerebellar cortex neurons. FBXO31 was localised to the centrosome (the microtubule organisation centre of eukaryotic cells) of cerebellar granule neurons. Overexpression of FBXO31 resulted in cells displaying non-polarised morphology. Furthermore, Parc6 (a centrosomal protein previously identified in regulating cellular polarity) was shown to be a substrate for the FBXO31 complex. In summary, these experiments suggested that the UPS regulates cellular polarity through the degradation of Parc6 via the E3-ligase FBXO31 (Vadhvani et al., 2013).

F-box protein complexes have also been implicated as regulators of neurite outgrowth and synaptic development in *C.elegans*. In touch receptor neurons (TRNs), mutation of the F-box protein MEC-15 results in decreased microtubule assembly, neurite outgrowth and synaptic development. This phenotype is rescued in double mutant *C. elegans* with mutations in co-chaperone proteins DAF-41, STI-1 or PPH-5. These co-chaperones work in concert with the chaperone proteins Hsp70/90. Hsp90 chaperones have been shown to inhibit neurite growth through the stabilisation of DLK-1 (delta like non-canonical Notch ligand 1) (Zheng et al., 2020). Previous studies have shown that DLK-1 is necessary for axon regeneration and has been associated with neuronal progenitor differentiation in murine and human cell culture models (Surmacz et al., 2012). DLK-1 is also regulated by the E3

ligase RPM-1 (Nakata et al., 2005). Hence, researchers concluded that a balance between the UPS and molecular chaperones is required for functioning neurite outgrowth and synapse development (Zheng et al., 2020).

Finally, studies carried out in *Drosophila* have shown the role the UPS has in synaptic pruning. A careful balance between E3 ligase hiw and the DUB faf are required for correct neurite organisation and synaptic bouton formation. Loss-of-function of hiw or overexpression of faf give rise to the same phenotype of aberrant neurite growth and disorganisation of synaptic boutons (Wan et al., 2000b, DiAntonio et al., 2001a, Collins et al., 2006). UbcD1, an E2-conjugating enzyme of the UPS cascade, has been shown to be involved in the degradation of C4da dendrites in *Drosophila*, aiding in synaptic elimination and allowing for maturation of C4da sensory neurons during metamorphosis to an adult life phase (Kuo et al., 2005, Kuo et al., 2006b). In both of these examples, there is evidence that the UPS is important in developing *Drosophila*, allowing for the maturation of synapses and important for the organisation of neuronal networks.

### 5.1.4 The UPS and Apoptosis

Apoptosis, or programmed cell death (PCD); is a cellular cascade of molecular steps triggered by cells that results in their death. This process is important for the removal of unwanted or abnormal cells and is required for animal development, the normal turnover of cells and for the function of a healthy immune system (Jacobson et al., 1997, Elmore, 2007).

Apoptosis can be triggered by three different molecular cascades: the extrinsic ('death receptor') pathway, the intrinsic ('mitochondrial') pathway or the perforin/granzyme pathway, although they all ultimately converge on the common 'execution pathway'. Apoptosis is an irreversible process once the final 'execution pathway' has been initiated. A schematic of the three different pathways of apoptosis is displayed in Figure 32.

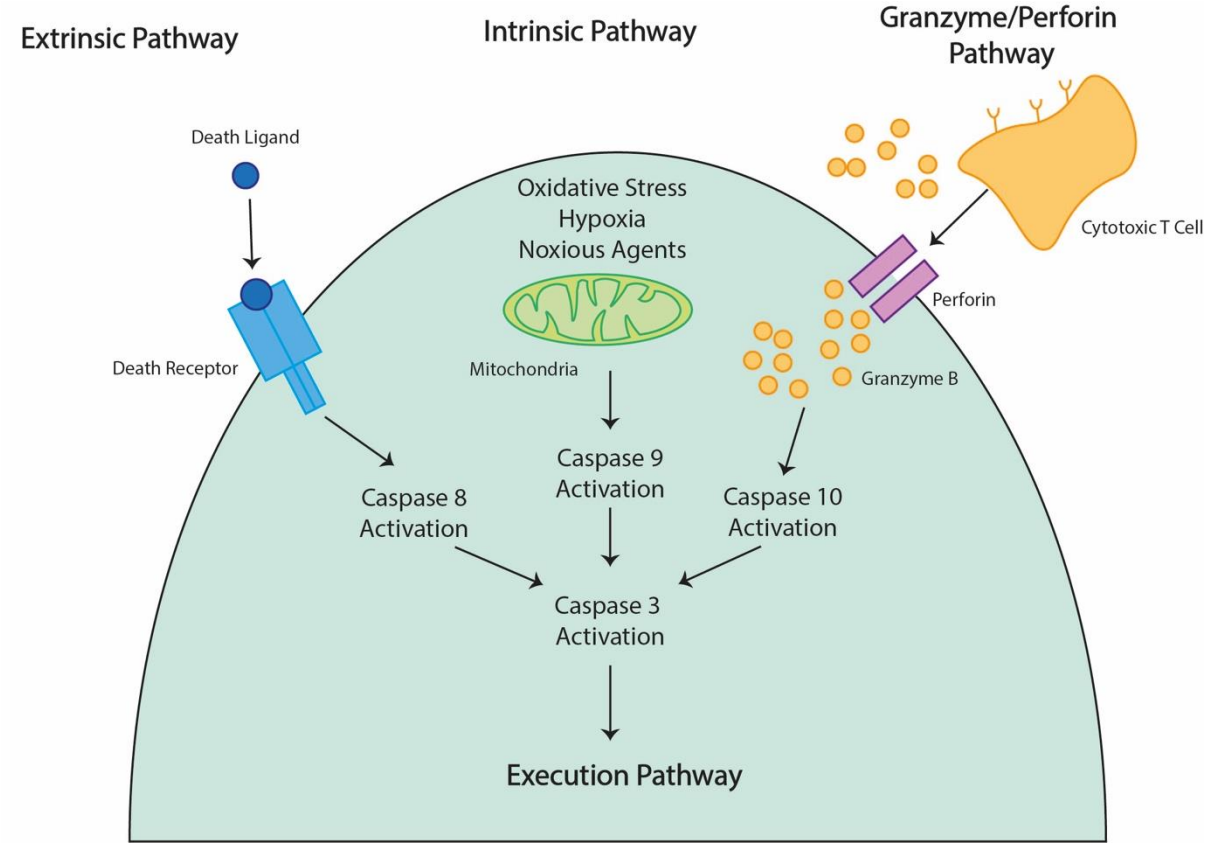


*Figure 32. A diagram showing the three different pathways to apoptosis.*

*The extrinsic pathway is triggered by external factors in the extracellular environment resulting in death ligands binding to the death receptors from the TNF receptor gene family. Downstream signalling results in caspase 8 activation and subsequent caspase 3 activation. The intrinsic pathway results from cellular stress cues from within the intracellular environment, resulting in the breakdown of the mitochondrial membrane and the release of factors from within the inter membrane space which can activate caspase 9. This triggers the caspase cascade resulting in caspase 3 activation. In the granzyme/perforin pathway, cytotoxic T cells recognise cancer cells or cells that have been virally infected. They release granzyme particles, which can access the intracellular environment of the target cell via perforins. Granzyme B granules trigger the activation of caspase 10, which results in the activation of caspase 3. All three pathways converge with the activation of caspase 3, irreversibly resulting in the execution pathway leading to the formation of apoptotic bodies which can be phagocytosed.*

Apoptosis is mediated by caspases, proteolytic complexes with which cleave proteins at aspartic acid residues, leading the breakdown of cellular components. Different caspases are activated depending on the pathway that triggers apoptosis. In the extrinsic pathway, an external ligand binds to death receptors, which are members of the TNF receptor family (Kumar et al., 2005). Activation of a death receptor results in downstream activation of caspase 8, which in turn causes the caspase cascade to begin and the terminal execution pathway to be triggered (Guicciardi and Gores, 2009).

In the intrinsic pathway, mitochondrial changes due to cellular stress (caused by noxious agents, reactive oxygen species or hypoxia, for example) results in formation of the apoptosome and the activation of caspase 9 which in turn triggers a signalling cascade that activates the terminal pathway (Fulda et al., 2010). In the perforin/granzyme pathway, cytotoxic T cells (which kill target cells such as cancer cells or viral infected cells) respond to the release of cytoplasmic granules called granzymes through perforin pores in the cell membrane. Granzyme B activates caspase 10, resulting in apoptosis via the execution pathway. Granzyme A mediates apoptosis via caspase independent mechanisms, activating DNAse NM23-H1 and resulting in cellular death (Fan et al., 2003).

The terminal execution pathway, triggered by the activation of caspase 8, 9 or 10, results in the activation of caspase 3 which in turn activates endonucleases and proteases, resulting in degradation of chromosomal DNA as well as nuclear and cytoskeletal proteins. As a result, cytoplasmic condensation, nuclear fragmentation, and the formation of apoptotic bodies occurs (Elmore, 2007). The apoptotic cell is then phagocytosed by phagocytic cells including macrophages and dendritic cells (Maderna and Godson, 2003).

Studies have shown that the UPS is involved in the regulation of both pro- and anti-apoptotic factors. p53, a transcription factor associated with cellular functions including control of mitosis, apoptosis, and differentiation, has been shown to be closely regulated by the UPS. p53 triggers apoptosis by activating the transcription of pro-apoptotic factors and is capable of triggering apoptosis through both the intrinsic and extrinsic pathways (Amaral et al., 2010). The half-life of p53 within cells is extended in the presence of cellular stress signals. This has been shown to be due to the inhibition of E3 ligases associated with p53 regulation and degradation. Around 20 E3 ligases have been identified so far which specifically regulate p53 levels, but Mdm2 has been identified as the primary E3 ligase for the degradation of p53 (Haupt et al., 1997, Kubbutat et al., 1997).

Pro-apoptotic factors specific to the intrinsic pathway of apoptosis have also been shown to be regulated by the UPS. During the intrinsic pathway of apoptosis, specific pro-apoptotic factors are recruited to the mitochondrial membrane, promoting the break-down of the mitochondrial outer membrane in order for cytochrome C to be released into the intracellular environment to activate the caspase cascade.

The UPS has been shown to regulate a number of pro-apoptotic factors associated with mitochondrial induced apoptosis. Cellular stress results in the activation of the Bcl-2 family of pro-apoptotic proteins which produce a pore in the mitochondrial membrane in order for the release of further apoptotic proteins from the mitochondrial inner membrane to occur (Siddiqui et al., 2015, Elmore, 2007, Abbas and Larisch, 2021). BID is an important member of the Bcl-2 family. Following cellular stress, BID cleaves to generate an active version, tBID, which binds to other Bcl-2 family members BAX and BAK to promote the formation of outer membrane pores on the mitochondria (Siddiqui et al., 2015). BID levels have been shown to be regulated by E3 ligases. The ITCH/AIP4 E3 ligase specifically ubiquitinates only the cleaved tBID, hence regulating apoptosis via downregulation of a pro-apoptotic factor (Azakir et al., 2010).

BAX is also regulated by the UPS, through the E3 ligases Parkin and IBRDC2. BAX is recruited to the mitochondrial membrane following apoptotic stimuli, initiating mitochondrial outer membrane permeabilisation (Hsu et al., 1997, Kuwana and Newmeyer, 2003). The permeabilisation of the mitochondrial outer membrane results in the release of further pro-apoptotic proteins from within mitochondria, hence this process needs to be highly regulated. Parkin and IBRDC2 are E3 ligases which regulate the levels of BAX. During apoptosis, inhibition of these E3 ligases results in higher levels of intracellular BAX available to initiate the permeabilisation of the mitochondrial membrane (Johnson et al., 2012, Benard et al., 2010).

## 5.2 Aims and Objectives

In Chapters 3 and 4 of this thesis, I demonstrated that proteasomal inhibition increases the frequency of glycinergic mIPSCs using both MG132 and bortezomib in a relatively rapid timescale. However, no effect on glutamatergic mEPSC frequency was observed. In the current chapter, I extend my studies of proteasome inhibition by examining its effects on the neuromuscular junction. First, using zebrafish EW muscle fibres as a model, as these are innervated by the PMNs used for study in Chapters 3 and 4, I used voltage clamp recordings of the EW fibres to examine the effects of proteasome inhibition on spontaneous neurotransmitter release at the NMJ. Subsequently, using immunohistochemical methods, I examined the effects of proteasome inhibition on the architecture of MN axons and neuromuscular synapses of larval zebrafish. Finally, I use acridine orange (AO) staining to examine the effects of proteasome inhibitors on apoptosis in the developing zebrafish spinal cord.

## 5.3 Results

### 5.3.1 The effects of proteasome inhibition on NMJ mEPC parameters

In order to examine the effects of proteasome inhibition on physiological properties of the NMJ, whole cell voltage clamp recordings were taken from EW muscle fibres following chronic (overnight) incubation with MG132, bortezomib or control conditions. mEPCs were isolated using saline containing sodium channel blocker TTX (1 µM) and a low concentration of tubocurarine (3 µM) to slow muscle contractions.

Larvae were first incubated with MG132 (10 µM, N = 9) or control (N = 10). The following morning, animals were spinalised and the red embryonic muscle was removed to expose the underlying white musculature. No significant change in white muscle mEPC frequency ($p = 0.7648$, MG132: 0.30 ± 0.29 Hz, controls: 0.34 ± 0.30 Hz; Figure 33A, C, E), amplitude ($p = 0.6297$, MG132: -525.2 ± 193.0 pA, controls: -341.7 ± 349.0 pA; Figure 33A, C, F), half-width ($p = 0.1988$, MG132: 0.99 ± 0.42 ms, controls: 1.10 ± 0.86 ms; Figure 33A, C, G) or rise time ($p = 0.2323$, MG132: 0.43 ± 0.10 ms, controls: 0.48 ± 0.16 ms; Figure 33 A, C, H) was determined between muscle cells recorded from larvae treated with MG132 compared to control. In summary, chronic incubation with MG132 (10 µM) had no effect on mEPC frequency or parameters compared to control treated EW muscle cells. The observed lack of increase in mEPC frequency following MG132 incubation could be due to concentration. Therefore, experiments were repeated as above using 40 µM MG132.

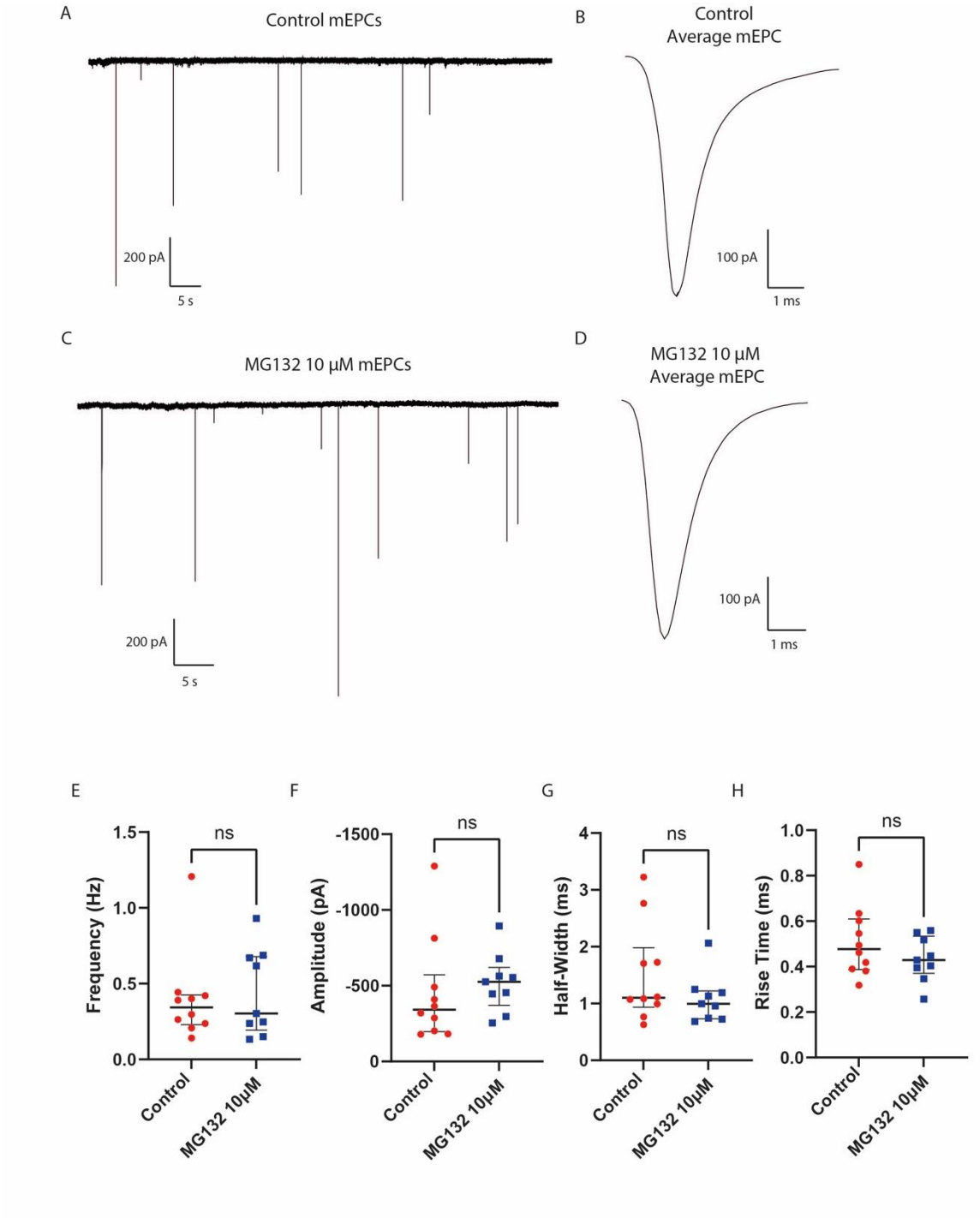


*Figure 33. Chronic incubation with proteasome inhibitor MG132 had no effect on mEPC parameters from EW muscle cells.*

*Zebrafish larvae were incubated chronically (overnight) with MG132 (10 µM) or control conditions and mEPCs were recorded from embryonic white muscle cells. A-B) A representative 60s voltage clamp trace of mEPCs isolated from an white embryonic muscle cell from larvae incubated overnight with control and an average mEPC (B) taken from the trace shown in A. C-D) A representative 60s voltage clamp trace of mEPCs isolated from an embryonic white muscle cell from larvae incubated overnight with 10 µM MG132 and an average mEPC (D) taken from the trace shown in C. E-H) Median with interquartile range plots for mEPC parameters taken from embryonic white muscle cells incubated with either control or MG132. No significant change was determined for mEPC frequency, average amplitude, half-width or rise time for cells treated with MG132 (10 µM) compared to controls*

Larvae were next treated overnight with bortezomib (50 µM, N = 10) or control (N = 10). A significant increase in the frequency ($p = 0.0005$, bortezomib: 1.40 ± 2.84 Hz, control: 0.29 ± 0.96 Hz; Figure 34 A, C, E) of mEPCs was determined for cells treated with bortezomib compared to control. No significant difference in average mEPC amplitude ($p = 0.7438$, bortezomib: -494.4 ± 150.0 pA, control: -463.4 ± 255.8 pA; Figure 34 A, C, F), half-width ($p = 0.9145$, bortezomib: 1.13 ± 0.38 ms, control: 0.92 ± 0.79 ms; Figure 34 A, C, G) or rise time ($p = 0.4359$, bortezomib: 0.43 ± 0.061 ms, control: 0.41 ± 0.094 ms; Figure 34 A, C, H).

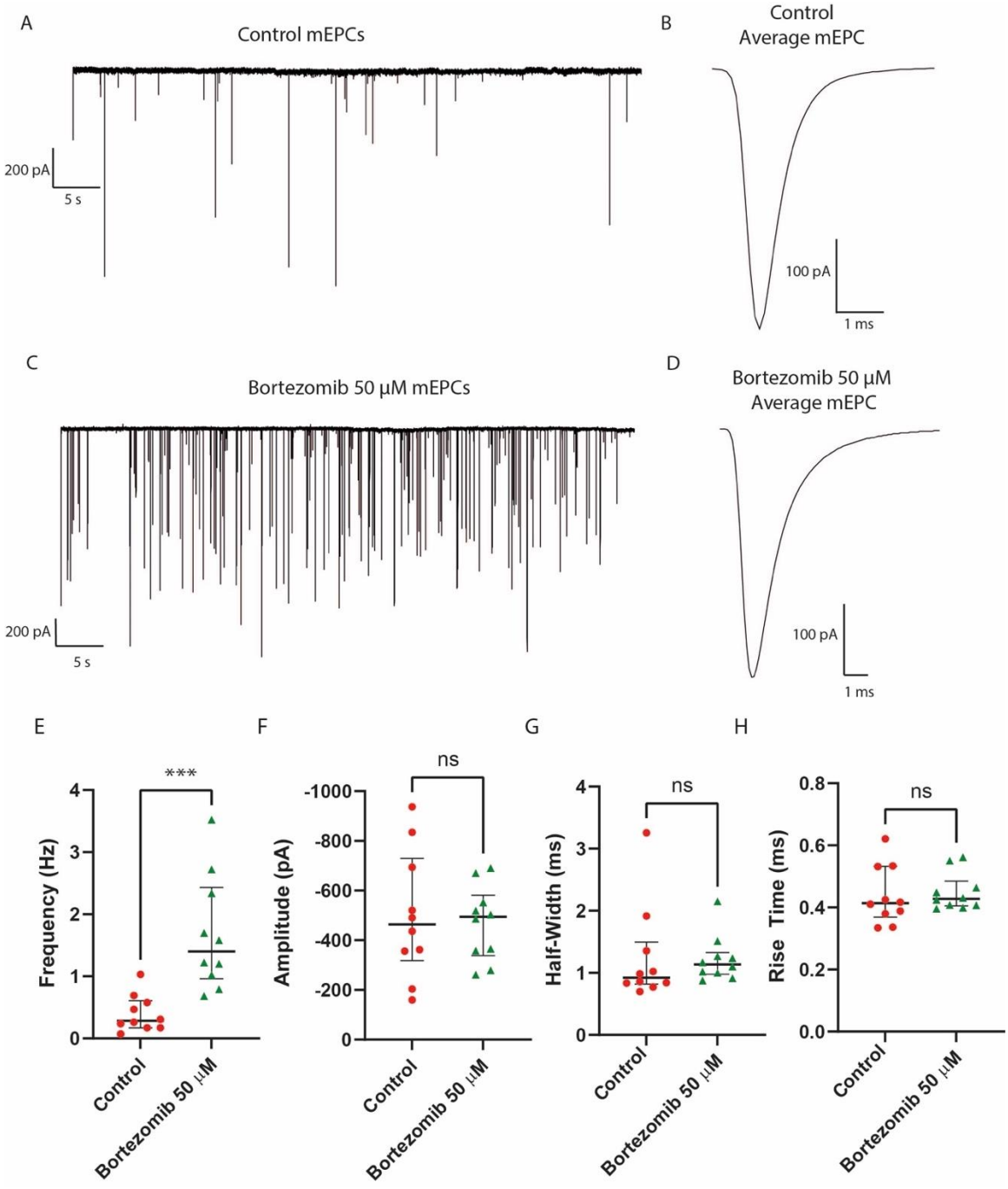


*Figure 34. Chronic incubation with proteasome inhibitor bortezomib increased mEPC frequency from EW muscle cells.*

*Zebrafish larvae were incubated overnight with bortezomib (50 µM) or control and whole-cell voltage clamp recordings of mEPCs were recorded. A-B) Representative 60s voltage clamp recordings from control EW muscle cells and an average mEPC (B) taken from A. C-D) A representative 60s voltage clamp recording of mEPCs taken from EW cells treated with bortezomib and an average mEPC (D) taken from C. E-H) Median with interquartile range plots of mEPC paramters from EW cells treated with either 50 µM bortezomib or control. No significant difference in average mEPC amplitude, half-width or rise time was determined for cells treated with bortezomib compared to control. A significant increase in mEPC frequency was observed for EW muscle cells treated with bortezomib compared to control. *** = $p < 0.0005$.*

Chronic (overnight) incubation with MG132 (40 µM, N = 10) resulted in no significant difference in mEPC frequency (p = 0.7981, MG132: 0.50 ± 0.43 Hz, controls: 0.52 ± 0.34 Hz: Figure 35A, C, E), amplitude (p = 0.5405, MG132: -609.3 ± 646.9 pA, controls: -655.6 ± 590.0 pA: Figure 35A, C, F), half-width (p = 0.6305, MG132: 0.79 ± 0.16 ms, controls: 0.82 ± 0.25 ms: Figure 35A, C, G) or rise time (p = 0.7959, MG132: 0.39 ± 0.048 ms, controls: 0.39 ± 0.042 ms: Figure 35A, C, H) between cells treated with MG132 compared to control treated cells.

Consistent with data collected for MG132 (10 µM), chronic incubation with MG132 (40 µM) resulted in no change in mEPC parameters. This contrasted to results obtained with bortezomib (50 µM), which showed a significant increase in mEPC frequency.

The observed increase in mEPC frequency following chronic bortezomib treatment could arise due to an increase in the number of synapses occurring on the muscle fibres or it could be due to an increase in release from the same number of synapses. In order to elucidate if this increase was due to changes in synapse number, I next investigated the innervation pattern of MNs and the formation of NMJs within the musculature.

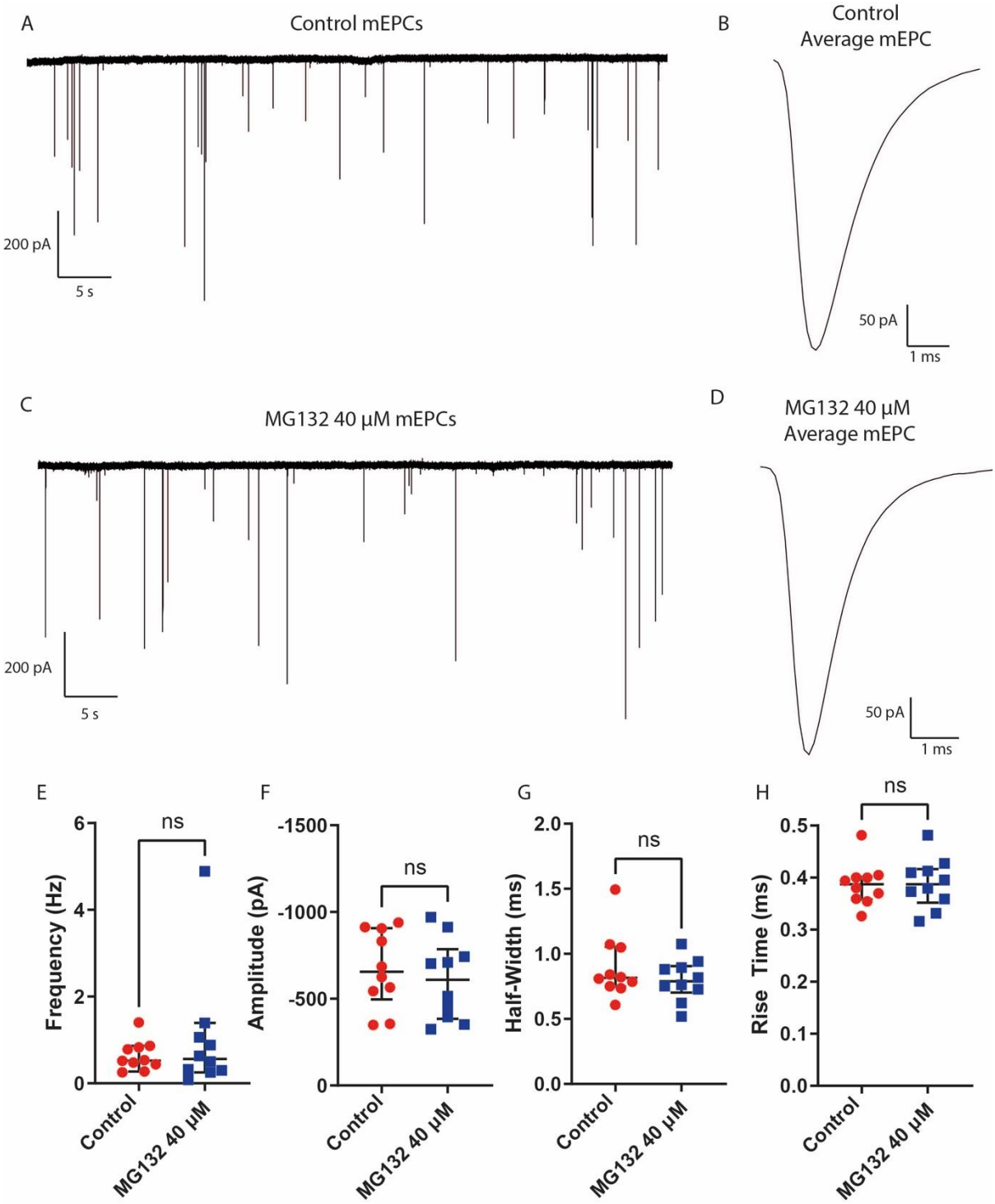


*Figure 35. Chronic incubation with MG132 (40 µM) had no significant effect on mEPC parameters from EW muscle cells.*

*Voltage-clamp recordings were taken of mEPCs isolated from EW muscle cells from larvae treated chronically (overnight) with either MG132 (40 µM) or control. A-B) Representative 60s voltage clamp recording of mEPCs isolated from EW muscle cells from larvae treated overnight with 0.04% DMSO and an average mEPC (B) taken from the trace displayed in A. C-D) A representative 60s voltage clamp recording of mEPCs isolated from EW muscle cells from larvae treated overnight with 40 µM MG132 and an average mEPC (D) taken from the trace displayed in C. E-H) Median with interquartile range plots displaying mEPC parameters from EW muscle cells from larvae treated with either 40 µM MG132 or 0.04% DMSO control. No significant difference in mEPC frequency, amplitude, half-width or rise time was detected for cells treated with 40 µM MG132 compared to control.*

### 5.3.2 The effect of proteasomal inhibition on the axonal and dendritic growth of motoneurons

To determine the effects of proteasome inhibition on motor axon branching, zebrafish larvae (3-dpf) were incubated overnight in either 10 µM MG132, 50 µM bortezomib or control saline. The following day larvae were fixed in PFA and stained using ZNP-1 antibodies, which recognise the presynaptic protein synaptotagmin-2 (Boon et al., 2009, Nozawa et al., 2017, Ahmed et al., 2018). Images were taken using the Olympus FV1000 confocal microscope using the x40 lens to focus on somites 6-9 (with somite 1 counted as the first somite at the rostral end of the spinal cord). Staining was analysed in three ways. The proportion of antibody stain was determined as a percentage of the analysed image. Images were then further analysed to visualise branching pattern in somite 7.

Overnight treatment with 10 µM MG132 caused no significant difference in the proportion of ZNP-1 antibody staining in four somites (two dorsal and two lateral) (%Antibody stain/background; $p = 0.3558$, MG132: N = 7, 17.87 ± 3.81 %, control*:* N = 8, 20.34 ± 5.43 %: Figure 36 A, B, E) compared to control larvae. A single lateral somite was then further analysed to determine branching pattern of labelled MNs and overall length of identified neural processes. Larvae treated overnight with MG132 also showed no significant difference in branch number ($p = 0.4301$, MG132: 109.0 ± 34, control: 127.0 ± 38: Figure 36 C, D, F) or overall neurite length ($p = 0.956$, MG132: 683.6 ± 163.5 µm, control: 656.8 ± 148.3 µm: Figure 36 C, D, G) compared to control treated larvae. In conclusion, chronic incubation with MG132 (10 µM) resulted in no significant difference in proportionate ZNP-1 staining, PMN branching or cable length compared to control PMNs.

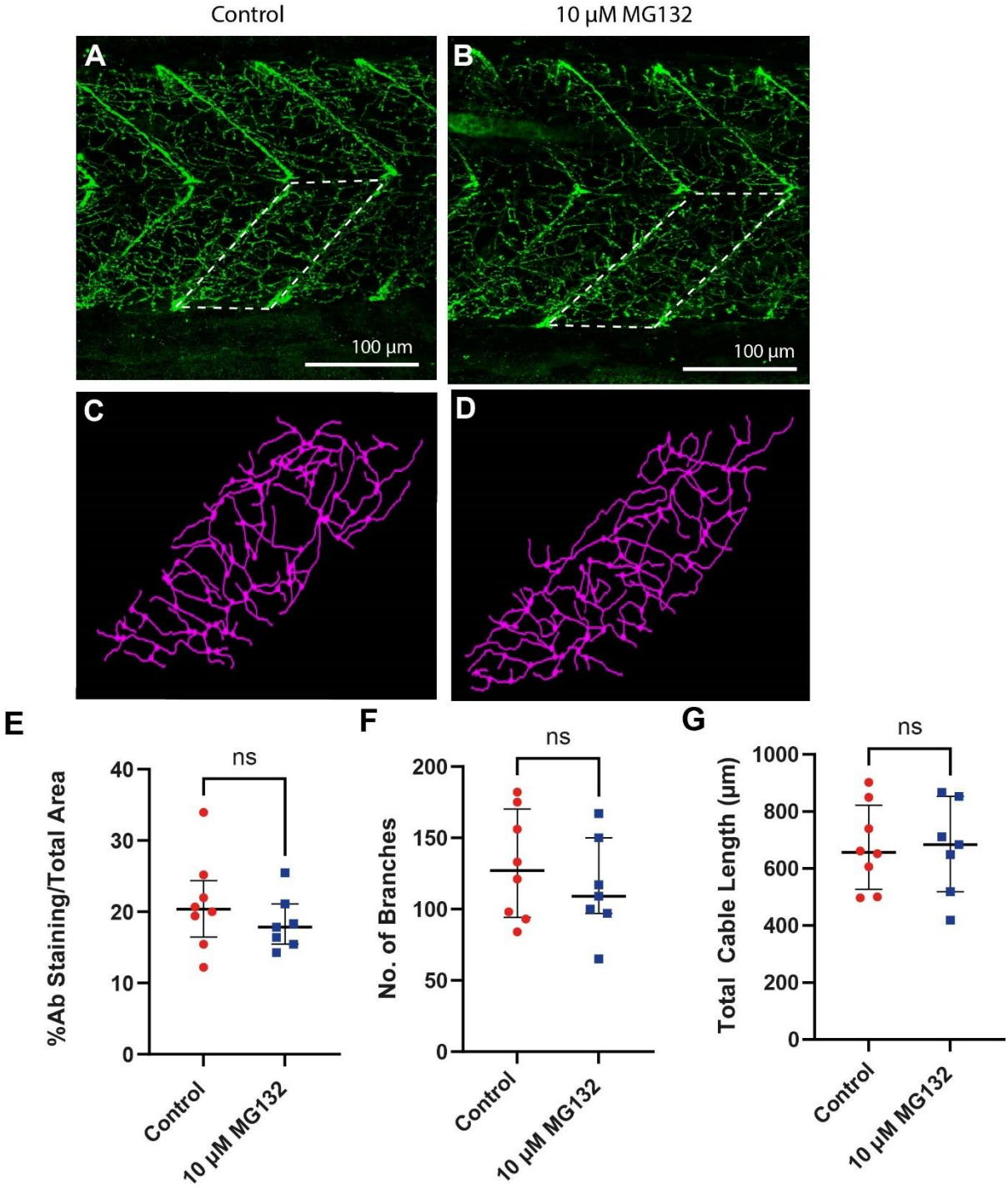


*Figure 36. Chronic incubation with proteasome inhibitor MG132 had no effect on PMN branching in larval zebrafish.*

*Zebrafish larvae were incubated in either MG132 (10 µM) or control conditions and then stained with anti-ZNP-1 antibodies. A-B) Confocal microscope z-stack images of ZNP-1 antibody staining in control (A) or MG132 (B). C-D) SNT tracing of highlighted hemisegments from A-B of ZNP-1 stained PMNs from larvae treated overnight with control (C) or MG132 (D). E-G) Median with interquartile range plots showing % antibody staining area (E), number of neurite branches (F) and the total cable length traced (G) compared between larvae treated with either MG132 or control for ZNP-1 staining. No significant difference was detected in ZNP-1 % staining, number of branches or total cable length between larvae treated with MG132 compared to control.*

Larvae were also treated overnight with bortezomib (50 µM) and stained with anti-ZNP-1. %Antibody stain/background was determined for each image. No significant difference in % antibody stain was detected for larvae treated with bortezomib stained for ZNP-1 ($p = 0.5432$, bortezomib: $N = 8$, $20.85 \pm 5.78$ %, control: $N = 8$, $21.56 \pm 3.44$ %: Figure 37 A, B, E) compared to control treated larvae. Following SNT analysis, no significant difference was determined for larvae treated overnight with bortezomib in branch number ($p = 0.238$, bortezomib: $88 \pm 47$, control: $130.5 \pm 41$: Figure 37 C, D, F) or overall neurite cable length ($p = 0.7867$, bortezomib*:* $640.4 \pm 255.3$ µm, control*:* 185.4 µm: Figure 37 C, D, G) compared to control treated larvae. In summary, these results suggest the proteasomal inhibition with both MG132 and bortezomib showed no difference in the branching pattern of MNs innervating the musculature.

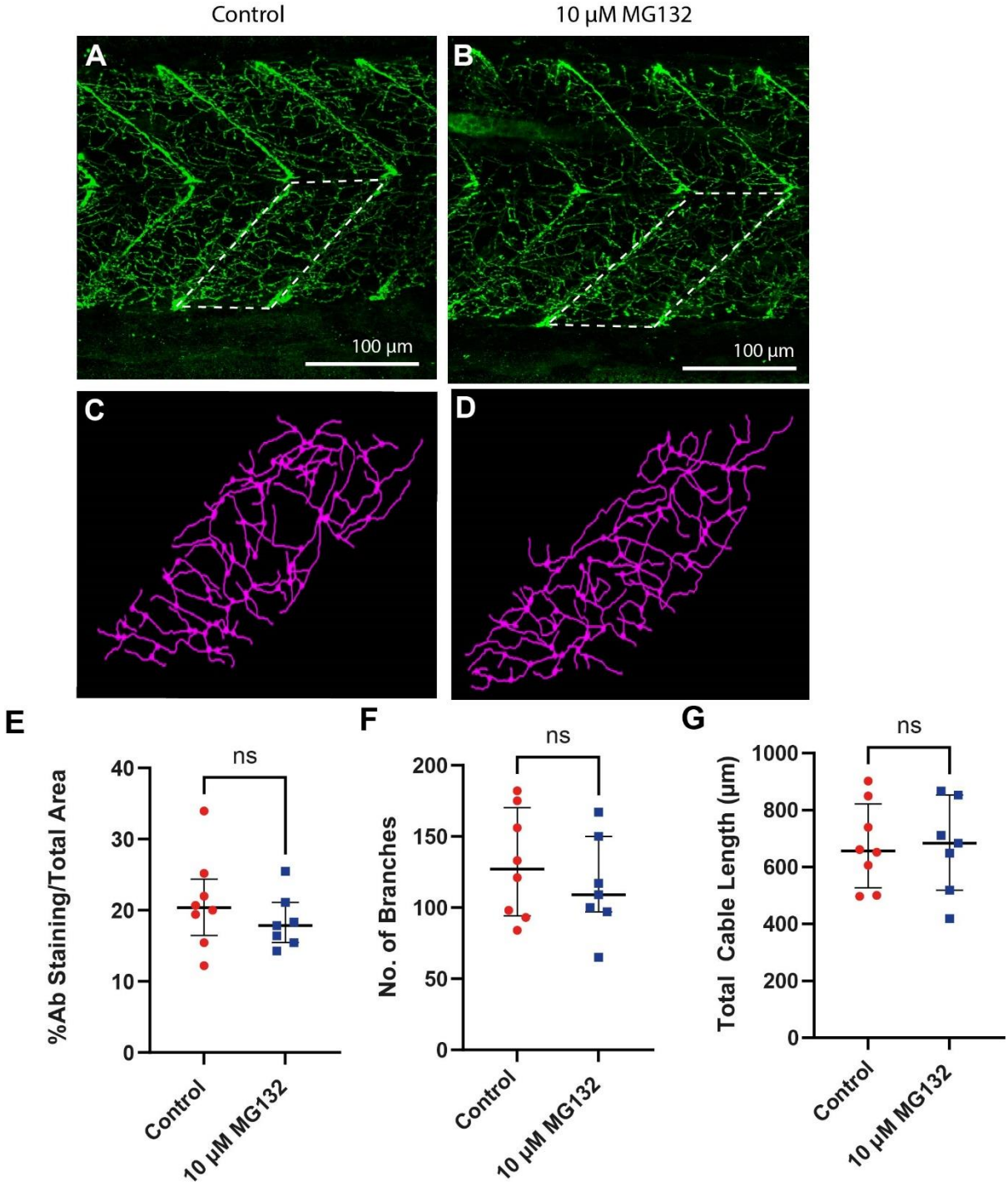


*Figure 37. Chronic incubation with proteasome inhibitor bortezomib did not affect PMN branching in larval zebrafish incubated overnight with bortezomib showed no significant difference in PMN branching or cable length.*

*Zebrafish larvae were incubated in either bortezomib (50 µM) or control and then stained with anti-ZNP-1 antibodies. A-B) Confocal microscope z-stack images of ZNP-1 antibody staining in control (A) or bortezomib (B). C-D) SNT tracing of highlighted hemisegments from A-B of ZNP-1 stained PMNs from larvae treated overnight with control conditions(C) or bortezomib (D). E-G) Median with interquartile range plots showing % antibody staining area (E), number of neurite branches (F) and the total cable length traced (G) compared between larvae treated with either bortezomib or control for ZNP-1 staining. No significant difference was detected in ZNP-1 % staining, number of branches or total cable length between larvae treated with bortezomib compared to control..*

### 5.3.3 The effect of proteasomal Inhibition on NMJ formation

In order to determine the effect of proteasomal inhibition on synapse formation, I incubated larval zebrafish overnight with either MG132 (10 µM), bortezomib (50 µM) or control conditions before carrying out co-staining with an antibody for SV2 and α-bungarotoxin-ATTO-633 in order to visualise the NMJ. Images were analysed using Coloc2 (an analysis option in Fiji). 4 different hemisegments were analysed individually per larvae (2 lateral and 2 dorsal segments) to determine the extent of co-localisation of SV2 and α-bgt stain.

Pearson's co-localisation co-efficient was determined and plotted in box plots displayed in Figure 38. No significant difference in Pearson's co-localisation coefficient was determined between larvae treated with 10 µM MG132 and control larvae (p = 0.6679, MG132*:* N = 5, 0.65 ± 0.08, control: N = 5, 0.61 ± 0.09: Figure 38 A-L, M). In addition to co-localisation analysis, I carried out total staining analysis to determine if there was an increase in α-bgt staining compared between MG132 treated larvae and 0.01% DMSO treated larvae. No significant difference in total staining with α-bgt staining was determined between MG132 treated larvae compared to control treated larvae (p = 0.091, MG132*:* N = 5, 11.30 ± 0.54 %, control: N = 5, 12.35 ± 1.44 %: Figure 38 A-L, N).

In summary, chronic MG132 treatment had no significant effect on co-localisation of pre- and post- NMJ synapses or the overall staining of NMJs compared to control. Experiments were next repeated with larvae treated overnight with bortezomib (50 µM) compared to control conditions.

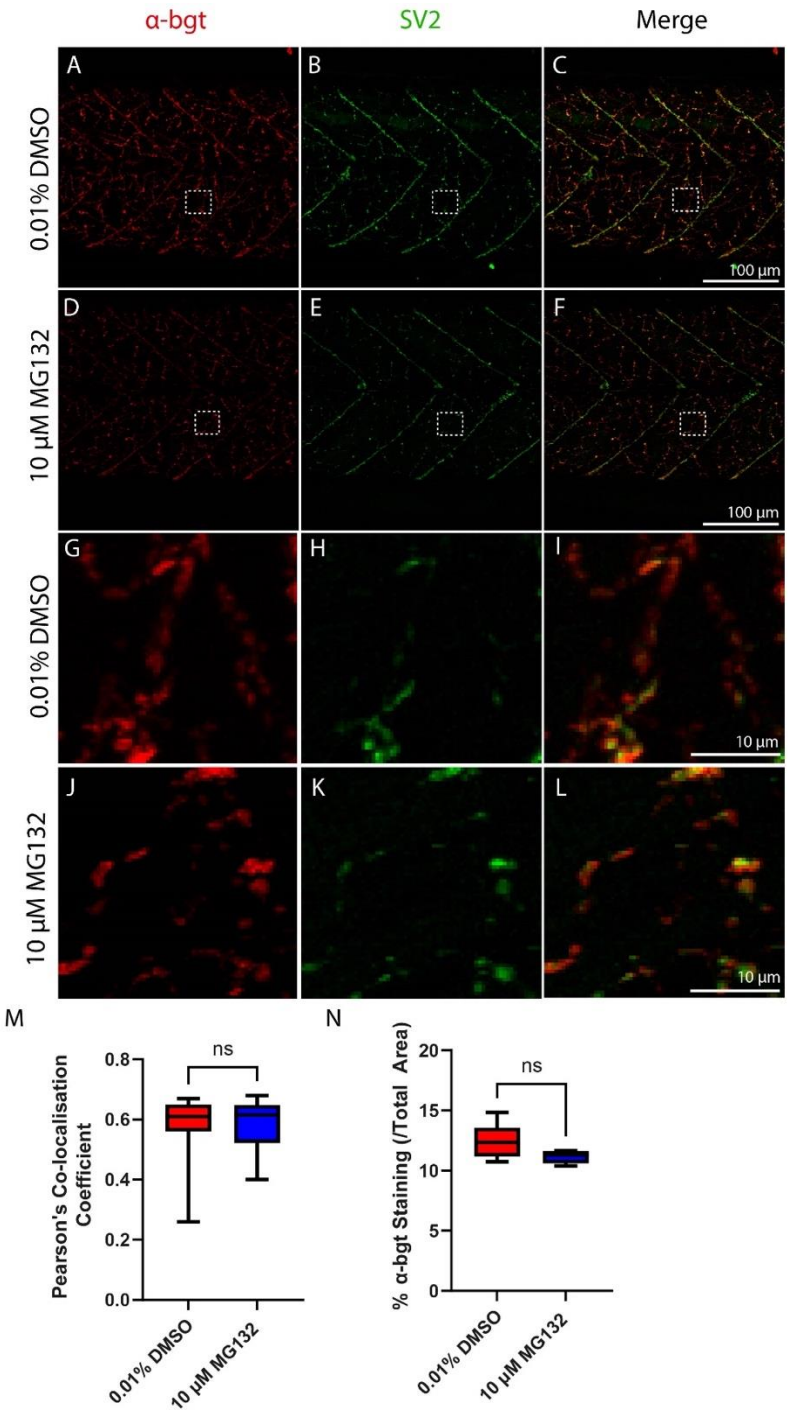


*Figure 38. Chronic incubation with proteasome inhibitor MG132 did not affect co-localisation or total staining of NMJ synapses..*

*Larvae (3-dpf) were treated overnight with MG132 (10 µM, N = 5) or control (N = 6) before being co-stained with anti-SV2 antibody and α-bungarotoxin-ATTO-633. A-G) x40 Confocal images of SV2 and α-bgt staining in larval zebrafish (4-dpf). A-C) α-bgt (A), SV2 (B) and merged staining (C) of larvae treated overnight with control conditions. D-F) α-bgt (D), SV2 (E) and merged staining (F) of larvae treated overnight with MG132. G-L) Zoomed in images of staining displayed in A-F from the boxes displayed. G-L) α-bgt (G), SV2 (H) and merged staining (I) from larvae treated overnight with control. J-L) α-bgt (J), SV2 (K) and merged staining (L) in larvae treated overnight with MG132. M) Box and whisker plots showing Pearson's co-localisation co-efficient for 4 different hemisegments analysed in each larvae treated with either MG132 or control. No significant difference in co-localisation coefficient was determined for larvae treated with MG132 compared to control. N) % Total α-bgt staining in larvae treated with MG132 compared to control. No significant difference was determined in total α-bgt staining in MG132 treated larvae compared to control.*

Experiments were next repeated with larvae treated overnight with bortezomib (50 µM) compared to control conditions. Data displayed in Figure 39 shows the results of overnight treatment with bortezomib (N =4) and control (N = 4) on the formation of NMJs. As with larvae treated overnight with MG132, overnight treatment with 50 µM bortezomib had no effect on the co-localisation of SV2 and α-bgt compared to larvae treated with 0.05% DMSO (p = 0.6860, *bortezomib:* 0.66 ± 0.1, *control*: 0.65 ± 0.28). The percentage of α-bgt staining was also determined for larvae treated with bortezomib compared to control treated larvae. No significant difference in α-bgt staining was determined between larvae treated with bortezomib (p = 0.8857, bortezomib*:* 13.12 ± 1.95%, *control*: 10.71 ± 1.45%) compared to control treated larvae. Data displayed in Figure 38 and Figure 39 suggest that overnight incubation with proteasome inhibitors MG132 and bortezomib have no effect on the formation of NMJs. This would suggest that increases in mEPC frequency observed in larvae treated overnight with bortezomib (Figure 34) are not due to an increase in the number of synapses onto the EW musculature from the PMNs.

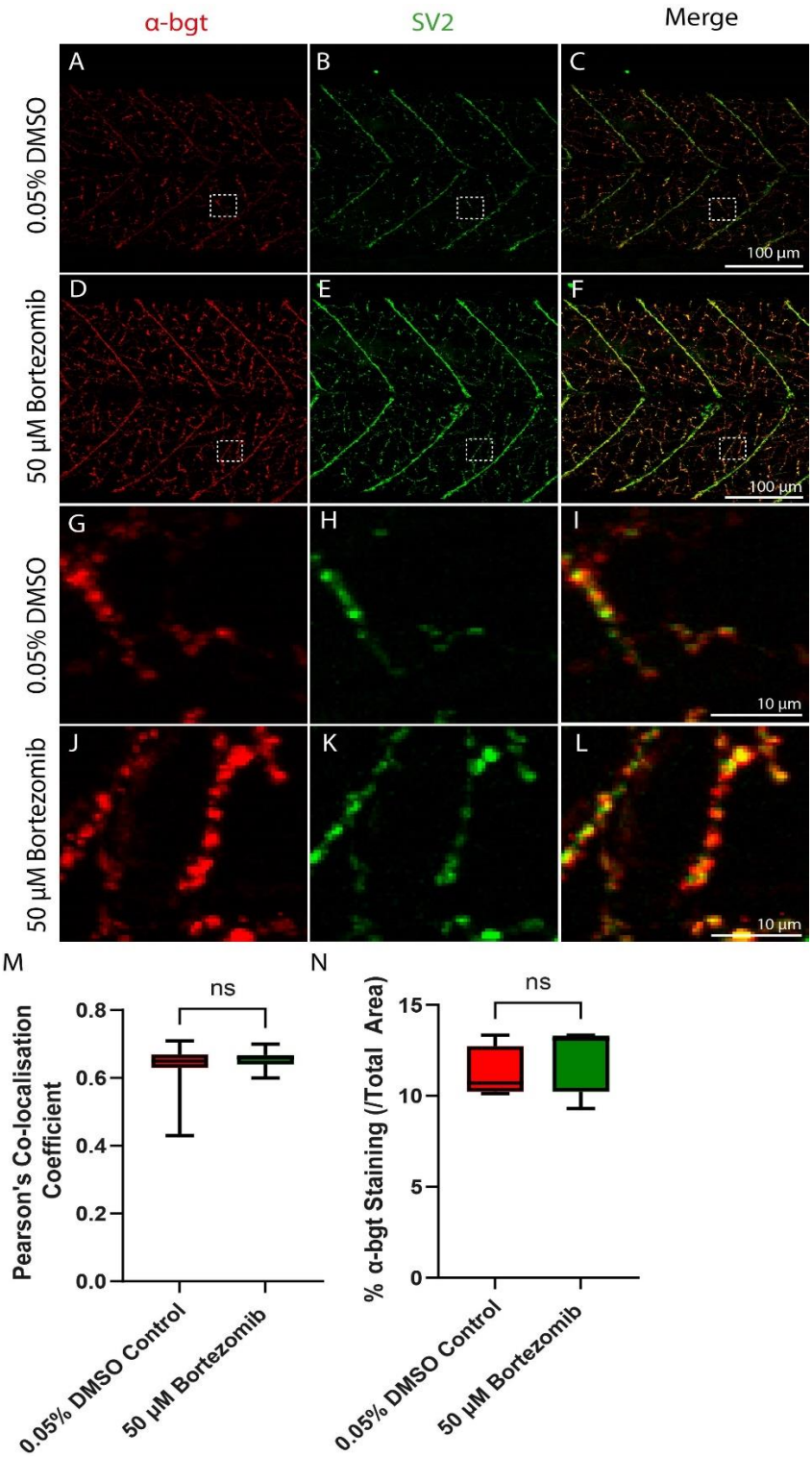


*Figure 39. Chronic incubation with bortezomib does not affect the formation of NMJ synapses.*

*Larvae (3-dpf) were treated overnight with bortezomib (50 µM, N = 4) or control (N = 4) before being co-stained with anti-SV2 antibody and α-bungarotoxin-ATTO-633. A-G) x40 Confocal images of SV2 and α-bgt staining in larval zebrafish (4-dpf). A-C) α-bgt (A), SV2 (B) and merged staining (C) of larvae treated overnight with control. D-F) α-bgt (D), SV2 (E) and merged staining (F) of larvae treated overnight with bortezomib. G-L) Zoomed in images of staining displayed in A-F from the boxes displayed. G-L) α-bgt (G), SV2 (H) and merged staining (I) from larvae treated overnight with control. J-L) α-bgt (J), SV2 (K) and merged staining (L) in larvae treated overnight with bortezomib. M) Box and whisker plots showing Pearson's co-localisation co-efficient for 4 different hemisegments analysed in each larvae treated with either bortezomib or control.. No significant difference in co-localisation coefficient was determined for larvae treated with bortezomib compared to control.*

### 5.3.4 The effect of proteasomal inhibition on apoptosis

The UPS is tightly linked to apoptosis, with the drug bortezomib showing the ability to induce apoptosis in multiple myeloma cells (Li et al., 2019). Acridine Orange (AO) is a vital nucleic acid dye that can be used to distinguish apoptotic tissues by binding to nucleic acids which have been released into the cytoplasm of apoptotic cells, allowing for fluorescent visualisation of cells undergoing apoptosis (Plemel et al., 2017, 2007). I therefore used AO staining to determine if chronic (overnight) treatment with MG132 or bortezomib increased apoptosis in larval zebrafish. Larvae were incubated overnight with proteasome inhibitors or appropriate control treatment and 10 ng/ml of AO dye. The following morning larvae were spinalised, mounted in fluorescent mounting media on microscope slides and imaged using an FV1000 Confocal microscope.

Following overnight incubation with MG132 (10 µM, N = 6) and AO, no difference in overall total staining with AO was determined for MG132 ($p = 0.6549$, MG132: 8.0 ± 3.02%, control: 9.14 ± 2.49 %: Figure 40 A-F, M) compared to larvae treated overnight with control conditions (N = 6). Overnight incubation with bortezomib (50 µM, N=6) and AO also did not show any difference in overall staining ($p = 0.5217$, bortezomib*:* 9.02 ± 4.03 %, control: 10.76 ± 3.74%: Figure 40G-L, M) compared to control treated larvae (N= 6). These results indicate that there was not an increase in apoptotic tissues due to overnight incubation with proteasome inhibitors MG132 or bortezomib.

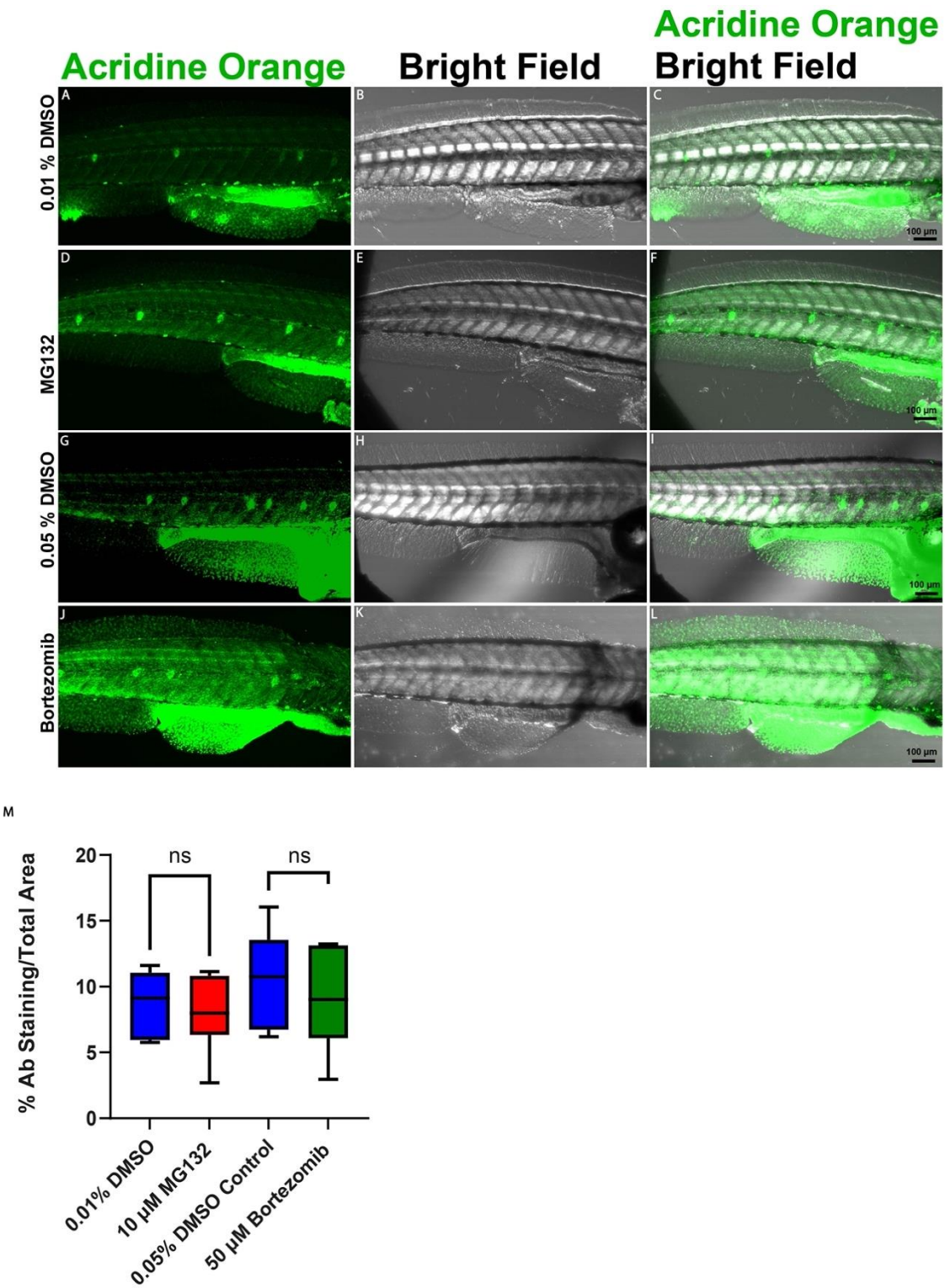


*Figure 40. Acridine Orange staining detected no difference in apoptotic tissue in larvae treated overnight with proteasome inhibitors MG132 or bortezomib.*

*Larvae (4-dpf) were treated overnight with either 10 µM MG132, 50 µM bortezomib or control conditions containing appropriate DMSO or 10 ng/ml AO. A-L) AO staining (left), bright field images (middle) and merged AO and bright field images (right) of larvae treated overnight with 0.01% DMSO (A-C), 10 µM MG132 (D-F), 0.05% DMSO (G-I) and 50 µM bortezomib (J-L). M) Median with interquartile range box plots showing %Ab staining compared to the total area of AO stain in larvae treated with proteasome inhibitors compared to control. No significant difference in AO stain was determined in control larvae compared to those treated with MG132 or bortezomib..*

## 5.4 Discussion

In Chapters 3 and 4 of this thesis, I showed that pharmacological inhibition of the proteasome increased the frequency of glycinergic mIPSCs in zebrafish PMNs across two different time periods, using two different proteasomal inhibitors. In the current chapter, I focused on the effect proteasome inhibition on physiological and anatomical properties of neuromuscular synapses.

During whole cell voltage clamp recordings of EW fibres, I found that mEPC frequency was increased following overnight incubation with 50 µM bortezomib, however mEPC frequency was not increased following either 10 µM or 40 µM MG132. The amplitude, half-width and rise time of mEPCs were unchanged following incubation with proteasome inhibitors compared to control DMSO.

I also examined the effect of proteasome inhibition on the outgrowth of motoneuron axons in the larval zebrafish spinal cord. Using ZNP-1 staining, I saw no difference in the overall staining in zebrafish larvae treated with control compared to those treated with either MG132 or bortezomib. I then focused on whether there were changes in the formation of NMJ synapses as a result of overnight incubation with proteasome inhibitors on larvae aged 3-dpf to 4-dpf using co-staining of SV2 and $\alpha$-bgt. Proteasomal inhibition with either MG132 or bortezomib had no effect on the overall formation of NMJs.

Finally, I examined the effects of chronic MG132 or bortezomib treatment on apoptosis using AO staining. I observed no significant difference in the proportion of AO stain in larvae treated with proteasome inhibitors (MG132 and bortezomib) compared to control treated larvae.

### 5.4.1 Effect of proteasome inhibition on mEPCs from EW muscle cells

Following chronic incubation with MG132, no significant difference in mEPC frequency, amplitude, half-width or rise time was observed. This was consistent with previous results obtained in Chapters 3 and 4 of this thesis. The NMJ is an excitatory synapse which releases the neurotransmitter acetylcholine. In Chapters 3 and 4, I showed that proteasomal inhibition had no effect on glutamatergic mEPSC frequency, hence I expected that the NMJ would not be affected by proteasomal inhibition. However, upon chronic incubation with

bortezomib, a significant increase in mEPC frequency was observed. I hypothesised that increased mEPC frequency at the NMJ following incubation with bortezomib, but not with MG132, could be due to higher specificity for the proteasome (Thibaudeau and Smith, 2019, Kisselev, 2021). Bortezomib was synthesised from peptide aldehyde inhibitors (including MG132) to contain a boronate group, hence increasing the specificity of peptide boronate inhibitors compared to conventional peptide aldehyde inhibitors (Thibaudeau and Smith, 2019). Following overnight incubation with MG132 (40 µM), no significant increase in the parameters of mEPCs was determined compared to control treated larvae.

Whilst increased specificity for the proteasome could be the reason for the differing changes in mEPC frequency seen here, an alternative explanation could be that MG132 and bortezomib can have differing effects in specific cell types. A previous study using oestrogen receptor (ER) positive breast cancer cells showed that MG132 treatment prevents the loss of ER$\alpha$ protein, whereas bortezomib treatment did not affect levels of this protein (Powers et al., 2010). There is also precedent to suggest that proteasome inhibitors require different concentrations to exert the same effect within cells. Notably, a study testing the specificity of proteasome inhibitors found that bortezomib inhibited $\beta$1 subunits in addition to $\beta$5 subunits, whereas MG132 had the ability to inhibit all proteasome catalytic subunits. Proteasomes have previously been shown to display heterogeneity within their subunit conformations, particularly during development or as a result of cellular stress (See Chapter 1) (Haass and Kloetzel, 1989, Yuan et al., 1996, Hutson et al., 1997, Aiken et al., 2011). However, MG132 was required to be at a much higher concentration to exert these effects, whereas bortezomib could inhibit its catalytic sites at a much lower concentration (Berkers et al., 2005). A previous study using oestrogen receptor-positive (ER+ ) breast cancer cell lines have shown that 30 nM bortezomib was capable of inhibiting 95% of the chymotrypsin-like activity of the proteasome within MCF7 cells (an immortal breast cancer cell line), whereas MG132 was required at 10 µM to achieve the equivalent level of inhibition (Powers et al., 2010). Further to this, studies have shown that the extent of proteasomal inhibition increases over time, as well as with increased concentration. Using the MM1.S cell line (B lymphoblast myeloma cell line) and SDS-Page of radiolabelled proteasome subunits, inhibition of the proteasome using bortezomib increased from 40% inhibition of $\beta$5 chymotrypsin-like activity following 1-hour incubation, to > 70% after 2-hour incubation. (Altun et al., 2005).

MG132 has also been shown to be less metabolically stable than bortezomib (Thibaudeau and Smith, 2019). In previous studies, MG132 has been shown to be degraded by certain enzymes including CYP3A family enzymes. Using a substrate depletion method, proteasome inhibitors epoxomicin, lactacystin, MG132 were shown to be rapidly metabolised by CYP3A enzymes in hepatocyte cultures, whereas bortezomib was not metabolised (Lee et al., 2010). Whilst CYP enzymes are mainly associated with the liver, certain families are expressed in other tissues (Woodland et al., 2008): CYP3A has been shown to be expressed within the CNS and has been implicated in the metabolism of certain psychoactive drugs, leading to drug resistance in certain brain regions (Ghosh et al., 2011, Wilkinson, 1996). Therefore, differential expression of enzymes could account for the differences in activity observed at PMN and neuromuscular synapses.

Further work potentially looking at longer incubation times could be interesting, as studies have shown that the extent of proteasomal inhibition increases over time. In studies using bortezomib, it has been shown that following shorter incubation times, β5 subunits are inhibited, whilst longer incubation times are required to inhibit β1 subunits in addition to β5 subunits. Whilst MG132 was not included in this study, it could suggest that inhibitors may require longer incubation times to inhibit all the catalytic sites within the proteasome. This could be due to location of the catalytic sites within the proteasome, as some may be more accessible for inhibitors to immediately bind to (Altun et al., 2005). Hence, whilst bortezomib was sufficient to show changes in mEPC frequency following overnight incubation, longer incubation times for MG132 could be required to see the same effect. Using another proteasome inhibitor which is more metabolically stable than MG132, but as specific as bortezomib, could be used to determine if the differences in pharmacology between MG132 and bortezomib caused the differences in mEPC frequency. Carfolizomib, another boronate proteasome inhibitor, could potentially be a better candidate to use in place of MG132, although carfolizomib is significantly more expensive than MG132 (Thibaudeau and Smith, 2019). However, due to project time and money constraints these experiments could not be carried out.

### 5.4.2 The effect of proteasome inhibition on MN neurite outgrowth using ZNP-1

The second aim of this chapter was to determine if inhibition of the proteasome affects the outgrowth from MNs in the zebrafish spinal cord. Previous studies have shown that inhibition of the proteasome affects the growth of neuronal process, including their arborisation patterns and organisation (Wan et al., 2000b, DiAntonio et al., 2001a, Collins et al., 2006), as well as being implicated in regulating axonal growth during synaptogenesis (Campbell and Holt, 2001). I therefore used immunohistochemistry to stain for ZNP-1, a protein associated with axons and dendrites of motoneurons.

First, I analysed the total percentage of stain of ZNP-1 in larvae treated overnight with proteasome inhibitors or control treatment. I saw no significant difference in ZNP-1 stain in larvae treated with control conditions compared to those treated with proteasome inhibitors. Furthermore, chronic incubation with proteasome inhibitors did not significantly increase the number of neurite branches or the overall cable length of PMNs compared to control conditions.

Results showing no difference in axonal and dendritic growth observed here were not consistent with previously described data, which showed that dysfunction of the UPS affects neurite outgrowth in other vertebrate (Campbell and Holt, 2001, Drinjakovic et al., 2010) and non-vertebrate species (Wan et al., 2000b, DiAntonio et al., 2001a, Collins et al., 2006). In the experiments carried out in this thesis, I applied proteasome inhibitors overnight to larvae from 3-dpf to 4-dpf. As at 4-dpf, PMN axons are well established (Myers, 1985, Myers et al., 1986b), I did not expect to see differences in overall axonal length. However, from 3-dpf to 4-dpf neurons within the spinal cord are still innervating the musculature (Myers et al., 1986b). The continued growth of motoneurons in this period are necessary for changes in swimming behaviour to occur from erratic burst swimming at 3-dpf, to more controlled beat-and-glide swimming observed at 4-dpf (Buss and Drapeau, 2001). Therefore, these results are interesting as they show that no neurite outgrowth and innervation of the musculature is unaffected by proteasomal inhibition at this stage of development.

### 5.4.3 The effect of proteasomal inhibition on NMJ formation

The UPS has been implicated in synapse formation and remodelling, hence in this chapter I aimed to investigate the effect of overnight incubation with proteasome inhibitors on the formation of synapses. Analysis of axons and dendrites within the spinal cord is difficult, as is densely populated and hence difficult to isolate individual neurons., MNs are the only axonal processes that innervate muscle fibres, hence isolation of individual processes is easier. As such, I focused on the formation of NMJs within the muscle fibres.

I observed no difference in the co-localisation of SV2 and $\alpha$-bgt between larvae treated with either MG132 compared to control or bortezomib compared to control. This suggests that proteasomal inhibition has no effect on the formation of complete synapses, with pre- and post- synaptic sites co-localising to the same degree in control and drug treated larvae. I also saw no significant difference in overall $\alpha$-bgt stain in larvae treated with MG132 or bortezomib compared to control treated larvae. These experiments suggest that NMJ formation is unaffected by proteasome inhibition, both in terms of the coupling of pre- and post- synaptic sites as well as the overall number of synapses formed.

Previously reported literature, which has suggested that proteasome inhibition effects synapse formation, contrasts with the findings I have presented here (Ding and Shen, 2008, Zheng et al., 2016, Türker et al., 2021). Multiple studies have been carried out in *Drosophila* and *C.elegans*, identifying key components of the UPS system in synapse formation. Loss of function of hiw and overexpression of faf, an E3 ligase and a DUB respectively, have been shown to produce the same phenotype of neurite overgrowth and increased synaptic boutons at the NMJ in *Drosophila* (Wan et al., 2000b, DiAntonio et al., 2001a, Collins et al., 2006). Another E3 ligase complex, APC, has been shown to localise at the pre-synaptic terminal at the *Drosophila* NMJ. Loss of function of APC also results in an overgrowth of synaptic boutons, due to accumulation of Liprin $\alpha$ (a synapse scaffolding protein) (van Roessel et al., 2004, Wise et al., 2013b). Further evidence from *C.elegans* has shown the role of E3 ligases in stabolising and organising the pre-synaptic terminal of the NMJ. RPM-1 is needed for the formation of the NMJ by regulating proteins involved in synapse formation (Zhen et al., 2000b, Yan et al., 2009).

The proteasome has also been shown to be involved in synaptic elimination. In transgenic mice, proteasomal degradation of PSD95 resulting in synapse elimination has

been associated with autism through the action of E3 ligase Mdm2 (Tsai et al., 2012). Further to this, in *Drosophila* during metamorphosis, E2-conjugating enzyme ubcD1 and E3-ligase DIAP1 have been associated with synaptic pruning and elimination of class IV dendritic arborisation sensory neurons (C4da) (Treier et al., 1992b, Kuo et al., 2005).

In the studies discussed above, genetic models were used and as such the focus was on the development of synapses as a result of dysfunctional UPS proteins. The aims of the experiments I carried out in this chapter were instead to look at the effect of synapse formation as a result of changes in synaptic plasticity of already formed neurons. By day 3, although neurite outgrowth will be continuing throughout the spinal cord, the majority of spinal neurons have already established innervations throughout the musculature (Myers, 1985, Myers et al., 1986b). Hence, I have shown here that proteasome inhibition does not affect the organisation of established pre- and post- synaptic sites, as SV2 and $\alpha$-bgt co-localisation was consistent across treatments. I have also shown that inhibition of the proteasome does not affect the formation of new synapses or eliminate existing synapses as a result of changes in synaptic plasticity.

### 5.4.4 The effect of proteasomal inhibition on apoptosis

Proteasome inhibitors including bortezomib and MG132 have been shown to induce apoptosis in a range of different cell types (Wójcik, 2002, Fribley and Wang, 2006). As such, I asked whether changes that had been seen in synaptic transmission could have been due to increase apoptotic tissue. I used AO staining to assess the effects of apoptosis. I observed no difference in the total fluorescence in larvae treated overnight with MG132 and bortezomib compared to control treated larvae. This suggests that there is no increase in apoptosis as a result of proteasome inhibitors MG132 and bortezomib.

Proteasomal inhibition prevents the degradation of proteins, resulting in protein accumulation which can cause inhibition of NF-$\kappa\beta$, an anti-apoptotic protein, and increases the levels of p53, Bax and Bcl-2 involved in the intrinsic pathway of apoptosis (Wójcik, 2002, Rajkumar et al., 2005). However, the accumulation of these proteins takes time as inhibition of the proteasome by MG132 and bortezomib increases overtime (Berkers et al., 2005). Therefore, in this study I might not be seeing the pro-apoptotic effect due to the length of

incubation. In order to observe proteasome inhibitor induced apoptosis, the incubation periods may need to be extended.

### 5.4.5 Conclusion

I have shown that inhibition of the proteasome overnight using bortezomib is sufficient to increase the frequency of EW muscle fibre mEPCs, whilst MG132 did not increase mEPC frequency. This indicates that inhibition of the proteasome with bortezomib can induce pre-synaptic changes in both INs innervating the MNs and PMNs innervating the musculature, as an increase in mIPSC frequency was observed in MNs and an increase in mEPCs was observed at the NMJ. I have also shown that the morphology of PMN axon and neurite outgrowth remains unaffected by proteasomal inhibition when incubated overnight between 3-dpf to 4-dpf larval zebrafish. I have also shown that NMJ formation is not affected by proteasome inhibition during overnight incubation. This shows that inhibition of the proteasome induces pre-synaptic plasticity but does not affect the overall morphology of neurons. This suggests that the plasticity displayed here involves intracellular mechanisms of synaptic vesicle release, rather than physical structural changes to outgrowth of neurons and the number of synapses present.

I have also shown that neither MG132 nor bortezomib treatment overnight increased apoptotic tissue in the larval zebrafish. This shows that proteasomal inhibition in this time frame does not induce apoptosis, and hence the physiological changes seen throughout these experiments have not been due to cell death.

As I have seen physiological changes in both PMNs and EW muscle cells as a result of proteasomal inhibition, with no changes to the morphology of the neurons, I next aimed to investigate if these physiological changes resulted in a change to the behaviour of larval zebrafish. As such, in Chapter 6 of this thesis I have investigated how overnight incubation with 10 µM MG132 and 50 µM bortezomib affects the free-swimming behaviour of larval zebrafish.

# Chapter 6 The Effect of Proteasomal Inhibition on the Free-Swimming Behaviour of Larval Zebrafish

## 6.1 Introduction

As I have previously shown that proteasome inhibition affects the physiological properties of motor network components, in this chapter I aim to assess how overnight incubation with proteasome inhibitors influences free-swimming behaviour of larval zebrafish. Below is an overview of the ontogeny of early zebrafish behaviours.

### 6.1.1 The Locomotion Repertoire of Larval Zebrafish

During the first 5 days of development, motor output of zebrafish larvae matures from simple coiling to free-swimming behaviour that is well suited to prey-capture behaviour and predator escape responses. Below, I discuss the full behaviour repertoire displayed by larval zebrafish during the first four days of development.

#### *6.1.1.1 Spontaneous Coiling Behaviour*

The first motor behaviour is observed at ~ 17-hpf in embryonic zebrafish and is characterised by spontaneous alternating trunk movement. These movements gradually develop into coiling behaviours. Coiling behaviour is characterised by periodic, slow tail flexions that last for hundreds of milliseconds in duration. Coiling is observed from ~ 17 hpf until 27 – 30-hpf, whilst the embryo is still contained within the chorion (egg sac). The frequency of coiling increases to a peak of 0.96 Hz at 19-hpf, before beginning to decline to 0.08 Hz by 26-hpf. Between 18 - 23-hpf, embryos contract continuously, but by 24-hpf, burst contractions are displayed resulting in three to five coils and then a period of inactivity (Saint-Amant and Drapeau, 1998, Roussel et al., 2021). By ~27-hpf coiling has developed into partial tail coils, with full tail coils associated with escape responses fully matured by 48-hpf, directly preceding hatching (Saint-Amant and Drapeau, 1998).

At this stage of development (~ 17-hpf), only four neuronal cell types have been found to be active- PMNs and three types of IN; VeLD (ventrolateral descending), CoPA (commissural primary ascending) and ipsilateral caudal (IC) (Saint-Amant and Drapeau, 2000). PMNs begin to innervate the musculature by ~17-hpf, with innervation occurring at the same time as coiling behaviour is first observed (Bernhardt et al., 1990). Coiling

behaviour is generated by spontaneous network activity (SNA), mediated by gap junctions providing depolarisation to MNs which can drive muscle contractions. SNA during coiling consists of periodic depolarisations and rhythmic membrane oscillations which continue to occur in the presence of glutamate, glycine and acetylcholine receptor blockers (Saint-Amant and Drapeau, 2000, Saint-Amant and Drapeau, 2001). However, TTX blocks SNA mediated activity, suggesting that sodium channels are important for the generation of SNA. Ipsilateral caudal (IC) INs exhibit bursting characteristic which are dependent on a persistent sodium current. This sodium current generates both low frequency membrane oscillations in IC INs to promote coiling behaviour and high frequency oscillations once bursting swimming has developed. As SNA activity decreases, so too does contraction frequency from 19-hpf until ~30-hpf when spontaneous contractions cease completely (Tong and McDearmid, 2012). Synaptic transmission begins to develop around 20 – 21-hpf, producing synaptic bursts (SB) of glycine. As newly formed synapses mature, SB amplitude increases until ~24-hpf. However, application of strychnine does not abolish periodic depolarisations, indicating that SBs are not required for coiling behaviour (Saint-Amant and Drapeau, 2000, Saint-Amant and Drapeau, 2001, Tong and McDearmid, 2012).

#### *6.1.1.2 Escape Responses*

Escape responses are one of the first forms of co-ordinated behaviour displayed by zebrafish. Whereas coiling occurs as a result of IC generation of periodic depolarisations through gap junctions, escape responses require intact motor circuits with synaptic transmission. Whilst hatching does not occur naturally until around 48-72 hpf, touch evoked responses occur prior to this period and larvae will respond to touch when still within their chorion (Kimmel et al., 1995). Touch evoked responses, with touches to either the tail or the head, first arise at ~21-hpf. A head or tail touch at ~21-hpf, resulted in similar responses of rapid coiling of up to 3 full coils, followed by slow relaxation. By 26-hpf (the point at which swimming behaviours begin to arise), touch evoked responses resulted in swimming behaviour in larvae which had been manually dechorionated. Touching the embryo on the head by this age resulted in the forward motion of the embryo by at least one body length. Frequency of tail beating increases from 15 Hz at 30-hpf, to 25 Hz by 36-hpf. Touching the tail results in a slightly increased frequency compared to head touching. Tail touching was

also far more likely to result in swimming behaviour compared to tactile stimulus to the head from 30-hpf onwards (Saint-Amant and Drapeau, 1998). By ~26 hpf, the axons from the first ventrally located SMNs have exited the spinal cord and begun to innervate the musculature, giving rise to the first swimming behaviour following tactile stimulus (Westerfield et al., 1986, Myers et al., 1986b).

The first type of startle response to arise in zebrafish larvae is the C-start response, characterised by a 'C' shape body bend followed by a propulsion through the water away from the stimuli that sparked the escape. C-start responses are generated through tactile touch to the head or can be sparked through auditory stimulation (Roberts et al., 2019, Sagasti et al., 2005, Gerlai, 2016). The C-start response can be observed directly following hatching, at ~44-hpf, however the response continues to mature throughout development as larvae become capable of free-swimming (Eaton and Hackett, 1984).

Escape response behaviour is mediated by supraspinal connections from the reticulospinal neurons in the hindbrain, which provide direct inputs to the MNs in the spinal cord (Metcalfe et al., 1986). The most well characterised of the reticulospinal neurons are the Mauthner neurons (M-cell; see Chapter 1), which receive inputs from the VIIIth cranial nerve (providing auditory information) and the optic nerve (providing visual information). The two M-cells are situated within the hindbrain of the zebrafish and are commissural excitatory neurons which have direct inputs to the MNs in the spinal cord (Eaton et al., 2001, Korn et al., 1992). Other homologues of the M-cell also exist, including Mid2cl and MiD3cm, which when ablated result in no escape response (Liu and Fetcho, 1999). Somatosensory information from the two M-Cells initiates the C-start response, with a single M-cell action potential resulting in activation of MNs on the contralateral side of the spinal cord, culminating in a 'C'-shaped body bend (Eaton and Nissanov, 1985, Eaton and Hackett, 1984). The C-start response can be broken down into two stages: stage 1 occurs at a latency of ~10 ms and comprises a body bend of 30 – 100 degrees around the centre of mass and subsequent head yawing (movement around the vertical axis), followed by stage 2 axial muscle acceleration which results in the propulsion of the fish at an angle of between 15 -135 degrees away from the initial stimuli (Eaton and Nissanov, 1985, Eaton and Hackett, 1984).

A further escape response illustrated in the larval zebrafish is the S-start response. As with a C-start response, the S-start has two stages, however stage 1 is broken down into

two constitutive parts. First, the caudal aspect of the larval trunk bends to adopt an 'S' shape in response to the initial stimuli and; second, the trunk subsequently bends to the 'C' shape configuration. Stage 2 comprises a rapid tail beat which propels the fish away from the stimuli (Webb, 1976). S-startle responses have been found to occur only during larval stages of development and occur in response to tactile stimuli to the tail, rather than to the head (Liu et al., 2012). S-start responses are generated through the simultaneous stimulation of both M-Cells, whereas C-start responses are generated through the activation of one M-Cell at a time (Liu and Hale, 2017).

#### *6.1.1.3 Burst Swimming*

Once larvae reach 2 to 3-dpf, they become capable of bursting swimming behaviour. At this stage, fish are largely inactive. However, tactile stimulation is sufficient to evoke locomotor activity characterised by periods of sustained, uninterrupted swimming that last for up to tens of seconds in duration. During larval stages, bursting swimming acts as a further form of escape response to evade predator capture. It is characterised by tail beats, allowing the larvae to travel distances of more than 10 body lengths, before coming to a complete stop. Tail beating is rapid, reaching frequencies of up to 100 Hz (Müller and van Leeuwen, 2004). Burst swimming is associated with large body bends, which occur towards the mid-body rather than more caudally which is associated with slower swimming. The yaw angle (side-to-side movement of the head) of burst swimming is also large compared to slower swimming, being between 14 to 27 ° (Budick and O'Malley, 2000). Yawing is important for turning behaviour with a larger yaw required for escape responses (Fish and Holzman, 2019, Budick and O'Malley, 2000). Control of bursting swimming increases as the larvae age, as at 2-dpf larvae often lack postural and directional stability leading to swimming in tight circles or rolling over during swimming episodes. By 3-dpf larvae have more control over their burst swimming episodes and display forward motion without rolling (Müller and van Leeuwen, 2004).

Burst swimming is underpinned by waves of rostrocaudally progressing body bends that alternate between the left and right halves of the spinal cord (Masino and Fetcho, 2005). Bursting swimming is driven by an early-developing scaffold of primary neurons (see Chapter 1). Fictive swimming preparations have been used extensively to study synaptic

drive involved in the maturation of swimming behaviour from burst swimming to beat-and-glide swimming. Fictive swimming involves the paralysis of the larvae using tubocurarine (ACh receptor blocker), which allows for electrophysiological recordings to be taken from spinal neurons (Buss and Drapeau, 2001, Masino and Fetcho, 2005). During fictive burst swimming, tonic depolarisation of the MNs occurs lasting for tens of seconds. A sustained pattern of rhythmic glutamatergic postsynaptic potentials (EPSPs) are also observed with a frequency of ~ 52 Hz. The synaptic drive for burst swimming is provided by glutamatergic INs, whilst input from glycinergic INs produces the left-to-right undulating body movement (Buss and Drapeau, 2001).

As the larvae develop, further MNs and INs are incorporated into the motor network, allowing of the maturation of behaviour from burst swimming at 2-dpf, to more intermittent style of swimming, beat-and-glide swimming, observed from 4-dpf. During escape swimming, firing of the PMNs results in a fast escape response, whilst for slower more rhythmic swimming movement the recruitment of smaller SMNs is required (Liu and Westerfield, 1988). Smaller, more dorsally located, latter born neurons control slow swimming, whilst larger, more ventrally located, earlier born neurons drive progressively faster swimming (McLean et al., 2007, McLean and Fetcho, 2009). It is this topographic map of MN and IN development and recruitment that allows swimming behaviour to mature from simple coiling to beat-and-glide swimming.

Body bends seen during burst swimming arise from contraction of EW and ER muscle fibres which drive the tail beats, propelling the larvae through the water. ER fibres are only recruited at the slowest swimming speeds, becoming derecruited as speed increases. During the end of bursting swimming, there is a period where only ER muscle fibres are active, as swimming frequency has decreased (van Raamsdonk et al., 1982, Buss and Drapeau, 2000). The alternating activation of MNs occurs due to inhibitory commissural INs, which inhibit neurons on the ipsilateral side (Buss and Drapeau, 2001), whilst excitatory drive for swimming is provided by V2a glutamatergic interneurons (Eklöf-Ljunggren et al., 2012, Ljunggren et al., 2014).

#### *6.1.1.4 Beat-and-Glide Swimming*

At 4-dpf, zebrafish become much more active and the motor pattern transitions to a form of locomotion termed beat-and-glide swimming. This swimming style is more intermittent than the sustained bursting swimming and is characterised by low frequency tail beats (~ 35 Hz) lasting ~ 200 ms, followed by longer 'glide' episodes lasting up to 400 ms in which the larvae propels through the water for a distance ~ 4.7 mm (Buss and Drapeau, 2001). During beat-and-glide swimming, maximal tail bending occurs at a more caudal point in the spinal cord when compared to burst swimming. Larvae turn frequently, displaying routine turns with a low yaw angle (~ 3 °) (Budick and O'Malley, 2000, Buss and Drapeau, 2001). Beat-and-glide swimming is intermittent, but as the larvae develop past 4-dpf, the amount of time dedicated to beat-and-glide swimming increases and periods of inactivity decrease (Hunter, 1972).

As with bursting swimming, beat-and-glide episodes comprise contractions of the musculature in a rostrocaudal direction that alternate between the left and right sides of the body (Masino and Fetcho, 2005). During fictive beat-and-glide swimming, bursts of tonic depolarisation of the MNs become more frequent and last for longer-periods of up to several minutes at a time compared to burst swimming. As with burst swimming, rhythmic EPSPs are also observed, however their frequency decreases to ~ 35 Hz indicative of slower tail-beats during this style of swimming (Buss and Drapeau, 2001). Synaptic depolarising drive from V2a excitatory INs is needed for beat-and-glide swimming, whilst inhibitory input from commissural inhibitory INs is needed for the alternating tail movement. It is this inhibitory input that drives the alternating body contractions which provide rhythmic tail beats (Buss and Drapeau, 2001, McLean, 2005).

Behavioural maturation from burst to beat-and-glide swimming is underpinned by the recruitment of later developing neurons into the motor network. As more, smaller SMNs develop, so too does the behavioural repertoire of the larval zebrafish allowing larvae to develop from simple spontaneous coiling movements, to controlled beat-and-glide episodes (McLean et al., 2007, McLean and Fetcho, 2009).

## 6.2 Aims and Objectives

In previous chapters I demonstrated that proteasome inhibition has a marked effect on synapses within the locomotor network (Chapters 3, 4, 5). Therefore, in this chapter I investigate whether this results in changes to locomotion output. To do this, I investigated the effect of chronic proteasomal inhibition on the free-swimming behaviour of larval zebrafish.

## 6.3 Results

### 6.3.1 The effect of proteasome inhibition on free-swimming behaviour of zebrafish larvae

To determine the effects of proteasome inhibition on swimming behaviour, larval zebrafish (4-dpf) were incubated overnight in MG132 (10 µM) or control saline. Larvae were then placed in the swimming arena and allowed to acclimatise for 10 minutes before being recorded for 5 minutes. Larvae treated with MG132 were first assessed for changes in total distance travelled, time spent swimming and the degree of thigmotaxis displayed compared to control larvae. Thigmotaxis is defined as 'wall-hugging' behaviour and gives an idea of the amount of time larvae spend at the edge of the arena compared to the centre (Schnörr et al., 2012). Thigmotaxis was defined as the period of time a larvae spent within 5 mm of the edge of the arena.

Total distance travelled by larvae treated with MG132 (N = 10) compared to control treated fish (N = 9) was not significantly different (p = 0.7802, MG132: 1938 ± 4743 mm, control: 1918 ± 4805 mm: Figure 41A, B). Larvae treated with MG132 showed no difference in total time spent swimming compared to control larvae (p = 0.1821, MG132: 21.00 ± 74.00 s, control: 35.00. ± 52.00: Figure 41 A, C). However, larvae treated with MG132 showed an increase in thigmotaxis (p = 0.0182, MG132: 64.11 ± 30.51 %, control: 22.44 ± 73.51 %: Figure 41A, D) compared to control larvae.

In summary, no change in total distance travelled or time spent swimming was observed following chronic treatment with MG132, but a significant increase in the percentage of time spent displaying thigmotaxis was observed.

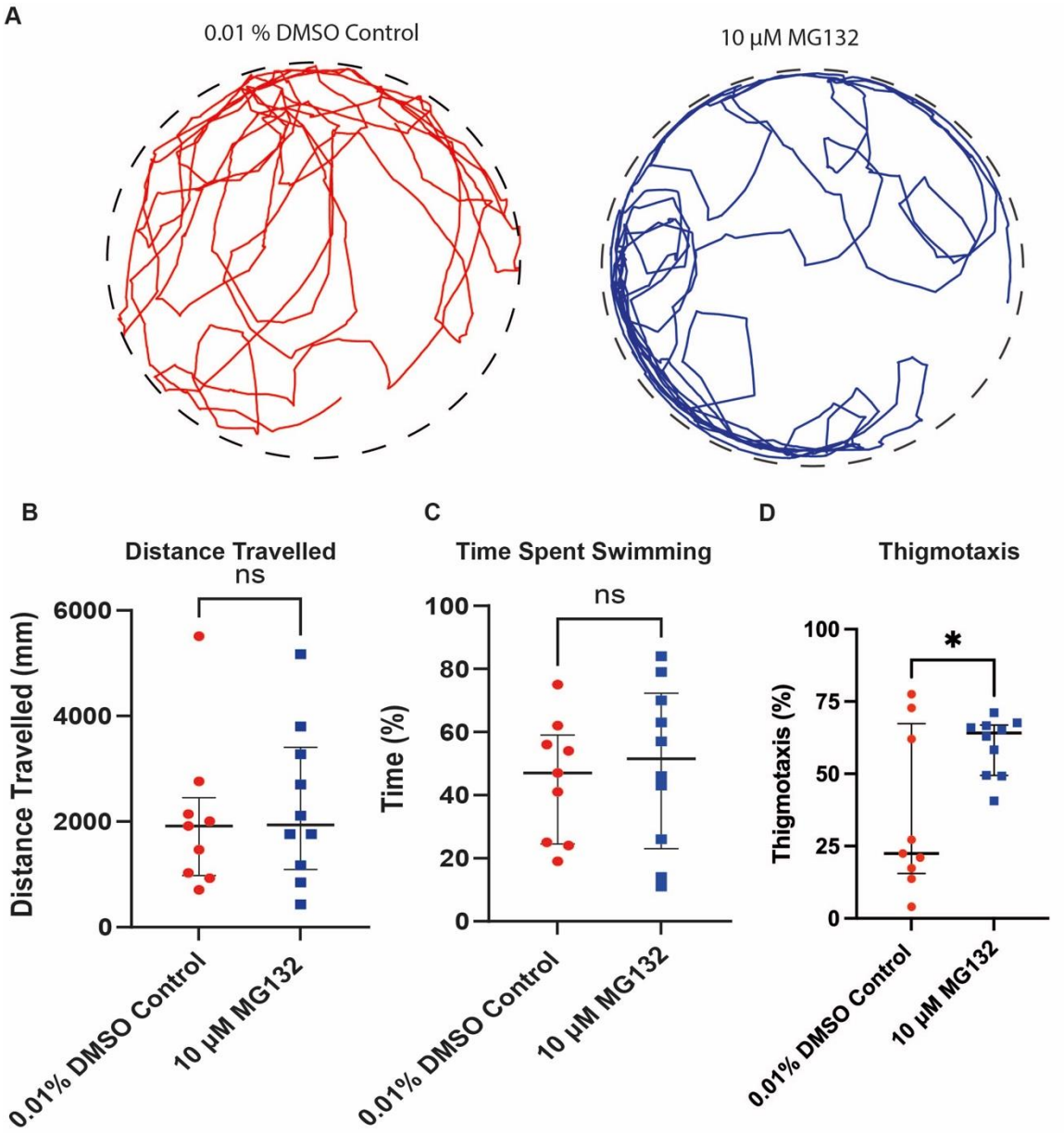


*Figure 41. The effect of overnight incubation with MG132 on the free-swimming behaviour of zebrafish larvae. Larvae were incubated with 10 µM MG1232 or 0.01% DMSO overnight. Larvae were then acclimatised for 10 minutes in the swimming arena before being recorded for 5 minutes free swimming. A) Representative tracking data for larval zebrafish treated with 0.01% DMSO (left) and 10 µM MG132 (right). B) Median with interquartile range plot showing the total distance travelled by larval zebrafish following treatment with 0.01% DMSO and 10 µM MG132. No difference in total distance travelled was determined between MG132 and control treated larvae. C) Median with interquartile range plot showing total time spent swimming as a percentage of time recorded. MG132 treated fish showed no significant difference in the total time spent swimming compared to control. D) Median with interquartile range plot showing the total percentage of thigmotaxis displayed by control and MG132 treated fish. Fish treated with MG132 showed a significantly higher degree of thigmotaxis compared to control treated larvae ($p = 0.0182$). Significant results are indicated with * ($p < 0.05$).*

The effects of bortezomib (50 µM) were next assessed. Overnight incubation with this drug resulted in no significant difference in distance travelled ($p = 0.0507$, bortezomib: N = 9, 836.3 ± 854.8 mm, control: N = 9, 1282 ± 1310 mm: Figure 42 A, B) or percentage of time spent swimming when compared to control treated larvae ($p = 0.1821$, bortezomib: 21.00 ± 74.00 %, control: 35.00 ± 52.00 %: Figure 42 A, C). A significant difference in thigmotaxis was also observed between bortezomib and control conditions ($p = <0.0001$, bortezomib: 78.82 ± 35.29 %, control: 8.667 ± 36.76 %: Figure 42 A, D).

In conclusion, in agreement with MG132 incubated larvae, chronic incubation with bortezomib showed no significant difference in overall distance travelled or time spent swimming, but did show an increase in the percentage of time displaying thigmotaxis.

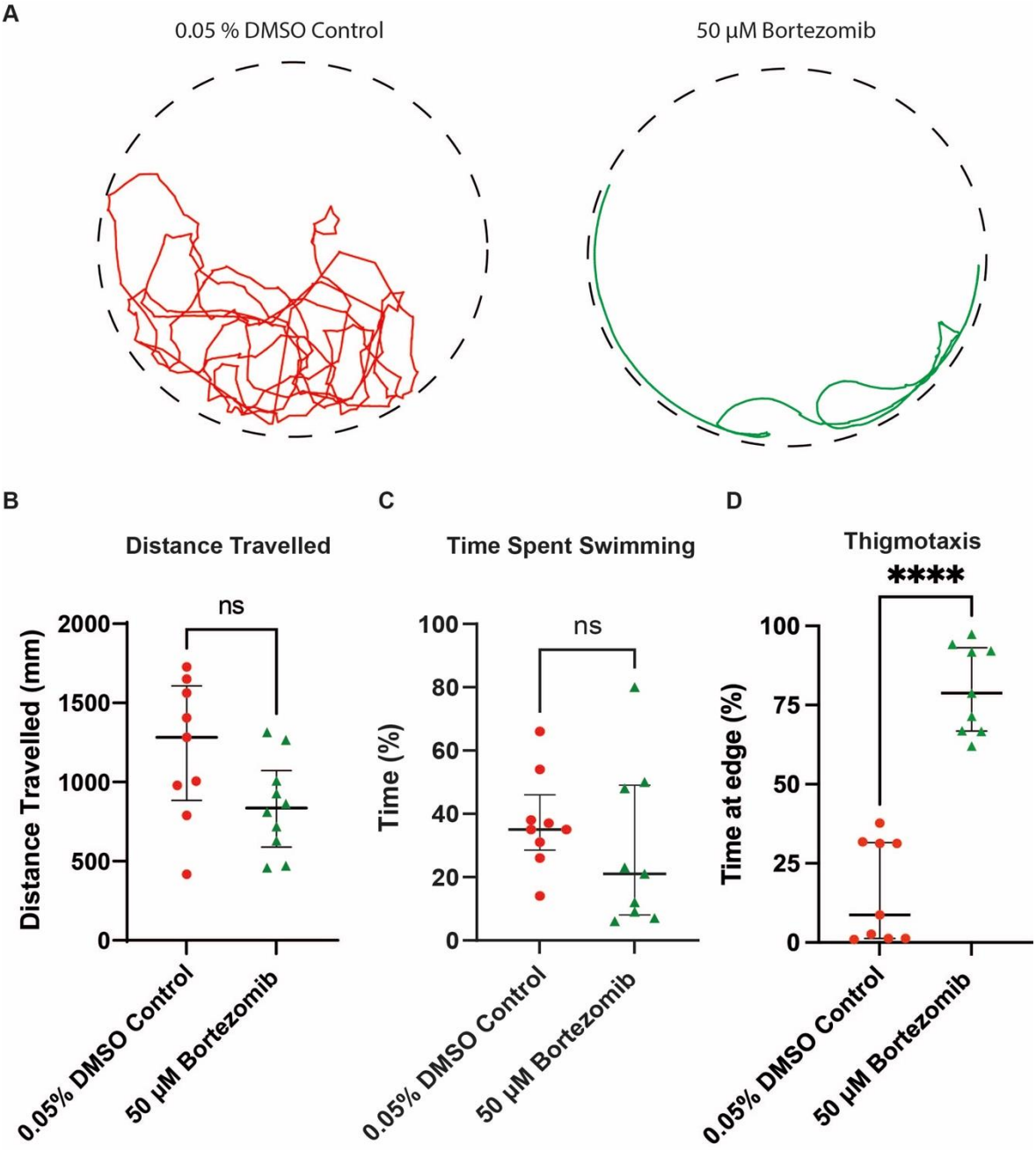


*Figure 42. The effect of overnight incubation with bortezomib on the free-swimming behaviour of zebrafish larvae. Larvae were incubated with 50 µM bortezomib or 0.05% DMSO overnight. Larvae were then acclimatised for 10 minutes in the swimming arena before being recorded for 5 minutes free-swimming. A) Representative tracking data for larval zebrafish treated with 0.05% DMSO (left) and 50 µM bortezomib (right). B) Median with interquartile range plot showing the total distance travelled by larval zebrafish following treatment with 0.05% DMSO and 50 µM bortezomib. No difference in total distance travelled was determined between 50 µM bortezomib and 0.05% DMSO control treated larvae. C) Median with interquartile range plot showing total time spent swimming as a percentage of time recorded. 50 µM bortezomib treated larvae showed no significant difference in the total time spent swimming compared to 0.05% DMSO control treated larvae. D) Median with interquartile range plot showing the total percentage of thigmotaxis displayed by control and 50 µM bortezomib treated larvae. Zebrafish larvae treated with bortezomib showed a significantly higher degree of thigmotaxis compared to control treated larvae ($p < 0.0001$). Significant results are indicated with **** ($p < 0.0001$).*

### 6.3.2 The effect of proteasome inhibition on velocity and bout length of beat glide swimming behaviour of zebrafish larvae

Free swimming videos were next analysed using JAABA (https://jaaba.sourceforge.net/; (Kabra et al., 2013) to identify bouts of beat-and-glide swimming. Raster plots were produced showing identified periods of beat-and-glide swimming for larvae treated with MG132 compared to control saline (Figure 43).Larvae treated overnight with MG132 showed no significant difference in the velocity ($p = 0.6028$, MG132: N = 10, 8,44 ± 14.56 mm/s, control: N = 9, 7.82 ± 17.13 mm/s: Figure 44A, B, C) of beat-and-glide swimming or the length ($p = 0.6105$, MG132: 0.33 ± 0.80 s, control: 0.33 ± 0.67 s: Figure 44 A, D) of beat-and-glide swimming bouts compared to control treated larvae (N = 9). The number of identified episodes of beat-and-glide swimming across the 5-minute recording was also not significantly different between control and MG132 treated larvae ($p = 0.7411$, MG132*:* 43 ± 61, control: 36 ± 40:Figure 43A, B, Figure 44 A, E).

In summary, chronic treatment with MG132 had no effect on the velocity, bout length or number of beat-and-glide episodes identified during free-swimming of zebrafish larvae.

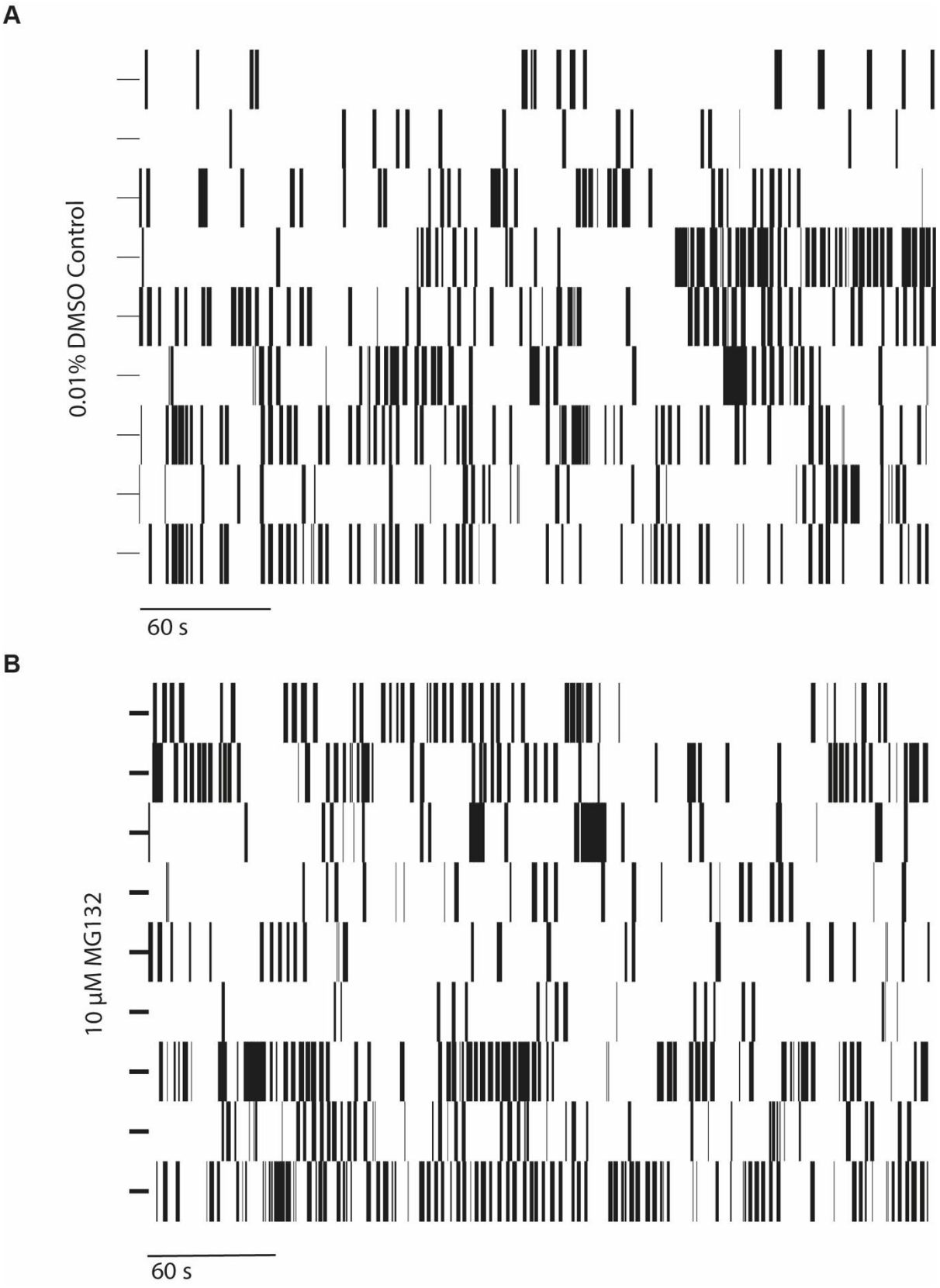


*Figure 43. Raster Plots of identified periods of beat-and-glide swimming for larvae treated with MG132 and control treated larvae.*
*Raster plot representing periods of beat-and-glide swimming for larvae treated with 0.01% DMSO control (A) and 10 µM MG132 (B). Black lines represent periods of beat-and-glide swimming. One row represents one larva*

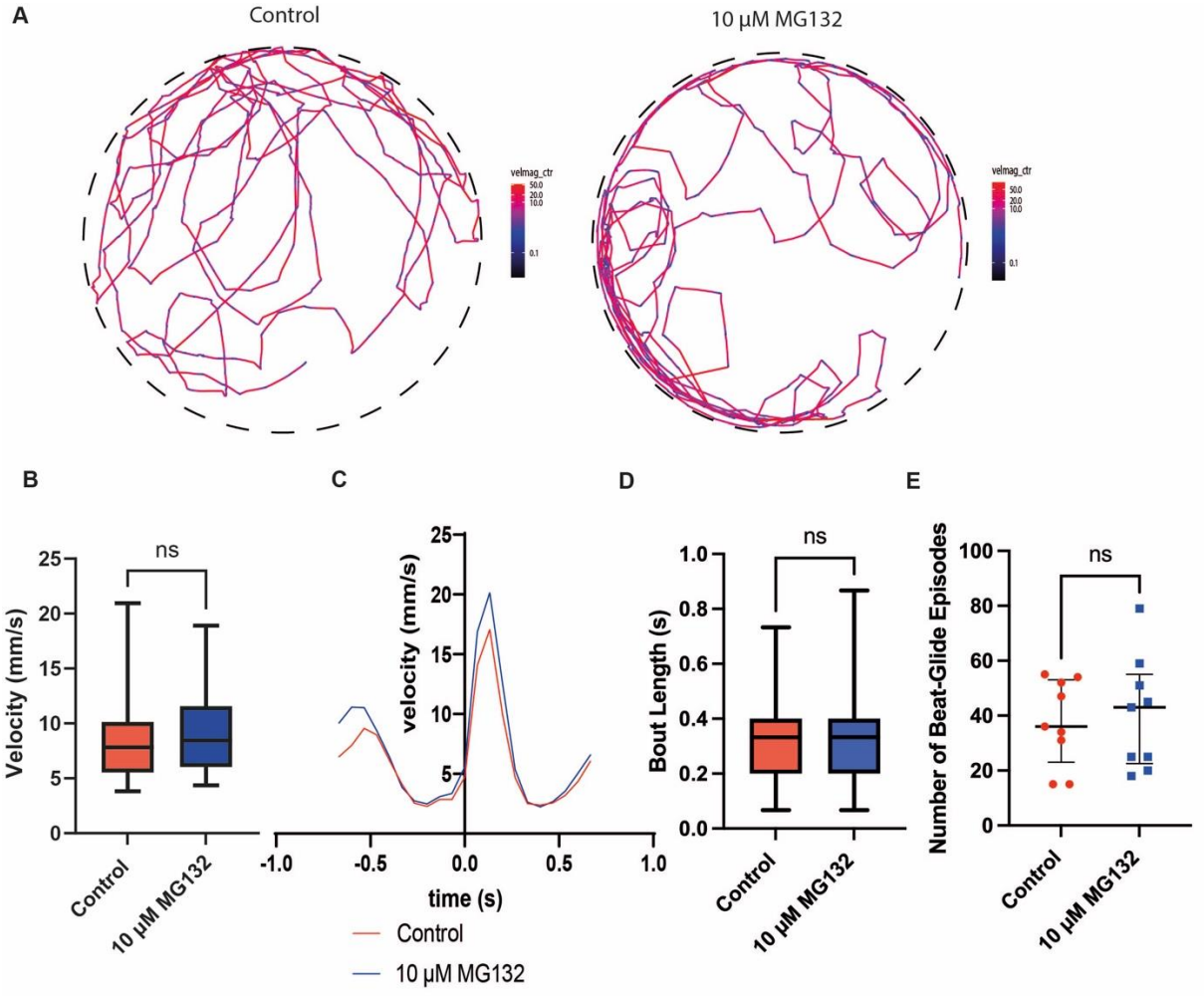


*Figure 44. The effect of overnight incubation with MG132 on beat-and-glide swimming behaviour of larval zebrafish.*

*Free-swimming videos were analysed to identify periods of beat-and-glide swimming using JAABA software. A) Representative traces of MG132 and control treated larvae showing the velocity of the larvae during swimming. B) Median with interquartile range plot showing the velocity of fish during identified beat-and-glide swimming episodes. No significant difference in the velocity of beat-and-glide episodes was detected between larvae treated with 10 µM MG132 compared to 0.01% DMSO control C) Mean velocity across the duration of individual beat-and-glide episodes. No significant difference in velocity was detected between larvae treated with MG132 compared to control larvae. D) Median with interquartile range plots showing identified beat-and-glide bout lengths from larvae treated with 10 µM MG132 compared to larvae treated with 0.01% DMSO. No significant difference in bout length was determined for larvae treated with MG132 compared to control larvae. E) Median with interquartile range plot showing the number of identified beat-and-glide episodes during 5 mins recording. No significant difference was detected between MG132 and DMSO treated larvae.*

Free-swimming videos of larvae treated with bortezomib (50 µM) were also analysed to identify periods of beat-and-glide swimming. A raster plot was produced showing identified periods of free swimming for each larvae treated with bortezomib or control saline (Figure 45). Larvae treated with bortezomib (N = 9) showed a significant increase in the mean velocity of beat-and-glide episodes ($p = 0.014$, bortezomib: N = 9, 6.72 ± 15.23 mm/s, control: N = 9, 5.36 ± 6.46 mm/s: Figure 46A, B, C) and an increase in the duration of identified beat-and-glide bouts ($p = >0.0001$, bortezomib: 0.33 ± 0.93 s, control: 0.27 ± 0.47 s: Figure 46 A, D) compared to control larvae. The number of beat-and-glide episodes were also identified across the 5-minute free-swimming period (Figure 46). A significant decrease in the number of beat-and-glide episodes were identified for bortezomib treated larvae compared to DMSO control treated larvae ($p = 0.0136$, bortezomib: 7 ± 30, control: 28 ± 52: Figure 46A, E).

In conclusion, chronic treatment with bortezomib increased velocity and bout duration of identified episodes of beat-and-glide swimming, whilst the overall number of beat-and-glide episodes reduced in frequency. This was in contrast to observations obtained following MG132 treatment which showed no change in velocity of duration of beat-and-glide episodes and no change in the number of identified episodes of beat-and-glide swimming.

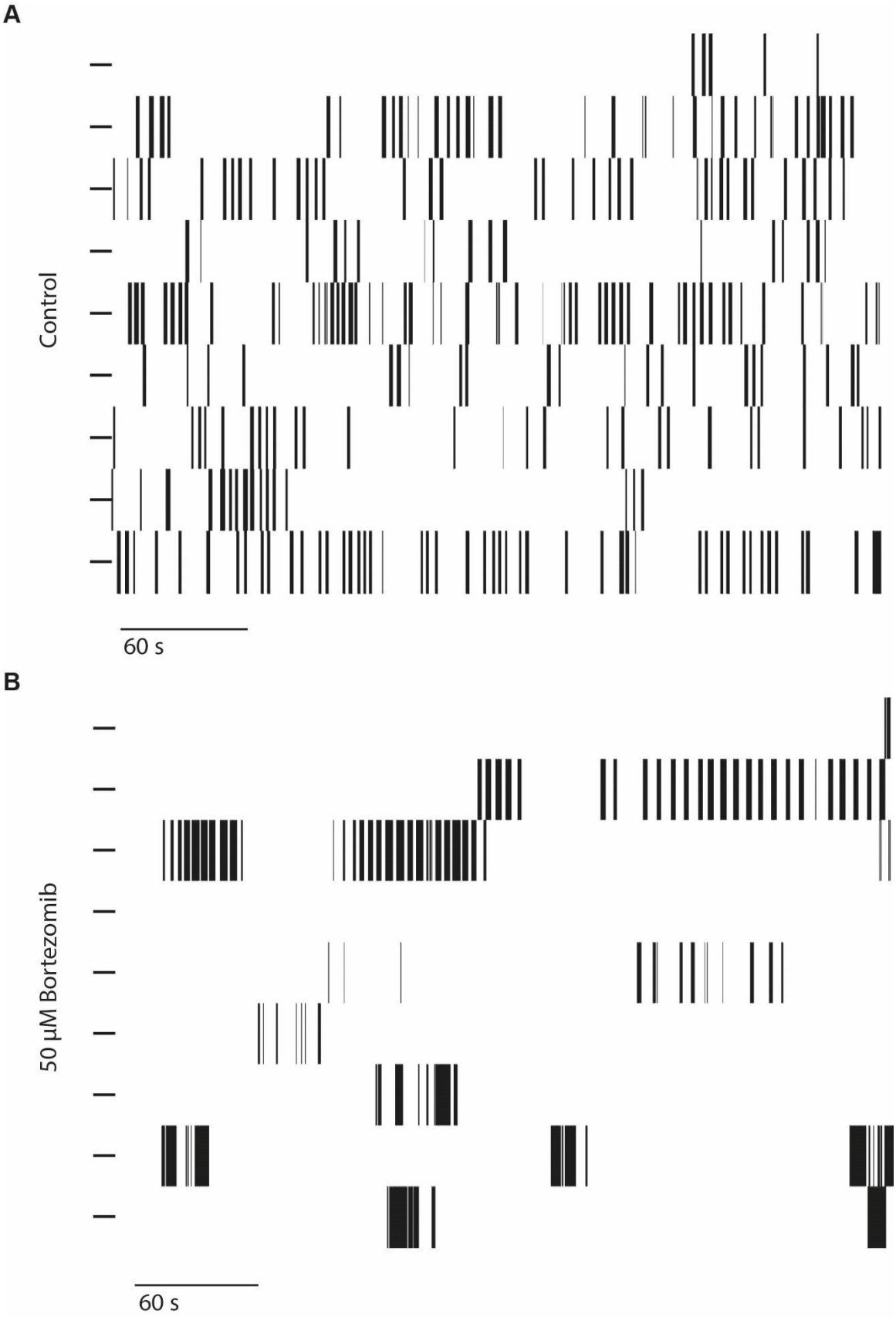


*Figure 45. Raster Plots of identified periods of beat-and-glide swimming for larvae treated with bortezomib and control treated larvae.*

*Raster Plots of identified periods of beat-and-glide swimming for larvae treated with bortezomib and control treated larvae.*

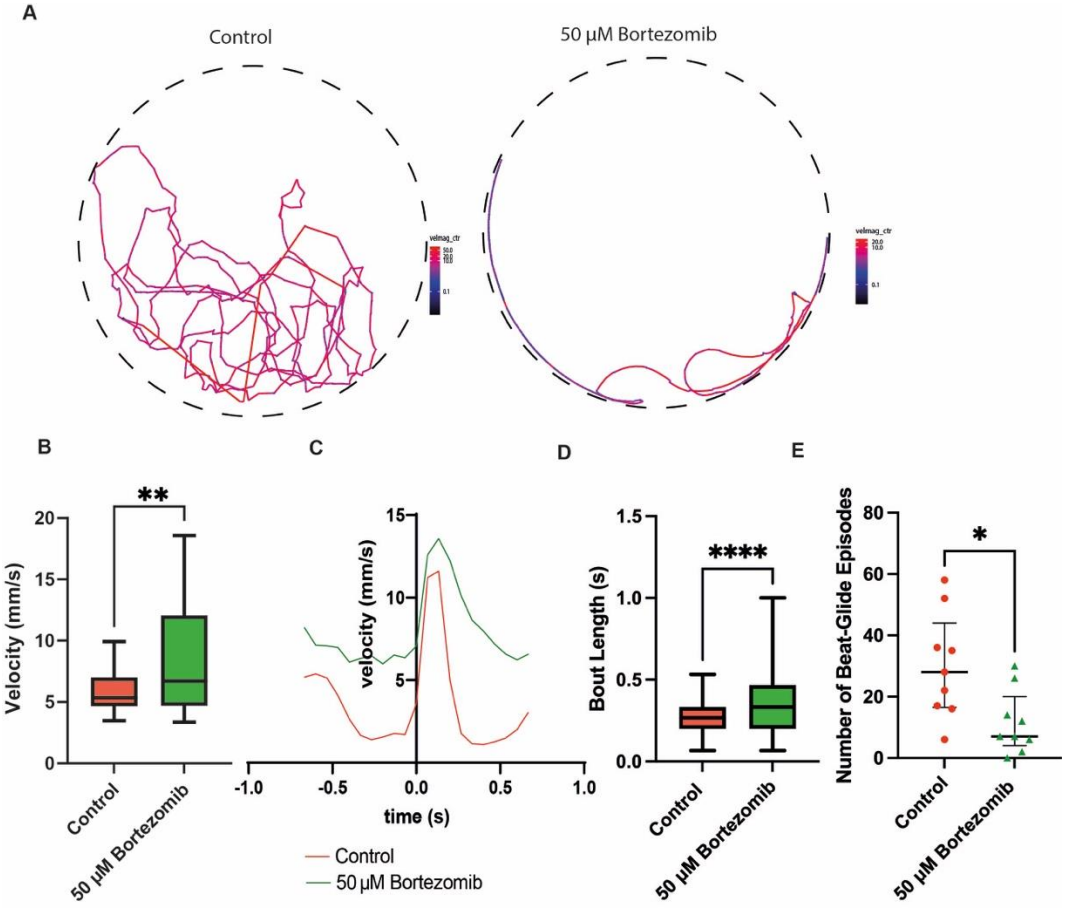


*Figure 46 The effect of overnight incubation with bortezomib on beat-and-glide swimming behaviour of larval zebrafish.*

*Free-swimming videos were analysed to identify periods of beat-and-glide swimming using JAABA software. A) Representative tracking data of bortezomib (left) and control (right) treated larvae showing the velocity of the larvae during free swimming. B) Median with interquartile range plot showing the velocity of fish during identified beat-and-glide swimming episodes. A significant increase in the velocity of beat-and-glide episodes was detected between larvae treated with 50 µM bortezomib compared to 0.05% DMSO control (p = 0.0014) C) Mean velocity across the duration of individual beat-and-glide episodes for larvae treated with bortezomib (green) and DMSO control (red). A significant increase in velocity was detected between larvae treated with bortezomib compared to control larvae (p = <0.0001). D) Median with interquartile range plots showing identified beat-and-glide bout lengths from larvae treated with 50 µM bortezomib compared to larvae treated with 0.05% DMSO. A significant increase in bout length was determined for larvae treated with bortezomib compared to control larvae (p = >0,0001). E) Median with interquartile range plot showing the number of identified beat-and-glide episodes during 5 mins recording. A significant decrease in the number of beat-and-glide episodes was detected for larvae treated with bortezomib compared to control (p = 0.0136) Significance values; ** = p ≤ 0.005, *** = p ≤ 0.0001*

## 6.4 Discussion

In Chapter 6, I have investigated the role of the proteasome in the locomotor behaviour of larval zebrafish using the pharmacological inhibitors MG132 and bortezomib. Following chronic incubation with proteasome inhibitors, I have shown that there is no difference in the total distance travelled or time spent swimming compared to control treated larvae. However, larvae treated with either MG132 or bortezomib showed increased thigmotaxis. I also identified that there was no significant difference in the velocity, mean bout length or number of beat-and-glide episodes identified in larval zebrafish treated with MG132 compared to controls. However, a significant increase in swimming velocity and bout length was determined for larvae treated with bortezomib. In addition, these larvae showed a significant decrease in the number of beat-and-glide episodes when compared to control treated larvae.

### 6.4.1 The effect of proteasome inhibition on free-swimming behaviour

In this chapter, I have shown that chronic proteasomal inhibition with MG132 or bortezomib did not affect the swimming distance or time spent swimming by larval zebrafish. In contrast, following bortezomib, but not MG132, treatment the velocity of swimming and the duration of beat-and-glide episodes increases. In Chapter 5 of this thesis, I showed that proteasomal inhibition with bortezomib, but not MG132 increased spontaneous neurotransmission at the NMJ. Throughout this thesis, I have studied spontaneous neurotransmission, however swimming behaviour is driven by evoked release events. Increased frequency of mEPPs could indicate an increase in neurotransmission during evoked release events, however further experiments investigating evoked release at the NMJ would be required to determine if this were the case.

Increased synaptic transmission at the NMJ could result in increased strength of muscle contraction, resulting in the changes to behavioural output observed here. ACh is released from MNs and binds to nicotinic AchR (nAchR) on the post-synaptic muscle fibre. Activation of nAChRs causes influx of sodium ions, causing a depolarisation of the membrane which results in activation of L-type calcium channels (Martyn et al., 2009). Muscle contraction is dependent on the concentration of cytosolic calcium, with increased calcium associated with stronger muscle contraction (Lamboley et al., 2015). Therefore,

increased ACh could result in increased nAchR activation, subsequently resulting in a larger influx of $Ca^{2+}$ to the muscle fibre, hence increasing the strength of muscle contraction. Beat-and-glide swimming is powered by an initial period of tail beating, which is driven by muscle contractions. The frequency of tail beats is unlikely to be altered by increased muscle contraction, as tail beat frequency is driven my glutamatergic drive to the MNs (Buss and Drapeau, 2001, Eklöf-Ljunggren et al., 2012). However, increased synaptic strength and subsequent increased muscle contraction, could be resulting in more powerful movement which could be propelling the larvae at a faster rate to increase the duration of swimming periods.

In addition to the increased velocity, bortezomib incubation, also decreased the number of beat-and-glide swimming episodes. This change in behaviour could also be attributed to increased ACh release. Overstimulation of nAChR due to an accumulation of ACh at the NMJ can result is muscle fatigue and is often seen in patients with myasthenia gravis (a muscle disease associated with decreased levels of acetylcholinesterase; (Gilhus, 2016). As ACh release increases the strength of muscle contractions, this could also be increasing the rate of muscle fatigue (Gandevia, 2001). As such the observed longer periods of inactivity between beat-and-glide episodes could also be caused by increased Ach release resulting in increased muscle fatigue.

An alternative explanation for this increased velocity and bout duration could be due to changes in supraspinal inputs to the spinal cord. Supraspinal neurons in the nMLF have been shown to modulate the duration and speed of swimming bouts (Severi et al., 2014). Hence, whilst the increased duration and speed of beat-and-glide swimming observed here could be due to increased synaptic input to the musculature due to proteasome inhibition, this study could indicate that proteasomal inhibition may also be altering the physiology of supraspinal neurons of the nMLF. As project restraints meant that I could only utilise spinalised preparations for this study, I was unable to test this hypothesis. However, this would be something of interest to look into going forward.

The observed increase in velocity following only bortezomib incubation was a surprising effect. In Chapters 3 and 4, I showed that proteasomal inhibition resulted in increased glycinergic synaptic transmission at the MNs. Glycinergic signalling is important for the alternating inhibition of MNs on the ipsilateral and contralateral side of the zebrafish resulting in undulating body movement (Buss and Drapeau, 2001). Application of strychnine

to larval zebrafish during NMDA-induced motor activity caused individual bursts of activity to shift from an alternating to a synchronised pattern. Strychnine also reduces the frequency of motor output, by increasing the frequency of action potentials (Buss and Drapeau, 2001). In *Xenopus* tadpoles, the use of a selective glycine antagonist, L-689560, inhibited fictive swimming, whilst the agonist, glycine or D-serine, increased fictive swimming (Issberner and Sillar, 2007). As such, it is conceivable that an increase in glycinergic transmission, as observed in this thesis, could have resulted in a change to motor output. However, throughout this thesis I have studied the effects of proteasomal inhibition on spontaneous neurotransmission, which differs from evoked neurotransmission (see Chapter 3 introduction). As such, it is also possible that evoked release of glycine increases following proteasomal inhibition, but the effect on swimming may be too subtle to detect with the methods used in this thesis. Further work would be required to investigate the effects of proteasomal inhibition on evoked release.

I also showed that larval zebrafish treated with proteasome inhibitors increased their level of thigmotaxis. Thigmotaxis is a behaviour associated with anxiety whereby animals show avoidance of open areas, instead swimming close to the boundaries of the arena in which they are swimming (Schnörr et al., 2012, Basnet et al., 2019). The main findings from this thesis have shown increased glycinergic synaptic input to MNs and increased synaptic input to the musculature. Thigmotaxis is linked to brain regions including the rostrodorsal telencephalon (Simon et al., 1994, Peitsaro et al., 2003). In adult zebrafish, injection with a histidine decarboxylase inhibitor resulted in increased thigmotaxis (Peitsaro et al., 2003). Histaminergic neurons are found to highly innervate the rostrodorsal telencephalon in adult zebrafish brains. Hence, there is some evidence to suggest that thigmotaxis is a result of changes to the histaminergic system (Peitsaro et al., 2003). In this thesis I have shown that proteasomal inhibition can induce increases in synaptic transmission in certain cell types. In the context of previous work carried out studying thigmotaxis, this could suggest that proteasome inhibition is inducing changes in synaptic transmission within neurons associated with thigmotaxis.

There is a lack of research into the causes of thigmotaxis and the brain regions involved. Previous research outlining thigmotatic behaviour in rodents has been focused on learning and memory deficits in models of Alzheimer's disease. Transgenic mice containing APP695 gene with the Swedish mutation (APP KM670) displayed increased thigmotatic

behaviour in the Morris Water Maze behavioural test. LTP was measured in this murine model and showed that LTP was normal at 10-13 weeks of age, but showed impairment with a reduction in LTP in 3 week old mice (Sri et al., 2019). Furthermore, THY-Tau22 transgenic mice, a genetic line which overexpressed human tau, also showed increased thigmotatic behaviour in the Morris Water Maze test. In LTD recordings, THY-Tau22 mice showed decreased maintenance of LTD at 9 months of age (Jeugd et al., 2011). In both studies, authors concluded that increased thigmotaxis was seen due to changes in learning and memory behaviour as a result of impaired LTP and LTD. However, in both transgenic mice lines plaques of aggregated protein (amyloid-β and tau in the APP-mice and THY-Tau22 mice respectively) were present in the brain (Jeugd et al., 2011, Sri et al., 2019). During inhibition of the proteasome, proteins cannot be efficiently degraded. As such, accumulation of proteins begins to occur within neurons. In the context of these previous findings of murine models which show protein aggregates, this could indicate that the increased thigmotaxis observed in my results are due to increased accumulation of proteins due to an inhibited proteasome.

### 6.4.2 Conclusions

In this chapter, I have shown that incubation with the proteasome inhibitor bortezomib does not affect time spent swimming or distance travelled but significantly increases the velocity and bout duration of beat-and-glide swimming episodes whilst also decreasing the number of observed beat-and-glide episodes. By contrast, MG132 had no effect on any of the locomotor parameters observed. Thus, the effects of these two proteasome inhibitors are complex, with contrasting effects on behavioural output. This is perhaps surprising as both inhibitors caused a rapid and consistent increase in glycinergic input to MNs during physiological recordings. Therefore, I posit that the differences observed in behaviour arise primarily from bortezomib's ability to selectively increase ACh transmission at the NMJ.

Both MG132 and bortezomib also increased thigmotaxis in larval zebrafish. However, as thigmotaxis is a behaviour associated with anxiety and hence, regions of the brain which could not be utilised in this study, I cannot comment on what could be causing this change in behaviour.

# Chapter 7 Discussion

In this thesis I have examined the effect of proteasome inhibition on the synaptic properties of neurons involved in generating motor output in larval zebrafish. I have assessed the physiology of MNs following overnight (Chapter 1) and 1-hour (Chapter 2) incubation with pharmacological inhibitors of the proteasome. I then assessed the branching outgrowth of PMNs following overnight incubation with proteasome inhibitors and their effects on the NMJ formation and physiology (Chapter 3). Finally, I investigated the effects of overnight proteasomal inhibition on the behaviour of free-swimming larval zebrafish (Chapter 4). Whilst previous experiments have assessed the effect of proteasomal inhibition on the electrophysiological properties of cultured hippocampal neurons (Rinetti and Schweizer, 2010) and dissected drosophila NMJ (Speese et al., 2003), these experiments were not carried out in an *in vivo* model. In this thesis, I have used the larval zebrafish as a model organism, as larvae can be used to easily link the physiology, morphology and resultant behaviour of the animal together, to assess the wider implications of proteasomal inhibition on an intact neuronal network.

In Chapter 3, I incubated larval zebrafish (3-dpf) overnight with proteasome inhibitors and assessed the intrinsic properties of PMNs using whole-cell voltage and current clamp recordings. I showed that glycinergic mIPSC frequency increased as a result of incubation with three different proteasome inhibitors (MG132, lactacystin and bortezomib), whilst glutamatergic mEPSCs showed no change in frequency. Equally, firing frequency was unaffected by proteasomal inhibition of PMNs. I showed that these effects occur over a shorter incubation period in chapter 4, with the increase in glycinergic mIPSCs observed with both MG132 and bortezomib after 1-hour incubation. In Chapter 5, I also showed that proteasomal inhibition with bortezomib is sufficient to induce changes in mEPCs from NMJs.

Taken together, the above results suggest that the inhibition of the proteasome is sufficient to induce changes in synaptic transmission in a synapse-specific manner. Changes to the frequency of neurotransmitter release indicate a pre-synaptic mode of action, as more vesicles are being released into the pre-synaptic cleft or that there has been an increase in the number of glycinergic synapses. Hence, in the developing zebrafish spinal cord, the proteasome appears to exert differential effects on regulation of excitatory and inhibitory synapses. This stands in contrast to the literature: inhibiting the proteasome in

mammalian hippocampal neurons showed increased release at both inhibitory and excitatory synapses following application of MG132 (Rinetti and Schweizer, 2010). Notwithstanding the aforementioned discrepancy, differences between inhibitory and excitatory synapses and vesicle release machinery could account for the differences observed in this thesis. Improved imaging techniques have shown differences in both the ultrastructure and dynamics of vesicle pools in nerve terminals of inhibitory and excitatory synapses, with inhibitory vesicle travelling shorter distances to fuse with the active zone and showing a shorter fusion time with a higher rate of kiss-and-run fusion (Park et al., 2020, Tao et al., 2018). Kiss-and-run fusion is where the vesicle transiently fuses to the membrane in order to open and release quanta into the synaptic cleft, before closing and being reused (Harata et al., 2006, de Toledo et al., 1993). Kiss-and-run fusion has been shown to be involved in both evoked and spontaneous vesicle release (Stevens and Williams, 2000). In the context of the increased spontaneous inhibitory neurotransmitter observed in this thesis, this could indicate that the proteasome regulates synaptic machinery involved in kiss-and-run fusion. There is evidence to suggest that munc-18 can regulate a switch to kiss-and-run fusion instead of full fusion release. Use of munc-18 mutants in lactotroph cell culture from rats showed that different mutations altered the morphology of vesicles, but also the time spent by vesicles at the synaptic membrane. As such these results suggested that munc-18 might control fusion kinetics at the plasma membrane (Jorgacevski et al., 2011, Burgoyne et al., 2001). The UPS is known to regulate munc-18 levels (Martin et al., 2014). Therefore, as inhibitory synapses show increased kiss-and-run fusion dynamics compared to excitatory synapses, inhibitory specific increase in neurotransmitter release could be due to differential vesicle fusion events seen between inhibitory and excitatory synapses.

Whilst differences in vesicle dynamics have been established using imaging techniques, there is less evidence for the differences in molecular release machinery at inhibitory and excitatory synapses. With that said, it is known that some synaptic proteins that are also substrates for the UPS have differing exocytotic roles at inhibitory and excitatory synapses. For example, the ELKS proteins (a protein involved in forming the active zone complex) increase the RRP size at excitatory synapses, but do not affect $Ca^{2+}$ influx, whilst ELKS proteins increase $Ca^{2+}$ influx and vesicular release probability at inhibitory synapses (Held et al., 2016, Liu et al., 2014). ELKS proteins have been shown to be targeted

for degradation by the proteasome (Jiang et al., 2010, Teixeira et al., 2013, Tada et al., 2010). As such, an increase in ELKS proteins at inhibitory synapses subsequent to proteasome inhibition could increase release probability in inhibitory synapses, but not excitatory synapses. Hence, this could account for the observed differences in vesicle release between inhibitory and excitatory synapses, as accumulation of the same protein in different cell types could result in differing effects to neurotransmission. Detailed molecular analysis of molecular machinery at synapses of the zebrafish spinal cord would help to determine if this could account for the differences observed between synapses in this thesis.

Differential regulation of neuronal plasma membrane proteasomes (NMPs) provide possible explanation for the selective increase in transmission at glycinergic synapses. These are 20S proteasome complexes associated with the neuronal plasma membrane (Ramachandran and Margolis, 2017). NMPs are capable of degrading intracellular nascent proteins and excreting peptides into the extracellular space which are then used as signalling molecules. Inhibiting NMPs in the *Xenopus* optic tectum has been shown to increase spontaneous neuronal activity due to accumulation of nascent proteins, including protein products from activity induced immediate early genes (IEGs; (Ramachandran et al., 2018, He et al., 2022). The exact mechanism by which nascent proteins increase spontaneous activity has yet to be elucidated. There is evidence to suggest that the composition of the nascent proteome varies depending on the activity pattern of the neuron. Homeostatic synaptic up-scaling or down-scaling in cultured rat hippocampal neurons did not cause changes to the size of the nascent proteome, but instead led to differential regulation of translation of the proteome with certain proteins being upregulated and others downregulated (Schanzenbächer et al., 2016, Hartman et al., 2006, Liu et al., 2018). This suggests that cell-type specific differences in nascent proteome could contribute to differing effects on neuronal activity, depending on the nascent proteins being degraded. Moreover, inhibition of NMPs could result in differing effects on neuronal activity based on the accumulation of nascent proteomes in different cell types. This may account for the differing effects on vesicular release at glutamatergic and glycinergic synapses in the zebrafish spinal cord.

Further work would be required to establish the existence of NMPs in larval zebrafish and to determine if the effects in synaptic transmission seen here are due to inhibition of

NMPs. Previous work on NMPs have been focused on network changes, rather than cell-specific changes in physiology. Hence, it would be interesting to determine if inhibition of NMPs specifically also contributes to an increase in synaptic transmission by using epoxomicin-biotin in conjunction with whole-cell patch clamp recordings. This would determine if the changes in spontaneous glycinergic transmission are due to inhibition specifically of NMPs. Recent advances in technology have made investigating the nascent proteome of individual cells easier and have begun to elucidate specific differences in the activity-induced nascent proteome of excitatory and inhibitory neurons (Schiapparelli et al., 2022). In the context of this project, further work could be carried out to investigate changes in the nascent proteome between inhibitory and excitatory INs in the zebrafish, to establish if certain proteins have been differentially translated within these cell types.

In Chapter 5 of this thesis, I assessed the effects of overnight inhibition of the proteasome on the morphology of PMNs and the formation of NMJs. Previous work had suggested that during development the proteasome is involved in both synaptogenesis and synaptic pruning (Wan et al., 2000b, DiAntonio et al., 2001a, Collins et al., 2006, Kuo et al., 2005, Kuo et al., 2006b, Ding and Shen, 2008), hence I investigated if the changes in mEPC properties following proteasome inhibition could have been due to changes in neurite innervation to the musculature and increased synapse formation.

I observed no difference in the overall cable length or branching pattern of PMNs following proteasomal inhibition, suggesting that the increase in mEPC frequency was not due to changes in MN innervation to EW muscle cells. Proteasomal inhibition also did not affect the degree of co-localisation of pre- and post-synaptic sites of NMJs, or the total percentage of α-bgt stain. This suggests that proteasomal inhibition does not affect synapse formation in 4-dpf larval zebrafish. Compared to the existing literature (Wan et al., 2000b, DiAntonio et al., 2001a, Collins et al., 2006), this could suggest that the proteasome has a distinct role during the development of synapses in the nervous system, but that inhibition of the proteasome does not cause synaptic pruning or continued formation of synapses in established neurons. PMNs arise in the spinal cord early in development and by day 4 have already innervated the musculature, although synapses are still forming and as such development is by no means complete (Myers, 1985, Myers et al., 1986b). I focused on these neurons to determine if changes in mEPC frequency, were due to changes in the outgrowth of PMNs. Further experiments could be carried out using larval zebrafish to

determine the effect of proteasomal inhibition on the development of spinal neurons through the use of longer incubation times with proteasome inhibitors starting on different days throughout development to establish if the proteasome affects the growth of axons and dendrites. This was beyond the scope of study in this thesis, which was focused primarily on the effects of the proteasome on synaptic plasticity.

In addition to looking at the formation of NMJs following proteasomal inhibition, I had also intended to investigate the formation of excitatory and inhibitory synapses within the spinal cord of larval zebrafish. I did this through staining for PSD95 and gephyrin post-synaptic proteins in sections of the zebrafish spinal cord, in order to visualise the excitatory and inhibitory synapses respectively (Yan et al., 2017). However, due to time constraints on the project I was not able to complete the optimisation of this experiment and I did not obtain valid results for either PSD-95 or gephyrin staining. This would be an interesting addition to be completed in future, as additional glycinergic synapses from inhibitory INs onto the MNs compared to glutamatergic IN inputs could account for the increased glycinergic mIPSCs recorded from MNs following proteasomal inhibition. PSD95 puncta outnumber gephyrin puncta in early embryonic stages (48 hpf), but gephyrin puncta continue to increase throughout development to eventually match the number of PSD95 puncta by larval stage (120 hpf) (Yan et al., 2017). Therefore, it would be interesting to investigate if the differences in pre-synaptic transmission of mIPSCs are due to changes in the number of inhibitory synapses compared to glutamatergic synapses during this period of development.

In the final chapter of this thesis, I showed that overnight inhibition of the proteasome causes changes to the free-swimming behaviour of larval zebrafish. Whilst the overall time spent swimming and the distance travelled did not significantly change as a result of proteasome inhibition, the degree of thigmotaxis did. Thigmotaxis is a behaviour associated with anxiety in many different species, including mammals and fish (Simon et al., 1994, Choleris et al., 2001, Colwill and Creton, 2011). The neuronal circuitry involved in thigmotaxis is less well known, although it has been linked to several different brain regions (Peitsaro et al., 2003, Yanai et al., 1998). In this thesis, project restrictions meant that only spinalised preparations could be used for electrophysiological experiments. As such, investigating thigmotaxis was not a primary objective when I planned Chapter 6 of this thesis and was instead picked up during analysis of free-swimming beat-and-glide

behaviour. This is because thigmotaxis is associated with regions of the brain, not with the neurons in the spinal cord. Hence, it is difficult for me to comment on the reason for these findings.

Changes to beat-and-glide swimming were observed following incubation with bortezomib, but not MG132. Overnight incubation with bortezomib increased the velocity and bout duration of beat-and-glide swimming, but also decreased the number of episodes of beat-and-glide swimming. This result stands in broad agreement with differences seen in electrophysiology at the NMJ between bortezomib incubation and MG132. In Chapter 5, I showed that bortezomib increased the frequency of mEPCs, whereas MG132 did not affect mEPC frequency. This would also explain the disparity in behavioural data, as increased input to the musculature with bortezomib could explain the increases in beat-and-glide speed and bout duration. As I recorded spontaneous release events in this thesis, I posit that increases in spontaneous neurotransmission would also be seen with evoked transmission. However, additional work would be needed to assess the effects of proteasomal inhibition on evoked neurotransmission.

Increased glycinergic signalling was observed following chronic application of both MG132 and bortezomib in Chapter 3. In zebrafish, glycinergic INs are involved in ensuring the alternating inhibition of MNs, leading to activation of muscle fibres on the ipsilateral and contralateral sides of the trunk alternatively. Previous work in *Xenopus* tadpoles has also shown that application of strychnine (glycine receptor blocker) reduced motor output. As such, glycinergic signalling has been shown to be important for locomotive behaviour. Therefore, it was a surprising result that MG132 did not display changes in free-swimming behaviour. The increase in glycinergic signalling I observed was due to increased spontaneous release events, which can be indicative of increased evoked release. As such, further work would be needed to determine if proteasomal inhibition affects the evoked release of glycine.

Differences in the pharmacology of the two inhibitors could account for the discrepancy between bortezomib induced changes to mEPC frequency and MG132. MG132 has been shown to be less metabolically stable than bortezomib, with CYP3 family of enzymes being shown to be able to degrade MG132 (Thibaudeau and Smith, 2019, Lee et al., 2010). CYP3 enzymes are found in tissues throughout the body, including within the neurons of the CNS, and are associated with drug metabolism (Lewis, 2003, Woodland et al.,

2008, Ghosh et al., 2011). As bortezomib is a more specific inhibitor of the proteasome compared to MG132 and has been shown to be sufficient to increase synaptic transmission in PMNs, it seems unlikely that this increase in mEPCs is due to off-target effects of the drug.

Whilst pharmacology is a useful tool for assessing the effects of proteasomal inhibition, there are disadvantages to using pharmacological agents. It can be difficult to determine the final concentration of a drug within an individual cell or to determine if the drugs have accessed all cells within the zebrafish, as larvae are bathed in drug solution and absorb the compounds through the skin. Drugs can also be metabolised or have off-target effects, hence it can be difficult to say with certainty that the drug is interacting with the target complex alone. In this thesis, I have mitigated for these effects by using multiple inhibitors.

An alternative to using pharmacology would be a genetic knockout model. Genetic knockouts of genes involved in the proteasome would allow for investigations into the effect of defective proteasomes on neuronal properties, whilst removing the off-target and toxicity effects that can occur when using pharmacological inhibitors. However, knock-out of proteasome subunit encoding genes are typically embryonic lethal. The proteasome is built of alpha and beta protein subunits and proteins involved in activating the proteasome encoded by four different gene families; PSMA, PSMB, PSMC and PSMD (Bard et al., 2018). PSMA and PSMB genes encode the alpha and beta proteasome subunits, hence knocking out PSMA or PSMB genes are embryonic lethal, as functional proteasomes cannot be formed. PSMC and PSMD genetic mutants and knockouts do exist, however functional 20S proteasomes can still be formed in these genetic models and so this does not allow for investigations into how defects in the catalytic subunits of the proteasome effect the model organism (Küry et al., 2017, Kröll-Hermi et al., 2020).

A conditional knockout of one of the PSMA or PSMB genes would be one way to investigate the effects of proteasome inhibition, without the need for pharmacology. This was beyond the scope of this thesis, as conditional knockouts in the zebrafish are a relatively new technology that is not as advanced as mammalian or invertebrate conditional knockouts (Friedel et al., 2011, Katsnelson, 2019). Advances in technology in recent years have allowed researchers to start producing zebrafish conditional knockout lines (Hans et al., 2021, Kalvaitytė and Balciunas, 2022). Producing a conditional knockout of the genes involved in the proteosome would be an interesting way of assessing the effect of inhibited

proteasomes on neuronal properties, whilst circumventing the issues surrounding pharmacology use. This could be an interesting direction to follow in future experiments.

## 7.1 Conclusion

In this thesis, I have shown that inhibition of the proteasome affects synaptic transmission through increasing the release of synaptic vesicles from pre-synaptic neurons. I have shown that this effect is specific to certain cell types, with increased glycinergic synaptic input onto MNs following proteasomal inhibition, but no increase in glutamatergic synaptic input. Inhibiting the proteasome induced increases in synaptic transmission over both short (1-hour) and chronic (overnight) time periods, with multiple different pharmacological inhibitors.

I have also shown that pharmacological inhibition of the proteasome affects synaptic inputs to the EW muscle fibres, with bortezomib inducing an increase in pre-synaptic vesicle release from the MNs. These results when taken with the increase in glycinergic synaptic inputs to the MNs, suggests that the proteasome has an important function in the release of synaptic vesicles in a synapse-type specific manner.

I have shown that proteasomal inhibition does not alter neurite innervation from PMNs onto the musculature. No changes to the number of NMJs from the PMNs to the musculature were observed as a result of proteasomal inhibition. This suggests that proteasomal inhibition affects synaptic plasticity through alterations to vesicle dynamics rather than through structural changes to the number of synapses or the innervation pattern of neurons.

Finally, I have shown that increased synaptic transmission as a result of proteasomal inhibition affects the behavioural output of the larval zebrafish. Proteasomal inhibition did not alter distance travelled or time spent swimming, however thigmotaxis did increase as a result. In addition to this, using bortezomib induced an increase in the overall bout duration and velocity of beat-and-glide swimming compared to control treated animals. This suggests that increased neurotransmission from MNs onto the EW musculature affects beat-and-glide swimming, by increasing the duration and velocity of bouts.

# References

References

2007. A Rapid Apoptosis Assay Measuring Relative Acridine Orange Fluorescence in Zebrafish Embryos. *Zebrafish,* 4**,** 113-116.

2012. The quest for quantitative microscopy. *Nature Methods,* 9**,** 627-627.

2022. MATLAB. R2022a ed.: The MathWorks Inc. .

ABBAS, R. & LARISCH, S. 2021. Killing by Degradation: Regulation of Apoptosis by the Ubiquitin-Proteasome-System. *Cells,* 10.

ADAMS, J. 2003. The proteasome: structure, function, and role in the cell. *Cancer Treat Rev,* 29 Suppl 1**,** 3-9.

AHMED, K. T., AMIN, M. R., SHAH, P. & ALI, D. W. 2018. Motor neuron development in zebrafish is altered by brief (5-hr) exposures to THC (Δ(9)-tetrahydrocannabinol) or CBD (cannabidiol) during gastrulation. *Sci Rep,* 8**,** 10518.

AIKEN, C. T., KAAKE, R. M., WANG, X. & HUANG, L. 2011. Oxidative stress-mediated regulation of proteasome complexes. *Mol Cell Proteomics,* 10**,** R110.006924.

ALFORD, S. & WILLIAMS, T. L. 1989. Endogenous activation of glycine and NMDA receptors in lamprey spinal cord during fictive locomotion. *The Journal of Neuroscience,* 9**,** 2792.

ALONSO, V. & FRIEDMAN, P. A. 2013. Minireview: ubiquitination-regulated G protein-coupled receptor signaling and trafficking. *Molecular Endocrinology,* 27**,** 558-572.

ALTUN, M., GALARDY, P. J., SHRINGARPURE, R., HIDESHIMA, T., LEBLANC, R., ANDERSON, K. C., PLOEGH, H. L. & KESSLER, B. M. 2005. Effects of PS-341 on the Activity and Composition of Proteasomes in Multiple Myeloma Cells. *Cancer Research,* 65**,** 7896-7901.

ALVAREZ-CASTELAO, B., SCHANZENBÄCHER, C. T., HANUS, C., GLOCK, C., TOM DIECK, S., DÖRRBAUM, A. R., BARTNIK, I., NASSIM-ASSIR, B., CIIRDAEVA, E., MUELLER, A., DIETERICH, D. C., TIRRELL, D. A., LANGER, J. D. & SCHUMAN, E. M. 2017. Cell-type-specific metabolic labeling of nascent proteomes in vivo. *Nature Biotechnology,* 35**,** 1196-1201.

AMARAL, J. D., XAVIER, J. M., STEER, C. J. & RODRIGUES, C. M. 2010. The role of p53 in apoptosis. *Discov Med,* 9**,** 145-52.

AMPATZIS, K., SONG, J., AUSBORN, J. & EL MANIRA, A. 2013. Pattern of innervation and recruitment of different classes of motoneurons in adult zebrafish. *J Neurosci,* 33**,** 10875-86.

AMPATZIS, K., SONG, J., AUSBORN, J. & EL MANIRA, A. 2014. Separate microcircuit modules of distinct v2a interneurons and motoneurons control the speed of locomotion. *Neuron,* 83**,** 934-43.

ANDRE, R. & TABRIZI, S. J. 2012. Misfolded PrP and a novel mechanism of proteasome inhibition. *Prion,* 6**,** 32-6.

ARAVAMUDAN, B. & BROADIE, K. 2003. Synaptic Drosophila UNC-13 is regulated by antagonistic G-protein pathways via a proteasome-dependent degradation mechanism. *J Neurobiol,* 54**,** 417-38.

ARBER, S. 2012. Motor Circuits in Action: Specification, Connectivity, and Function. *Neuron,* 74**,** 975-989.

ARMSTRONG, R. A., LANTOS, P. L. & CAIRNS, N. J. 2008a. What determines the molecular composition of abnormal protein aggregates in neurodegenerative disease? *Neuropathology,* 28**,** 351-365.

ARMSTRONG, R. A., LANTOS, P. L. & CAIRNS, N. J. 2008b. What determines the molecular composition of abnormal protein aggregates in neurodegenerative disease? *Neuropathology,* 28**,** 351-65.

AUSBORN, J., MAHMOOD, R. & EL MANIRA, A. 2012. Decoding the rules of recruitment of excitatory interneurons in the adult zebrafish locomotor network. *Proc Natl Acad Sci U S A,* 109**,** E3631-9.

AZAKIR, B. A., DESROCHERS, G. & ANGERS, A. 2010. The ubiquitin ligase ITCH mediates the antiapoptotic activity of epidermal growth factor by promoting the ubiquitylation and degradation of the truncated C-terminal portion of Bid. *The FEBS journal,* 277**,** 1319-1330.

BACHILLER, S., ALONSO-BELLIDO, I. M., REAL, L. M., PÉREZ-VILLEGAS, E. M., VENERO, J. L., DEIERBORG, T., ARMENGOL, J. & RUIZ, R. 2020. The Ubiquitin Proteasome System in Neuromuscular Disorders: Moving Beyond Movement. *Int J Mol Sci,* 21.

BARBERIS, A., PETRINI, E. M. & MOZRZYMAS, J. 2011. Impact of Synaptic Neurotransmitter Concentration Time Course on the Kinetics and Pharmacological Modulation of Inhibitory Synaptic Currents. *Frontiers in Cellular Neuroscience,* 5.

BARD, J. A. M., GOODALL, E. A., GREENE, E. R., JONSSON, E., DONG, K. C. & MARTIN, A. 2018. Structure and Function of the 26S Proteasome. *Annu Rev Biochem,* 87**,** 697-724.

BARGHOUT, S. H. & SCHIMMER, A. D. 2021. E1 Enzymes as Therapeutic Targets in Cancer. *Pharmacol Rev,* 73**,** 1-58.

BASISTY, N., MEYER, J. G. & SCHILLING, B. 2018. Protein Turnover in Aging and Longevity. *Proteomics,* 18**,** e1700108.

BASNET, R. M., ZIZIOLI, D., TAWEEDET, S., FINAZZI, D. & MEMO, M. 2019. Zebrafish Larvae as a Behavioral Model in Neuropharmacology. *Biomedicines,* 7.

BELLES, B., MALÉCOT, C. O., HESCHELER, J. & TRAUTWEIN, W. 1988. "Run-down" of the Ca current during long whole-cell recordings in guinea pig heart cells: role of phosphorylation and intracellular calcium. *Pflugers Arch,* 411**,** 353-60.

BELLO-ROJAS, S., ISTRATE, A. E., KISHORE, S. & MCLEAN, D. L. 2019. Central and peripheral innervation patterns of defined axial motor units in larval zebrafish. *J Comp Neurol,* 527**,** 2557-2572.

BENARD, G., NEUTZNER, A., PENG, G., WANG, C., LIVAK, F., YOULE, R. J. & KARBOWSKI, M. 2010. IBRDC2, an IBR-type E3 ubiquitin ligase, is a regulatory factor for Bax and apoptosis activation. *Embo j,* 29**,** 1458-71.

BERG, E. M., BJÖRNFORS, E. R., PALLUCCHI, I., PICTON, L. D. & EL MANIRA, A. 2018a. Principles Governing Locomotion in Vertebrates: Lessons From Zebrafish. *Front Neural Circuits,* 12**,** 73.

BERG, E. M., BJÖRNFORS, R. E., PALLUCCHI, I., PICTON, L. D. & EL MANIRA, A. 2018b. Principles Governing Locomotion in Vertebrates: Lessons from Zebrafish. *Frontiers in Neural Circuits,* 12.

BERKERS, C. R., VERDOES, M., LICHTMAN, E., FIEBIGER, E., KESSLER, B. M., ANDERSON, K. C., PLOEGH, H. L., OVAA, H. & GALARDY, P. J. 2005. Activity probe for in vivo profiling of the specificity of proteasome inhibitor bortezomib. *Nature Methods,* 2**,** 357-362.

BERNALES, S., MCDONALD, K. L. & WALTER, P. 2006. Autophagy counterbalances endoplasmic reticulum expansion during the unfolded protein response. *PLoS biology,* 4**,** e423-e423.
BERNHARDT, R. R., CHITNIS, A. B., LINDAMERS, L. & KUWADA, J. Y. 1990. Identification of Spinal Neurons in the Embryonic and Larval Zebrafish. *The Journal of Comparative Neurobiology,* 302**,** 603-616.
BETZ, A., ASHERY, U., RICKMANN, M., AUGUSTIN, I., NEHER, E., SÜDHOF, T. C., RETTIG, J. & BROSE, N. 1998. Munc13-1 is a presynaptic phorbol ester receptor that enhances neurotransmitter release. *Neuron,* 21**,** 123-36.
BHATTACHARYYA, B. J., WILSON, S. M., JUNG, H. & MILLER, R. J. 2012. Altered neurotransmitter release machinery in mice deficient for the deubiquitinating enzyme Usp14. *Am J Physiol Cell Physiol,* 302**,** C698-708.
BINGOL, B. & SCHUMAN, E. M. 2006. Activity-dependent dynamics and sequestration of proteasomes in dendritic spines. *Nature,* 441**,** 1144-1148.
BINGOL, B., WANG, C. F., ARNOTT, D., CHENG, D., PENG, J. & SHENG, M. 2010. Autophosphorylated CaMKIIalpha acts as a scaffold to recruit proteasomes to dendritic spines. *Cell,* 140**,** 567-78.
BLISS, T. V. & LØMO, T. 1973. Long-lasting potentiation of synaptic transmission in the dentate area of the anaesthetized rabbit following stimulation of the perforant path. *The Journal of physiology,* 232**,** 331-356.
BLONDELLE, J., TALLAPAKA, K., SETO, J. T., GHASSEMIAN, M., CLARK, M., LAITILA, J. M., BOURNAZOS, A., SINGER, J. D. & LANGE, S. 2019. Cullin-3–dependent deregulation of ACTN1 represents a pathogenic mechanism in nemaline myopathy. *JCI insight,* 4.
BOLTE, S. & CORDELIÈRES, F. P. 2006. A guided tour into subcellular colocalization analysis in light microscopy. *Journal of microscopy,* 224**,** 213-232.
BONAM, S. R., WANG, F. & MULLER, S. 2019. Lysosomes as a therapeutic target. *Nature Reviews Drug Discovery,* 18**,** 923-948.
BONGIORNO, D., SCHUETZ, F., PORONNIK, P. & ADAMS, D. J. 2011. Regulation of voltage-gated ion channels in excitable cells by the ubiquitin ligases Nedd4 and Nedd4-2. *Channels (Austin),* 5**,** 79-88.
BOON, K. L., XIAO, S., MCWHORTER, M. L., DONN, T., WOLF-SAXON, E., BOHNSACK, M. T., MOENS, C. B. & BEATTIE, C. E. 2009. Zebrafish survival motor neuron mutants exhibit presynaptic neuromuscular junction defects. *Hum Mol Genet,* 18**,** 3615-25.
BOWLING, H., BHATTACHARYA, A., ZHANG, G., LEBOWITZ, J. Z., ALAM, D., SMITH, P. T., KIRSHENBAUM, K., NEUBERT, T. A., VOGEL, C., CHAO, M. V. & KLANN, E. 2016. BONLAC: A combinatorial proteomic technique to measure stimulus-induced translational profiles in brain slices. *Neuropharmacology,* 100**,** 76-89.
BRANSON, K., ROBIE, A. A., BENDER, J., PERONA, P. & DICKINSON, M. H. 2009. High-throughput ethomics in large groups of Drosophila. *Nature Methods,* 6**,** 451-457.
BRILL, R. W. & DIZON, A. E. 1979. Red and white muscle fibre activity in swimming skipjack tuna, Katsuwonus pelamis (L.). *Journal of Fish Biology,* 15**,** 679-685.
BROWN, D. A. & PASSMORE, G. M. 2009. Neural KCNQ (kv7) channels. *British journal of pharmacology,* 156**,** 1185-1195.
BRUSTEIN, E. & DRAPEAU, P. 2005. Serotoninergic Modulation of Chloride Homeostasis during Maturation of the Locomotor Network in Zebrafish. *The Journal of Neuroscience,* 25**,** 10607.

BUCKINGHAM, S. D. & ALI, D. W. 2004. Sodium and potassium currents of larval zebrafish muscle fibres. *J Exp Biol,* 207**,** 841-52.

BUDICK, S. A. & O'MALLEY, D. M. 2000. Locomotor repertoire of the larval zebrafish: swimming, turning and prey capture. *Journal of Experimental Biology,* 203**,** 2565-2579.

BURBEA, M., DREIER, L., DITTMAN, J. S., GRUNWALD, M. E. & KAPLAN, J. M. 2002a. Ubiquitin and AP180 Regulate the Abundance of GLR-1 Glutamate Receptors at Postsynaptic Elements in C. elegans. *Neuron,* 35**,** 107-120.

BURBEA, M., DREIER, L., DITTMAN, J. S., GRUNWALD, M. E. & KAPLAN, J. M. 2002b. Ubiquitin and AP180 regulate the abundance of GLR-1 glutamate receptors at postsynaptic elements in C. elegans. *Neuron,* 35**,** 107-20.

BURGOYNE, R. D., FISHER, R. J. & GRAHAM, M. E. 2001. Regulation of kiss-and-run exocytosis. *Trends in Cell Biology,* 11**,** 404-405.

BUSS, R. R. & DRAPEAU, P. 2000. Physiological properties of zebrafish embryonic red and white muscle fibers during early development. *Journal of neurophysiology,* 84**,** 1545-1557.

BUSS, R. R. & DRAPEAU, P. 2001. Synaptic drive to motoneurons during fictive swimming in the developing zebrafish. *J Neurophysiol,* 86**,** 197-210.

BUSS, R. R. & DRAPEAU, P. 2002. Activation of embryonic red and white muscle fibers during fictive swimming in the developing zebrafish. *Journal of neurophysiology,* 87**,** 1244-1251.

CABOT, J., BUSHNELL, A., ALESSI, V. & MENDELL, N. 1995. Postsynaptic gephyrin immunoreactivity exhibits a nearly one-to-one correspondence with gamma-aminobutyric acid-like immunogold-labeled synaptic inputs to sympathetic preganglionic neurons. *Journal of Comparative Neurology,* 356**,** 418-432.

CALLISTER, R. & GRAHAM, B. 2010. Early history of glycine receptor biology in mammalian spinal cord circuits. *Frontiers in Molecular Neuroscience,* 3.

CAMPBELL, D. S. & HOLT, C. E. 2001. Chemotropic responses of retinal growth cones mediated by rapid local protein synthesis and degradation. *Neuron,* 32**,** 1013-1026.

CARROLL, R. C., BEATTIE, E. C., XIA, H., LÜSCHER, C., ALTSCHULER, Y., NICOLL, R. A., MALENKA, R. C. & VON ZASTROW, M. 1999. Dynamin-dependent endocytosis of ionotropic glutamate receptors. *Proceedings of the National Academy of Sciences,* 96**,** 14112-14117.

CHAPMAN, A., SMITH, S., RIDER, C. & BEESLEY, P. 1994. Multiple ubiquitin conjugates are present in rat brain synaptic membranes and postsynaptic densities. *Neuroscience letters,* 168**,** 238-242.

CHAPMAN, D. C., HUBERT, W. A. & JACKSON, U. T. 1988. Influence of Access to Air and of Salinity on Gas Bladder Inflation in Striped Bass. *The Progressive Fish-Culturist,* 50**,** 23-27.

CHEN, G.-F., XU, T.-H., YAN, Y., ZHOU, Y.-R., JIANG, Y., MELCHER, K. & XU, H. E. 2017a. Amyloid beta: structure, biology and structure-based therapeutic development. *Acta Pharmacologica Sinica,* 38**,** 1205-1235.

CHEN, P. C., QIN, L. N., LI, X. M., WALTERS, B. J., WILSON, J. A., MEI, L. & WILSON, S. M. 2009. The proteasome-associated deubiquitinating enzyme Usp14 is essential for the maintenance of synaptic ubiquitin levels and the development of neuromuscular junctions. *J Neurosci,* 29**,** 10909-19.

CHEN, X., YANG, Q., XIAO, L., TANG, D., DOU, Q. P. & LIU, J. 2017b. Metal-based proteasomal deubiquitinase inhibitors as potential anticancer agents. *Cancer metastasis reviews,* 36**,** 655-668.

CHOLERIS, E., THOMAS, A. W., KAVALIERS, M. & PRATO, F. S. 2001. A detailed ethological analysis of the mouse open field test: effects of diazepam, chlordiazepoxide and an extremely low frequency pulsed magnetic field. *Neuroscience & Biobehavioral Reviews,* 25**,** 235-260.

CHOW, D. M., ZUCHOWSKI, K. A. & FETCHO, J. R. 2017. In Vivo Measurement of Glycine Receptor Turnover and Synaptic Size Reveals Differences between Functional Classes of Motoneurons in Zebrafish. *Curr Biol,* 27**,** 1173-1183.

CHOW, L. W. C. & LEUNG, Y.-M. 2020. The versatile Kv channels in the nervous system: actions beyond action potentials. *Cellular and Molecular Life Sciences,* 77**,** 2473-2482.

CIECHANOVER, A., ELIAS, S., HELLER, H. & HERSHKO, A. 1982. "Covalent affinity" purification of ubiquitin-activating enzyme. *J Biol Chem,* 257**,** 2537-42.

COHEN, A. H. & HARRIS-WARRICK, R. M. 1984. Strychnine eliminates alternating motor output during fictive locomotion in the lamprey. *Brain Res,* 293**,** 164-7.

COHEN, L. D., ZUCHMAN, R., SOROKINA, O., MÜLLER, A., DIETERICH, D. C., ARMSTRONG, J. D., ZIV, T. & ZIV, N. E. 2013. Metabolic turnover of synaptic proteins: kinetics, interdependencies and implications for synaptic maintenance. *PLoS One,* 8**,** e63191.

COLLEDGE, M., SNYDER, E. M., CROZIER, R. A., SODERLING, J. A., JIN, Y., LANGEBERG, L. K., LU, H., BEAR, M. F. & SCOTT, J. D. 2003. Ubiquitination regulates PSD-95 degradation and AMPA receptor surface expression. *Neuron,* 40**,** 595-607.

COLLINGRIDGE, G. L., PEINEAU, S., HOWLAND, J. G. & WANG, Y. T. 2010. Long-term depression in the CNS. *Nature Reviews Neuroscience,* 11**,** 459-473.

COLLINS, C. A., WAIRKAR, Y. P., JOHNSON, S. L. & DIANTONIO, A. 2006. Highwire Restrains Synaptic Growth by Attenuating a MAP Kinase Signal. *Neuron,* 51**,** 57-69.

COLWILL, R. M. & CRETON, R. 2011. Locomotor behaviors in zebrafish (Danio rerio) larvae. *Behavioural Processes,* 86**,** 222-229.

COSKER, K. E. & EICKHOLT, B. J. 2007. Phosphoinositide 3-kinase signalling events controlling axonal morphogenesis. *Biochem Soc Trans,* 35**,** 207-10.

CRAWFORD, D. C., RAMIREZ, D. M., TRAUTERMAN, B., MONTEGGIA, L. M. & KAVALALI, E. T. 2017. Selective molecular impairment of spontaneous neurotransmission modulates synaptic efficacy. *Nat Commun,* 8**,** 14436.

CRAWFORD, L. J. A., WALKER, B., OVAA, H., CHAUHAN, D., ANDERSON, K. C., MORRIS, T. C. M. & IRVINE, A. E. 2006. Comparative Selectivity and Specificity of the Proteasome Inhibitors BzLLLCOCHO, PS-341, and MG-132. *Cancer Research,* 66**,** 6379-6386.

CRIMMINS, S., JIN, Y., WHEELER, C., HUFFMAN, A. K., CHAPMAN, C., DOBRUNZ, L. E., LEVEY, A., ROTH, K. A., WILSON, J. A. & WILSON, S. M. 2006. Transgenic Rescue of <em>ataxia</em> Mice with Neuronal-Specific Expression of Ubiquitin-Specific Protease 14. *The Journal of Neuroscience,* 26**,** 11423.

CROALL, D. E. & ERSFELD, K. 2007. The calpains: modular designs and functional diversity. *Genome Biology,* 8**,** 218.

CUERVO, A. M. & DICE, J. F. 1998. Lysosomes, a meeting point of proteins, chaperones, and proteases. *J Mol Med (Berl),* 76**,** 6-12.

DAHLMANN, B. 2016. Mammalian proteasome subtypes: Their diversity in structure and function. *Arch Biochem Biophys,* 591**,** 132-40.

DAHLMANN, B., RUPPERT, T., KUEHN, L., MERFORTH, S. & KLOETZEL, P.-M. 2000. Different proteasome subtypes in a single tissue exhibit different enzymatic properties11Edited by R. Huber. *Journal of Molecular Biology,* 303**,** 643-653.

DALE, G. E., LEIGH, P. N., LUTHERT, P., ANDERTON, B. H. & ROBERTS, G. W. 1991. Neurofibrillary tangles in dementia pugilistica are ubiquitinated. *Journal of Neurology, Neurosurgery & Psychiatry,* 54**,** 116.

DAROCZI, B., KARI, G., REN, Q., DICKER, A. P. & RODECK, U. 2009. Nuclear factor kappaB inhibitors alleviate and the proteasome inhibitor PS-341 exacerbates radiation toxicity in zebrafish embryos. *Mol Cancer Ther,* 8**,** 2625-34.

DAVIDSON, W. S., JONAS, A., CLAYTON, D. F. & GEORGE, J. M. 1998. Stabilization of α-synuclein secondary structure upon binding to synthetic membranes. *Journal of Biological Chemistry,* 273**,** 9443-9449.

DAWSON, T. M. & DAWSON, V. L. 2010. The role of parkin in familial and sporadic Parkinson's disease. *Movement disorders : official journal of the Movement Disorder Society,* 25 Suppl 1**,** S32-S39.

DAWSON, T. M. & DAWSON, V. L. 2014. Parkin plays a role in sporadic Parkinson's disease. *Neuro-degenerative diseases,* 13**,** 69-71.

DE TOLEDO, G. A., FERNÁNDEZ-CHACÓN, R. & FERNÁNDEZ, J. M. 1993. Release of secretory products during transient vesicle fusion. *Nature,* 363**,** 554-558.

DEL MONTE, F. & AGNETTI, G. 2014. Protein post-translational modifications and misfolding: new concepts in heart failure. *Proteomics. Clinical applications,* 8**,** 534-542.

DELL'ANGELICA, E. C., MULLINS, C., CAPLAN, S. & BONIFACINO, J. S. 2000. Lysosome-related organelles. *The FASEB Journal,* 14**,** 1265-1278.

DENG, L., KAESER, P. S., XU, W. & SÜDHOF, T. C. 2011. RIM Proteins Activate Vesicle Priming by Reversing Autoinhibitory Homodimerization of Munc13. *Neuron,* 69**,** 317-331.

DERIZIOTIS, P., ANDRÉ, R., SMITH, D. M., GOOLD, R., KINGHORN, K. J., KRISTIANSEN, M., NATHAN, J. A., ROSENZWEIG, R., KRUTAUZ, D., GLICKMAN, M. H., COLLINGE, J., GOLDBERG, A. L. & TABRIZI, S. J. 2011. Misfolded PrP impairs the UPS by interaction with the 20S proteasome and inhibition of substrate entry. *The EMBO Journal,* 30**,** 3065-3077.

DESHAIES, R. J. & JOAZEIRO, C. A. 2009. RING domain E3 ubiquitin ligases. *Annu Rev Biochem,* 78**,** 399-434.

DEVAUX, J., ABIDI, A., ROUBERTIE, A., MOLINARI, F., BECQ, H., LACOSTE, C., VILLARD, L., MILH, M. & ANIKSZTEJN, L. 2016. A Kv7.2 mutation associated with early onset epileptic encephalopathy with suppression-burst enhances Kv7/M channel activity. *Epilepsia,* 57**,** e87-93.

DEVOTO, S. H., MELANÇON, E., EISEN, J. S. & WESTERFIELD, M. 1996. Identification of separate slow and fast muscle precursor cells in vivo, prior to somite formation. *Development,* 122**,** 3371-80.

DIAMOND, J. S. & JAHR, C. E. 1995. Asynchronous release of synaptic vesicles determines the time course of the AMPA receptor-mediated EPSC. *Neuron,* 15**,** 1097-1107.

DIANTONIO, A., HAGHIGHI, A. P., PORTMAN, S. L., LEE, J. D., AMARANTO, A. M. & GOODMAN, C. S. 2001a. Ubiquitination-dependent mechanisms regulate synaptic growth and function. *Nature,* 412**,** 449-52.

DIANTONIO, A., HAGHIGHI, A. P., PORTMAN, S. L., LEE, J. D., AMARANTO, A. M. & GOODMAN, C. S. 2001b. Ubiquitination-dependent mechanisms regulate synaptic growth and function. *Nature,* 412**,** 449-452.

DICE, J. F. 2007. Chaperone-Mediated Autophagy. *Autophagy,* 3**,** 295-299.
DICK, L. R., CRUIKSHANK, A. A., DESTREE, A. T., GRENIER, L., MCCORMACK, T. A., MELANDRI, F. D., NUNES, S. L., PALOMBELLA, V. J., PARENT, L. A., PLAMONDON, L. & STEIN, R. L. 1997. Mechanistic Studies on the Inactivation of the Proteasome by Lactacystin in Cultured Cells *. *Journal of Biological Chemistry,* 272**,** 182-188.
DING, F., BORREGUERO, J. M., BULDYREY, S. V., STANLEY, H. E. & DOKHOLYAN, N. V. 2003. Mechanism for the alpha-helix to beta-hairpin transition. *Proteins,* 53**,** 220-8.
DING, F., LAROCQUE, J. J. & DOKHOLYAN, N. V. 2005. Direct Observation of Protein Folding, Aggregation, and a Prion-like Conformational Conversion *. *Journal of Biological Chemistry,* 280**,** 40235-40240.
DING, M. & SHEN, K. 2008. The role of the ubiquitin proteasome system in synapse remodeling and neurodegenerative diseases. *Bioessays,* 30**,** 1075-83.
DONG, C., BACH, S. V., HAYNES, K. A. & HEGDE, A. N. 2014. Proteasome modulates positive and negative translational regulators in long-term synaptic plasticity. *Journal of Neuroscience,* 34**,** 3171-3182.
DONG, C., UPADHYA, S. C., DING, L., SMITH, T. K. & HEGDE, A. N. 2008. Proteasome inhibition enhances the induction and impairs the maintenance of late-phase long-term potentiation. *Learning & memory,* 15**,** 335-347.
DOWNES, G. B. & GRANATO, M. 2006. Supraspinal input is dispensable to generate glycine-mediated locomotive behaviors in the zebrafish embryo. *Journal of Neurobiology,* 66**,** 437-451.
DREIER, L., BURBEA, M. & KAPLAN, J. M. 2005. LIN-23-mediated degradation of beta-catenin regulates the abundance of GLR-1 glutamate receptors in the ventral nerve cord of C. elegans. *Neuron,* 46**,** 51-64.
DREWS, O., WILDGRUBER, R., ZONG, C., SUKOP, U., NISSUM, M., WEBER, G., GOMES, A. V. & PING, P. 2007. Mammalian proteasome subpopulations with distinct molecular compositions and proteolytic activities. *Mol Cell Proteomics,* 6**,** 2021-31.
DRINJAKOVIC, J., JUNG, H., CAMPBELL, D. S., STROCHLIC, L., DWIVEDY, A. & HOLT, C. E. 2010. E3 ligase Nedd4 promotes axon branching by downregulating PTEN. *Neuron,* 65**,** 341-57.
DUNN, W. A. 1994. Autophagy and related mechanisms of lysosome-mediated protein degradation. *Trends in Cell Biology,* 4**,** 139-143.
EATON, R., LEE, R. & FOREMAN, M. 2001. The Mauthner cell and other identified neurons of the brainstem escape network of fish. *Progress in neurobiology,* 63**,** 467-485.
EATON, R. C., BOMBARDIERI, R. A. & MEYER, D. L. 1977. The Mauthner-initiated startle response in teleost fish. *Journal of Experimental Biology,* 66**,** 65-81.
EATON, R. C. & HACKETT, J. T. The Role of the Mauthner Cell in Fast-Starts Involving Escape in Teleost Fishes. 1984.
EATON, R. C. & NISSANOV, J. 1985. A review of Mauthner-initiated escape behavior and its possible role in hatching in the immature zebrafish, Brachydanio rerio. *Environmental Biology of Fishes,* 12**,** 265-279.
EHLERS, M. D. 2003. Activity level controls postsynaptic composition and signaling via the ubiquitin-proteasome system. *Nat Neurosci,* 6**,** 231-42.
EKLÖF-LJUNGGREN, E., HAUPT, S., AUSBORN, J., DEHNISCH, I., UHLÉN, P., HIGASHIJIMA, S.-I. & EL MANIRA, A. 2012. Origin of excitation underlying locomotion in the spinal circuit of zebrafish. *Proceedings of the National Academy of Sciences,* 109**,** 5511-5516.

ELMORE, S. 2007. Apoptosis: a review of programmed cell death. *Toxicol Pathol,* 35**,** 495-516.
FAN, Z., BERESFORD, P. J., OH, D. Y., ZHANG, D. & LIEBERMAN, J. 2003. Tumor suppressor NM23-H1 is a granzyme A-activated DNase during CTL-mediated apoptosis, and the nucleosome assembly protein SET is its inhibitor. *Cell,* 112**,** 659-72.
FATT, P. & KATZ, B. 1950. Some Observations on Biological Noise. *Nature,* 166**,** 597-598.
FATT, P. & KATZ, B. 1952. Spontaneous subthreshold activity at motor nerve endings. *The Journal of physiology,* 117**,** 109-128.
FAUST, T. E., GUNNER, G. & SCHAFER, D. P. 2021. Mechanisms governing activity-dependent synaptic pruning in the developing mammalian CNS. *Nat Rev Neurosci,* 22**,** 657-673.
FENG, G., TINTRUP, H., KIRSCH, J., NICHOL, M. C., KUHSE, J., BETZ, H. & SANES, J. R. 1998. Dual requirement for gephyrin in glycine receptor clustering and molybdoenzyme activity. *Science,* 282**,** 1321-1324.
FENG, Y., HE, D., YAO, Z. & KLIONSKY, D. J. 2014. The machinery of macroautophagy. *Cell Research,* 24**,** 24-41.
FETCHO, J. R. 1992. The Spinal Motor System in Early Vertebrates and Some of Its Evolutionary Changes. *Brain, Behavior and Evolution,* 40**,** 82-97.
FETCHO, J. R. & FABER, D. S. 1988. Identification of motoneurons and interneurons in the spinal network for escapes initiated by the mauthner cell in goldfish. *The Journal of Neuroscience,* 8**,** 4192.
FINLEY, D., SADIS, S., MONIA, B. P., BOUCHER, P., ECKER, D. J., CROOKE, S. T. & CHAU, V. 1994. Inhibition of proteolysis and cell cycle progression in a multiubiquitination-deficient yeast mutant. *Mol Cell Biol,* 14**,** 5501-9.
FISH, F. E. & HOLZMAN, R. 2019. Swimming Turned on Its Head: Stability and Maneuverability of the Shrimpfish (Aeoliscus punctulatus). *Integr Org Biol,* 1**,** obz025.
FON, E. A. & EDWARDS, R. H. 2001. Molecular mechanisms of neurotransmitter release. *Muscle Nerve,* 24**,** 581-601.
FOTIA, A. B., EKBERG, J., ADAMS, D. J., COOK, D. I., PORONNIK, P. & KUMAR, S. 2004. Regulation of neuronal voltage-gated sodium channels by the ubiquitin-protein ligases Nedd4 and Nedd4-2. *J Biol Chem,* 279**,** 28930-5.
FRANK, C. A., KENNEDY, M. J., GOOLD, C. P., MAREK, K. W. & DAVIS, G. W. 2006. Mechanisms underlying the rapid induction and sustained expression of synaptic homeostasis. *Neuron,* 52**,** 663-77.
FREDJ, N. B. & BURRONE, J. 2009. A resting pool of vesicles is responsible for spontaneous vesicle fusion at the synapse. *Nat Neurosci,* 12**,** 751-8.
FREUDENBURG, W., GAUTAM, M., CHAKRABORTY, P., JAMES, J., RICHARDS, J., SALVATORI, A. S., BALDWIN, A., SCHRIEWER, J., BULLER, R. M. L., CORBETT, J. A. & SKOWYRA, D. 2013. Reduction in ATP Levels Triggers Immunoproteasome Activation by the 11S (PA28) Regulator during Early Antiviral Response Mediated by IFNβ in Mouse Pancreatic β-Cells. *PLOS ONE,* 8**,** e52408.
FRIBLEY, A. & WANG, C. Y. 2006. Proteasome inhibitor induces apoptosis through induction of endoplasmic reticulum stress. *Cancer Biol Ther,* 5**,** 745-8.
FRIEDEL, R. H., WURST, W., WEFERS, B. & KÜHN, R. 2011. Generating conditional knockout mice. *Methods Mol Biol,* 693**,** 205-31.
FULDA, S., GORMAN, A. M., HORI, O. & SAMALI, A. 2010. Cellular stress responses: cell survival and cell death. *International journal of cell biology,* 2010.

FULGA, T. A. & VAN VACTOR, D. 2008. Synapses and growth cones on two sides of a highwire. *Neuron,* 57**,** 339-44.
GAFFIELD, M. A. & BETZ, W. J. 2006. Imaging synaptic vesicle exocytosis and endocytosis with FM dyes. *Nature Protocols,* 1**,** 2916-2921.
GAHTAN, E., TANGER, P. & BAIER, H. 2005. Visual prey capture in larval zebrafish is controlled by identified reticulospinal neurons downstream of the tectum. *Journal of Neuroscience,* 25**,** 9294-9303.
GANDEVIA, S. C. 2001. Spinal and supraspinal factors in human muscle fatigue. *Physiol Rev,* 81**,** 1725-89.
GEORGE, A. J., HOFFIZ, Y. C., CHARLES, A. J., ZHU, Y. & MABB, A. M. 2018. A Comprehensive Atlas of E3 Ubiquitin Ligase Mutations in Neurological Disorders. *Frontiers in genetics,* 9**,** 29-29.
GERLAI, R. 2016. Learning and memory in zebrafish (Danio rerio). *Methods Cell Biol,* 134**,** 551-86.
GHOSH, C., MARCHI, N., DESAI, N. K., PUVENNA, V., HOSSAIN, M., GONZALEZ-MARTINEZ, J., ALEXOPOULOS, A. V. & JANIGRO, D. 2011. Cellular localization and functional significance of CYP3A4 in the human epileptic brain. *Epilepsia,* 52**,** 562-71.
GILHUS, N. E. 2016. Myasthenia Gravis. *N Engl J Med,* 375**,** 2570-2581.
GLENNER, G. G. & WONG, C. W. 1984. Alzheimer's disease: initial report of the purification and characterization of a novel cerebrovascular amyloid protein. *Biochemical and biophysical research communications,* 120**,** 885-890.
GOEL, P., MANNING, J. A. & KUMAR, S. 2015. NEDD4-2 (NEDD4L): the ubiquitin ligase for multiple membrane proteins. *Gene,* 557**,** 1-10.
GOLDBERG, A. L. 1998. Proteasome inhibitors: valuable new tools for cell biologists. *Trends in cell biology,* 8**,** 397-403.
GOMES, A. V., YOUNG, G. W., WANG, Y., ZONG, C., EGHBALI, M., DREWS, O., LU, H., STEFANI, E. & PING, P. 2009. Contrasting Proteome Biology and Functional Heterogeneity of the 20 S Proteasome Complexes in Mammalian Tissues. *Molecular & Cellular Proteomics,* 8**,** 302-315.
GOOLISH, E. M. & OKUTAKE, K. 1999. Lack of gas bladder inflation by the larvae of zebrafish in the absence of an air-water interface. *Journal of Fish Biology,* 55**,** 1054-1063.
GOULDING, M. 2009. Circuits controlling vertebrate locomotion: moving in a new direction. *Nature Reviews Neuroscience,* 10**,** 507-518.
GRILLNER, S. 2003. The motor infrastructure: from ion channels to neuronal networks. *Nature Reviews Neuroscience,* 4**,** 573-586.
GRILLNER, S. & EL MANIRA, A. 2020. Current Principles of Motor Control, with Special Reference to Vertebrate Locomotion. *Physiol Rev,* 100**,** 271-320.
GRILLNER, S. & KOZLOV, A. 2021. The CPGs for Limbed Locomotion–Facts and Fiction. *International Journal of Molecular Sciences,* 22**,** 5882.
GROEMER, T. W. & KLINGAUF, J. 2007. Synaptic vesicles recycling spontaneously and during activity belong to the same vesicle pool. *Nat Neurosci,* 10**,** 145-7.
GROETTRUP, M., PELZER, C., SCHMIDTKE, G. & HOFMANN, K. 2008. Activating the ubiquitin family: UBA6 challenges the field. *Trends in Biochemical Sciences,* 33**,** 230-237.
GUICCIARDI, M. E. & GORES, G. J. 2009. Life and death by death receptors. *The FASEB Journal,* 23**,** 1625-1637.

GUPTA, R., LAN, M., MOJSILOVIC-PETROVIC, J., CHOI, W. H., SAFREN, N., BARMADA, S., LEE, M. J. & KALB, R. 2017. The Proline/Arginine Dipeptide from Hexanucleotide Repeat Expanded C9ORF72 Inhibits the Proteasome. *eNeuro,* 4**,** ENEURO.0249-16.2017.

HAASS, C. & KLOETZEL, P. M. 1989. The Drosophila proteasome undergoes changes in its subunit pattern during development. *Exp Cell Res,* 180**,** 243-52.

HAKIM, V., COHEN, L. D., ZUCHMAN, R., ZIV, T. & ZIV, N. E. 2016. The effects of proteasomal inhibition on synaptic proteostasis. *Embo j,* 35**,** 2238-2262.

HAN, L., TALWAR, S., WANG, Q., SHAN, Q. & LYNCH, J. W. 2013. Phosphorylation of α3 glycine receptors induces a conformational change in the glycine-binding site. *ACS Chem Neurosci,* 4**,** 1361-70.

HANS, S., ZÖLLER, D., HAMMER, J., STUCKE, J., SPIES, S., KESAVAN, G., KROEHNE, V., EGUIGUREN, J. S., EZHKOVA, D., PETZOLD, A., DAHL, A. & BRAND, M. 2021. Cre-Controlled CRISPR mutagenesis provides fast and easy conditional gene inactivation in zebrafish. *Nature Communications,* 12**,** 1125.

HARATA, N. C., ARAVANIS, A. M. & TSIEN, R. W. 2006. Kiss-and-run and full-collapse fusion as modes of exo-endocytosis in neurosecretion. *Journal of Neurochemistry,* 97**,** 1546-1570.

HARDY, J. A. & HIGGINS, G. A. 1992. Alzheimer's disease: the amyloid cascade hypothesis. *Science,* 256**,** 184-5.

HARTMAN, K. N., PAL, S. K., BURRONE, J. & MURTHY, V. N. 2006. Activity-dependent regulation of inhibitory synaptic transmission in hippocampal neurons. *Nature neuroscience,* 9**,** 642-649.

HAUPT, Y., MAYA, R., KAZAZ, A. & OREN, M. 1997. Mdm2 promotes the rapid degradation of p53. *Nature,* 387**,** 296-299.

HE, H.-Y., RAMACHANDRAN, K., MCLAIN, N., FAULKNER, R., AHSAN, A., BERA, R., MARGOLIS, S. S. & CLINE, H. T. 2022. Neuronal membrane proteasomes homeostatically regulate neural circuit activity in vivo and are required for learning-induced behavioral plasticity. *bioRxiv***,** 2022.01.29.478314.

HE, M., ZHOU, Z., SHAH, A. A., ZOU, H., TAO, J., CHEN, Q. & WAN, Y. 2016. The emerging role of deubiquitinating enzymes in genomic integrity, diseases, and therapeutics. *Cell & Bioscience,* 6**,** 62.

HECKMAN, C. J. & ENOKA, R. M. 2012. Motor unit. *Compr Physiol,* 2**,** 2629-82.

HEGDE, A. N. 2010. The ubiquitin-proteasome pathway and synaptic plasticity. *Learn Mem,* 17**,** 314-27.

HEGDE, A. N. 2017. Proteolysis, synaptic plasticity and memory. *Neurobiology of learning and memory,* 138**,** 98-110.

HELD, R. G., LIU, C. & KAESER, P. S. 2016. ELKS controls the pool of readily releasable vesicles at excitatory synapses through its N-terminal coiled-coil domains. *Elife,* 5.

HERSHKO, A., LESHINSKY, E., GANOTH, D. & HELLER, H. 1984. ATP-dependent degradation of ubiquitin-protein conjugates. *Proc Natl Acad Sci U S A,* 81**,** 1619-23.

HETZ, C. & PAPA, F. R. 2018. The Unfolded Protein Response and Cell Fate Control. *Molecular Cell,* 69**,** 169-181.

HETZ, C. & SAXENA, S. 2017a. ER stress and the unfolded protein response in neurodegeneration. *Nature Reviews Neurology,* 13**,** 477-491.

HETZ, C. & SAXENA, S. 2017b. ER stress and the unfolded protein response in neurodegeneration. *Nature Reviews Neurology,* 13**,** 477.

HEUSER, J., REESE, T., DENNIS, M., JAN, Y., JAN, L. & EVANS, L. 1979. Synaptic vesicle exocytosis captured by quick freezing and correlated with quantal transmitter release. *The Journal of cell biology,* 81**,** 275-300.

HIGH, B., COLE, A. A., CHEN, X. & REESE, T. S. 2015. Electron microscopic tomography reveals discrete transcleft elements at excitatory and inhibitory synapses. *Frontiers in synaptic neuroscience,* 7**,** 9.

HILLE, B. 1992. Potassium channels and chloride channels. In Ionic Channels of Excitable Membrane. *Edited by Hill B***,** 130-133.

HIPP, M. S., KASTURI, P. & HARTL, F. U. 2019. The proteostasis network and its decline in ageing. *Nature Reviews Molecular Cell Biology,* 20**,** 421-435.

HOLLWAY, G. E., BRYSON-RICHARDSON, R. J., BERGER, S., COLE, N. J., HALL, T. E. & CURRIE, P. D. 2007. Whole-somite rotation generates muscle progenitor cell compartments in the developing zebrafish embryo. *Developmental cell,* 12**,** 207-219.

HOWE, K., CLARK, M. D., TORROJA, C. F., TORRANCE, J., BERTHELOT, C., MUFFATO, M., COLLINS, J. E., HUMPHRAY, S., MCLAREN, K., MATTHEWS, L., MCLAREN, S., SEALY, I., CACCAMO, M., CHURCHER, C., SCOTT, C., BARRETT, J. C., KOCH, R., RAUCH, G. J., WHITE, S., CHOW, W., KILIAN, B., QUINTAIS, L. T., GUERRA-ASSUNÇÃO, J. A., ZHOU, Y., GU, Y., YEN, J., VOGEL, J. H., EYRE, T., REDMOND, S., BANERJEE, R., CHI, J., FU, B., LANGLEY, E., MAGUIRE, S. F., LAIRD, G. K., LLOYD, D., KENYON, E., DONALDSON, S., SEHRA, H., ALMEIDA-KING, J., LOVELAND, J., TREVANION, S., JONES, M., QUAIL, M., WILLEY, D., HUNT, A., BURTON, J., SIMS, S., MCLAY, K., PLUMB, B., DAVIS, J., CLEE, C., OLIVER, K., CLARK, R., RIDDLE, C., ELLIOT, D., THREADGOLD, G., HARDEN, G., WARE, D., BEGUM, S., MORTIMORE, B., KERRY, G., HEATH, P., PHILLIMORE, B., TRACEY, A., CORBY, N., DUNN, M., JOHNSON, C., WOOD, J., CLARK, S., PELAN, S., GRIFFITHS, G., SMITH, M., GLITHERO, R., HOWDEN, P., BARKER, N., LLOYD, C., STEVENS, C., HARLEY, J., HOLT, K., PANAGIOTIDIS, G., LOVELL, J., BEASLEY, H., HENDERSON, C., GORDON, D., AUGER, K., WRIGHT, D., COLLINS, J., RAISEN, C., DYER, L., LEUNG, K., ROBERTSON, L., AMBRIDGE, K., LEONGAMORNLERT, D., MCGUIRE, S., GILDERTHORP, R., GRIFFITHS, C., MANTHRAVADI, D., NICHOL, S., BARKER, G., et al. 2013. The zebrafish reference genome sequence and its relationship to the human genome. *Nature,* 496**,** 498-503.

HSU, Y.-T., WOLTER, K. G. & YOULE, R. J. 1997. Cytosol-to-membrane redistribution of Bax and Bcl-XL during apoptosis. *Proceedings of the National Academy of Sciences,* 94**,** 3668-3672.

HUANG, E. P. 1998. Synaptic plasticity: Going through phases with LTP. *Current Biology,* 8**,** R350-R352.

HUNTER, J. R. 1972. Swimming and feeding behavior of larval anchovy Engraulis mordax. *Fish. Bull,* 70**,** 821-838.

HUTSON, M. R., RHODES, M. R. & KIRBY, M. L. 1997. Differential Expression of a Proteasomal Subunit during Chick Development. *Biochemical and Biophysical Research Communications,* 234**,** 216-223.

IMAMURA, S., YABU, T. & YAMASHITA, M. 2012. Protective Role of Cell Division Cycle 48 (CDC48) Protein against Neurodegeneration via Ubiquitin-Proteasome System Dysfunction during Zebrafish Development. *The Journal of biological chemistry,* 287**,** 23047-56.

ISAACSON, J. S. & WALMSLEY, B. 1995. Counting quanta: Direct measurements of transmitter release at a central synapse. *Neuron,* 15**,** 875-884.

ISLAM, S., CHEN, X., ESTRADA-MONDRAGON, A. & LYNCH, J. W. 2018. Phosphorylation of the α2 glycine receptor induces an extracellular conformational change and slows the rise and decay rates of glycinergic synaptic currents. *bioRxiv*, 434357.

ISSBERNER, J. P. & SILLAR, K. T. 2007. The contribution of the NMDA receptor glycine site to rhythm generation during fictive swimming in Xenopus laevis tadpoles. *European Journal of Neuroscience,* 26, 2556-2564.

ITO, M. & KANO, M. 1982. Long-lasting depression of parallel fiber-Purkinje cell transmission induced by conjunctive stimulation of parallel fibers and climbing fibers in the cerebellar cortex. *Neurosci Lett,* 33, 253-8.

IVANOVA, D., DIRKS, A. & FEJTOVA, A. 2016. Bassoon and piccolo regulate ubiquitination and link presynaptic molecular dynamics with activity-regulated gene expression. *J Physiol,* 594, 5441-8.

JACOBSON, M. D., WEIL, M. & RAFF, M. C. 1997. Programmed Cell Death in Animal Development. *Cell,* 88, 347-354.

JAKAWICH, S. K., NEELY, R. M., DJAKOVIC, S. N., PATRICK, G. N. & SUTTON, M. A. 2010. An essential postsynaptic role for the ubiquitin proteasome system in slow homeostatic synaptic plasticity in cultured hippocampal neurons. *Neuroscience,* 171, 1016-1031.

JELÍNKOVÁ, A., MALÍNSKÁ, K. & PETRÁŠEK, J. 2019. Using FM Dyes to Study Endomembranes and Their Dynamics in Plants and Cell Suspensions. *Methods Mol Biol,* 1992, 173-187.

JEUGD, A. V. D., AHMED, T., BURNOUF, S., BELARBI, K., HAMDAME, M., GROSJEAN, M.-E., HUMEZ, S., BALSCHUN, D., BLUM, D., BUÉE, L. & D'HOOGE, R. 2011. Hippocampal tauopathy in tau transgenic mice coincides with impaired hippocampus-dependent learning and memory, and attenuated late-phase long-term depression of synaptic transmission. *Neurobiology of Learning and Memory,* 95, 296-304.

JIANG, X., LITKOWSKI, P. E., TAYLOR, A. A., LIN, Y., SNIDER, B. J. & MOULDER, K. L. 2010. A role for the ubiquitin-proteasome system in activity-dependent presynaptic silencing. *J Neurosci,* 30, 1798-809.

JIN, I., PUTHANVEETTIL, S., UDO, H., KARL, K., KANDEL, E. R. & HAWKINS, R. D. 2012a. Spontaneous transmitter release is critical for the induction of long-term and intermediate-term facilitation in Aplysia. *Proceedings of the National Academy of Sciences,* 109, 9131-9136.

JIN, I., UDO, H., RAYMAN, J. B., PUTHANVEETTIL, S., KANDEL, E. R. & HAWKINS, R. D. 2012b. Spontaneous transmitter release recruits postsynaptic mechanisms of long-term and intermediate-term facilitation in Aplysia. *Proc Natl Acad Sci U S A,* 109, 9137-42.

JOHNSON, B. N., BERGER, A. K., CORTESE, G. P. & LAVOIE, M. J. 2012. The ubiquitin E3 ligase parkin regulates the proapoptotic function of Bax. *Proc Natl Acad Sci U S A,* 109, 6283-8.

JORGACEVSKI, J., POTOKAR, M., GRILC, S., KREFT, M., LIU, W., BARCLAY, J. W., BÜCKERS, J., MEDDA, R., HELL, S. W., PARPURA, V., BURGOYNE, R. D. & ZOREC, R. 2011. Munc18-1 tuning of vesicle merger and fusion pore properties. *J Neurosci,* 31, 9055-66.

JUO, P. & KAPLAN, J. M. 2004. The Anaphase-Promoting Complex Regulates the Abundance of GLR-1 Glutamate Receptors in the Ventral Nerve Cord of C. elegans. *Current Biology,* 14, 2057-2062.

KABRA, M., ROBIE, A. A., RIVERA-ALBA, M., BRANSON, S. & BRANSON, K. 2013. JAABA: interactive machine learning for automatic annotation of animal behavior. *Nature Methods,* 10, 64-67.

KAESER, P. S. & REGEHR, W. G. 2014. Molecular mechanisms for synchronous, asynchronous, and spontaneous neurotransmitter release. *Annu Rev Physiol,* 76**,** 333-63.
KALLA, S., STERN, M., BASU, J., VAROQUEAUX, F., REIM, K., ROSENMUND, C., ZIV, N. E. & BROSE, N. 2006. Molecular dynamics of a presynaptic active zone protein studied in Munc13-1-enhanced yellow fluorescent protein knock-in mutant mice. *J Neurosci,* 26**,** 13054-66.
KALVAITYTĖ, M. & BALCIUNAS, D. 2022. Conditional mutagenesis strategies in zebrafish. *Trends Genet,* 38**,** 856-868.
KANO, M. & WATANABE, T. 2019. Developmental synapse remodeling in the cerebellum and visual thalamus. *F1000Research,* 8**,** F1000 Faculty Rev-1191.
KATSNELSON, A. 2019. Editing zebrafish becomes conditional. *Lab Animal,* 48**,** 48-48.
KATZ, B. 1969. The release of neural transmitter substances. *Liverpool University Press***,** 5-39.
KATZ, B. & MILEDI, R. 1963. A study of spontaneous miniature potentials in spinal motoneurones. *The Journal of Physiology,* 168**,** 389-422.
KATZ, B. & MILEDI, R. 1967. The timing of calcium action during neuromuscular transmission. *The Journal of Physiology,* 189**,** 535-544.
KATZ, P. S. 2016. Evolution of central pattern generators and rhythmic behaviours. *Philos Trans R Soc Lond B Biol Sci,* 371**,** 20150057.
KAVALALI, E. T. 2015. The mechanisms and functions of spontaneous neurotransmitter release. *Nature Reviews Neuroscience,* 16**,** 5-16.
KAVALALI, E. T., CHUNG, C., KHVOTCHEV, M., LEITZ, J., NOSYREVA, E., RAINGO, J. & RAMIREZ, D. M. 2011. Spontaneous neurotransmission: an independent pathway for neuronal signaling? *Physiology (Bethesda),* 26**,** 45-53.
KHAN, T. M., BENAICH, N., MALONE, C. F., BERNARDOS, R. L., RUSSELL, A. R., DOWNES, G. B., BARRESI, M. J. & HUTSON, L. D. 2012. Vincristine and bortezomib cause axon outgrowth and behavioral defects in larval zebrafish. *J Peripher Nerv Syst,* 17**,** 76-89.
KIDD, T., RUSSELL, C., GOODMAN, C. S. & TEAR, G. 1998. Dosage-sensitive and complementary functions of roundabout and commissureless control axon crossing of the CNS midline. *Neuron,* 20**,** 25-33.
KIM, E. C., ZHANG, J., PANG, W., WANG, S., LEE, K. Y., CAVARETTA, J. P., WALTERS, J., PROCKO, E., TSAI, N.-P. & CHUNG, H. J. 2018. Reduced axonal surface expression and phosphoinositide sensitivity in Kv7 channels disrupts their function to inhibit neuronal excitability in Kcnq2 epileptic encephalopathy. *Neurobiology of disease,* 118**,** 76-93.
KIM, H. T. & GOLDBERG, A. L. 2017. The deubiquitinating enzyme Usp14 allosterically inhibits multiple proteasomal activities and ubiquitin-independent proteolysis. *Journal of Biological Chemistry,* 292**,** 9830-9839.
KIMMEL, C. B., BALLARD, W. W., KIMMEL, S. R., ULLMANN, B. & SCHILLING, T. F. 1995. Stages of Embryonic Development of the Zebrafish. *Developmental Dynamics,* 203**,** 253-210.
KIMMEL, C. B., POWELL, S. L. & METCALFE, W. K. 1982. Brain neurons which project to the spinal cord in young larvae of the zebrafish. *Journal of Comparative Neurology,* 205**,** 112-127.
KISSELEV, A. F. 2021. Site-Specific Proteasome Inhibitors. *Biomolecules,* 12.
KISSELEV, A. F. & GOLDBERG, A. L. 2001. Proteasome inhibitors: from research tools to drug candidates. *Chemistry & biology,* 8**,** 739-758.

KLARE, N., SEEGER, M., JANEK, K., JUNGBLUT, P. R. & DAHLMANN, B. 2007. Intermediate-type 20 S proteasomes in HeLa cells: "asymmetric" subunit composition, diversity and adaptation. *J Mol Biol,* 373**,** 1-10.

KONISHI, Y., STEGMÜLLER, J., MATSUDA, T., BONNI, S. & BONNI, A. 2004. Cdh1-APC controls axonal growth and patterning in the mammalian brain. *Science,* 303**,** 1026-1030.

KORN, H. & FABER, D. S. 2005. The Mauthner Cell Half a Century Later: A Neurobiological Model for Decision-Making? *Neuron,* 47**,** 13-28.

KORN, H., ODA, Y. & FABER, D. S. 1992. Long-term potentiation of inhibitory circuits and synapses in the central nervous system. *Proceedings of the National Academy of Sciences,* 89**,** 440-443.

KOWALSKI, J. R. & JUO, P. 2012a. The role of deubiquitinating enzymes in synaptic function and nervous system diseases. *Neural Plast,* 2012**,** 892749.

KOWALSKI, J. R. & JUO, P. 2012b. The Role of Deubiquitinating Enzymes in Synaptic Function and Nervous System Diseases. *Neural Plasticity,* 2012**,** 892749.

KOYANO, F., YAMANO, K., KOSAKO, H., TANAKA, K. & MATSUDA, N. 2019. Parkin recruitment to impaired mitochondria for nonselective ubiquitylation is facilitated by MITOL. *The Journal of biological chemistry,* 294**,** 10300-10314.

KOZLOWSKI, L., STOKLOSA, T., OMURA, S., WÓJCIK, C., WOJTUKIEWICZ, M. Z., WOROWSKI, K. & OSTROWSKA, H. 2001. Lactacystin inhibits cathepsin A activity in melanoma cell lines. *Tumour Biol,* 22**,** 211-5.

KRISTARIYANTO, Y. A., CHOI, S.-Y., REHMAN, S. A. A., RITORTO, M. S., CAMPBELL, D. G., MORRICE, N. A., TOTH, R. & KULATHU, Y. 2015. Assembly and structure of Lys33-linked polyubiquitin reveals distinct conformations. *Biochemical Journal,* 467**,** 345.

KRÖLL-HERMI, A., EBSTEIN, F., STOETZEL, C., GEOFFROY, V., SCHAEFER, E., SCHEIDECKER, S., BÄR, S., TAKAMIYA, M., KAWAKAMI, K., ZIEBA, B. A., STUDER, F., PELLETIER, V., EYERMANN, C., SPEEG-SCHATZ, C., LAUGEL, V., LIPSKER, D., SANDRON, F., MCGINN, S., BOLAND, A., DELEUZE, J. F., KUHN, L., CHICHER, J., HAMMANN, P., FRIANT, S., ETARD, C., KRÜGER, E., MULLER, J., STRÄHLE, U. & DOLLFUS, H. 2020. Proteasome subunit PSMC3 variants cause neurosensory syndrome combining deafness and cataract due to proteotoxic stress. *EMBO Mol Med,* 12**,** e11861.

KUBBUTAT, M. H., JONES, S. N. & VOUSDEN, K. H. 1997. Regulation of p53 stability by Mdm2. *Nature,* 387**,** 299-303.

KUMAR DESHMUKH, F., YAFFE, D., OLSHINA, M. A., BEN-NISSAN, G. & SHARON, M. 2019. The Contribution of the 20S Proteasome to Proteostasis. *Biomolecules,* 9**,** 190.

KUMAR, R., HERBERT, P. E. & WARRENS, A. N. 2005. An introduction to death receptors in apoptosis. *International Journal of Surgery,* 3**,** 268-277.

KUO, C. T., JAN, L. Y. & JAN, Y. N. 2005. Dendrite-specific remodeling of Drosophila sensory neurons requires matrix metalloproteases, ubiquitin-proteasome, and ecdysone signaling. *Proc Natl Acad Sci U S A,* 102**,** 15230-5.

KUO, C. T., ZHU, S., YOUNGER, S., JAN, L. Y. & JAN, Y. N. 2006a. Identification of E2/E3 Ubiquitinating Enzymes and Caspase Activity Regulating Drosophila Sensory Neuron Dendrite Pruning. *Neuron,* 51**,** 283-290.

KUO, C. T., ZHU, S., YOUNGER, S., JAN, L. Y. & JAN, Y. N. 2006b. Identification of E2/E3 ubiquitinating enzymes and caspase activity regulating Drosophila sensory neuron dendrite pruning. *Neuron,* 51**,** 283-90.

KÜRY, S., BESNARD, T., EBSTEIN, F., KHAN, T. N., GAMBIN, T., DOUGLAS, J., BACINO, C. A., CRAIGEN, W. J., SANDERS, S. J., LEHMANN, A., LATYPOVA, X., KHAN, K., PACAULT, M.,

SACHAROW, S., GLASER, K., BIETH, E., PERRIN-SABOURIN, L., JACQUEMONT, M.-L., CHO, M. T., ROEDER, E., DENOMMÉ-PICHON, A.-S., MONAGHAN, K. G., YUAN, B., XIA, F., SIMON, S., BONNEAU, D., PARENT, P., GILBERT-DUSSARDIER, B., ODENT, S., TOUTAIN, A., PASQUIER, L., BARBOUTH, D., SHAW, C. A., PATEL, A., SMITH, J. L., BI, W., SCHMITT, S., DEB, W., NIZON, M., MERCIER, S., VINCENT, M., ROORYCK, C., MALAN, V., BRICEÑO, I., GÓMEZ, A., NUGENT, K. M., GIBSON, J. B., COGNÉ, B., LUPSKI, J. R., STESSMAN, H. A. F., EICHLER, E. E., RETTERER, K., YANG, Y., REDON, R., KATSANIS, N., ROSENFELD, J. A., KLOETZEL, P.-M., GOLZIO, C., BÉZIEAU, S., STANKIEWICZ, P. & ISIDOR, B. 2017. De Novo Disruption of the Proteasome Regulatory Subunit PSMD12 Causes a Syndromic Neurodevelopmental Disorder. *The American Journal of Human Genetics,* 100**,** 352-363.

KUWANA, T. & NEWMEYER, D. D. 2003. Bcl-2-family proteins and the role of mitochondria in apoptosis. *Current opinion in cell biology,* 15**,** 691-699.

LAEDERMANN, C. J., CACHEMAILLE, M., KIRSCHMANN, G., PERTIN, M., GOSSELIN, R. D., CHANG, I., ALBESA, M., TOWNE, C., SCHNEIDER, B. L., KELLENBERGER, S., ABRIEL, H. & DECOSTERD, I. 2013. Dysregulation of voltage-gated sodium channels by ubiquitin ligase NEDD4-2 in neuropathic pain. *J Clin Invest,* 123**,** 3002-13.

LAMBOLEY, C. R., WYCKELSMA, V. L., DUTKA, T. L., MCKENNA, M. J., MURPHY, R. M. & LAMB, G. D. 2015. Contractile properties and sarcoplasmic reticulum calcium content in type I and type II skeletal muscle fibres in active aged humans. *J Physiol,* 593**,** 2499-514.

LECKER, S. H., GOLDBERG, A. L. & MITCH, W. E. 2006. Protein Degradation by the Ubiquitin-Proteasome Pathway in Normal and Disease States. *Journal American Society of Nephrology,* 17**,** 1807-1819.

LEE, C. & HAM, S. 2011. Characterizing amyloid-beta protein misfolding from molecular dynamics simulations with explicit water. *Journal of Computational Chemistry,* 32**,** 349-355.

LEE, C., SCHWARTZ, M. P., PRAKASH, S., IWAKURA, M. & MATOUSCHEK, A. 2001. ATP-dependent proteases degrade their substrates by processively unraveling them from the degradation signal. *Molecular cell,* 7**,** 627-637.

LEE, C.-M., KUMAR, V., RILEY, R. I. & MORGAN, E. T. 2010. Metabolism and Action of Proteasome Inhibitors in Primary Human Hepatocytes. *Drug Metabolism and Disposition,* 38**,** 2166.

LEENDERS, A. G., SCHOLTEN, G., WIEGANT, V. M., DA SILVA, F. H. & GHIJSEN, W. E. 1999. Activity-dependent neurotransmitter release kinetics: correlation with changes in morphological distributions of small and large vesicles in central nerve terminals. *Eur J Neurosci,* 11**,** 4269-77.

LESCAT, L., VÉRON, V., MOUROT, B., PÉRON, S., CHENAIS, N., DIAS, K., RIERA-HEREDIA, N., BEAUMATIN, F., PINEL, K. & PRIAULT, M. 2020. Chaperone-mediated autophagy in the light of evolution: Insight from fish. *Molecular Biology and Evolution,* 37**,** 2887-2899.

LEWIS, D. F. 2003. Human cytochromes P450 associated with the phase 1 metabolism of drugs and other xenobiotics: a compilation of substrates and inhibitors of the CYP1, CYP2 and CYP3 families. *Current medicinal chemistry,* 10**,** 1955-1972.

LI, C. H. & LEE, C. K. 1993. Minimum cross entropy thresholding. *Pattern Recognition,* 26**,** 617-625.

LI, H., KULKARNI, G. & WADSWORTH, W. G. 2008. RPM-1, a <em>Caenorhabditis elegans</em> Protein That Functions in Presynaptic Differentiation, Negatively Regulates Axon Outgrowth by Controlling SAX-3/robo and UNC-5/UNC5 Activity. *The Journal of Neuroscience,* 28**,** 3595.

LI, J., ZHANG, X., SHEN, J., GUO, J., WANG, X. & LIU, J. 2019. Bortezomib promotes apoptosis of multiple myeloma cells by regulating HSP27. *Mol Med Rep,* 20**,** 2410-2418.

LI, Q., KORTE, M. & SAJIKUMAR, S. 2015. Ubiquitin-Proteasome System Inhibition Promotes Long-Term Depression and Synaptic Tagging/Capture. *Cerebral Cortex,* 26**,** 2541-2548.

LI, W.-W., LI, J. & BAO, J.-K. 2012. Microautophagy: lesser-known self-eating. *Cellular and Molecular Life Sciences,* 69**,** 1125-1136.

LIAO, E. H., HUNG, W., ABRAMS, B. & ZHEN, M. 2004. An SCF-like ubiquitin ligase complex that controls presynaptic differentiation. *Nature,* 430**,** 345-350.

LIM, R., ALVAREZ, F. J. & WALMSLEY, B. 1999. Quantal size is correlated with receptor cluster area at glycinergic synapses in the rat brainstem. *J Physiol,* 516 ( Pt 2)**,** 505-12.

LIMANAQI, F., BIAGIONI, F., BUSCETI, C. L., RYSKALIN, L., SOLDANI, P., FRATI, A. & FORNAI, F. 2019. Cell Clearing Systems Bridging Neuro-Immunity and Synaptic Plasticity. *Int J Mol Sci,* 20.

LIN, A. W. & MAN, H.-Y. 2013. Ubiquitination of Neurotransmitter Receptors and Postsynaptic Scaffolding Proteins. *Neural Plasticity,* 2013**,** 432057.

LIN, M. T., LUJÁN, R., WATANABE, M., ADELMAN, J. P. & MAYLIE, J. 2008. SK2 channel plasticity contributes to LTP at Schaffer collateral-CA1 synapses. *Nat Neurosci,* 11**,** 170-7.

LITTLETON, J. T., STERN, M., PERIN, M. & BELLEN, H. J. 1994. Calcium dependence of neurotransmitter release and rate of spontaneous vesicle fusions are altered in Drosophila synaptotagmin mutants. *Proceedings of the National Academy of Sciences,* 91**,** 10888-10892.

LIU, C., BICKFORD, L. S., HELD, R. G., NYITRAI, H., SÜDHOF, T. C. & KAESER, P. S. 2014. The active zone protein family ELKS supports Ca2+ influx at nerve terminals of inhibitory hippocampal neurons. *J Neurosci,* 34**,** 12289-303.

LIU, C.-W. & JACOBSON, A. D. 2013. Functions of the 19S complex in proteasomal degradation. *Trends in biochemical sciences,* 38**,** 103-110.

LIU, C. W., CORBOY, M. J., DEMARTINO, G. N. & THOMAS, P. J. 2003. Endoproteolytic activity of the proteasome. *Science,* 299**,** 408-11.

LIU, D. W. & WESTERFIELD, M. 1988. Function of identified motoneurones and co-ordination of primary and secondary motor systems during zebra fish swimming. *J Physiol,* 403**,** 73-89.

LIU, H.-H., MCCLATCHY, D. B., SCHIAPPARELLI, L., SHEN, W., YATES, J. R., III & CLINE, H. T. 2018. Role of the visual experience-dependent nascent proteome in neuronal plasticity. *eLife,* 7**,** e33420.

LIU, K. S. & FETCHO, J. R. 1999. Laser Ablations Reveal Functional Relationships of Segmental Hindbrain Neurons in Zebrafish. *Neuron,* 23**,** 325-335.

LIU, Y., SUGIURA, Y., SÜDHOF, T. C. & LIN, W. 2019. Ablation of All Synaptobrevin vSNAREs Blocks Evoked But Not Spontaneous Neurotransmitter Release at Neuromuscular Synapses. *The Journal of Neuroscience,* 39**,** 6049-6066.

LIU, Y.-C., BAILEY, I. & HALE, M. E. 2012. Alternative startle motor patterns and behaviors in the larval zebrafish (Danio rerio). *Journal of Comparative Physiology A,* 198**,** 11-24.
LIU, Y.-C. & HALE, M. E. 2017. Local Spinal Cord Circuits and Bilateral Mauthner Cell Activity Function Together to Drive Alternative Startle Behaviors. *Current Biology,* 27**,** 697-704.
LIVNEH, I., COHEN-KAPLAN, V., COHEN-ROSENZWEIG, C., AVNI, N. & CIECHANOVER, A. 2016. The life cycle of the 26S proteasome: from birth, through regulation and function, and onto its death. *Cell Research,* 26**,** 869-885.
LJUNGGREN, E. E., HAUPT, S., AUSBORN, J., AMPATZIS, K. & EL MANIRA, A. 2014. Optogenetic activation of excitatory premotor interneurons is sufficient to generate coordinated locomotor activity in larval zebrafish. *Journal of Neuroscience,* 34**,** 134-139.
LONGAIR, M. H., BAKER, D. A. & ARMSTRONG, J. D. 2011. Simple Neurite Tracer: open source software for reconstruction, visualization and analysis of neuronal processes. *Bioinformatics,* 27**,** 2453-4.
LU, Y., CHRISTIAN, K. & LU, B. 2008. BDNF: a key regulator for protein synthesis-dependent LTP and long-term memory? *Neurobiol Learn Mem,* 89**,** 312-23.
LU, Z., JE, H.-S., YOUNG, P., GROSS, J., LU, B. & FENG, G. 2007. Regulation of synaptic growth and maturation by a synapse-associated E3 ubiquitin ligase at the neuromuscular junction. *The Journal of cell biology,* 177**,** 1077-1089.
LUQUE, M. A., BELTRAN-MATAS, P., MARIN, M. C., TORRES, B. & HERRERO, L. 2017. Excitability is increased in hippocampal CA1 pyramidal cells of Fmr1 knockout mice. *PLoS One,* 12**,** e0185067.
MADERNA, P. & GODSON, C. 2003. Phagocytosis of apoptotic cells and the resolution of inflammation. *Biochimica et Biophysica Acta (BBA) - Molecular Basis of Disease,* 1639**,** 141-151.
MAGBY, J. P. & RICHARDSON, J. R. 2015. Role of calcium and calpain in the downregulation of voltage-gated sodium channel expression by the pyrethroid pesticide deltamethrin. *J Biochem Mol Toxicol,* 29**,** 129-34.
MALENKA, R. C., NICOLL & A, R. 1999. Long-term potentiation--a decade of progress? *Science,* 285**,** 1870-1874.
MARTIN, S., PAPADOPULOS, A., TOMATIS, VANESA M., SIERECKI, E., MALINTAN, NANCY T., GORMAL, RACHEL S., GILES, N., JOHNSTON, WAYNE A., ALEXANDROV, K., GAMBIN, Y., COLLINS, BRETT M. & MEUNIER, FREDERIC A. 2014. Increased Polyubiquitination and Proteasomal Degradation of a Munc18-1 Disease-Linked Mutant Causes Temperature-Sensitive Defect in Exocytosis. *Cell Reports,* 9**,** 206-218.
MARTINEZ, A., LECTEZ, B., RAMIREZ, J., POPP, O., SUTHERLAND, J. D., URBÉ, S., DITTMAR, G., CLAGUE, M. J. & MAYOR, U. 2017. Quantitative proteomic analysis of Parkin substrates in Drosophila neurons. *Molecular Neurodegeneration,* 12**,** 29.
MARTYN, J. A. J., FAGERLUND, M. J. & ERIKSSON, L. I. 2009. Basic principles of neuromuscular transmission. *Anaesthesia,* 64**,** 1-9.
MASINO, M. A. & FETCHO, J. R. 2005. Fictive Swimming Motor Patterns in Wild Type and Mutant Larval Zebrafish. *Journal of Neurophysiology,* 93**,** 3177-3188.
MASON, G. G. F., HENDIL, K. B. & RIVETT, A. J. 1996. Phosphorylation of Proteasomes in Mammalian Cells. *European Journal of Biochemistry,* 238**,** 453-462.

MASPERO, E., VALENTINI, E., MARI, S., CECATIELLO, V., SOFFIENTINI, P., PASQUALATO, S. & POLO, S. 2013. Structure of a ubiquitin-loaded HECT ligase reveals the molecular basis for catalytic priming. *Nat Struct Mol Biol,* 20**,** 696-701.

MAXIMOV, A., SHIN, O. H., LIU, X. & SÜDHOF, T. C. 2007. Synaptotagmin-12, a synaptic vesicle phosphoprotein that modulates spontaneous neurotransmitter release. *J Cell Biol,* 176**,** 113-24.

MCKINNEY, R. A., CAPOGNA, M., DÜRR, R., GÄHWILER, B. H. & THOMPSON, S. M. 1999. Miniature synaptic events maintain dendritic spines via AMPA receptor activation. *Nat Neurosci,* 2**,** 44-9.

MCLEAN, D. L., FAN, J., HIGASHIJIMA, S.-I., HALE, M. E. & FETCHO, J. R. 2007. A topographic map of recruitment in spinal cord. *Nature Letters,* 446**,** 71-75.

MCLEAN, D. L. & FETCHO, J. R. 2009. Spinal Interneurons Differentiate Sequentially from Those Driving the Fastest Swimming Movements in Larval Zebrafish to Those Driving the Slowest Ones. *The Journal of Neuroscience,* 29**,** 13566-13577.

MCLEAN, D. L. F., JOSEPH R Oral Communications: Beat-and-glide swimming in larval zebrafish is an emergent property of their spinal network [Conference Presentation]. The Physiological Society 2005 University of Bristol.

MENELAOU, E. & MCLEAN, D. L. 2012. A Gradient in Endogenous Rhythmicity and Oscillatory Drive Matches Recruitment Order in an Axial Motor Pool. *The Journal of Neuroscience,* 32**,** 10925-10939.

MENELAOU, E. & MCLEAN, D. L. 2019. Hierarchical control of locomotion by distinct types of spinal V2a interneurons in zebrafish. *Nature Communications,* 10**,** 4197.

MENÉNDEZ-BENITO, V., VERHOEF, L. G., MASUCCI, M. G. & DANTUMA, N. P. 2005. Endoplasmic reticulum stress compromises the ubiquitin-proteasome system. *Hum Mol Genet,* 14**,** 2787-99.

METCALFE, W. K., MENDELSON, B. & KIMMEL, C. B. 1986. Segmental homologies among reticulospinal neurons in the hindbrain of the zebrafish larva. *Journal of Comparative Neurology,* 251**,** 147-159.

METZGER, M. B., PRUNEDA, J. N., KLEVIT, R. E. & WEISSMAN, A. M. 2014a. RING-type E3 ligases: master manipulators of E2 ubiquitin-conjugating enzymes and ubiquitination. *Biochim Biophys Acta,* 1843**,** 47-60.

METZGER, M. B., PRUNEDA, J. N., KLEVIT, R. E. & WEISSMAN, A. M. 2014b. RING-type E3 ligases: master manipulators of E2 ubiquitin-conjugating enzymes and ubiquitination. *Biochimica et biophysica acta,* 1843**,** 47-60.

MEYER, R. D., SRINIVASAN, S., SINGH, A. J., MAHONEY, J. E., GHARAHASSANLOU, K. R. & RAHIMI, N. 2011. PEST motif serine and tyrosine phosphorylation controls vascular endothelial growth factor receptor 2 stability and downregulation. *Molecular and cellular biology,* 31**,** 2010-2025.

MING, G.-L., WONG, S. T., HENLEY, J., YUAN, X.-B., SONG, H.-J., SPITZER, N. C. & POO, M.-M. 2002. Adaptation in the chemotactic guidance of nerve growth cones. *Nature,* 417**,** 411-418.

MORREALE, F. E. & WALDEN, H. 2016. Types of Ubiquitin Ligases. *Cell,* 165**,** 248-248.e1.

MÜLLER, S., GULI, X., HEY, J., EINSLE, A., PFANZ, D., SUDMANN, V., KIRSCHSTEIN, T. & KÖHLING, R. 2018. Acute epileptiform activity induced by gabazine involves proteasomal rather than lysosomal degradation of KCa2. 2 channels. *Neurobiology of Disease,* 112**,** 79-84.

MÜLLER, U. K. & VAN LEEUWEN, J. L. 2004. Swimming of larval zebrafish: ontogeny of body waves and implications for locomotory development. *Journal of Experimental Biology,* 207**,** 853-868.

MYAT, A., HENRY, P., MCCABE, V., FLINTOFT, L., ROTIN, D. & TEAR, G. 2002. Drosophila Nedd4, a ubiquitin ligase, is recruited by Commissureless to control cell surface levels of the roundabout receptor. *Neuron,* 35**,** 447-459.

MYERS, P. Z. 1985. Spinal motoneurons of the larval zebrafish. *J Comp Neurol,* 236**,** 555-61.

MYERS, P. Z., EISEN, J. S. & WESTERFIELD, M. 1986a. Development and axonal outgrowth of identified motoneurons in the zebrafish. *Journal of Neuroscience,* 6**,** 2278-2289.

MYERS, P. Z., EISEN, J. S. & WESTERFIELD, M. 1986b. Development and axonal outgrowth of identified motoneurons in the zebrafish. *J Neurosci,* 6**,** 2278-89.

MYUNG, J., KIM, K. B. & CREWS, C. M. 2001. The ubiquitin-proteasome pathway and proteasome inhibitors. *Medicinal Research Reviews,* 21**,** 245-273.

NAKATA, K., ABRAMS, B., GRILL, B., GONCHAROV, A., HUANG, X., CHISHOLM, A. D. & JIN, Y. 2005. Regulation of a DLK-1 and p38 MAP kinase pathway by the ubiquitin ligase RPM-1 is required for presynaptic development. *Cell,* 120**,** 407-20.

NISHINO, A., OKAMURA, Y., PISCOPO, S. & BROWN, E. R. 2010. A glycine receptor is involved in the organization of swimming movements in an invertebrate chordate. *BMC Neuroscience,* 11**,** 6.

NOGALSKA, A., D'AGOSTINO, C., ENGEL, W. K., CACCIOTTOLO, M., ASADA, S., MORI, K. & ASKANAS, V. 2015. Activation of the Unfolded Protein Response in Sporadic Inclusion-Body Myositis but Not in Hereditary GNE Inclusion-Body Myopathy. *J Neuropathol Exp Neurol,* 74**,** 538-46.

NOSYREVA, E., SZABLA, K., AUTRY, A. E., RYAZANOV, A. G., MONTEGGIA, L. M. & KAVALALI, E. T. 2013. Acute suppression of spontaneous neurotransmission drives synaptic potentiation. *J Neurosci,* 33**,** 6990-7002.

NOZAWA, K., LIN, Y., KUBODERA, R., SHIMIZU, Y., TANAKA, H. & OHSHIMA, T. 2017. Zebrafish Mecp2 is required for proper axonal elongation of motor neurons and synapse formation. *Developmental Neurobiology,* 77**,** 1101-1113.

OGINO, K., LOW, S. E., YAMADA, K., SAINT-AMANT, L., ZHOU, W., MUTO, A., ASAKAWA, K., NAKAI, J., KAWAKAMI, K., KUWADA, J. Y. & HIRATA, H. 2015. RING finger protein 121 facilitates the degradation and membrane localization of voltage-gated sodium channels. *Proceedings of the National Academy of Sciences,* 112**,** 2859-2864.

OLESKEVICH, S., ALVAREZ, F. J. & WALMSLEY, B. 1999. Glycinergic Miniature Synaptic Currents and Receptor Cluster Sizes Differ Between Spinal Cord Interneurons. *Journal of Neurophysiology,* 82**,** 312-319.

OLSEN, S. K. & LIMA, C. D. 2013. Structure of a ubiquitin E1-E2 complex: insights to E1-E2 thioester transfer. *Mol Cell,* 49**,** 884-96.

ŌMURA, S. & CRUMP, A. 2019. Lactacystin: first-in-class proteasome inhibitor still excelling and an exemplar for future antibiotic research. *The Journal of Antibiotics,* 72**,** 189-201.

OSTROWSKA, H., WOJCIK, C., OMURA, S. & WOROWSKI, K. 1997. Lactacystin, a Specific Inhibitor of the Proteasome, Inhibits Human Platelet Lysosomal Cathepsin A-like Enzyme. *Biochemical and Biophysical Research Communications,* 234**,** 729-732.

PALMER, A., RIVETT, A. J., THOMSON, S., HENDIL, K. B., BUTCHER, G. W., FUERTES, G. & KNECHT, E. 1996. Subpopulations of proteasomes in rat liver nuclei, microsomes and cytosol. *Biochem J,* 316 ( Pt 2)**,** 401-7.

PANDELIDES, Z., USSERY, E. J., OVERTURF, M. D., GUCHARDI, J. & HOLDWAY, D. A. 2021. Inhibition of swim bladder inflation in Japanese medaka (Oryzias latipes) embryos following exposure to select pharmaceuticals alone and in combination. *Aquatic Toxicology,* 234**,** 105796.

PARICHY, D. M., ELIZONDO, M. R., MILLS, M. G., GORDON, T. N. & ENGESZER, R. E. 2009. Normal table of postembryonic zebrafish development: staging by externally visible anatomy of the living fish. *Dev Dyn,* 238**,** 2975-3015.

PARK, C., CHEN, X., TIAN, C.-L., PARK, G. N., CHENOUARD, N., LEE, H., YEO, X. Y., JUNG, S., BI, G., TSIEN, R. W. & PARK, H. 2020. Inhibitory synaptic vesicles have unique dynamics and exocytosis properties. *bioRxiv***,** 2020.09.21.289314.

PARZYCH, K. R. & KLIONSKY, D. J. 2014. An overview of autophagy: morphology, mechanism, and regulation. *Antioxidants & redox signaling,* 20**,** 460-473.

PATRICK, G. N., BINGOL, B., WELD, H. A. & SCHUMAN, E. M. 2003. Ubiquitin-mediated proteasome activity is required for agonist-induced endocytosis of GluRs. *Current Biology,* 13**,** 2073-2081.

PAYNE, J. A., RIVERA, C., VOIPIO, J. & KAILA, K. 2003. Cation–chloride co-transporters in neuronal communication, development and trauma. *Trends in neurosciences,* 26**,** 199-206.

PEITSARO, N., KASLIN, J., ANICHTCHIK, O. V. & PANULA, P. 2003. Modulation of the histaminergic system and behaviour by α-fluoromethylhistidine in zebrafish. *Journal of Neurochemistry,* 86**,** 432-441.

PETERS, J.-M. 2006. The anaphase promoting complex/cyclosome: a machine designed to destroy. *Nature Reviews Molecular Cell Biology,* 7**,** 644-656.

PETERSEN, S. A., FETTER, R. D., NOORDERMEER, J. N., GOODMAN, C. S. & DIANTONIO, A. 1997. Genetic analysis of glutamate receptors in Drosophila reveals a retrograde signal regulating presynaptic transmitter release. *Neuron,* 19**,** 1237-48.

PLATKIEWICZ, J. & BRETTE, R. 2010. A threshold equation for action potential initiation. *PLoS Comput Biol,* 6**,** e1000850.

PLEMEL, J. R., CAPRARIELLO, A. V., KEOUGH, M. B., HENRY, T. J., TSUTSUI, S., CHU, T. H., SCHENK, G. J., KLAVER, R., YONG, V. W. & STYS, P. K. 2017. Unique spectral signatures of the nucleic acid dye acridine orange can distinguish cell death by apoptosis and necroptosis. *Journal of Cell Biology,* 216**,** 1163-1181.

POWERS, G. L., ELLISON-ZELSKI, S. J., CASA, A. J., LEE, A. V. & ALARID, E. T. 2010. Proteasome inhibition represses ERα gene expression in ER+ cells: a new link between proteasome activity and estrogen signaling in breast cancer. *Oncogene,* 29**,** 1509-1518.

PRAKASH, S., TIAN, L., RATLIFF, K. S., LEHOTZKY, R. E. & MATOUSCHEK, A. 2004. An unstructured initiation site is required for efficient proteasome-mediated degradation. *Nat Struct Mol Biol,* 11**,** 830-7.

PRICE, J. C., GUAN, S., BURLINGAME, A., PRUSINER, S. B. & GHAEMMAGHAMI, S. 2010. Analysis of proteome dynamics in the mouse brain. *Proc Natl Acad Sci U S A,* 107**,** 14508-13.

PRIOR, P., SCHMITT, B., GRENNINGLOH, G., PRIBILLA, I., MULTHAUP, G., BEYREUTHER, K., MAULET, Y., WERNER, P., LANGOSCH, D. & KIRSCH, J. 1992. Primary structure and alternative splice variants of gephyrin, a putative glycine receptor-tubulin linker protein. *Neuron,* 8**,** 1161-1170.

R DEVELOPMENT CORE TEAM 2022. R: A language and environment for statistical computing. R Foundation for Statistical Computing
RAEDLER, L. 2015. Velcade (Bortezomib) Receives 2 New FDA Indications: For Retreatment of Patients with Multiple Myeloma and for First-Line Treatment of Patients with Mantle-Cell Lymphoma. *Am Health Drug Benefits,* 8**,** 135-40.
RAJKUMAR, S. V., RICHARDSON, P. G., HIDESHIMA, T. & ANDERSON, K. C. 2005. Proteasome Inhibition As a Novel Therapeutic Target in Human Cancer. *Journal of Clinical Oncology,* 23**,** 630-639.
RAMACHANDRAN, K. V., FU, J. M., SCHAFFER, T. B., NA, C. H., DELANNOY, M. & MARGOLIS, S. S. 2018. Activity-Dependent Degradation of the Nascentome by the Neuronal Membrane Proteasome. *Mol Cell,* 71**,** 169-177.e6.
RAMACHANDRAN, K. V. & MARGOLIS, S. S. 2017. A mammalian nervous-system-specific plasma membrane proteasome complex that modulates neuronal function. *Nature Structural & Molecular Biology,* 24**,** 419-430.
RAMIREZ, D. M. & KAVALALI, E. T. 2011. Differential regulation of spontaneous and evoked neurotransmitter release at central synapses. *Curr Opin Neurobiol,* 21**,** 275-82.
RAMIREZ, D. M. O., CRAWFORD, D. C., CHANADAY, N. L., TRAUTERMAN, B., MONTEGGIA, L. M. & KAVALALI, E. T. 2017. Loss of Doc2-Dependent Spontaneous Neurotransmission Augments Glutamatergic Synaptic Strength. *J Neurosci,* 37**,** 6224-6230.
RAMOS, P. C., MARQUES, A. J., LONDON, M. K. & DOHMEN, R. J. 2004. Role of C-terminal extensions of subunits beta2 and beta7 in assembly and activity of eukaryotic proteasomes. *J Biol Chem,* 279**,** 14323-30.
RECHSTEINER, M. PEST sequences are signals for rapid intracellular proteolysis. Seminars in cell biology, 1990. 433-440.
REESE, A. L. & KAVALALI, E. T. 2015. Spontaneous neurotransmission signals through store-driven Ca(2+) transients to maintain synaptic homeostasis. *eLife,* 4**,** e09262.
REN, Q. G., LIAO, X. M., CHEN, X. Q., LIU, G. P. & WANG, J. Z. 2007. Effects of tau phosphorylation on proteasome activity. *FEBS Lett,* 581**,** 1521-8.
REYNOLDS, A., BRUSTEIN, E., LIAO, M., MERCADO, A., BABILONIA, E., MOUNT, D. B. & DRAPEAU, P. 2008. Neurogenic role of the depolarizing chloride gradient revealed by global overexpression of KCC2 from the onset of development. *Journal of Neuroscience,* 28**,** 1588-1597.
RILEY, B. E., LOUGHEED, J. C., CALLAWAY, K., VELASQUEZ, M., BRECHT, E., NGUYEN, L., SHALER, T., WALKER, D., YANG, Y., REGNSTROM, K., DIEP, L., ZHANG, Z., CHIOU, S., BOVA, M., ARTIS, D. R., YAO, N., BAKER, J., YEDNOCK, T. & JOHNSTON, J. A. 2013. Structure and function of Parkin E3 ubiquitin ligase reveals aspects of RING and HECT ligases. *Nature communications,* 4**,** 1982-1982.
RINETTI, G. V. & SCHWEIZER, F. E. 2010. Ubiquitination Acutely Regulates Presynaptic Neurotransmitter Release in Mammalian Neurons. *Journal of Neuroscience,* 30**,** 3157-3166.
RIZZOLI, S. O. & BETZ, W. J. 2005. Synaptic vesicle pools. *Nat Rev Neurosci,* 6**,** 57-69.
ROBERTS, A. C., CHORNAK, J., ALZAGATITI, J. B., LY, D. T., BILL, B. R., TRINKELLER, J., PEARCE, K. C., CHOE, R. C., CAMPBELL, C. S., WONG, D., DEUTSCH, E., HERNANDEZ, S. & GLANZMAN, D. L. 2019. Rapid habituation of a touch-induced escape response in Zebrafish (Danio rerio) Larvae. *PLoS One,* 14**,** e0214374.
ROCK, K. L., GRAMM, C., ROTHSTEIN, L., CLARK, K., STEIN, R., DICK, L., HWANG, D. & GOLDBERG, A. L. 1994. Inhibitors of the proteasome block the degradation of most

cell proteins and the generation of peptides presented on MHC class I molecules. *Cell,* 78**,** 761-71.
RODRÍGUEZ CRUZ, P. M., COSSINS, J., BEESON, D. & VINCENT, A. 2020. The Neuromuscular Junction in Health and Disease: Molecular Mechanisms Governing Synaptic Formation and Homeostasis. *Front Mol Neurosci,* 13**,** 610964.
RONCHI, V. P. & HAAS, A. L. 2012. Measuring rates of ubiquitin chain formation as a functional readout of ligase activity. *Methods Mol Biol,* 832**,** 197-218.
ROSAS, M. G., LORENZATTI, A., PORCEL DE PERALTA, M. S., CALCATERRA, N. B. & COUX, G. 2019. Proteasomal inhibition attenuates craniofacial malformations in a zebrafish model of Treacher Collins Syndrome. *Biochem Pharmacol,* 163**,** 362-370.
ROSE, J. K., KAUN, K. R., CHEN, S. H. & RANKIN, C. H. 2003. GLR-1, a non-NMDA glutamate receptor homolog, is critical for long-term memory in Caenorhabditis elegans. *J Neurosci,* 23**,** 9595-9.
ROUGIER, J.-S., BEMMELEN, M. X. V., BRUCE, M. C., JESPERSEN, T., GAVILLET, B., APOTHÉLOZ, F., CORDONIER, S., STAUB, O., ROTIN, D. & ABRIEL, H. 2005. Molecular determinants of voltage-gated sodium channel regulation by the Nedd4/Nedd4-like proteins. *American Journal of Physiology-Cell Physiology,* 288**,** C692-C701.
ROUSSEL, Y., GAUDREAU, S. F., KACER, E. R., SENGUPTA, M. & BUI, T. V. 2021. Modeling spinal locomotor circuits for movements in developing zebrafish. *Elife,* 10.
RUBIO, M. D., WOOD, K., HAROUTUNIAN, V. & MEADOR-WOODRUFF, J. H. 2013. Dysfunction of the ubiquitin proteasome and ubiquitin-like systems in schizophrenia. *Neuropsychopharmacology,* 38**,** 1910-1920.
SAGASTI, A., GUIDO, M. R., RAIBLE, D. W. & SCHIER, A. F. 2005. Repulsive interactions shape the morphologies and functional arrangement of zebrafish peripheral sensory arbors. *Curr Biol,* 15**,** 804-14.
SAINT-AMANT, L. & DRAPEAU, P. 1998. Time course of the development of motor behaviors in the zebrafish embryo. *Journal of Neurobiology,* 37**,** 622-632.
SAINT-AMANT, L. & DRAPEAU, P. 2000. Motoneuron activity patterns related to the earliest behavior of the zebrafish embryo. *Journal of Neuroscience,* 20**,** 3964-3972.
SAINT-AMANT, L. & DRAPEAU, P. 2001. Synchronization of an embryonic network of identified spinal interneurons solely by electrical coupling. *Neuron,* 31**,** 1035-1046.
SAINT-AMANT, L. & DRAPEAU, P. 1998. Time course of the development of motor behaviors in the zebrafish embryo. *Journal of neurobiology,* 37**,** 622-632.
SANES, J. R. & LICHTMAN, J. W. 2001. Induction, assembly, maturation and maintenance of a postsynaptic apparatus. *Nature Reviews Neuroscience,* 2**,** 791-805.
SARA, Y., VIRMANI, T., DEÁK, F., LIU, X. & KAVALALI, E. T. 2005. An Isolated Pool of Vesicles Recycles at Rest and Drives Spontaneous Neurotransmission. *Neuron,* 45**,** 563-573.
SATO-MAEDA, M., OBINATA, M. & SHOJI, W. 2008. Position fine-tuning of caudal primary motoneurons in the zebrafish spinal cord. *Development,* 135**,** 323-32.
SATOU, C., KIMURA, Y., KOHASHI, T., HORIKAWA, K., TAKEDA, H., ODA, Y. & HIGASHIJIMA, S. 2009. Functional role of a specialized class of spinal commissural inhibitory neurons during fast escapes in zebrafish. *J Neurosci,* 29**,** 6780-93.
SATOU, C., SUGIOKA, T., UEMURA, Y., SHIMAZAKI, T., ZMARZ, P., KIMURA, Y. & HIGASHIJIMA, S.-I. 2020. Functional Diversity of Glycinergic Commissural Inhibitory Neurons in Larval Zebrafish. *Cell Reports,* 30**,** 3036-3050.e4.
SCHAEFER, A. M., HADWIGER, G. D. & NONET, M. L. 2000. rpm-1, a conserved neuronal gene that regulates targeting and synaptogenesis in C. elegans. *Neuron,* 26**,** 345-56.

SCHANZENBÄCHER, C. T., SAMBANDAN, S., LANGER, J. D. & SCHUMAN, E. M. 2016. Nascent Proteome Remodeling following Homeostatic Scaling at Hippocampal Synapses. *Neuron,* 92**,** 358-371.
SCHIAPPARELLI, L. M., XIE, Y., SHARMA, P., MCCLATCHY, D. B., MA, Y., YATES, J. R., 3RD, MAXIMOV, A. & CLINE, H. T. 2022. Activity-Induced Cortical Glutamatergic Neuron Nascent Proteins. *J Neurosci,* 42**,** 7900-7920.
SCHINDELIN, J., ARGANDA-CARRERAS, I., FRISE, E., KAYNIG, V., LONGAIR, M., PIETZSCH, T., PREIBISCH, S., RUEDEN, C., SAALFELD, S., SCHMID, B., TINEVEZ, J.-Y., WHITE, D. J., HARTENSTEIN, V., ELICEIRI, K., TOMANCAK, P. & CARDONA, A. 2012. Fiji: an open-source platform for biological-image analysis. *Nature Methods,* 9**,** 676-682.
SCHMID, K., BÖHMER, G. & GEBAUER, K. 1991. Glycine receptor-mediated fast synaptic inhibition in the brainstem respiratory system. *Respiration physiology,* 84**,** 351-361.
SCHMID, K., FOUTZ, A. S. & DENAVIT-SAUBIÉ, M. 1996. Inhibitions mediated by glycine and GABAA receptors shape the discharge pattern of bulbar respiratory neurons. *Brain research,* 710**,** 150-160.
SCHNÖRR, S. J., STEENBERGEN, P. J., RICHARDSON, M. K. & CHAMPAGNE, D. L. 2012. Assessment of thigmotaxis in larval zebrafish. *Zebrafish protocols for neurobehavioral research.* Springer.
SCHRADER, E. K., HARSTAD, K. G. & MATOUSCHEK, A. 2009. Targeting proteins for degradation. *Nature Chemical Biology,* 5**,** 815-822.
SCHUCK, S. 2020. Microautophagy – distinct molecular mechanisms handle cargoes of many sizes. *Journal of Cell Science,* 133.
SCHULMAN, B. A. & HARPER, J. W. 2009. Ubiquitin-like protein activation by E1 enzymes: the apex for downstream signalling pathways. *Nature reviews. Molecular cell biology,* 10**,** 319-331.
SCHWARZ, L. A., HALL, B. J. & PATRICK, G. N. 2010. Activity-dependent ubiquitination of GluA1 mediates a distinct AMPA receptor endocytosis and sorting pathway. *Journal of Neuroscience,* 30**,** 16718-16729.
SEVERI, K. E., PORTUGUES, R., MARQUES, J. C., O'MALLEY, D. M., ORGER, M. B. & ENGERT, F. 2014. Neural control and modulation of swimming speed in the larval zebrafish. *Neuron,* 83**,** 692-707.
SHAMSI, T. N., ATHAR, T., PARVEEN, R. & FATIMA, S. 2017a. A review on protein misfolding, aggregation and strategies to prevent related ailments. *Int J Biol Macromol,* 105**,** 993-1000.
SHAMSI, T. N., ATHAR, T., PARVEEN, R. & FATIMA, S. 2017b. A review on protein misfolding, aggregation and strategies to prevent related ailments. *International Journal of Biological Macromolecules,* 105**,** 993-1000.
SHENG, M. 2001. Molecular organization of the postsynaptic specialization. *Proceedings of the National Academy of Sciences,* 98**,** 7058-7061.
SHIVU, B., SESHADRI, S., LI, J., OBERG, K. A., UVERSKY, V. N. & FINK, A. L. 2013. Distinct β-sheet structure in protein aggregates determined by ATR-FTIR spectroscopy. *Biochemistry,* 52**,** 5176-83.
SIDDIQUI, W. A., AHAD, A. & AHSAN, H. 2015. The mystery of BCL2 family: Bcl-2 proteins and apoptosis: an update. *Archives of Toxicology,* 89**,** 289-317.
SIES, H. 1999. Glutathione and its role in cellular functions. *Free Radic Biol Med,* 27**,** 916-21.
SIMON, P., DUPUIS, R. & COSTENTIN, J. 1994. Thigmotaxis as an index of anxiety in mice. Influence of dopaminergic transmissions. *Behavioural brain research,* 61**,** 59-64.

SNYDER, H., MENSAH, K., HSU, C., HASHIMOTO, M., SURGUCHEVA, I. G., FESTOFF, B., SURGUCHOV, A., MASLIAH, E., MATOUSCHEK, A. & WOLOZIN, B. 2005. beta-Synuclein reduces proteasomal inhibition by alpha-synuclein but not gamma-synuclein. *J Biol Chem,* 280**,** 7562-9.

SONG, J., AMPATZIS, K., BJÖRNFORS, E. R. & EL MANIRA, A. 2016. Motor neurons control locomotor circuit function retrogradely via gap junctions. *Nature,* 529**,** 399-402.

SONG, J., DAHLBERG, E. & EL MANIRA, A. 2018. V2a interneuron diversity tailors spinal circuit organization to control the vigor of locomotor movements. *Nature Communications,* 9**,** 3370.

SONG, J., PALLUCCHI, I., AUSBORN, J., AMPATZIS, K., BERTUZZI, M., FONTANEL, P., PICTON, L. D. & EL MANIRA, A. 2020. Multiple Rhythm-Generating Circuits Act in Tandem with Pacemaker Properties to Control the Start and Speed of Locomotion. *Neuron,* 105**,** 1048-1061.e4.

SPEESE, S. D., TROTTA, N., RODESCH, C. K., ARAVAMUDAN, B. & BROADIE, K. 2003. The ubiquitin proteasome system acutely regulates presynaptic protein turnover and synaptic efficacy. *Curr Biol,* 13**,** 899-910.

SPILLANTINI, M. G., SCHMIDT, M. L., LEE, V. M. Y., TROJANOWSKI, J. Q., JAKES, R. & GOEDERT, M. 1997. α-Synuclein in Lewy bodies. *Nature,* 388**,** 839-840.

SRI, S., PEGASIOU, C.-M., CAVE, C. A., HOUGH, K., WOOD, N., GOMEZ-NICOLA, D., DEINHARDT, K., BANNERMAN, D., PERRY, V. H. & VARGAS-CABALLERO, M. 2019. Emergence of synaptic and cognitive impairment in a mature-onset APP mouse model of Alzheimer's disease. *Acta Neuropathologica Communications,* 7**,** 25.

SRINIVASAN, B., SAMADDAR, S., MYLAVARAPU, S. V. S., CLEMENT, J. P. & BANERJEE, S. 2021. Homeostatic scaling is driven by a translation-dependent degradation axis that recruits miRISC remodeling. *PLoS Biol,* 19**,** e3001432.

STEFANI, M. 2008. Protein folding and misfolding on surfaces. *International journal of molecular sciences,* 9**,** 2515-2542.

STEIN, W. 2014. Sensory Input to Central Pattern Generators.

STELLABOTTE, F. & DEVOTO, S. H. 2007. The teleost dermomyotome. *Developmental dynamics: an official publication of the American Association of Anatomists,* 236**,** 2432-2443.

STELLABOTTE, F., DOBBS-MCAULIFFE, B., FERNÁNDEZ, D. A., FENG, X. & DEVOTO, S. H. 2007. Dynamic somite cell rearrangements lead to distinct waves of myotome growth.

STEVENS, C. F. & WILLIAMS, J. H. 2000. "Kiss and run" exocytosis at hippocampal synapses. *Proceedings of the National Academy of Sciences,* 97**,** 12828-12833.

STEWART, M. D., RITTERHOFF, T., KLEVIT, R. E. & BRZOVIC, P. S. 2016. E2 enzymes: more than just middle men. *Cell Research,* 26**,** 423-440.

STICKNEY, H. L., BARRESI, M. J. & DEVOTO, S. H. 2000. Somite development in zebrafish. *Dev Dyn,* 219**,** 287-303.

SURMACZ, B., NOISA, P., RISNER-JANICZEK, J. R., HUI, K., UNGLESS, M., CUI, W. & LI, M. 2012. DLK1 promotes neurogenesis of human and mouse pluripotent stem cell-derived neural progenitors via modulating Notch and BMP signalling. *Stem Cell Rev Rep,* 8**,** 459-71.

SWOPE, S. L., MOSS, S. J., BLACKSTONE, C. D. & HUGANIR, R. L. 1992. Phosphorylation of ligand-gated ion channels: a possible mode of synaptic plasticity. *The FASEB Journal,* 6**,** 2514-2523.

TADA, H., OKANO, H. J., TAKAGI, H., SHIBATA, S., YAO, I., MATSUMOTO, M., SAIGA, T., NAKAYAMA, K. I., KASHIMA, H., TAKAHASHI, T., SETOU, M. & OKANO, H. 2010. Fbxo45, a novel ubiquitin ligase, regulates synaptic activity. *J Biol Chem,* 285**,** 3840-3849.

TANAKA, K. 2009. The proteasome: overview of structure and functions. *Proceedings of the Japan Academy. Series B, Physical and biological sciences,* 85**,** 12-36.

TAO, C.-L., LIU, Y.-T., SUN, R., ZHANG, B., QI, L., SHIVAKOTI, S., TIAN, C.-L., ZHANG, P., LAU, P.-M. & ZHOU, Z. H. 2018. Differentiation and characterization of excitatory and inhibitory synapses by cryo-electron tomography and correlative microscopy. *Journal of Neuroscience,* 38**,** 1493-1510.

TEIXEIRA, F. R., MANFIOLLI, A. O., SOARES, C. S., BAQUI, M. M. A., KOIDE, T. & GOMES, M. D. 2013. The F-box Protein FBXO25 Promotes the Proteasome-dependent Degradation of ELK-1 Protein *<sup> </sup>. *Journal of Biological Chemistry,* 288**,** 28152-28162.

THIBAUDEAU, T. A. & SMITH, D. M. 2019. A Practical Review of Proteasome Pharmacology. *Pharmacological reviews,* 71**,** 170-197.

THIELE, T. R., DONOVAN, J. C. & BAIER, H. 2014. Descending control of swim posture by a midbrain nucleus in zebrafish. *Neuron,* 83**,** 679-691.

TONG, H. & MCDEARMID, J. R. 2012. Pacemaker and plateau potentials shape output of a developing locomotor network. *Curr Biol,* 22**,** 2285-93.

TREIER, M., SEUFERT, W. & JENTSCH, S. 1992a. Drosophila UbcD1 encodes a highly conserved ubiquitin-conjugating enzyme involved in selective protein degradation. *Embo j,* 11**,** 367-72.

TREIER, M., SEUFERT, W. & JENTSCH, S. 1992b. Drosophila UbcD1 encodes a highly conserved ubiquitin-conjugating enzyme involved in selective protein degradation. *The EMBO journal,* 11**,** 367-372.

TSAI, N.-P., WILKERSON, JULIA R., GUO, W., MAKSIMOVA, M. A., DEMARTINO, GEORGE N., COWAN, CHRISTOPHER W. & HUBER, KIMBERLY M. 2012. Multiple Autism-Linked Genes Mediate Synapse Elimination via Proteasomal Degradation of a Synaptic Scaffold PSD-95. *Cell,* 151**,** 1581-1594.

TSIMOKHA, A. S., ARTAMONOVA, T. O., DIAKONOV, E. E., KHODORKOVSKII, M. A. & TOMILIN, A. N. 2020. Post-Translational Modifications of Extracellular Proteasome. *Molecules,* 25.

TSUBUKI, S., SAITO, Y., TOMIOKA, M., ITO, H. & KAWASHIMA, S. 1996. Differential inhibition of calpain and proteasome activities by peptidyl aldehydes of di-leucine and tri-leucine. *J Biochem,* 119**,** 572-6.

TÜRKER, F., COOK, E. K. & MARGOLIS, S. S. 2021. The proteasome and its role in the nervous system. *Cell Chemical Biology,* 28**,** 903-917.

TUTTLE, M. D., COMELLAS, G., NIEUWKOOP, A. J., COVELL, D. J., BERTHOLD, D. A., KLOEPPER, K. D., COURTNEY, J. M., KIM, J. K., BARCLAY, A. M., KENDALL, A., WAN, W., STUBBS, G., SCHWIETERS, C. D., LEE, V. M., GEORGE, J. M. & RIENSTRA, C. M. 2016. Solid-state NMR structure of a pathogenic fibril of full-length human α-synuclein. *Nat Struct Mol Biol,* 23**,** 409-15.

TWYMAN, R. E. & MACDONALD, R. L. 1991. Kinetic properties of the glycine receptor main- and sub-conductance states of mouse spinal cord neurones in culture. *J Physiol,* 435**,** 303-31.

TYAGARAJAN, S. K., GHOSH, H., YÉVENES, G. E., NIKONENKO, I., EBELING, C., SCHWERDEL, C., SIDLER, C., ZEILHOFER, H. U., GERRITS, B., MULLER, D. & FRITSCHY, J.-M. 2011. Regulation of GABAergic synapse formation and plasticity by GSK3β-dependent phosphorylation of gephyrin. *Proceedings of the National Academy of Sciences,* 108**,** 379-384.

TYLER, W. J. & POZZO-MILLER, L. 2003. Miniature synaptic transmission and BDNF modulate dendritic spine growth and form in rat CA1 neurones. *The Journal of Physiology,* 553**,** 497-509.

UPADHYA, S. C., DING, L., SMITH, T. K. & HEGDE, A. N. 2006. Differential regulation of proteasome activity in the nucleus and the synaptic terminals. *Neurochemistry International,* 48**,** 296-305.

VADHVANI, M., SCHWEDHELM-DOMEYER, N., MUKHERJEE, C. & STEGMÜLLER, J. 2013. The centrosomal E3 ubiquitin ligase FBXO31-SCF regulates neuronal morphogenesis and migration. *PLoS One,* 8**,** e57530.

VALASTYAN, J. S. & LINDQUIST, S. 2014. Mechanisms of protein-folding diseases at a glance. *Disease Models & Mechanisms,* 7**,** 9.

VAN DER KLOOT, W., COLASANTE, C., CAMERON, R. & MOLGÓ, J. 2000. Recycling and refilling of transmitter quanta at the frog neuromuscular junction. *The Journal of Physiology,* 523**,** 247-258.

VAN RAAMSDONK, W., POOL, C. W. & TE KRONNIE, G. 1978. Differentiation of muscle fiber types in the teleost Brachydanio rerio. *Anat Embryol (Berl),* 153**,** 137-55.

VAN RAAMSDONK, W., VAN'T VEER, L., VEEKEN, K., HEYTING, C. & POOL, C. W. 1982. Differentiation of muscle fiber types in the teleost Brachydanio rerio, the zebrafish. Posthatching development. *Anat Embryol (Berl),* 164**,** 51-62.

VAN ROESSEL, P., ELLIOTT, D. A., ROBINSON, I. M., PROKOP, A. & BRAND, A. H. 2004. Independent Regulation of Synaptic Size and Activity by the Anaphase-Promoting Complex. *Cell,* 119**,** 707-718.

VON REYN, C. R., SPAETHLING, J. M., MESFIN, M. N., MA, M., NEUMAR, R. W., SMITH, D. H., SIMAN, R. & MEANEY, D. F. 2009. Calpain mediates proteolysis of the voltage-gated sodium channel alpha-subunit. *J Neurosci,* 29**,** 10350-6.

WAN, H. I., DIANTONIO, A., FETTER, R. D., BERGSTROM, K., STRAUSS, R. & GOODMAN, C. S. 2000a. Highwire Regulates Synaptic Growth in Drosophila. *Neuron,* 26**,** 313-329.

WAN, H. I., DIANTONIO, A., FETTER, R. D., BERGSTROM, K., STRAUSS, R. & GOODMAN, C. S. 2000b. Highwire regulates synaptic growth in Drosophila. *Neuron,* 26**,** 313-29.

WANG, W.-C. & MCLEAN, DAVID L. 2014. Selective Responses to Tonic Descending Commands by Temporal Summation in a Spinal Motor Pool. *Neuron,* 83**,** 708-721.

WANG, Y., OKAMOTO, M., SCHMITZ, F., HOFMANN, K. & SÜDHOF, T. C. 1997. Rim is a putative Rab3 effector in regulating synaptic-vesicle fusion. *Nature,* 388**,** 593-598.

WEBB, P. W. 1976. The effect of size on the fast-start performance of rainbow trout Salmo gairdneri, and a consideration of piscivorous predator-prey interactions. *Journal of Experimental Biology,* 65**,** 157-177.

WEBER, J., POLO, S. & MASPERO, E. 2019. HECT E3 Ligases: A Tale With Multiple Facets. *Frontiers in physiology,* 10**,** 370-370.

WENTZEL, C., DELVENDAHL, I., SYDLIK, S., GEORGIEV, O. & MÜLLER, M. 2018. Dysbindin links presynaptic proteasome function to homeostatic recruitment of low release probability vesicles. *Nature Communications,* 9**,** 267.

WESTERFIELD, M., MCMURRAY, J. V. & EISEN, J. S. 1986. Identified motoneurons and their innervation of axial muscles in the zebrafish. *J Neurosci,* 6**,** 2267-77.
WILKINSON, G. R. 1996. Cytochrome P4503A (CYP3A) metabolism: prediction of in vivo activity in humans. *J Pharmacokinet Biopharm,* 24**,** 475-90.
WILKINSON, K., URBAN, M. & HAAS, A. 1980. Ubiquitin is the ATP-dependent proteolysis factor I of rabbit reticulocytes. *Journal of Biological Chemistry,* 255**,** 7529-7532.
WILLEMS, A. R., SCHWAB, M. & TYERS, M. 2004. A hitchhiker's guide to the cullin ubiquitin ligases: SCF and its kin. *Biochimica et Biophysica Acta (BBA) - Molecular Cell Research,* 1695**,** 133-170.
WILLEUMIER, K., PULST, S. M. & SCHWEIZER, F. E. 2006. Proteasome inhibition triggers activity-dependent increase in the size of the recycling vesicle pool in cultured hippocampal neurons. *J Neurosci,* 26**,** 11333-41.
WILLIAMS, C., CHEN, W., LEE, C.-H., YAEGER, D., VYLETA, N. P. & SMITH, S. M. 2012. Coactivation of multiple tightly coupled calcium channels triggers spontaneous release of GABA. *Nature neuroscience,* 15**,** 1195-1197.
WILLIAMS, C. L. & SMITH, S. M. 2018. Calcium dependence of spontaneous neurotransmitter release. *J Neurosci Res,* 96**,** 335-347.
WILSON, D. & WYMAN, R. 1965. Motor output patterns during random and rhythmic stimulation of locust thoracic ganglia. *Biophysical Journal,* 5**,** 121-143.
WILSON, R. S. & NAIRN, A. C. 2018. Cell-Type-Specific Proteomics: A Neuroscience Perspective. *Proteomes,* 6.
WILSON, S. M., BHATTACHARYYA, B., RACHEL, R. A., COPPOLA, V., TESSAROLLO, L., HOUSEHOLDER, D. B., FLETCHER, C. F., MILLER, R. J., COPELAND, N. G. & JENKINS, N. A. 2002. Synaptic defects in ataxia mice result from a mutation in Usp14, encoding a ubiquitin-specific protease. *Nat Genet,* 32**,** 420-5.
WINDER, S. J., LIPSCOMB, L., ANGELA PARKIN, C. & JUUSOLA, M. 2011. The proteasomal inhibitor MG132 prevents muscular dystrophy in zebrafish. *PLoS currents,* 3**,** RRN1286-RRN1286.
WISE, A., SCHATOFF, E., FLORES, J., HUA, S.-Y., UEDA, A., WU, C.-F. & VENKATESH, T. 2013a. Drosophila-Cdh1 (Rap/Fzr) a regulatory subunit of APC/C is required for synaptic morphology, synaptic transmission and locomotion. *International Journal of Developmental Neuroscience,* 31**,** 624-633.
WISE, A., SCHATOFF, E., FLORES, J., HUA, S. Y., UEDA, A., WU, C. F. & VENKATESH, T. 2013b. Drosophila-Cdh1 (Rap/Fzr) a regulatory subunit of APC/C is required for synaptic morphology, synaptic transmission and locomotion. *Int J Dev Neurosci,* 31**,** 624-33.
WÓJCIK, C. 2002. Regulation of apoptosis by the ubiquitin and proteasome pathway. *J Cell Mol Med,* 6**,** 25-48.
WOODLAND, C., HUANG, T. T., GRYZ, E., BENDAYAN, R. & FAWCETT, J. P. 2008. Expression, activity and regulation of CYP3A in human and rodent brain. *Drug Metab Rev,* 40**,** 149-68.
WU, H. Y. & LYNCH, D. R. 2006. Calpain and synaptic function. *Mol Neurobiol,* 33**,** 215-36.
XIE, J. D., CHEN, S. R., CHEN, H. & PAN, H. L. 2017. Bortezomib induces neuropathic pain through protein kinase C-mediated activation of presynaptic NMDA receptors in the spinal cord. *Neuropharmacology,* 123**,** 477-487.
XU, J., PANG, Z. P., SHIN, O. H. & SÜDHOF, T. C. 2009. Synaptotagmin-1 functions as a Ca2+ sensor for spontaneous release. *Nat Neurosci,* 12**,** 759-66.

YAN, D., WU, Z., CHISHOLM, A. D. & JIN, Y. 2009. The DLK-1 Kinase Promotes mRNA Stability and Local Translation in C. elegans Synapses and Axon Regeneration. *Cell,* 138**,** 1005-1018.

YAN, Q., ZHAI, L., ZHANG, B. & DALLMAN, J. E. 2017. Spatial patterning of excitatory and inhibitory neuropil territories during spinal circuit development. *J Comp Neurol,* 525**,** 1649-1667.

YANAI, K., SON, L. Z., ENDOU, M., SAKURAI, E., NAKAGAWASAI, O., TADANO, T., KISARA, K., INOUE, I., WATANABE, T. & WATANABE, T. 1998. Behavioural characterization and amounts of brain monoamines and their metabolites in mice lacking histamine H1 receptors. *Neuroscience,* 87**,** 479-87.

YANG, C. & WANG, X. 2021. Lysosome biogenesis: Regulation and functions. *J Cell Biol,* 220.

YAO, I., TAKAGI, H., AGETA, H., KAHYO, T., SATO, S., HATANAKA, K., FUKUDA, Y., CHIBA, T., MORONE, N., YUASA, S., INOKUCHI, K., OHTSUKA, T., MACGREGOR, G. R., TANAKA, K. & SETOU, M. 2007. SCRAPPER-Dependent Ubiquitination of Active Zone Protein RIM1 Regulates Synaptic Vesicle Release. *Cell,* 130**,** 943-957.

YOUNG, P., DEVERAUX, Q., BEAL, R. E., PICKART, C. M. & RECHSTEINER, M. 1998. Characterization of two polyubiquitin binding sites in the 26 S protease subunit 5a. *J Biol Chem,* 273**,** 5461-7.

YU, L., CHEN, Y. & TOOZE, S. A. 2018. Autophagy pathway: Cellular and molecular mechanisms. *Autophagy,* 14**,** 207-215.

YUAN, X., MILLER, M. & BELOTE, J. M. 1996. Duplicated proteasome subunit genes in Drosophila melanogaster encoding testes-specific isoforms. *Genetics,* 144**,** 147-157.

ZHANG, C.-W., HANG, L., YAO, T.-P. & LIM, K.-L. 2016. Parkin Regulation and Neurodegenerative Disorders. *Frontiers in aging neuroscience,* 7**,** 248-248.

ZHAO, Y., HEGDE, A. N. & MARTIN, K. C. 2003. The ubiquitin proteasome system functions as an inhibitory constraint on synaptic strengthening. *Curr Biol,* 13**,** 887-98.

ZHEN, M., HUANG, X., BAMBER, B. & JIN, Y. 2000a. Regulation of presynaptic terminal organization by C. elegans RPM-1, a putative guanine nucleotide exchanger with a RING-H2 finger domain. *Neuron,* 26**,** 331-343.

ZHEN, M., HUANG, X., BAMBER, B. & JIN, Y. 2000b. Regulation of presynaptic terminal organization by C. elegans RPM-1, a putative guanine nucleotide exchanger with a RING-H2 finger domain. *Neuron,* 26**,** 331-43.

ZHENG, C., ATLAS, E., LEE, H. M. T., JAO, S. L. J., NGUYEN, K. C. Q., HALL, D. H. & CHALFIE, M. 2020. Opposing effects of an F-box protein and the HSP90 chaperone network on microtubule stability and neurite growth in Caenorhabditis elegans. *Development,* 147.

ZHENG, Q., HUANG, T., ZHANG, L., ZHOU, Y., LUO, H., XU, H. & WANG, X. 2016. Dysregulation of Ubiquitin-Proteasome System in Neurodegenerative Diseases. *Frontiers in Aging Neuroscience,* 8**,** 303.